



Universiteit
Leiden

The Netherlands

Lipid model membrane systems as a tool for unraveling the underlying factors for skin barrier dysfunction

Uche, L.E.

Citation

Uche, L. E. (2021, December 14). *Lipid model membrane systems as a tool for unraveling the underlying factors for skin barrier dysfunction*. Retrieved from <https://hdl.handle.net/1887/3246835>

Version: Publisher's Version

License: [Licence agreement concerning inclusion of doctoral thesis in the Institutional Repository of the University of Leiden](#)

Downloaded from: <https://hdl.handle.net/1887/3246835>

Note: To cite this publication please use the final published version (if applicable).

Lipid model membrane systems as a tool for unraveling the underlying factors for skin barrier dysfunction

Lorretta Uche

Lipid model membrane systems as a tool for unraveling the underlying factors for skin barrier dysfunction

PhD thesis, with summary in Dutch

The research described in this thesis was performed at the Leiden Academic Center for Drug Research, Leiden University, Leiden, The Netherlands.

Cover image: X-ray diffraction pattern of a simple stratum corneum lipid model. The equidistant positions of concentric rings indicate a lamellar phase.

Layout: Douwe Oppewal
Printed by: Ipskamp Printing, Enschede

ISBN: 78-94-6421-548-9

Copyright © 2021, Lorretta Uche. All rights reserved. No part of this thesis may be reproduced or transmitted in any form or by any means without the written permission of the author.

Lipid model membrane systems as a tool for unraveling the underlying factors for skin barrier dysfunction

Proefschrift

ter verkrijging van
de graad van doctor aan de Universiteit Leiden,
op gezag van rector magnificus prof.dr.ir. H. Bijl,
volgens besluit van het college voor promoties
te verdedigen op 14 december 2021
klokke 10:00 uur

door

Lorretta Uche
geboren te Urualla, Nigeria
in 1969

Promotor

Prof. dr. J.A. Bouwstra

Co-Promotor

Dr. C.M. Beddoes

Promotiecommissie

Prof. dr. H. Irth, Universiteit Leiden (voorzitter)

Prof. dr. J. Kuiper, Universiteit Leiden (secretaris)

Prof. dr. R. Rissmann, Universiteit Leiden

Prof. dr. A. Kros, Universiteit Leiden

Prof. dr. J. Lawrence, University of Manchester

Dr. O. Lopez Serrano, Institute of Advanced Chemistry of Catalonia

**To my husband for making this journey with me and my family
for their unwavering support and love**

TABLE OF CONTENTS

Chapter 1

Introduction, aim, and outline of this thesis 9

Chapter 2

Barrier capability of skin lipid models: Effect of ceramides and free fatty acid composition 35

Chapter 3

High concentration of the ester-linked ω -hydroxy ceramide increases the permeability in skin lipid model membranes 65

Chapter 4

New insight into phase behavior and permeability of skin lipid models based on sphingosine and phytosphingosine ceramides 91

Chapter 5

Increased levels of short-chain ceramides modify the lipid organization and reduce the lipid barrier of the skin model membrane 127

Chapter 6

Summary and perspectives 159

Appendices

Nederlandse samenvatting 174

Curriculum Vitae 182

List of publications 183



1

Introduction, aim, and outline
of this thesis

INTRODUCTION

The skin structure and barrier function

The skin is the largest organ of the body, weighing 12 to 15 percent of the total body mass, and covering 1.5-2 m² of the surface area [1-3]. Its primary function is the protection of the body against invasion by exogenous substances including dust, pathogens, chemicals, and ultraviolet radiation [4-10]. In addition to barring indiscriminate permeation of substances, the skin also prevents uncontrolled loss of water from inside the body to the external environment, referred to as transepidermal water loss (TEWL) [11, 12]. In effect, the skin is a two-way barrier, determining both the inward and outward movement of substances across the human body. Other important biological functions of the skin include thermoregulation, vitamin D synthesis, excretion of urea and salts as well as serving as a sensory organ for transmitting external environmental information, such as pain and heat [10, 13].

The skin is composed of three main morphological layers, from the innermost layer to the surface: hypodermis, dermis, and epidermis (figure 1A). The hypodermis or subcutaneous tissue attaches the skin to the underlying bones and muscles.

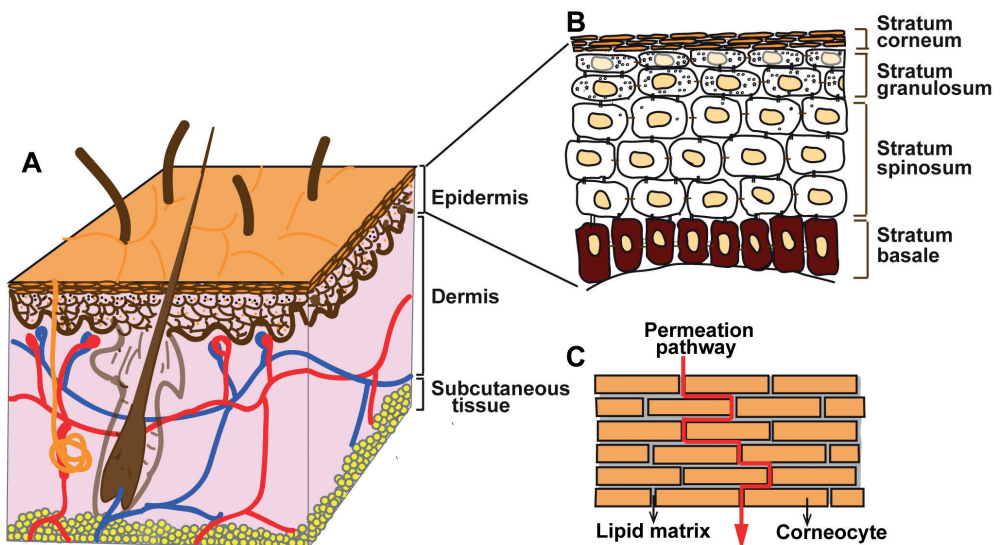


Figure 1. Schematic structure of the skin.

A) The skin consists of three major layers: Epidermis, dermis, and subcutaneous tissue. B) The epidermis is subdivided into four layers stratum basale (SB), stratum spinosum (SS), stratum granulosum (SG), and stratum corneum (SC). C) In SC the corneocytes are embedded in a lipid matrix often referred to as a brick-and-mortar structure. The intercellular lipid matrix is the main permeation pathway for substances into the body.

The next layer is the dermis, which is primarily made up of connective tissue, collagen, and elastin, responsible for the skin's resilience, flexibility, and elasticity. The skin appendages including the sweat gland and hair follicle units cut across the dermis to the skin surface. The outermost layer of the skin is the epidermis and varies in thickness from 50 to 150 μm . It is composed of four layers characterized by different stages of keratinocyte (major cell type in the epidermis) differentiation. Moving from the lowest layer upwards to the skin surface, these layers are stratum basale (SB), stratum spinosum (SS), stratum granulosum (SG), and stratum corneum (SC) (figure 1B). The SB, SS, and SG constitute the viable epidermis while the SC is the non-viable epidermis. The keratinocytes are generated by stem cells in the basal layer. After proliferation through mitosis, the keratinocytes migrate from the SB upwards, towards the surface of the epidermis, undergoing several stages of cell differentiation, changing composition and shape. During this process, the keratinocytes synthesize the SC structural proteins and lipids. At the SS, the keratinocytes are spherical, contain a nucleus and cell organelles, and are tightly connected by protein bridges referred to as desmosomes. Also, the initial formation of the membrane coating granules (lamellar bodies) occurs [14]. These granules contain the precursors of the barrier lipids and a series of hydrolytic enzymes and function as lipid-transporters.

At the SG, the keratinocytes flattened, while the keratohyalin granules (mainly containing proteins) and lamellar bodies are present at high concentrations [15-18]. The keratohyalin granules contain primarily the epidermal proteins: profilaggrin, loricrin, involucrin, and keratin [19-22]. The lamellar bodies contain polar lipids including glucosylceramides, sphingomyelin, phospholipids, (as well as the respective catabolic enzymes: β -glucocerebrosidase, sphingomyelinase, and phospholipase A2), and free sterols. During the terminal differentiation of the keratinocytes to form their final product, the corneocytes, cellular organelles are destroyed by the action of enzymes and the keratinocytes are flattened, highly differentiated, the content of the keratohyalin granules is released. Profilaggrin is enzymatically converted into filaggrin, which aggregates keratin through the formation of disulfide bonds between keratin fibers. The corneocytes are then filled with the water-retaining keratin. The precursor proteins loricrin and involucrin, are cross-linked by the action of transglutaminase to form the stable, rigid cornified cell envelope. Filaggrin was shown to be a component of the cell envelope [23]. Simultaneously, the lamellar bodies migrate to the apical periphery of the uppermost granular cells and fuse with the membrane of the keratinocytes. The lipids and lipid processing enzymes are extruded via

exocytosis into the intercellular space at the SG-SC interface [15, 16, 18, 24-27]. The lipids are processed to form a highly organized intercellular lamellar matrix. Finally, the cell envelope surrounds the corneocytes and is embedded in the intercellular lipid matrix [4-6, 12]. The cell envelope has a layer of covalently bounded polar lipids. A major lipid class bound to the cornified envelope consists of an ultra-long carbon chain length (C30-C34) omega-hydroxy fatty acids in amide linkage with sphingoid base and attached mainly to the glutamate residues of involucrin [28-30]. This lipid monolayer referred to as cornified lipid envelope (CLE) provides a hydrophobic interface between the hydrophilic protein cell envelope and the highly hydrophobic intercellular lipid matrix. The lipid monolayer is postulated to act as a template for the subsequent addition of the intercellular lipids forming the lipid matrix, orienting the intercellular lipid lamellae parallel to the corneocyte surface [31, 32].

SC structure

The SC is 10-15 micron thick and composed of 10-20 layers of corneocytes arranged approximately parallel to the skin surface and linked by corneodesmosomes [4-6, 12, 33]. The structure of the SC has been described as being comparable to brick and mortar (figure 1C), with the corneocytes as the bricks and intercellular lipids as the mortar [34]. The highly impermeable nature of the cornified envelopes encapsulating the corneocyte redirects penetrating substances mainly through the tortuous pathway of intercellular lipids, which is the only continuous pathway for diffusion through the SC [35-38]. The intercellular lipids are thus key in maintaining the skin barrier function and alterations in lipid composition and/or organization may play a role in skin barrier dysfunction [34]. This is seen by lipid extraction of the epidermis increasing the recorded water permeation [11, 39-41]. Keratinocytes from the SC are eventually shed from the surface (desquamation). The desquamation process is due to the activity of proteolytic enzymes and lipolytic enzymes acting respectively on the corneodesmosomes and intercellular lipids.

SC lipid composition

The major lipid classes generated at the SG-SC interface are ceramides (CERs), cholesterol (CHOL), and free fatty acids (FFAs) [6, 34, 42-44]. These lipids are in an approximately equimolar ratio in the human SC [45]. A low concentration of CHOL sulphate is also present in the SC and plays a key role in the regulation of desquamation [46]. The FFAs are mostly saturated and exhibit a chain length distribution between 12 and 30 carbon atoms, with the most prevalent chain

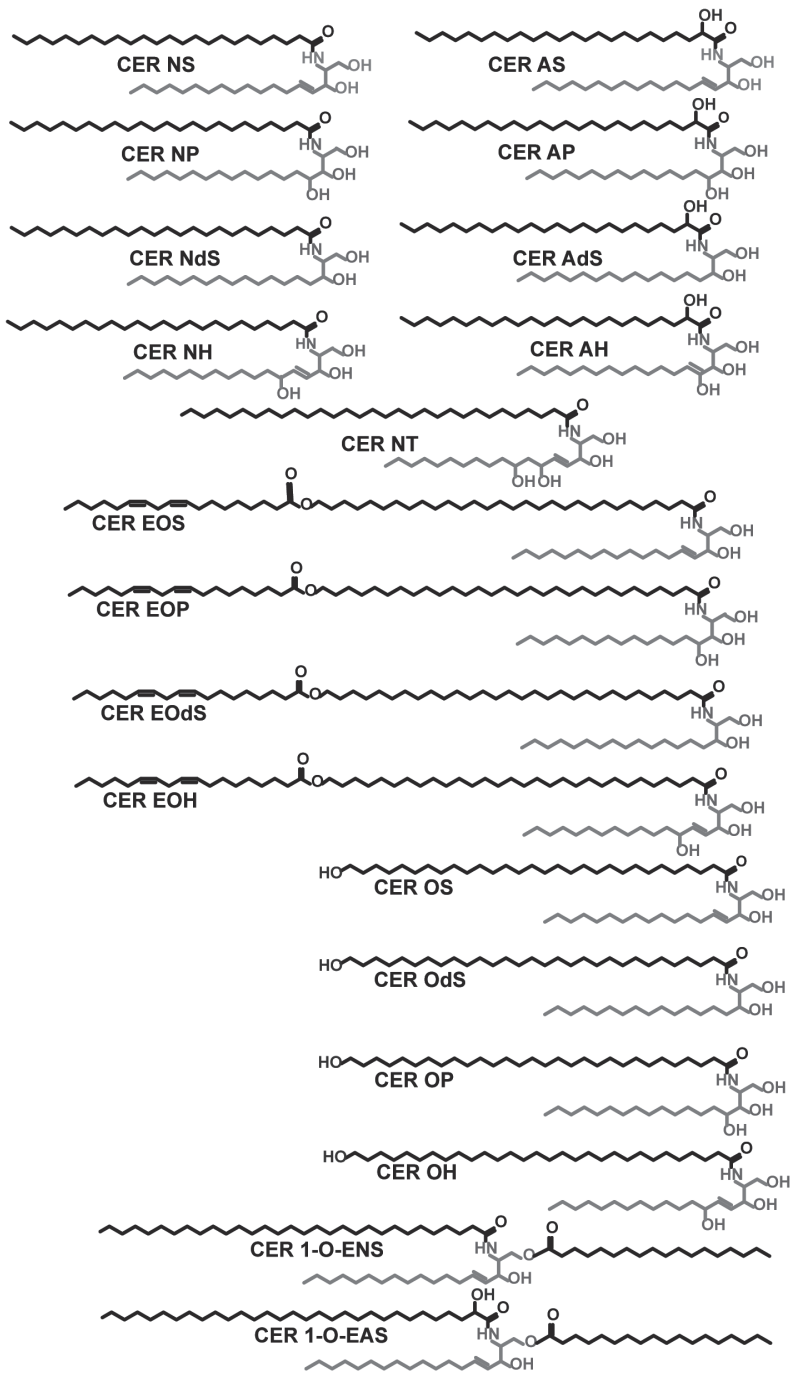


Figure 2. CER subclasses in the SC matrix.

CERs consist of a sphingoid base linked to a FA chain. The acyl chain can either be non-hydroxylated (N), α-hydroxylated (A), ω-hydroxylated (O), or esterified ω-hydroxylated (EO), while the sphingoid base is either sphingosine (S), dihydrosphingosine (dS), phytosphingosine (P), 6-hydroxysphingosine (H), or dihydroxy dihydrosphingosine (T).

lengths being 22, 24, and 26 carbon atoms [47, 48]. The CERs are made up of fatty acid linked to a sphingoid base via an amide bond between the carboxyl group of the fatty acid and the amino group of the sphingoid base (figure 2). The most abundant sphingoid base chain length is 18 carbon atoms [49, 50]. The sphingoid base head group is either sphingosine (S), phytosphingosine (P), 6-hydroxy sphingosine (HS), dihydrosphingosine (DS), or dihydroxy dihydrosphingosine (T). The fatty acid acyl chain is either non hydroxylated (N), α -hydroxylated (A), or omega hydroxylated (O). The most abundant chain lengths of the non-hydroxylated and the α -hydroxylated fatty acids are 24 to 26 carbon atoms. The omega hydroxylated fatty acid is of an ultra-long carbon chain length varying between 30 to 34 carbon atoms (although shorter chain lengths are also present) and subsequently esterified to an unsaturated fatty acid, usually, linoleic acid, esterified omega hydroxyl fatty acid (EO) also referred to as acylCER. Two recently identified CERs contain an additional acyl chain at position 1 of the sphingosine base chain (1-O-acylCER) [51]. The different combinations of the sphingoid bases linked to the variety of acyl chains result in at least 18 CER subclasses currently identified in the human SC (figure 2) [50, 52-60]. The generally adopted nomenclature for CER is based on Motta et al, [61] in which the CERs are denoted with 2-3 letters, defining the type of sphingoid base and linked fatty acid acyl chain.

Synthesis of the SC lipids

Some lipids are taken up by the epidermis from extracutaneous sources, such as the dietary lipids (e.g. essential FFAs and cholesterol esters), but most lipids are generated in the viable keratinocytes (de novo synthesis). It is a complex network of synthetic pathways involving many enzymes.

FFAs with a chain length of up to 16 carbon atoms are synthesized by fatty acid synthase using acetyl-coenzyme A and malonyl-coenzyme. Synthesized FFA C16 or FA supplied from dietary sources are then elongated in chain lengths by a series of 7 elongases (ELOVL1-7) in the endoplasmic reticulum and occurs with two carbons per cycle, hence synthesis occurs with the preference of even-numbered carbon chains [62]. The elongases are specific for a particular fatty acid chain length [41, 62]. ELOVL1 and ELOVL4 elongate FFAs with a carbon chain length of C20-C26 and \geq C26 respectively. ELOVL3 elongates FFA C18-C20 whereas ELOVL6 elongates FFA C16 to generate FFA C18. Besides elongation, the FAs can be converted to monounsaturated fatty acids (MUFAs) by stearoyl-coenzyme A desaturases. The elongation of MUFAs is catalyzed by ELOVL3, 7, and 1, whereas ELOVL5 is involved in the elongation of polyunsaturated fatty

acids (PUFAs). Subsequently, the synthesized FFAs can be used for CER synthesis or transformed into phospholipids and then stored in the lamellar bodies (LBs). During lamellar body extrusion at the SG-SC interface, secretory phospholipase A2 converts phospholipids back to FFAs.

CER synthesis occurs in the endoplasmatic reticulum of the keratinocytes. The variety in the CER subclasses arises from the final stages in the CER synthesis pathway in the body. In the first step, the enzyme serine palmitoyl catalyzes the condensation of L-serine and palmitoyl-CoA into 3-keto-dihydrosphingosine, which is consecutively reduced to dihydrosphingosine. Dihydrosphingosine is then acetylated by one of the 6 CER synthases (CERS₁₋₆) to form dihydro-CER using acyl-CoAs as FA donors [63]. Each CER synthase has specificity for fatty acid chain length and saturation. (CERS₁, C18; CERS₂, C22, and C24; CERS₄, C20, C22 and C24; and CERS₅ and CERS₆, C16), except for CERS₃, which exhibits broad substrate specificity toward medium- to long-chain fatty acyl-CoAs (short-chain having \leq C18; medium-chain, C18–C22; and long-chain, \geq C26) [64]. CERS₃ specifically synthesizes the acylCERs and together with CERS₄ are the major CERs in the skin. Finally, the dihydro-CERs are desaturated to sphingosine CER or hydroxylated to phytosphingosine CER subclasses by dihydro-CER desaturase 1 and 2, respectively. In addition to hydroxylase activity, dihydro-CER desaturase 2 also has weak desaturase activity that can create sphingosine CER. CERs can also be produced by the salvage pathway, in which sphingosine generated by the deacylation of CER is re-acylated by as yet undetermined factors [63].

After synthesis, the primary hydroxy group of the CER is linked to either a glucose or phosphocholine group by the action of the enzymes glucosylceramide synthase and sphingomyelin synthase, respectively. The products glucosylceramides and sphingomyelin are packed in lamellar bodies, and released together with their catabolic enzymes at the SG-SC interface during the terminal differentiation of keratinocytes into corneocytes.

SC lipid organization

The SC intercellular lipids are present in stacks of lamellae arranged parallel to the skin surface. The presence of the lamellar layers in the SC was first observed using freeze-fracture electron microscopy [65]. Thereafter, the broad-narrow-broad sequence of electron translucent bands was visualized after ruthenium tetroxide fixation of the SC [66-68]. The lipids adopt a highly ordered, 3-dimensional structure of stacked densely packed lipid layers. X-ray diffraction studies revealed the coexistence of two crystalline lamellar phases of 13 nm repeat distance known as the long periodicity phase (LPP) and 6 nm

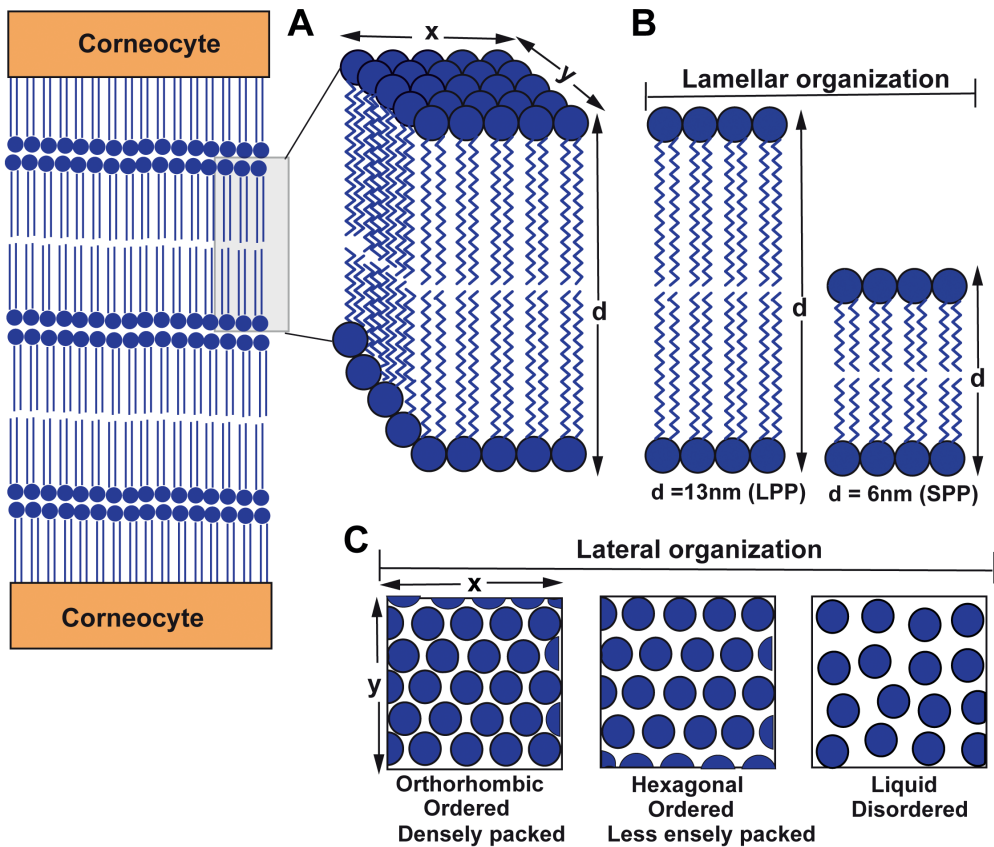


Figure 3. Organization of the lipids within the SC.

A) The lipids are stacked in layers (lamellae) in between the corneocytes. B) Two lamellar phases coexist with a repeat distance of either 13 nm (LPP) or 6 nm (SPP). C) Within the lamellae (lateral organization) three arrangements are possible: either an orthorhombic, hexagonal, or liquid packing.

repeat distance known as the short periodicity phase (SPP) [69-72]. The LPP is a trilayer structure that is unique in the SC and considered to be important for the skin barrier function [73, 74]. Perpendicular to the basal layer of the lamellae, the lipid organization is referred to as the lateral organization. In this organization the lipids can be ordered, adopting either the dense orthorhombic or less dense hexagonal packing or lipids can be disordered (liquid) [75-77]. Infrared spectroscopic studies showed that the majority of the SC lipids in human skin adopt the densely packed phase, which is necessary to limit the permeability through the skin [78, 79].

SC in skin diseases with an impaired barrier

Skin barrier dysfunction indicated by increased trans-epidermal water loss is habitually observed in inflammatory skin diseases including autosomal recessive congenital ichthyosis (ARCI), Netherton syndrome, psoriasis, and atopic dermatitis (AD) [32, 80-84]. The SC lipid composition of diseased skin differs from that of healthy skin and is considered to play a role in the impaired skin barrier function [85]. Netherton syndrome is a severe, rare genetic skin disorder characterized by congenital erythroderma, hair shaft defects, and severe atopic manifestations [83, 86-88]. In Netherton syndrome patients' skin, the level of acylCERs is reduced while there is an increased level of short-chain FFAs and CERs (particularly CER NS and CER AS), unsaturated CERs, and MUFAs [83]. Consequently, an altered lamellar organization and increased disordering of the lipids were observed.

ARCI is a rare skin disease characterized by abnormal desquamation over the whole body [84, 89]. In ARCI patients, the impaired CERS₃ via genetic defects results in alterations of the sphingolipid metabolism. This includes reduced levels of ultra-long chain CERs, and a disturbed epidermal permeability barrier function [57, 84, 90, 91]. Likewise, deficiency of CERS₃ in mice resulted in complete loss of ultra-long chain CERs (\geq C26), altered lamellar organization, and a non-functional CLE [92-94]. Enzymatic oxidation of the linoleate ester in CER EOS by lipoxygenases (LOXs) is required for the formation of the CLE. In ARCI patients, Loss-of-function of 12R-lipoxygenase (12R-LOX) or epidermal lipoxygenase-3 (eLOX3) by gene mutations resulted in the absence of CLE on the surface of the cornified cell envelope [32]. Consequently, lamellar structures were defective and barrier function was severely impaired, indicating the importance of the CLE for a proper lamellar organization [95]. Psoriasis is another chronic inflammatory skin disease that is characterized by both increased desquamation and keratinocyte hyperproliferation in lesional skin leading to incomplete differentiation in distinct regions [82, 96]. In the lesional areas, the SC is thickened to about 10 times the situation in healthy skin [82]. Analysis of the lipid composition of psoriatic skin showed a reduction in CER subclasses: EOS, CER NP, and CER AP, whereas CER NS, and CER AS increased [61, 82]. Regarding the other lipid classes, psoriasis scales have been shown to contain an increased level of CHOL and a decreased level of FFA in comparison to SC of normal skin [96].

AD is a chronic, multifactorial, inflammatory skin disease characterized by redness, itching, dryness, and lesions [97]. In industrialized nations, the incidence of AD has increased to about 15-30% in children, and 2-10% in adults making it the most prevalent skin disease [98]. Due to the combined facts of its increasing

prevalence, its devastating effect on the quality of life, and consequential financial burden, AD remains of vital research interest [98-102]. Initially, AD was thought to be solely an allergic response [103, 104]. However, the loss-of-function mutations in the filaggrin gene appeared to be a major predisposing risk factor for developing AD [81, 105-107]. Filaggrin is an important protein for the maintenance of structural integrity and the breakdown products are part of the natural moisturizing factor (NMF), necessary for proper SC hydration [105, 108-110]. Reduced barrier function was subsequently demonstrated in certain AD patients unrelated to loss-of-function mutation of the filaggrin gene suggesting the involvement of factors other than filaggrin genotype in barrier dysfunction of those patients [57]. In AD patients' skin, the expression of certain enzymes involved in lipid metabolism differs when compared with control skin [57]. The activity of Sphingomyelinase and β -glucocerebrosidase, which catalyzes the conversion of their respective lipid precursors, sphingomyelin and glucosylceramide to CERs were shown to be reduced in lesional and non-lesional AD skin. [111, 112]. This correlated with reduced SC CER content and barrier dysfunction. Conversion by sphingomyelinase generates only CER subclasses NS and AS, while CER formation via glucocerebrosidase may result in various subclass [112].

It has been reported that the enzymes sphingomyelin deacylase and glucosylceramide deacylase that stimulates the cleavage of the acyl chain from the glucosylceramide and sphingomyelin are increased in activity, resulting in a decreased CER level [113-115]. It has been proposed that in AD, the activity of Ceramidases, which catalyzes the breakdown of CERs to a sphingoid base and a fatty acid chain is increased [57]. This resulted in accumulation of the CER metabolite, sphingosine-1-phosphate, which stimulated the release of the inflammatory mediators (tumor necrosis factor alpha (TNF- α) and interleukin (IL)-8) from the keratinocytes [116].

A strong correlation has been observed between changes in SC lipid composition and barrier function impairment in AD patients [117-119]. The lipid composition of AD patients' skin shows a reduction in the level of CER NP, CER NH, and the acylCERs, while there is an increase in levels of CER NS and AS [117, 118, 120, 121]. With regards to chain length variation, increased levels of short-chain CER particularly in the CER subclasses CER NS and CER AS was reported in diseased skin. CERs with a total chain length (sphingoid base chain + fatty acid chain) of 34 carbon atoms increased significantly in AD patients [112, 117, 118] when compared with controls. An increase in the level of lipid adopting the hexagonal lateral packing was observed. Apart from the increase in the level

of short-chain CERs, an increased level of short-chain FFAs was also observed. Reduced levels of ELOVL1 and ELOVL4 reported in the AD murine model suggests that a reduced average chain length of CERs and FFAs in SC of AD patients may be caused by a reduced expression and/or activity of these elongases [57, 122].

Alterations in lipid composition observed in diseased skin result in changes in lipid organization and possibly contribute to the barrier function impairment. Studying the effect of the changes in the lipid composition on the organization of the SC lipids is therefore an important aspect for investigating the factors for barrier dysfunction in diseased skin. However, the complexity of the SC structure makes it difficult to delineate the link between lipid organization and lipid composition in healthy and diseased human skin. As several alterations in the lipid composition of diseased skin occur simultaneously, it is not possible to determine the effect of the individual alterations in the lipid composition on lipid organization and barrier function in clinical studies. Lipid models in which the lipid composition can be varied at will and as desired, including mimicking that of diseased skin, offers an attractive option to achieve this feat.

SC lipid models.

SC lipid models range from simple ternary systems containing a CER, CHOL, and a FFA to more complex models incorporating a large number of lipid subclasses and chain lengths. The unique SC lipid organization has been mimicked by lipid model mixtures prepared with either isolated [72, 123-127] or synthetic [128-131] CERs together with CHOL, and FFAs. Previous X-ray diffraction studies carried out with mixtures prepared from isolated pig CER [123] or human CER [124, 127] and CHOL revealed the formation of two lamellar phases, the SPP and LPP mimicking the lipid organization in native human SC in which the SPP and LPP with a repeat distance of approximately 6 and 13 nm are present. The repeat distances of the lamellar phases formed by the pig CER: CHOL mixture were slightly shorter, being 5.2 and 12.2 nm, while the human CER: CHOL mixture mainly formed an LPP. Analysis of the WAXD data of both lipid mixtures showed that the lipids adopted a hexagonal lateral packing. The addition of long-chain FFA in both mixtures induced a phase transition from a hexagonal to an orthorhombic packing but also promoted the SPP formation in the human CER: CHOL mixture. Absence of CER EOS in the isolated human CER: CHOL mixture resulted in the predominance of the SPP [124] indicating the importance of CER EOS for the LPP formation.

Studies were performed in which the natural CER EOS in a human CER:CHOL:FFA mixture was replaced by synthetic CER EOS linoleate (double unsaturation) or CER EOS oleate (single unsaturation), or CER EOS stearate

(saturated) [132]. The liquid phase was more prominently formed and the LPP less prominent in presence of CER EOS oleate compared to the linoleate, while both the liquid phase and the LPP were not detected in presence of the stearate [132, 133] indicating that a certain level of unsaturation in the C18 chain of EO CER is required for LPP formation. X-ray and infrared spectroscopy studies showed that CER EOS linoleate and CER EOS oleate have a similar influence on lipid phase behavior in SC models [133].

The use of isolated CERs is limited by the laborious and lengthy procedure required for the isolation of CERs from human skin. Moreover, human skin is not as readily available. Synthetic CERs are used as an alternative and offer the additional advantage of having a well-defined chain length favorable for reproducibility of experimental data and interpretation of results. Equimolar mixtures of CHOL, FFAs, and synthetic CERs (mimicking the composition of pig CERs) formed the SPP and LPP and adopted the orthorhombic packing, closely resembling the lamellar and lateral native SC lipid organization [129]. As the synthetic CER composition can be altered as desired, SC lipid models can be employed to obtain detailed insight regarding the role of the individual lipid classes and subclasses in SC lipid organization. For instance, CER EOS was shown to be crucial for the formation of the LPP [129, 134]. Substitution of CER EOS by CER EOP reduced the formation of the long periodicity lamellar phase [129]. Though complex lipid mixtures prepared with synthetic CERs offer an attractive tool to unravel the importance of the molecular structure of individual CER for proper lipid organization, detailed interpretation of the interaction of the CER subclasses is complicated by the presence of diverse CER headgroups.

The interpretation of the interaction and lipid phase behavior in simple systems can be more detailed than in complex systems as interference from multiple lipid subclasses does not arise. Furthermore, it is easier to include deuterated lipids to obtain additional information. Previous studies of a simple SC model comprising an equimolar ratio of CHOL, palmitic acid (FA C16), and a CER reported differences in the physical properties such as phase transition temperature when the CER headgroup was varied [135-137]. However, chain length mismatch between the CER and FFA chains in these simple systems often resulted in the formation of separate domains of the lipid species. In other simple systems, FA C16 was replaced with lignoceric acid (FA C24), which is the most abundant FA chain length in the native SC [138, 139]. Despite the important role of the LPP in the characteristic SC lipid organization, these systems did not contain CER EOS and thus did not form the LPP. Examining the effect of lipid composition on the lipid organization and molecular interaction within the LPP

is important for a comprehensive and detailed understanding of the processes, factors, and mechanisms underlying skin barrier function.

Model membrane system for assessment of barrier function

To obtain detailed insight regarding the role the individual lipid classes and subclasses play in the skin barrier function, SC lipid model membranes are developed on a porous membrane. This system can be clamped in a diffusion cell to be able to perform permeation studies [73]. As the lipid composition in the model can easily be modified, the lipid model membranes enable to study of the relationship between lipid composition, molecular organization, and barrier function. The model membranes offer the opportunity to mimic the lipid composition and organization in healthy as well as in diseased skin. Barrier function properties of the SC lipid model membranes can be evaluated with various techniques. The inside-out barrier can be determined by measuring trans-epidermal water loss (TEWL). The outside-in barrier function can be examined by the measurement of the amount of a model drug permeating a membrane per unit area per unit time (flux) in diffusion experiments.

A previous study evaluated the barrier integrity of the SC model membrane that mimicked pigCER composition using diffusion studies of three model compounds with different lipophilicities: benzoic acid, para-aminobenzoic acid (PABA), ethyl PABA and butyl PABA [73]. Isolated human SC was used as a control sample. The permeation profile of all these compounds across the model membrane revealed a similar flux as observed in human SC, demonstrating the suitability of the model membrane as a substitute for the native SC. In that study, modification of the lipid composition of the pigCER model, generating a model membrane that lacks CER EOS, was accompanied by a two-fold increase in permeability indicating the importance of CER EOS not only in the lamellar organization but also for proper skin lipid barrier function. The pigCER model membrane as control was subsequently modified to mimic several alterations in the lipid composition observed in diseased skin [140]. When the pigCER model was altered to mimic the composition in recessive X-linked ichthyosis by incorporating high levels of CHOL sulphate, the model membrane displayed a two-fold increase in permeability compared to the pigCER control model. The barrier impairment was attributed to the formation of separate phases and the reduction in packing density. To mimic aspects of the lipid composition of psoriasis patients' skin, the level of CHOL in the model mixture was increased and the level of FFA was reduced. The permeability and lamellar organization were similar to those of the control though psoriasis skin is characterized by

impaired barrier function. Thus, the reported changes may not be responsible for the observed impaired barrier function in vivo [140]. A reduction in CER chain length and FFA chain length which may have a profound effect on permeability were not investigated as no information was available on the CER and FFA chain length distribution in psoriasis SC at that time [140]. The psoriatic skin model was modified to incorporate the reported CER composition of psoriatic scales thereby mimicking the psoriasis patients' skin more closely [141]. Lower permeability was observed across the psoriatic skin model than across the pigCER model and SC, which was suggested to be probably due to the higher level of phase-separated crystalline CHOL. In another study, the pigCER model composition was altered by the incorporation of increased levels of monounsaturated fatty acids, as observed in the skin of Netherton syndrome patients [131]. The permeability of the model membrane increased with the degree of unsaturation and was attributed to the phase transition of the lipid chains from orthorhombic to the less dense hexagonal phase.

To determine whether the reported changes in lipid composition contribute to the impaired barrier function of atopic dermatitis skin, it is important to design a model membrane that can mimic the lipid composition of atopic skin as closely as possible. PigCER model has been used as control in the studies with the diseased skin models described above. However, the pigCER mixture contained short-chain CER and high levels of CER NS which are not present in healthy human skin. There is therefore a need for a SC model that will mimic human CER composition and lipid organization as the result obtained with such a model can be better extrapolated directly to the in-vivo situation.

AIM OF THIS THESIS

The studies described in this thesis aimed to unravel the underlying factors and mechanisms for the impaired skin barrier function in AD using complex model membrane systems mimicking the human SC lipid composition and simple model membranes to obtain more detailed information.

OUTLINE OF THIS THESIS

Studies in **Chapter 2** describe the development of a lipid model membrane mimicking the lipid composition and lipid organization of human SC by replacing the pigCER composition with a CER composition that mimics closely that in human SC. To establish the resemblance of the skin model to the native skin, the lipid organization and permeability of the lipid model membrane were compared with those in SC of the native skin. In subsequent studies, the lipid composition was altered to mimic several aspects of the lipid composition in AD skin. The changes in lipid composition investigated in this study include i) incorporation of short-chain length CERs with a total chain length of 34 C atoms. ii) Increased levels of CER NS and CER AS and reduction in the level of CER NP. iii) Reduction in CER EOS concentration and iv) Increased level of short-chain FFAs. As the penetration through these membranes can also be measured, the lipid membrane models enabled a systematic examination of the effect of the various changes reported in the lipid composition of AD patients' skin on the permeability and lipid organization of the model membrane. Similar deviations in lipid composition are observed in some other inflammatory skin diseases including Netherton syndrome and psoriasis [82, 83].

In the subsequent chapters, simple model systems mimicking important aspects of the native skin lipid organization were prepared for a more detailed study based on the changes in CER composition of AD patients' skin investigated in chapter 2.

Chapter 3 describes studies involving varying levels of CER EOS in the SC lipid model. The level is altered in AD, but also in other inflammatory skin diseases [32, 80-84]. As CER EOS concentration affects the formation of the LPP, SC models with gradually increasing levels of CER EOS (10/30/50/70/90) mol% were employed for a detailed investigation of the influence of CER EOS concentration on lamellar organization, LPP unit cell structure, lateral organization, and permeability of the model membrane. The LPP intensity distribution in the models was compared to that previously observed for the complex SC model and native SC [144] to determine the similarity of their LPP structures. The mechanism underlying the changes in permeability with varying concentrations of CER EOS was investigated.

The simple models used in the subsequent studies were prepared as an equimolar mixture of CERs, CHOL, and FFA with CER EOS constituting 40% of the CER fraction. This high CER EOS concentration opposed to the physiological 10% (approximate) [57, 145] was necessary to prepare lipid models forming only

the LPP [136, 146, 147] with a similar structure to that of the native skin (hereafter referred to as LPP model).

In **Chapter 4**, a detailed study is presented that describes the effect of CER headgroup variation on the lipid organization and barrier function of LPP models focusing on the sphingosine- and phytosphingosine-based CERs as their levels are altered in AD and psoriasis. Biophysical techniques were employed to determine the mechanisms for the differences in the lipid phase behavior and permeability of the models containing the different CER head groups.

In **Chapter 5**, studies are reported in which the level of the long acyl chain length CER NS(C24) in the simple LPP model was gradually substituted with short-chain CER NS(C16) as observed in AD but also in Netherton syndrome patients' skin to systematically evaluate the effect of the acyl chain length of CERs on the permeability and phase behavior of model membranes. Finally, the overall findings are summarized and the future perspectives are presented in **Chapter 6**.

REFERENCES

1. Moore, L.; Chien, Y. W., Transdermal drug delivery: a review of pharmaceuticals, pharmacokinetics, and pharmacodynamics. *Crit. Rev. Ther. Drug Carrier Syst.* **1988**, *4* (4), 285-349.
2. Swann, G., The skin is the body's largest organ. *J. vis. commun. in med.* **2010**, *33*, 148-9.
3. Burton, R. F., Estimating body surface area from mass and height: theory and the formula of Du Bois and Du Bois. *Ann. Hum. Biol.* **2008**, *35* (2), 170-84.
4. Blank, I. H., Cutaneous barriers. *J. Invest. Dermatol.* **1965**, *45* (4), 249-256.
5. Elias, P. M., Epidermal barrier function - Intercellular lamellar lipid structures, origin, composition, and metabolism. *J. Control. Release* **1991**, *15* (3), 199-208.
6. Elias, P. M.; Goerke, J.; Friend, D. S., Mammalian epidermal barrier layer lipids: composition and influence on structure. *J. Invest. Dermatol.* **1977**, *69* (6), 535-46.
7. Lee, S. H.; Jeong, S. K.; Ahn, S. K., An update of the defensive barrier function of skin. *Yonsei Med. J.* **2006**, *47* (3), 293-306.
8. Proksch, E.; Brandner, J. M.; Jensen, J. M., The skin: an indispensable barrier. *Exp. Dermatol.* **2008**, *17* (12), 1063-72.
9. Wickett, R. R.; Visscher, M. O., Structure and function of the epidermal barrier. *Am. J. Infect. Control* **2006**, *34* (10), S98-S110.
10. Chuong, C. M.; Nickoloff, B. J.; Elias, P. M.; Goldsmith, L. A.; Macher, E.; Maderson, P. A.; Sundberg, J. P.; Tagami, H.; Plonka, P. M.; Thestrup-Pedersen, K.; Bernard, B. A.; Schroder, J. M.; Dotto, P.; Chang, C. H.; Williams, M. L.; Feingold, K. R.; King, L. E.; Kligman, A. M.; Rees, J. L.; Christophers, E., What is the 'true' function of skin? Viewpoint 1. *Exp. Dermatol.* **2002**, *11* (2), 159-163.
11. Madison, K. C., Barrier function of the skin: "la raison d'être" of the epidermis. *J. Invest. Dermatol.* **2003**, *121* (2), 231-41.
12. Scheuplein, R. J.; Blank, I. H., Permeability of the skin. *Physiol. Rev.* **1971**, *51* (4), 702-47.
13. Baroni, A.; Buommino, E.; De Gregorio, V.; Ruocco, E.; Ruocco, V.; Wolf, R., Structure, and function of the epidermis related to barrier properties. *Clin. Dermatol.* **2012**, *30* (3), 257-62.
14. Selby, C. C., An electron microscope study of thin sections of human skin. II. Superficial cell layers of footpad epidermis. *J. Invest. Dermatol.* **1957**, *29* (2), 131-49.
15. Odland, G. F., A Submicroscopic Granular Component in Human Epidermis**From the Department of Anatomy, University of Washington, Seattle, Washington. *J. Invest. Dermatol.* **1960**, *34* (1), 11-15.
16. Landmann, L., Lamellar granules in mammalian, avian, and reptilian epidermis. *J. Ultrastruct. Res.* **1980**, *72* (3), 245-63.
17. Elias, P. M.; Brown, B. E.; Fritsch, P.; Goerke, J.; Gray, G. M.; White, R. J., Localization and Composition of Lipids in Neonatal Mouse Stratum Granulosum and Stratum Corneum. *J. Invest. Dermatol.* **1979**, *73* (5, Part 1), 339-348.
18. Freinkel, R. K.; Traczyk, T. N., Lipid Composition and Acid Hydrolase Content of Lamellar Granules of Fetal Rat Epidermis. *J. Invest. Dermatol.* **1985**, *85* (4), 295-298.
19. Burdett, I. D., Aspects of the structure and assembly of desmosomes. *Micron* **1998**, *29* (4), 309-28.
20. Fuchs, E.; Raghavan, S., Getting under the skin of epidermal morphogenesis. *Nat. Rev. Genet.* **2002**, *3* (3), 199-209.

21. Harding, C. R.; Scott, I. R., Histidine-rich proteins (filaggrins): structural and functional heterogeneity during epidermal differentiation. *J. Mol. Biol.* **1983**, *170* (3), 651-73.
22. Steven, A. C.; Steinert, P. M., Protein composition of cornified cell envelopes of epidermal keratinocytes. *J. Cell. Sci.* **1994**, *107* (Pt 2), 693-700.
23. Simon, M.; Haftek, M.; Sebbag, M.; Montézin, M.; Girbal-Neuhausser, E.; Schmitt, D.; Serre, G., Evidence that filaggrin is a component of cornified cell envelopes in human plantar epidermis. *Biochem. J.* **1996**, *317* (Pt 1) (Pt 1), 173-7.
24. Elias, P. M.; McNutt, N. S.; Friend, D. S., Membrane alterations during cornification of mammalian squamous epithelia: a freeze-fracture, tracer, and thin-section study. *Anat. Rec.* **1977**, *189* (4), 577-94.
25. Wertz, P. W.; Downing, D. T.; Freinkel, R. K.; Traczyk, T. N., Sphingolipids of the stratum corneum and lamellar granules of fetal rat epidermis. *J. Invest. Dermatol.* **1984**, *83* (3), 193-195.
26. Fartasch, M.; Bassukas, I. D.; Diepgen, T. L., Structural Relationship between Epidermal Lipid Lamellae, Lamellar Bodies and Desmosomes in Human Epidermis - an Ultrastructural-Study. *Br. J. Dermatol.* **1993**, *128* (1), 1-9.
27. Menon, G. K.; Feingold, K. R.; Elias, P. M., Lamellar Body Secretory Response to Barrier Disruption. *J. Invest. Dermatol.* **1992**, *98* (3), 279-289.
28. Swartzendruber, D. C.; Wertz, P. W.; Madison, K. C.; Downing, D. T., Evidence That the Corneocyte Has a Chemically Bound Lipid Envelope. *J. Invest. Dermatol.* **1987**, *88* (6), 709-713.
29. Wertz, P. W.; Downing, D. T., Covalently bound ω -hydroxyacylsphingosine in the stratum corneum. *Biochim. Biophys. Acta* **1987**, *917* (1), 108-111.
30. Wertz, P. W.; Swartzendruber, D. C.; Kitko, D. J.; Madison, K. C.; Downing, D. T., The Role of the Corneocyte Lipid Envelopes in Cohesion of the Stratum Corneum. *J. Invest. Dermatol.* **1989**, *93* (1), 169-172.
31. Wertz, P. W.; Madison, K. C.; Downing, D. T., Covalently Bound Lipids of Human Stratum Corneum. *J. Invest. Dermatol.* **1989**, *92* (1), 109-111.
32. Crumrine, D.; Khnykin, D.; Krieg, P.; Man, M.-Q.; Celli, A.; Mauro, T. M.; Wakefield, J. S.; Menon, G.; Mauldin, E.; Miner, J. H.; Lin, M.-H.; Brash, A. R.; Sprecher, E.; Radner, F. P. W.; Choate, K.; Roop, D.; Uchida, Y.; Gruber, R.; Schmuth, M.; Elias, P. M., Mutations in Recessive Congenital Ichthyoses Illuminate the Origin and Functions of the Corneocyte Lipid Envelope. *J. Invest. Dermatol.* **2019**, *139* (4), 760-768.
33. Holbrook, K. A.; Odland, G. F., Regional Differences in the Thickness (Cell Layers) of the Human Stratum Corneum: An Ultrastructural Analysis. *J. Invest. Dermatol.* **1974**, *62* (4), 415-422.
34. Elias, P. M., Epidermal lipids, membranes, and keratinization. *Int. J. Dermatol.* **1981**, *20* (1), 1-19.
35. Bodde, H. E.; Kruithof, M. A. M.; Brussee, J.; Koerten, H. K., Visualization of normal and enhanced HgCl₂ transport through human-skin invitro. *Int. J. Pharm.* **1989**, *53* (1), 13-24.
36. Talreja, P. S.; Kleene, N. K.; Pickens, W. L.; Wang, T. F.; Kasting, G. B., Visualization of the lipid barrier and measurement of lipid pathlength in human stratum corneum. *AAPS Pharmsci.* **2001**, *3* (2), art. no. 13.
37. Johnson, M. E.; Blankschtein, D.; Langer, R., Evaluation of Solute Permeation through the Stratum Corneum: Lateral Bilayer Diffusion as the Primary Transport Mechanism. *J. Pharm. Sci.* **1997**, *86* (10), 1162-1172.
38. Feingold, K. R., Thematic review series: skin lipids. The role of epidermal lipids in cutaneous permeability barrier homeostasis. *J. Lipid Res.* **2007**, *48* (12), 2531-46.
39. Onken, H. D.; Moyer, C. A., The water barrier in human epidermis. Physical and chemical nature. *Arch. Dermatol.* **1963**, *87*, 584-90.

40. Sweeney, T. M.; Downing, D. T., The role of lipids in the epidermal barrier to water diffusion. *J. Invest. Dermatol.* **1970**, *55* (2), 135-40.
41. Grubauer, G.; Feingold, K. R.; Harris, R. M.; Elias, P. M., Lipid-Content and Lipid Type as Determinants of the Epidermal Permeability Barrier. *J. Lipid Res.* **1989**, *30* (1), 89-96.
42. Gray, G. M.; Yardley, H. J., Lipid compositions of cells isolated from pig, human, and rat epidermis. *J. Lipid Res.* **1975**, *16* (6), 434-440.
43. Weerheim, A.; Ponc, M., Determination of stratum corneum lipid profile by tape stripping in combination with high-performance thin-layer chromatography. *Arch. Dermatol. Res.* **2001**, *293* (4), 191-199.
44. Wertz, P.W.; van den Bergh, B., The physical, chemical and functional properties of lipids in the skin and other biological barriers. *Chem. Phys. Lipids* **1998**, *91* (2), 85-96.
45. Mao-Qiang, M.; Feingold, K. R.; Thornfeldt, C. R.; Elias, P. M., Optimization of Physiological Lipid Mixtures for Barrier Repair. *J. Investig Dermatol.* **1996**, *106* (5), 1096-1101.
46. Elias, P. M.; Williams, M. L.; Maloney, M. E.; Bonifas, J. A.; Brown, B. E.; Grayson, S.; Epstein, E. H., Jr., Stratum corneum lipids in disorders of cornification. Steroid sulfatase and cholesterol sulfate in normal desquamation and the pathogenesis of recessive X-linked ichthyosis. *J. clin. investig.* **1984**, *74* (4), 1414-21.
47. Wertz, P.W.; Downing D.T., *Physiology, biochemistry and molecular biology of the skin.* second ed.; Oxford University Press: New York, 1991; Vol. 1, p 205-236.
48. Norlen, L.; Nicander, I.; Lundsjo, A.; Cronholm, T.; Forslind, B., A new HPLC-based method for the quantitative analysis of inner stratum corneum lipids with special reference to the free fatty acid fraction. *Arch. Dermatol. Res.* **1998**, *290* (9), 508-16.
49. Farwanah, H.; Wohlrab, J.; Neubert, R. H.; Raith, K., Profiling of human stratum corneum ceramides by means of normal phase LC/APCI-MS. *Anal. Bioanal. Chem.* **2005**, *383* (4), 632-7.
50. Masukawa, Y.; Narita, H.; Shimizu, E.; Kondo, N.; Sugai, Y.; Oba, T.; Homma, R.; Ishikawa, J.; Takagi, Y.; Kitahara, T.; Takema, Y.; Kita, K., Characterization of overall ceramide species in human Stratum corneum. *J. Lipid Res.* **2008**, *49* (7), 1466-1476.
51. Rabionet, M.; Bayerle, A.; Marsching, C.; Jennemann, R.; Gröne, H.-J.; Yildiz, Y.; Wachten, D.; Shaw, W.; Shayman, J. A.; Sandhoff, R., 1-O-acylceramides are natural components of human and mouse epidermis. *J. Lipid Res.* **2013**, *54* (12), 3312-3321.
52. Robson, K. J.; Stewart, M. E.; Michelsen, S.; Lazo, N. D.; Downing, D. T., 6-Hydroxy-4-sphingenine in human epidermal ceramides. *J. Lipid Res.* **1994**, *35* (11), 2060-8.
53. Stewart, M. E.; Downing, D. T., A new 6-hydroxy-4-sphingenine-containing ceramide in human skin. *J. Lipid Res.* **1999**, *40* (8), 1434-9.
54. van Smeden, J.; Hoppel, L.; van der Heijden, R.; Hankemeier, T.; Vreeken, R. J.; Bouwstra, J. A., LC/MS analysis of stratum corneum lipids: ceramide profiling and discovery. *J. Lipid Res.* **2011**, *52* (6), 1211-21.
55. Rabionet, M.; Gorgas, K.; Sandhoff, R., Ceramide synthesis in the epidermis. *Biochim. Biophys. Acta* **2014**, *1841* (3), 422-34.
56. Wertz, P.W.; Miethke, M. C.; Long, S. A.; Strauss, J. S.; Downing, D. T., The Composition of the ceramides from human stratum-corneum and from comedones. *J. Invest. Dermatol.* **1985**, *84* (5), 410-412.
57. van Smeden, J.; Bouwstra, J. A., Stratum corneum lipids: Their role for the skin barrier function in healthy subjects and atopic dermatitis patients. *Curr. Probl. Dermatol.* **2016**, *49*, 8-26.
58. t'Kindt, R.; Jorge, L.; Dumont, E.; Couturon, P.; David, F.; Sandra, P.; Sandra, K., Profiling and characterizing skin ceramides using reversed-phase liquid chromatography-quadrupole time-of-flight mass spectrometry. *Anal. Chem.* **2012**, *84* (1), 403-411.

59. Ponec, M.; Weerheim, A.; Lankhorst, P.; Wertz, P., New Acylceramide in Native and Reconstructed Epidermis. *J. Invest. Dermatol.* **2003**, *120* (4), 581-588.
60. Boiten, W.; Absalah, S.; Vreeken, R.; Bouwstra, J.; van Smeden, J., Quantitative analysis of ceramides using a novel lipidomics approach with three dimensional response modelling. *Biochimica et Biophysica Acta* **2016**, *1861* (11), 1652-1661.
61. Motta, S.; Monti, M.; Sesana, S.; Caputo, R.; Carelli, S.; Ghidoni, R., Ceramide composition of the psoriatic scale. *Biochim. Biophys. Acta* **1993**, *1182* (2), 147-51.
62. Uchida, Y., The role of fatty acid elongation in epidermal structure and function. *Dermatoendocrinol* **2011**, *3* (2), 65-9.
63. Mizutani, Y.; Mitsutake, S.; Tsuji, K.; Kihara, A.; Igarashi, Y., Ceramide biosynthesis in keratinocyte and its role in skin function. *Biochimie* **2009**, *91* (6), 784-90.
64. Mizutani, Y.; Kihara, A.; Chiba, H.; Tojo, H.; Igarashi, Y., 2-Hydroxy-ceramide synthesis by ceramide synthase family: enzymatic basis for the preference of FA chain length. *J. Lipid Res.* **2008**, *49* (11), 2356-2364.
65. Breathnach, A. S.; Goodman, T.; Stolinski, C.; Gross, M., Freeze-fracture replication of cells of stratum corneum of human epidermis. *J. Anat.* **1973**, *114* (Pt 1), 65-81.
66. Elias, P. M.; Friend, D. S., The permeability barrier in mammalian epidermis. *J. Cell. Biol.* **1975**, *65* (1), 180-91.
67. Madison, K. C.; Swartzendruber, D. C.; Wertz, P. W.; Downing, D. T., Presence of intact intercellular lipid lamellae in the upper layers of the stratum corneum. *J. Invest. Dermatol.* **1987**, *88* (6), 714-8.
68. Swartzendruber, D. C.; Wertz, P. W.; Kitko, D. J.; Madison, K. C.; Downing, D. T., Molecular models of the intercellular lipid lamellae in mammalian stratum corneum. *J. Invest. Dermatol.* **1989**, *92* (2), 251-7.
69. Bouwstra, J. A.; Gooris, G. S.; Bras, W.; Downing, D. T., Lipid organization in pig stratum-corneum. *J. Lipid Res.* **1995**, *36* (4), 685-695.
70. Hill, J. R.; Wertz, P. W., Molecular models of the intercellular lipid lamellae from epidermal stratum corneum. *Biochim. Biophys. Acta* **2003**, *1616* (2), 121-6.
71. White, S. H.; Mirejovsky, D.; King, G. I., Structure of lamellar lipid domains and corneocyte envelopes of murine stratum corneum. An X-ray diffraction study. *Biochemistry* **1988**, *27* (10), 3725-32.
72. McIntosh, T. J.; Stewart, M. E.; Downing, D. T., X-ray diffraction analysis of isolated skin lipids: reconstitution of intercellular lipid domains. *Biochemistry* **1996**, *35* (12), 3649-53.
73. de Jager, M.; Groenink, W.; Bielsa i Guivernau, R.; Andersson, E.; Angelova, N.; Ponec, M.; Bouwstra, J., A novel in vitro percutaneous penetration model: evaluation of barrier properties with p-aminobenzoic acid and two of its derivatives. *Pharm. Res.* **2006**, *23* (5), 951-60.
74. Groen, D.; Poole, D. S.; Gooris, G. S.; Bouwstra, J. A., Is an orthorhombic lateral packing and a proper lamellar organization important for the skin barrier function? *Biochim. Biophys. Acta* **2011**, *1808* (6), 1529-1537.
75. Bouwstra, J.; Gooris, G.; Ponec, M., The lipid organisation of the skin barrier: liquid and crystalline domains coexist in lamellar phases. *J. biol. phys.* **2002**, *28* (2), 211-23.
76. Mendelsohn, R.; Flach, C. R.; Moore, D. J., Determination of molecular conformation and permeation in skin via IR spectroscopy, microscopy, and imaging. *Biochim. Biophys. Acta* **2006**, *1758* (7), 923-933.
77. Boncheva, M.; Damien, F.; Normand, V., Molecular organization of the lipid matrix in intact stratum corneum using ATR-FTIR spectroscopy. *Biochim. Biophys. Acta* **2008**, *1778* (5), 1344-55.

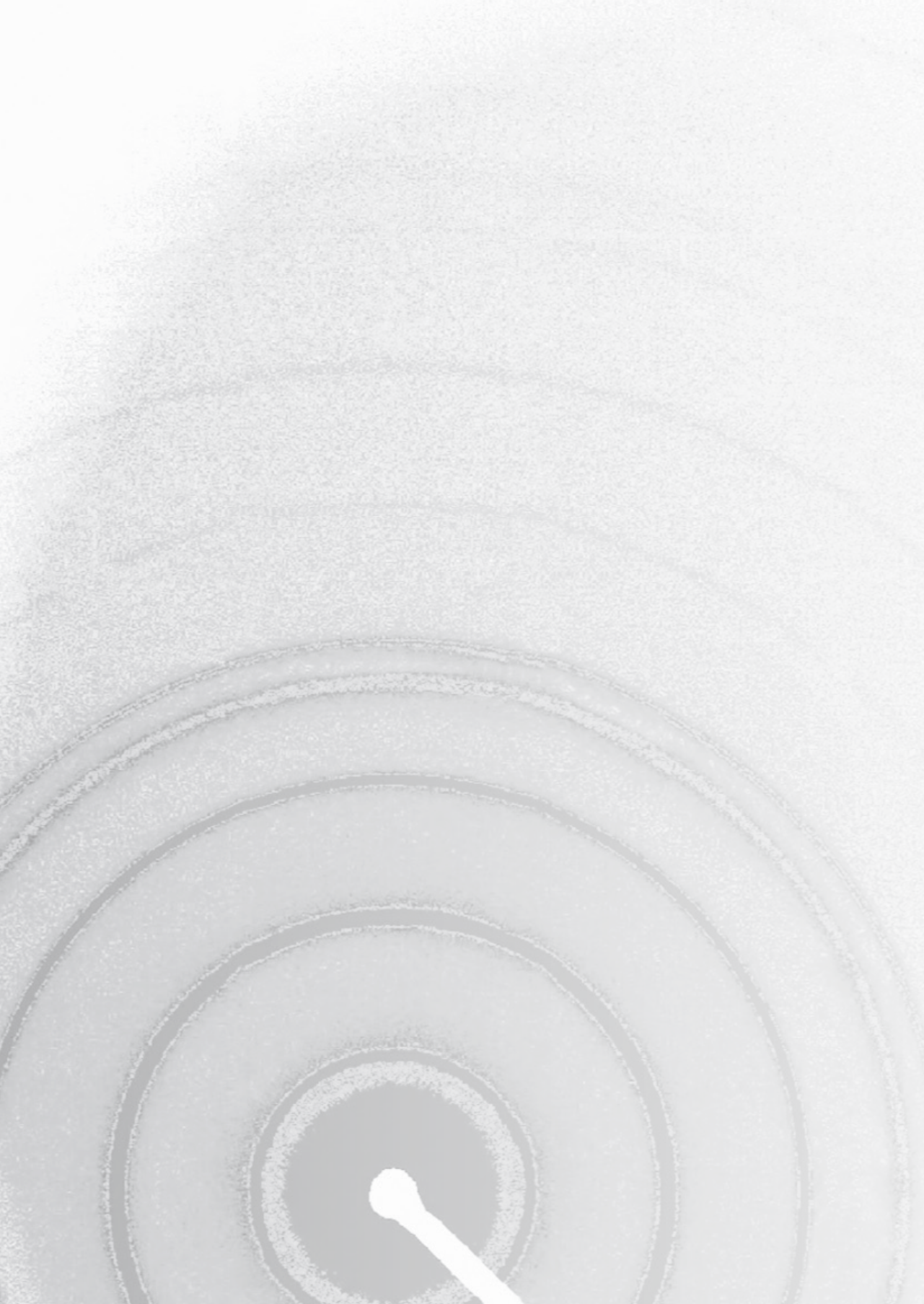
78. Damien, F.; Boncheva, M., The extent of orthorhombic lipid phases in the stratum corneum determines the barrier efficiency of human skin in vivo. *J. Invest. Dermatol.* **2010**, *130* (2), 611-614.
79. Bouwstra, J. A.; Dubbelaar, F. E.; Gooris, G. S.; Ponc, M., The lipid organisation in the skin barrier. *Acta Derm-Venerol.* **2000**, *208*, 23-30.
80. Jensen, J. M.; Folster-Holst, R.; Baranowsky, A.; Schunck, M.; Winoto-Morbach, S.; Neumann, C.; Schutze, S.; Proksch, E., Impaired sphingomyelinase activity and epidermal differentiation in atopic dermatitis. *J. Invest. Dermatol.* **2004**, *122* (6), 1423-31.
81. Jakasa, I.; Koster, E. S.; Calkoen, F.; Irwin McLean, W. H.; Campbell, L. E.; Bos, J. D.; Verberk, M. M.; Kezic, S., Skin Barrier Function in Healthy Subjects and Patients with Atopic Dermatitis in Relation to Filaggrin Loss-of-Function Mutations. *J. Invest. Dermatol.* **2011**, *131* (2), 540-542.
82. Motta, S.; Monti, M.; Sesana, S.; Mellesi, L.; Ghidoni, R.; Caputo, R., Abnormality of water barrier function in psoriasis. Role of ceramide fractions. *Arch. Dermatol.* **1994**, *130* (4), 452-6.
83. van Smeden, J.; Janssens, M.; Boiten, W. A.; van Drongelen, V.; Furio, L.; Vreeken, R. J.; Hovnanian, A.; Bouwstra, J. A., Intercellular skin barrier lipid composition, and organization in Netherton syndrome patients. *J. Invest. Dermatol.* **2014**, *134* (5), 1238-1245.
84. Eckl, K. M.; Tidhar, R.; Thiele, H.; Oji, V.; Hausser, I.; Brodesser, S.; Preil, M.; Önal-Akan, A.; Stock, F.; Müller, D., Impaired Epidermal Ceramide Synthesis Causes Autosomal Recessive Congenital Ichthyosis and Reveals the Importance of Ceramide Acyl Chain Length. *J. Invest. Dermatol.* **2013**, *133* (9), 2202-2211.
85. van Smeden, J.; Janssens, M.; Gooris, G. S.; Bouwstra, J. A., The important role of stratum corneum lipids for the cutaneous barrier function. *Biochim. Biophys. Acta* **2014**, *1841* (3), 295-313.
86. Bitoun, E.; Chavanas, S.; Irvine, A. D.; Lonie, L.; Bodemer, C.; Paradisi, M.; Hamel-Teillac, D.; Ansai, S.; Mitsuhashi, Y.; Taïeb, A.; de Prost, Y.; Zambruno, G.; Harper, J. I.; Hovnanian, A., Netherton syndrome: disease expression and spectrum of SPINK5 mutations in 21 families. *J. Invest. Dermatol.* **2002**, *118* (2), 352-61.
87. Chavanas, S.; Bodemer, C.; Rochat, A.; Hamel-Teillac, D.; Ali, M.; Irvine, A. D.; Bonafé, J.-L.; Wilkinson, J.; Taïeb, A.; Barrandon, Y.; Harper, J. I.; de Prost, Y.; Hovnanian, A., Mutations in SPINK5, encoding a serine protease inhibitor, cause Netherton syndrome. *Nat. Genet.* **2000**, *25* (2), 141-142.
88. van Smeden, J.; Al-Khakany, H.; Wang, Y.; Visscher, D.; Stephens, N.; Absalah, S.; Overkleeft, H. S.; Aerts, J.; Hovnanian, A.; Bouwstra, J. A., Skin barrier lipid enzyme activity in Netherton patients is associated with protease activity and ceramide abnormalities. *J. Lipid. Res.* **2020**, *61* (6), 859-869.
89. Radner, F. P.; Marrakchi, S.; Kirchmeier, P.; Kim, G. J.; Ribierre, F.; Kamoun, B.; Abid, L.; Leipoldt, M.; Turki, H.; Schempp, W.; Heilig, R.; Lathrop, M.; Fischer, J., Mutations in CERS3 cause autosomal recessive congenital ichthyosis in humans. *PLoS genetics* **2013**, *9* (6), e1003536.
90. Meguro, S.; Arai, Y.; Masukawa, Y.; Uie, K.; Tokimitsu, I., Relationship between covalently bound ceramides and transepidermal water loss (TEWL). *Arch. Dermatol. Res.* **2000**, *292* (9), 463-8.
91. Behne, M.; Uchida, Y.; Seki, T.; de Montellano, P. O.; Elias, P. M.; Holleran, W. M., Omega-hydroxyceramides are required for corneocyte lipid envelope (CLE) formation and normal epidermal permeability barrier function. *J. Invest. Dermatol.* **2000**, *114* (1), 185-92.

92. Jennemann, R.; Rabionet, M.; Gorgas, K.; Epstein, S.; Dalpke, A.; Rothermel, U.; Bayerle, A.; van der Hoeven, F.; Imgrund, S.; Kirsch, J.; Nickel, W.; Willecke, K.; Riezman, H.; Gröne, H. J.; Sandhoff, R., Loss of ceramide synthase 3 causes lethal skin barrier disruption. *Hum. mol. genet.* **2012**, *21* (3), 586-608.
93. Jobard, F.; Lefèvre, C.; Karaduman, A.; Blanchet-Bardon, C.; Emre, S.; Weissenbach, J.; Ozgüc, M.; Lathrop, M.; Prud'homme, J. F.; Fischer, J., Lipoxygenase-3 (ALOXE3) and 12(R)-lipoxygenase (ALOX12B) are mutated in non-bullous congenital ichthyosiform erythroderma (NCIE) linked to chromosome 17p13.1. *Hum. mol. genet.* **2002**, *11* (1), 107-13.
94. Akiyama, M., Corneocyte lipid envelope (CLE), the key structure for skin barrier function and ichthyosis pathogenesis. *J. Dermatol. Sci.* **2017**, *88* (1), 3-9.
95. Epp, N.; Fürstenberger, G.; Müller, K.; de Juanes, S.; Leitges, M.; Hausser, I.; Thieme, F.; Liebisch, G.; Schmitz, G.; Krieg, P., 12R-lipoxygenase deficiency disrupts epidermal barrier function. *J. Cell Biol.* **2007**, *177* (1), 173-182.
96. Motta, S.; Sesana, S.; Ghidoni, R.; Monti, M., Content of the different lipid classes in psoriatic scale. *Arch. Dermatol. Res.* **1995**, *287* (7), 691-694.
97. Proksch, E.; Folster-Holst, R.; Jensen, J. M., Skin barrier function, epidermal proliferation and differentiation in eczema. *J. Dermatol. Sci.* **2006**, *43* (3), 159-69.
98. Alanne, S.; Nermes, M.; Soderlund, R.; Laitinen, K., Quality of life in infants with atopic dermatitis and healthy infants: a follow-up from birth to 24 months. *Acta Paediatr.* **2011**, *100* (8), e65-70.
99. Su, J. C.; Kemp, A. S.; Varigos, G. A.; Nolan, T. M., Atopic eczema: its impact on the family and financial cost. *Arch. Dis. Child.* **1997**, *76* (2), 159-62.
100. Mortz, C. G.; Andersen, K. E.; Dellgren, C.; Barington, T.; Bindslev-Jensen, C., Atopic dermatitis from adolescence to adulthood in the TOACS cohort: prevalence, persistence, and comorbidities. *Allergy* **2015**, *70* (7), 836-45.
101. Sandhu, J. K.; Salame, N.; Ehsani-Chimeh, N.; Armstrong, A. W., Economic burden of cutaneous infections in children and adults with atopic dermatitis. *Pediatr. Dermatol.* **2019**, *36* (3), 303-310.
102. Lifschitz, C., The impact of atopic dermatitis on quality of life. *Ann. Nutr. Metab.* **2015**, *66* Suppl 1, 34-40.
103. Hata, M.; Tokura, Y.; Takigawa, M.; Sato, M.; Shioya, Y.; Fujikura, Y.; Imokawa, G., Assessment of epidermal barrier function by photoacoustic spectrometry in relation to its importance in the pathogenesis of atopic dermatitis. *Lab. Invest.* **2002**, *82*, 1451.
104. Williams, H. C., *Atopic Dermatitis*. Cambridge University Press: Cambridge 2000.
105. Irvine, A. D.; McLean, W. H.; Leung, D. Y., Filaggrin mutations associated with skin and allergic diseases. *N. Engl. J. Med.* **2011**, *365* (14), 1315-27.
106. O'Regan, G. M.; Sandilands, A.; McLean, W. H. I.; Irvine, A. D., Filaggrin in atopic dermatitis. *J. Allergy Clin. Immunol.* **2008**, *122* (4), 689-693.
107. Palmer, C. N.; Irvine, A. D.; Terron-Kwiatkowski, A.; Zhao, Y.; Liao, H.; Lee, S. P.; Goudie, D. R.; Sandilands, A.; Campbell, L. E.; Smith, F. J.; O'Regan, G. M.; Watson, R. M.; Cecil, J. E.; Bale, S. J.; Compton, J. G.; DiGiovanna, J. J.; Fleckman, P.; Lewis-Jones, S.; Arseculeratne, G.; Sergeant, A.; Munro, C. S.; El Houate, B.; McElreavey, K.; Halkjaer, L. B.; Bisgaard, H.; Mukhopadhyay, S.; McLean, W. H., Common loss-of-function variants of the epidermal barrier protein filaggrin are a major predisposing factor for atopic dermatitis. *Nat. Genet.* **2006**, *38* (4), 441-6.
108. Rodriguez, E.; Illig, T.; Weidinger, S., Filaggrin loss-of-function mutations and association with allergic diseases. *Pharmacogenomics* **2008**, *9* (4), 399-413.
109. Hudson, T. J., Skin barrier function and allergic risk. *Nat. Genet.* **2006**, *38* (4), 399-400.

110. McGrath, J. A., Filaggrin and the great epidermal barrier grief. *Australas J. Dermatol.* **2008**, *49* (2), 67-73; quiz 73-4.
111. Jensen, J. M.; Folster-Holst, R.; Baranowsky, A.; Schunck, M.; Winoto-Morbach, S.; Neumann, C.; Schutze, S.; Proksch, E., Impaired sphingomyelinase activity and epidermal differentiation in atopic dermatitis. *J Invest Dermatol* **2004**, *122* (6), 1423-31.
112. Boer, D. E. C.; van Smeden, J.; Al-Khakany, H.; Melnik, E.; van Dijk, R.; Absalah, S.; Vreeken, R. J.; Haenen, C. C. P.; Lavrijsen, A. P. M.; Overkleeft, H. S.; Aerts, J. M. F. G.; Bouwstra, J. A., Skin of atopic dermatitis patients shows disturbed β -glucocerebrosidase and acid sphingomyelinase activity that relates to changes in stratum corneum lipid composition. *Biochim. Biophys. Acta* **2020**, *1865* (6), 158673.
113. Hara, J.; Higuchi, K.; Okamoto, R.; Kawashima, M.; Imokawa, G., High-expression of sphingomyelin deacylase is an important determinant of ceramide deficiency leading to barrier disruption in atopic dermatitis. *J. Invest. Dermatol.* **2000**, *115* (3), 406-413.
114. Ishibashi, M.; Arikawa, J.; Okamoto, R.; Kawashima, M.; Takagi, Y.; Ohguchi, K.; Imokawa, G., Abnormal expression of the novel epidermal enzyme, glucosylceramide deacylase, and the accumulation of its enzymatic reaction product, glucosylsphingosine, in the skin of patients with atopic dermatitis. *Lab. Invest.* **2003**, *83* (3), 397-408.
115. Murata, Y.; Ogata, J.; Higaki, Y.; Kawashima, M.; Yada, Y.; Higuchi, K.; Tsuchiya, T.; Kawaminami, S.; Imokawa, G., Abnormal Expression of Sphingomyelin Acylase in Atopic Dermatitis: An Etiologic Factor for Ceramide Deficiency? *J. Invest. Dermatol.* **1996**, *106* (6), 1242-1249.
116. Oizumi, A.; Nakayama, H.; Okino, N.; Iwahara, C.; Kina, K.; Matsumoto, R.; Ogawa, H.; Takamori, K.; Ito, M.; Suga, Y.; Iwabuchi, K., Pseudomonas-derived ceramidase induces production of inflammatory mediators from human keratinocytes via sphingosine-1-phosphate. *PLoS One* **2014**, *9* (2), e89402.
117. Ishikawa, J.; Narita, H.; Kondo, N.; Hotta, M.; Takagi, Y.; Masukawa, Y.; Kitahara, T.; Takema, Y.; Koyano, S.; Yamazaki, S.; Hatamochi, A., Changes in the ceramide profile of atopic dermatitis patients. *J. Invest. Dermatol.* **2010**, *130* (10), 2511-4.
118. Janssens, M.; van Smeden, J.; Gooris, G. S.; Bras, W.; Portale, G.; Caspers, P. J.; Vreeken, R. J.; Hankemeier, T.; Kezic, S.; Wolterbeek, R.; Lavrijsen, A. P.; Bouwstra, J. A., Increase in short-chain ceramides correlates with an altered lipid organization and decreased barrier function in atopic eczema patients. *J. Lipid Res.* **2012**, *53* (12), 2755-66.
119. Janssens, M.; van Smeden, J.; Gooris, G. S.; Bras, W.; Portale, G.; Caspers, P. J.; Vreeken, R. J.; Kezic, S.; Lavrijsen, A. P.; Bouwstra, J. A., Lamellar lipid organization and ceramide composition in the stratum corneum of patients with atopic eczema. *J. Invest. Dermatol.* **2011**, *131* (10), 2136-8.
120. Di Nardo, A.; Wertz, P.; Giannetti, A.; Seidenari, S., Ceramide and cholesterol composition of the skin of patients with atopic dermatitis. *Acta Derm-Venereol.* **1998**, *78* (1), 27-30.
121. Imokawa, G.; Abe, A.; Jin, K.; Higaki, Y.; Kawashima, M.; Hidano, A., Decreased level of ceramides in stratum corneum of atopic dermatitis: an etiologic factor in atopic dry skin? *J. Invest. Dermatol.* **1991**, *96* (4), 523-6.
122. Park, Y.-H.; Jang, W.-H.; Seo, J. A.; Park, M.; Lee, T. R.; Park, Y.-H.; Kim, D. K.; Lim, K.-M., Decrease of Ceramides with Very Long-Chain Fatty Acids and Downregulation of Elongases in a Murine Atopic Dermatitis Model. *J. Investig. Dermatol.* **2012**, *132* (2), 476-479.
123. Bouwstra, J. A.; Gooris, G. S.; Cheng, K.; Weerheim, A.; Bras, W.; Ponec, M., Phase behavior of isolated skin lipids. *J. Lipid Res.* **1996**, *37* (5), 999-1011.
124. Bouwstra, J. A.; Gooris, G. S.; Dubbelaar, F. E.; Ponec, M., Phase behavior of lipid mixtures based on human ceramides: coexistence of crystalline and liquid phases. *J. Lipid Res.* **2001**, *42* (11), 1759-70.

125. Gooris, G. S.; Bouwstra, J. A., Infrared spectroscopic study of stratum corneum model membranes prepared from human ceramides, cholesterol, and fatty acids. *Biophys. J.* **2007**, *92* (8), 2785-95.
126. Caussin, J.; Gooris, G. S.; Janssens, M.; Bouwstra, J. A., Lipid organization in human and porcine stratum corneum differs widely, while lipid mixtures with porcine ceramides model human stratum corneum lipid organization very closely. *Biochim. Biophys. Acta* **2008**, *1778* (6), 1472-1482.
127. Bouwstra, J. A.; Gooris, G. S.; Dubbelaar, F. E.; Weerheim, A. M.; Ponec, M., pH, cholesterol sulfate, and fatty acids affect the stratum corneum lipid organization. *J. Investig. Dermatol. Symp. Proc.* **1998**, *3* (2), 69-74.
128. de Jager, M. W.; Gooris, G. S.; Dolbnya, I. P.; Bras, W.; Ponec, M.; Bouwstra, J. A., Novel lipid mixtures based on synthetic ceramides reproduce the unique stratum corneum lipid organization. *J. Lipid Res.* **2004**, *45* (5), 923-32.
129. de Jager, M. W.; Gooris, G. S.; Ponec, M.; Bouwstra, J. A., Lipid mixtures prepared with well-defined synthetic ceramides closely mimic the unique stratum corneum lipid phase behavior. *J. Lipid Res.* **2005**, *46* (12), 2649-2656.
130. Mojumdar, E. H.; Gooris, G. S.; Bouwstra, J. A., Phase behavior of skin lipid mixtures: the effect of cholesterol on lipid organization. *Soft Matter* **2015**, *11* (21), 4326-4336.
131. Mojumdar, E. H.; Helder, R. W.; Gooris, G. S.; Bouwstra, J. A., Monounsaturated fatty acids reduce the barrier of stratum corneum lipid membranes by enhancing the formation of a hexagonal lateral packing. *Langmuir* **2014**, *30* (22), 6534-43.
132. Bouwstra, J. A.; Gooris, G. S.; Dubbelaar, F. E.; Ponec, M., Phase behavior of stratum corneum lipid mixtures based on human ceramides: the role of natural and synthetic ceramide 1. *J. Invest. Dermatol.* **2002**, *118* (4), 606-17.
133. de Sousa Neto, D.; Gooris, G.; Bouwstra, J., Effect of the omega-acylceramides on the lipid organization of stratum corneum model membranes evaluated by X-ray diffraction and FTIR studies (Part I). *Chem. Phys. Lipids* **2011**, *164* (3), 184-95.
134. Opalka, L.; Kovacik, A.; Maixner, J.; Vavrova, K., Omega-O-Acylceramides in skin lipid membranes: effects of concentration, sphingoid base, and model complexity on microstructure and permeability. *Langmuir* **2016**, *32* (48), 12894-12904.
135. Moore, D. J.; Rerek, M. E.; Mendelsohn, R., Lipid domains and orthorhombic phases in model stratum corneum: evidence from Fourier transform infrared spectroscopy studies. *Biochem. Biophys. Res. Co.* **1997**, *231* (3), 797-801.
136. Velkova, V.; Lafleur, M., Influence of the lipid composition on the organization of skin lipid model mixtures: An infrared spectroscopy investigation. *Chem. Phys. Lipids* **2002**, *117* (1), 63-74.
137. Moore, D. J.; Rerek, M. E., Insights into the molecular organization of lipids in the skin barrier from infrared spectroscopy studies of stratum corneum lipid models. *Acta Derm-Venereol.* **2000**, 16-22.
138. Skolova, B.; Kovacik, A.; Tesar, O.; Opalka, L.; Vavrova, K., Phytosphingosine, sphingosine and dihydrosphingosine ceramides in model skin lipid membranes: permeability and biophysics. *Biochim. Biophys. Acta* **2017**, *1859* (5), 824-834.
139. Skolova, B.; Jandovska, K.; Pullmannova, P.; Tesar, O.; Roh, J.; Hrabalek, A.; Vavrova, K., The role of the trans double bond in skin barrier sphingolipids: permeability and infrared spectroscopic study of model ceramide and dihydroceramide membranes. *Langmuir* **2014**, *30* (19), 5527-35.
140. Groen, D.; Poole, D. S.; Gooris, G. S.; Bouwstra, J. A., Investigating the barrier function of skin lipid models with varying compositions. *Eur. J. Pharm. Biopharm.* **2011**, *79* (2), 334-342.
141. Basse, L. H.; Groen, D.; Bouwstra, J. A., Permeability and lipid organization of a novel psoriasis stratum corneum substitute. *Int. J. Pharm.* **2013**, *457* (1), 275-282.

142. Groen, D.; Gooris, G. S.; Bouwstra, J. A., New insights into the stratum corneum lipid organization by X-ray diffraction analysis. *Biophys. J.* **2009**, *97* (8), 2242-2249.
143. T'Kindt, R.; Jorge, L.; Dumont, E.; Couturon, P.; David, F.; Sandra, P.; Sandra, K., Profiling and Characterizing Skin Ceramides Using Reversed-Phase Liquid Chromatography–Quadrupole Time-Of-Flight Mass Spectrometry. *Anal. Chem.* **2012**, *84*, 403.
144. Gooris, G. S.; Kamran, M.; Kros, A.; Moore, D. J.; Bouwstra, J. A., Interactions of dipalmitoylphosphatidylcholine with ceramide-based mixtures. *Biochim. Biophys. Acta* **2018**, *1860* (6), 1272-1281.
145. Mojumdar, E. H.; Gooris, G. S.; Groen, D.; Barlow, D. J.; Lawrence, M. J.; Deme, B.; Bouwstra, J. A., Stratum corneum lipid matrix: Location of acyl ceramide and cholesterol in the unit cell of the long periodicity phase. *Biochim. Biophys. Acta* **2016**, *1858* (8), 1926-34.



2

Barrier capability of skin lipid models: Effect of ceramides and free fatty acid composition

2

Authors and affiliations:

Lorretta.E. Uche¹, Gerrit.S. Gooris¹, Joke.A. Bouwstra¹ and Charlotte.M. Beddoes¹

¹Division of Drug Delivery Technology, Cluster BioTherapeutics, Leiden Academic Centre for Drug Research, Leiden University, Netherlands

Adapted from: Langmuir, 2019. 35(47): p. 15376-15388.

ABSTRACT

The skin is an effective barrier that prevents the influx of harmful substances from the environment and the efflux of body fluid. This barrier function is ascribed to the intercellular lipids present in the outermost layer of the skin referred to as the stratum corneum (SC). These lipids are composed mainly of ceramides (CERs), cholesterol, and free fatty acids (FFAs). Alterations in the SC lipid composition and barrier function impairment occur in several skin diseases including atopic dermatitis (AD). As the etiology of AD is multifactorial, establishing the relationship between the changes in SC lipid composition and barrier function impairment in the patients remains a challenge. Here, we employed model membrane systems to investigate the contribution of various anomalies in the SC CER and FFA composition observed in AD patients' skin to the barrier dysfunction. Using ethyl-p-aminobenzoate permeation and transepidermal water loss values as markers for barrier function, we determined that the alterations in SC lipid composition contribute to the impaired barrier function in AD patients. By the use of biophysical techniques, we established that the largest reduction in barrier capability was observed in the model with an increased fraction of short-chain FFAs, evident by the decrease in chain packing density. Modulations in the CER subclass composition impacted the lamellar organization while having a smaller effect on the barrier function. These findings provide evidence that AD therapies normalizing the FFA composition are at least as important as normalizing CER composition.

Keywords

Atopic dermatitis; Ceramide; Free fatty acids; Infrared spectroscopy; Permeability; Stratum corneum; X-ray scattering.

INTRODUCTION

Lipids can act as structural components for cell membranes but are also important for signaling and energy storage [1-6]. In most viable cell membranes the most important components are phospholipids, sphingolipids, and cholesterol (CHOL). A special group of sphingolipids is the ceramides (CERs). In the outermost layer of the epidermis, the stratum corneum (SC), these CERs together with cholesterol and free fatty acids (FFAs) are the most important components of the lipid matrix, a structure that is crucial in maintaining the skin barrier function [7]. A major difference between the SC lipid composition and other biological membranes is that the former is basically devoid of phospholipids. The SC lipid matrix surrounds the individual keratin-filled terminally differentiated cells, the corneocytes. The SC structure has been described as being analogous to bricks and mortar structure, the corneocyte being the bricks and the intercellular lipids the mortar [8]. X-ray diffraction studies have revealed that the intercellular lipids are assembled in two co-existing lamellar phases with periodicities of ~13 nm and ~6 nm known as the long and short periodicity phases (LPP and SPP) respectively [9, 10]. Within the lamellae, the majority of the SC lipids preferably adopt a dense orthorhombic lateral packing at skin temperature (30-32 °C), while a portion of the lipids adopts the less dense hexagonal packing [11, 12]. This is distinctive from most biological cell membranes, which often form a liquid (ordered) phase. The ordered lipid packing in SC is induced by; i) the FFAs with predominantly saturated chains, with carbon chain lengths ranging between 12 and 30, the majority of the FFA having a chain length of 22, 24, or 26 carbon atoms [13, 14] and ii) the CERs with a small head group and long hydrocarbon tails. The CERs can vary in the headgroup structure and chain length. Currently, at least 18 subclasses of CERs have been identified in the human SC [15-17]. The commonly adopted nomenclature for CER is based on Motta et al [18], in which the CERs are designated with 2-3 letters, defining the type of sphingoid base and linked fatty acid acyl chain (Figure 1).

Alterations in the SC lipid composition has been reported in one of the most prevalent, chronic inflammatory skin disease referred to as atopic dermatitis (AD). In industrialized nations, the incidence of AD has increased to about 15-30% in children and 2-10% in adults [19]. The etiology of AD is multifactorial, involving the interaction of immunological, genetic, and environmental factors [20]. A compromised skin barrier, indicated by increased water transport across the SC, is characteristic of patients with AD [21, 22]. Several studies have reported that the reduced skin barrier function is associated with changes in lipid composition. The following changes in lipid composition were described

in AD patients' skin compared to healthy skin: i) a reduction in the levels of CER NP, CER NH, CER EO classes, while CER NS and AS were increased [23-26], ii) a reduction in chain length of FFAs [27] and CERs, specifically increased level of CERs AS and NS (C16) with a total chain length of 34 carbon atoms [23, 26]. As these changes in lipid composition occur simultaneously [21, 28, 29], it is not yet established which of them is the underlying factor of the impaired skin barrier.

In the current study, we investigated in a systematic way, which changes in SC lipid composition reported in AD patients, resulted in the most dramatic changes in the lipid organization, thereby possibly increasing the lipid barrier dysfunctionality. Healthy skin model based on the SC lipid composition and diseased skin models that mimicked different aspects of the altered lipid composition in atopic dermatitis patients' skin was developed. We showed that an increased level of short-chain FFAs resulted in a more drastic reduction in barrier function than compositional changes of the CERs. Knowledge from this study could aid in design of rational therapy for the treatment of inflammatory skin diseases in which compositional changes in SC lipids are implicated.

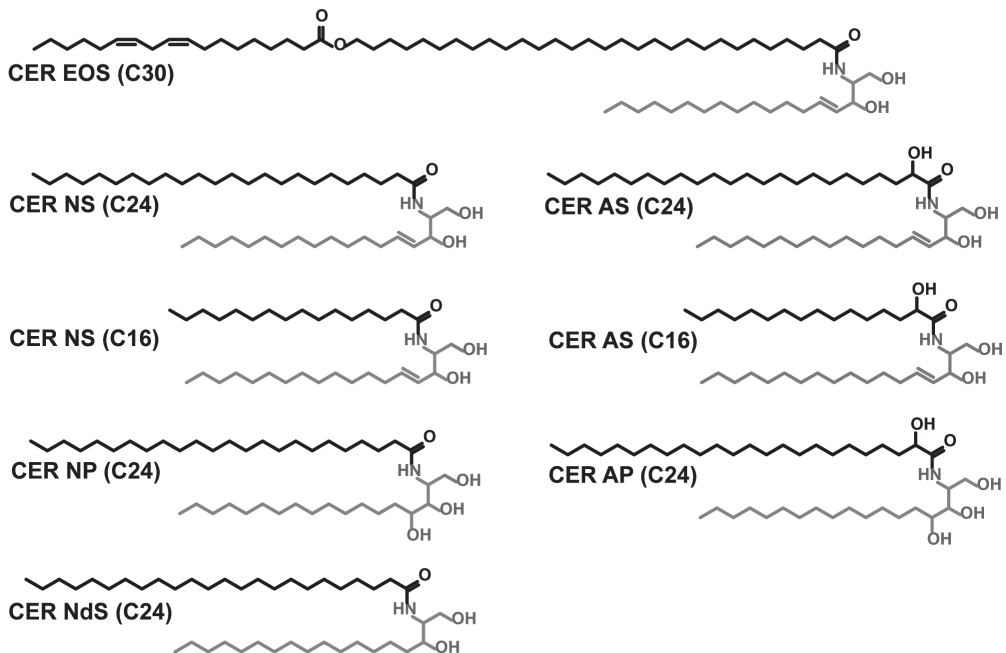


Figure 1: Molecular structure of the CERs used in the study.

CERs consist of a sphingoid base (marked in grey) linked to a fatty acid acyl chain (marked in black) via an amide bond. The fatty acid acyl chain is either non-hydroxylated [N], α -hydroxylated [A], or ω -esterified [EO], while the sphingoid base is either sphingosine [S] or phytosphingosine [P].

EXPERIMENTAL SECTION

Materials

The synthetic CERs: N-(tetracosanoyl)-sphingosine (CER NS), N-(tetracosanoyl)-phytosphingosine (CER NP), N-(2R-hydroxy-tetracosanoyl)-sphingosine (CER AS), N-(2R-hydroxy-tetracosanoyl)-phytosphingosine (CER AP) of acyl carbon chain length C24 and N-(30-Linoleoyloxy-triacontanoyl)-sphingosine (EOS C30) used in this study were generously donated by Evonik (Essen, Germany). CERs NS and AS C16 and N-(tetracosanoyl)-dihydrosphingosine (CER NdS C24) were purchased from Avanti. The CERs were of $\geq 90\%$ purity. The FFAs, ethyl-p-aminobenzoate (E-PABA), CHOL and acetate buffer salts were acquired from Sigma- Aldrich Chemie GmbH (Schnelldorf, Germany). The perdeuterated FFAs (DFFAs) with chain lengths of C18 and C20 were obtained from Cambridge Isotope Laboratories (Andover, Massachusetts). The DFFAs with chain lengths of C16 and C22 were purchased from Larodan (Malmö, Sweden). The DFFA with a chain length of C24 was obtained from Arc Laboratories B.V. (Apeldoorn, The Netherlands). All organic solvents were procured from Labscan Ltd. (Dublin, Ireland). All other reagents were of analytical grade and used without further purification. The water was of Millipore quality, obtained through a Milli-Q Integral Water Purification System (Millipore, Bedford, MA). Nucleopore polycarbonate filter disks (pore size 0.05 μm) were acquired from Whatman (Kent, UK).

Isolation of SC from native skin

SC was isolated from abdominal or mammary skin, which was obtained within 24 h after cosmetic surgery. The skin surface was first cleaned with 70% ethanol and Milli-Q water thereafter. The skin was dermatomed to a thickness of ~ 0.6 mm. The SC was separated from the epidermis by trypsin digestion; 0.1% in phosphate-buffered saline (PBS 0.1 M solution: NaCl, Na_2HPO_4 , KH_2PO_4 , and KCl in milli-Q water with a concentration of 8.13, 1.14, 0.20 and 0.19 g/l respectively at pH 7.4), after overnight incubation at 4 °C and subsequently at 37 °C for 1 h. The SC was then placed in a 0.1% solution of trypsin inhibitor, rinsed twice with Milli-Q water, and allowed to dry. The SC was stored in a silica-containing, opaque, sealed box, under nitrogen in order to prevent oxidation of the intercellular SC lipids. The isolated native SC was subsequently used in diffusion studies.

Preparation of the model lipid mixtures

Five SC lipid models (healthy and diseased skin) were prepared as equimolar mixtures of CER, CHOL, and FFAs. The lipid composition of the healthy skin

model (denoted as Healthy) was based on the native SC lipid composition [15, 30]. The most prevalent CERs in human skin were included in the model, except for CERs comprised of 6-hydroxy sphingoid bases that were not available. As CER EOS constitutes over 50% of the total CER EO class present in the human CER [15], it represented the CER EO in the healthy skin model. To prepare the diseased skin models, the lipid composition of the healthy skin model was adjusted, to mimic various aberrations reported in the skin of AD patients. The changes made are; i) replacing a fraction of CER NS (C24) and CER AS (C24) with by CER NS (C16) and CER AS (C16) respectively, denoted as Dis-CER_{ch}; ii) besides the presence of CERs NS and AS (C16), a reduction of the level of CER EOS and NP subclasses was included, counterbalanced by an increase in the levels of CER NS and AS subclasses, referred to as Dis-CER_{ch-SbC}; iii) increased fraction of short-chain FFAs referred to as Dis-FFA_{ch} and iv) Combination of all the changes in CERs & FFAs referred to as Dis-Combi. The CERs and FFAs composition of the models are presented in Tables 1 and 2 respectively. Additional models were prepared in which FFAs were replaced by their deuterated counterparts. The resulting models are denoted by D- before the model name (D-Healthy, D-Dis-CER_{ch}, D-Dis-CER_{ch-SbC}, D-Dis-FFA_{ch}, and D-Dis-Combi). Other models were prepared in which either CER NS (C24) or CER NS (C16) fatty acid acyl chain in the Dis-CER_{ch} model was substituted by their deuterated counterparts (D-CER NS (C24) or D-CER NS (C16)) resulting in Dis-CER_{ch-D-NS (C24)} and Dis-CER_{ch-D-NS (C16)} respectively.

Table 1: CER composition of the various models used in the study.

CER name and chain length	Model name & CER molar ratio (%)						
	Healthy	Dis-CER _{ch}	Dis-CER _{ch-D-NS (C24)}	Dis-CER _{ch-D-NS (C16)}	Dis-CER _{ch-SbC}	Dis-FFA _{ch}	Dis-Combi
CER EOS (C30)	15	15	15	15	7	15	7
CER NdS (C24)	13	13	13	13	13	13	13
CER NS (C24)	13	6.5	-	6.5	12	13	12
D-CER NS (C24)	-	-	6.5	-	-	-	-
CER NS (C16)	-	6.5	6.5	-	12	-	12
D-CER NS (C16)	-	-	-	6.5	-	-	-
CER NP (C24)	30	30	30	30	16	30	16
CER AS (C24)	13	6.5	6.5	6.5	12	13	12
CER AS (C16)	-	6.5	6.5	6.5	12	-	12
CER AP (C24)*	16	16	16	16	16	16	16
Total	100	100	100	100	100	100	100

* In our study, we used the native D-isomer of CER AP and CER AS which unlike the unnatural L-isomer has been shown to display native-like behavior[31]

Table 2: FFA composition of the various models used in the study.

FFA name and chain length	Model name & FFA molar ratio (%)		
	Healthy	Dis-CER _{ch} /Dis-CER _{ch-SbC}	Dis-FFA _{ch} /Dis-combi
Palmitic Acid (C16)	1.8	1.8	26
Stearic Acid (C18)	4.0	4.0	19
Arachidic Acid (C20)	7.6	7.6	10
Behenic Acid (C22)	47.8	47.8	21
Lignoceric Acid (C24)	38.8	38.8	24
Total	100	100	100

Preparation of SC model membranes for permeability studies and transepidermal water loss (TEWL) measurements

To prepare the SC model membranes, 0.9 mg of the appropriate lipid composition was dissolved in 200 μ l hexane:ethanol (2:1) solution. The solution was sprayed over an area of 10 x 10 mm², on a nucleopore polycarbonate filter disk with 0.05 μ m pore size (Whatman, Kent, UK), using a Linomat IV device with an extended y-axis arm (Camag, Muttenz, Switzerland) under a gentle stream of nitrogen. The solution was sprayed at 14 μ l/sec at an approximate distance of 1 mm between the nozzle and the spraying surface. The samples were equilibrated for 10 min at 85 °C, which was sufficient to ensure that the lipid mixtures had fully melted and then gradually cooled to room temperature. The heating and cooling cycle was repeated once more.

Permeability studies

The permeation studies were performed using PermeGear in-line diffusion cells (Bethlehem PA, USA) with a diffusion area of 0.28 cm². The sprayed membranes in various lipid compositions were mounted in the diffusion cells and hydrated for 1 h with the acceptor phase consisting of PBS at pH 7.4 before the experiment. Before use, the PBS was filtered and degassed for 30 min under vacuum to remove any dissolved air. The donor phase was a saturated E-PABA solution (0.65mg/ml) in pH 5 acetate buffer. The solution was stirred with a magnetic stirrer, perfused at a flow rate of about 2 ml/h, and degassed continuously by an online degasser. The experiment was performed under occlusive conditions, by closing the opening of the donor compartment with adhesive tape. The temperature of the membranes was maintained at 32 °C mimicking the skin temperature. The acceptor fluid was collected over 15 h at 1-h intervals. At the end of the diffusion study, the volume per collected fraction of PBS was determined by weight and the concentration of E-PABA was determined by UPLC. Permeation of multiple

samples of each model was analyzed $n > 6$. The steady-state flux values were calculated from the plots of E-PABA flux values versus time, at a time interval between the 5th and 15th hour.

Ultra performance liquid chromatography (UPLC)

The analysis of E-PABA was undertaken with Acquity UPLC systems (Waters Co., Milford, MA, USA). The UPLC systems consisted of a quaternary solvent manager (a high-pressure pump), a tunable ultraviolet/visible absorbance detector, and a sample manager. UPLC special analytical column packed with 1.7 μm , bridged, ethyl siloxane, hybrid particles, was used as the stationary phase. The column temperature was set at 40 °C. The mobile phase was composed of mixtures of 0.1% trifluoroacetic acid in acetonitrile: milli-Q water at 40:60 (v/v) ratio. The flow rate of the mobile phase was set at 1 ml/min. 10 μl of the sample was injected on the column. The detector wavelength was set at 286 nm. Data were collected and processed by MassLynx and TargetLynx software V4.1 SCN951 (Waters Co., Milford, USA).

0.5 mg/ml E-PABA stock solution in a 1:1 solution of methanol and milli-Q water was prepared. Eight different concentrations were prepared by serial dilutions of the stock solution with milli-Q water to plot the standard curve. The linearity of the relationship was evaluated in a concentration range of 0.1 -10 $\mu\text{g/ml}$ covering the range of concentrations obtained when analyzing the concentration of E-PABA permeating the model membranes. The calibration curves were obtained using least square linear regression and the linearity was confirmed with the R^2 values. The UPLC method was previously validated for E-PABA analysis as per ICH (International conference on harmonization) guidelines with respect to linearity, precision, limit of detection (LOD), and limit of quantification (LOQ) [32-34].

TEWL measurements

An AquaFlux (AF200, Biox Systems Ltd., London, UK) was used to measure the TEWL of the lipid models. The measurement has been previously described elsewhere [35]. Briefly, the sprayed membranes were mounted in a diffusion cell. The TEWL device was then coupled vertically with the donor compartment of the diffusion cell using a special measurement cap (Biox Systems Limited, UK) in order to seal the compartment and ensure vapour tight connectivity. The TEWL values for the models studied were recorded over a period of 30 min, after which an average reading during the final 10 min of the measurement was calculated, $n = 7$.

Sample preparation for FTIR and X-ray diffraction studies

The appropriate lipid composition was dissolved in chloroform:methanol (2:1) to a concentration of 5 mg/ml. Either 1.5 mg was sprayed over an area of 10 × 10 mm on an AgBr window (for FTIR studies) or 1 mg was sprayed over an area of 2 × 4 mm on mica (for X-ray diffraction studies) using a Linomat IV device (Camag, Muttenz, Switzerland) with an extended y-axis arm and equilibrated as described earlier (section 2.3). The samples were equilibrated for 10 min at 85 °C. The heating and cooling cycle was repeated once more. Finally, the samples were hydrated in deuterated acetate buffer (pH 5.0) and incubated at 37 °C for at least 15 h before measurements to ensure that the samples were fully hydrated.

FTIR measurements

FTIR measurements were implemented with a Varian 670-IR spectrometer (Agilent Technologies, Inc., Santa Clara, CA) equipped with a broad-band mercury cadmium telluride detector, cooled by liquid nitrogen. The samples were purged continuously under dry air, starting 30 min prior to data acquisition. The spectra were collected in transmission mode and acquired by the co-addition of 256 scans at 1 cm⁻¹ resolution, over 4 min. In order to examine the thermotropic phase behavior, the sample was measured between 0-100 °C at a heating rate of 0.25 °C/ min, resulting in a 1 °C temperature rise per recorded spectrum. The spectra were deconvoluted using a half-width of 4 cm⁻¹, and an enhancement factor of 1.7. The software used was Agilent resolution pro (Agilent Technologies, Palo Alto CA, USA). Samples were measured over a range of 600–4000 cm⁻¹. The CH₂ symmetric stretching modes (2845–2855 cm⁻¹) and CD₂ symmetric stretching modes (2080–2100 cm⁻¹), referred to as $\nu_s\text{CH}_2$ and $\nu_s\text{CD}_2$ modes respectively, were chosen to examine the conformational ordering and phase transition of the lipid chains. The conformational ordering was determined at 10 °C, which was prior to the orthorhombic to hexagonal phase transition. The linear regression curve fitting method was used to determine the mid-transition temperature described previously [36]. The CH₂ rocking vibration mode (719–730 cm⁻¹) and scissoring mode (1462–1473 cm⁻¹) referred to as ρCH_2 and δCH_2 respectively were evaluated to monitor the lateral packing, while the CD₂ scissoring modes (1085–1095 cm⁻¹) was examined for determination of the mixing properties of the lipid chains. Multiple samples were measured for each condition, $n > 2$.

X-ray diffraction studies

The small- and wide-angle X-ray diffraction (SAXD and WAXD) diffraction measurements were performed at the European Synchrotron Radiation Facility (ESRF, Grenoble) at station BM26B. SAXD images were collected using a Pilatus 1M detector with 981 x 1043 pixels of 172 μm spatial resolution while the WAXD patterns were collected using a 300K Pilatus detector with 1475 x 195 pixels of 172 μm spatial resolution. The SAXD detector was calibrated using silver behenate while the WAXD detector was calibrated using the two strongest reflections of high-density polyethylene (HDPE). The X-ray wavelength was set at 0.1033 nm. The sample-to-detector distances were 1.98 m and 0.31 m for SAXD and WAXD respectively. The samples were hydrated for 24 h in milli-Q water prior to mounting in parallel to the primary beam in a sample holder with temperature controlled at 25 °C. The diffraction patterns of the samples were acquired in two positions. At each position, the samples were measured for 90 sec. The scattering intensity (I) was measured as a function of the scattering vector (q). The latter is defined as $q = \frac{4\pi \sin \theta}{\lambda}$, where θ is the scattering angle and λ is the wavelength. From the positions of a series of equidistant peaks (q_h), the periodicity of a lamellar phase was calculated using the equation $d = \frac{2h\pi}{q_h}$ in which h is the order of the diffraction peak. The one-dimensional intensity profiles used in these calculations were obtained by the reduction of the 2D SAXD pattern from Cartesian (x,y) to polar (ρ,θ) coordinates and integrated over an θ range. WAXD was used to obtain the diffraction patterns related to the lateral packing of lipids. The diffraction pattern was subsequently collected between 25 and 85 °C in order to examine the temperature-induced phase changes in various models. Each sample condition was measured, $n > 2$.

Data analysis

Unpaired t-test was performed for analysis of the permeability studies data for the healthy skin model versus native skin. One-way ANOVA with Dunnett's multiple comparison test was performed to analyze the permeability studies' and FTIR data for the healthy against the diseased skin models. The significance level for rejection of null hypothesis was set at $P < 0.05$ (*), $P < 0.01$ (**), $P < 0.001$ (***) and $P < 0.0001$ (****).

RESULTS

The healthy skin model membrane properties mimic that of human SC

First, we determined whether the lipid properties of the healthy skin model membrane mimic those of human SC. The lamellar and lateral lipid organization of the healthy skin model were characterized by SAXD and FTIR respectively. The SAXD profile exhibits two lamellar phases with repeat distances of 12.8 and 5.4 nm corresponding to the LPP and SPP in the native human SC, respectively [9, 10] (figure 2A). With respect to the lateral lipid organization, the thermotropic response of the ρCH_2 mode is provided in figure 2B. The ρCH_2 contour is split into two peaks positioned at ~ 720 and 730 cm^{-1} . The splitting is a result of the short-range coupling of adjacent ρCH_2 modes and occurs only in a phase possessing orthorhombic packed chains, as observed in human SC [37]. As the temperature increases, the 730 cm^{-1} peak, which is attributed exclusively to the orthorhombic phase reduces in intensity, implying a loss in orthorhombic packing within the lipid population. At $32\text{ }^\circ\text{C}$, the peak appears as a weak shoulder, indicating a significant reduction in the proportion of lipids adopting an orthorhombic packing and finally disappears at $36\text{ }^\circ\text{C}$, signaling a complete orthorhombic to hexagonal phase transition of the lipids. The permeation of E-PABA through the isolated native human SC and healthy skin model membrane were compared. The E-PABA steady-state flux is presented in (figure 2C). There is no significant difference in

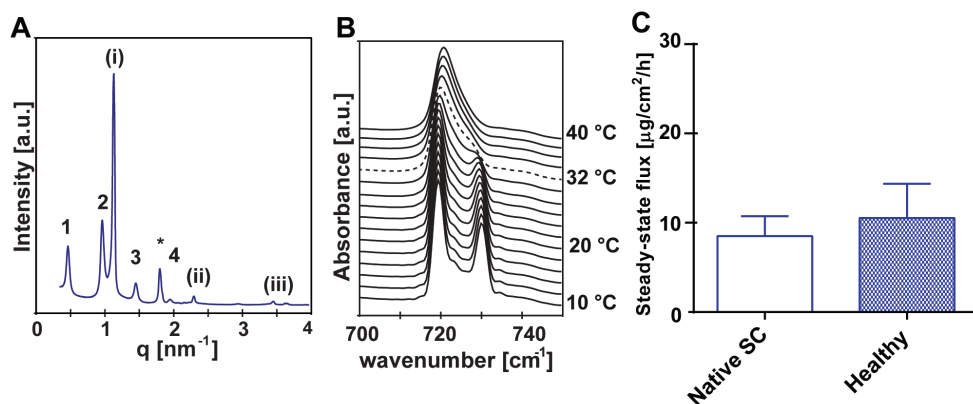


Figure 2: Characterization of the healthy skin model.

A) SAXD profile at $25\text{ }^\circ\text{C}$. The arabic numbers (1, 2, 3,4) indicate the diffraction orders of the LPP, $d = 12.8$ positioned at $q = 0.49, 0.98, 1.46$ and 1.96 nm^{-1} . The roman numbers (i, ii, iii) indicate the diffraction orders of the SPP, $d = 5.4$, positioned at $q = 1.16, 2.3$ and 3.48 nm^{-1} . B) The thermotropic response of the ρCH_2 modes. The presence of two peaks positioned at ~ 720 and 730 cm^{-1} indicate orthorhombic lateral packing while a single peak at $\sim 720\text{ cm}^{-1}$ indicates hexagonal lateral packing. C) The average steady-state flux of E-PABA across the native SC and healthy skin model (5-15 h). Data presented as the mean \pm SD, $n \geq 6$, significance level ($P < 0.05$).

permeability between the native SC and the healthy skin model membrane. As the healthy skin model membrane properties are sufficiently similar to that of the lipid matrix in human SC, the composition of the membrane was modulated to mimic several aspects of the lipid composition in SC of AD.

Changes in lipid composition resulted in increased permeability in AD patients' skin models

In order to examine whether the changes in the lipid composition affect the lipid barrier function, the permeability of the healthy and diseased model membranes was monitored. The average fluxes of E-PABA across the models are displayed in figure 3A. The E-PABA's average steady-state flux values are plotted in figure 3B. The highest E-PABA steady-state flux was observed in Dis-combi, where the alterations in the CER and FFA composition were combined.

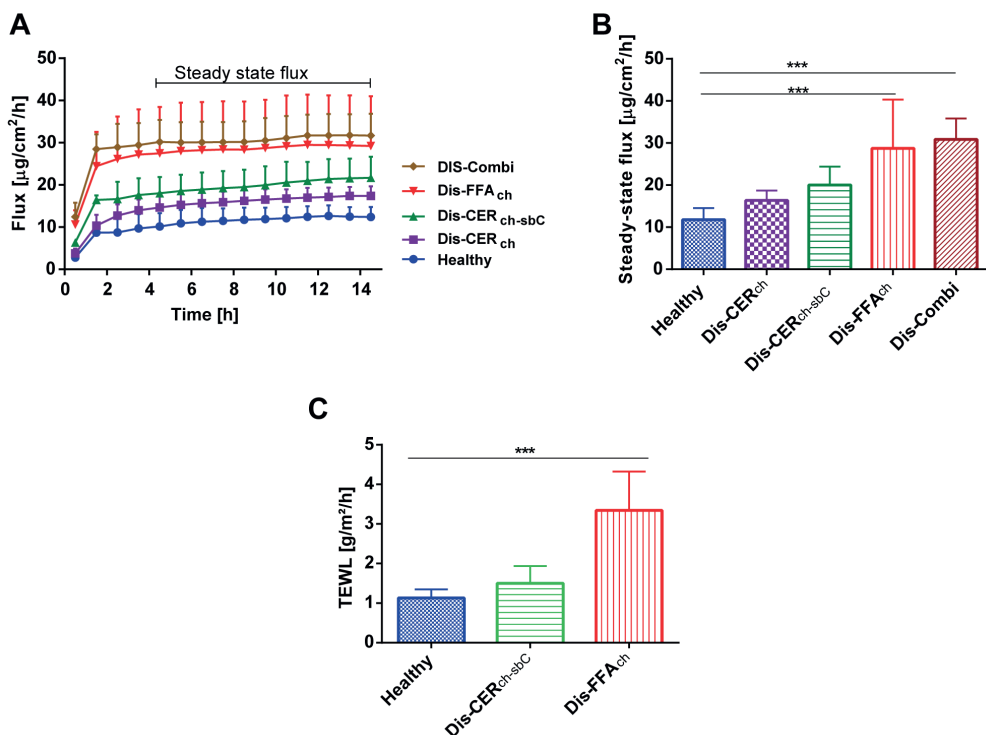


Figure 3: Permeability of the model membranes.

A) The flux of E-PABA across the model membranes over 15 h. B) The average steady-state flux of E-PABA across the model membranes (5-15 h). Data presented as the means \pm SD, $n \geq 6$. E-PABA steady-state flux was significantly higher in the models containing an increased level of short-chain FFAs compared to the healthy skin model, *** ($P < 0.001$). C) TEWL across the model membranes, Dis FFA_{ch} showing significantly higher permeability compared to the healthy skin model, $n = 7$, *** $P < 0.001$.

The flux was significantly higher compared to that of the healthy skin model. To determine which change in composition contributed the most to the reduced SC lipid barrier, the contribution of each of the anomalies in the CER and FFA composition on permeability was examined. First, the CER composition was examined. Replacing 50% of the CER NS and CER AS (C24) by CER NS and CER AS (C16), respectively (Model Dis-CER_{ch}) resulted in a slight but not significant increase in E-PABA flux compared to the healthy skin model. In the next step, the total CERs NS and AS (C24) fraction were increased, of which 50% were the C16 counterparts, while CERs NP and EOS were reduced. This resulted in a further increase (not statistically significant) in permeability. In contrast, when focusing on the FFA composition, the E-PABA steady-state flux across Dis-FFA_{ch}, which contains increased levels of short-chain FFAs, was significantly higher than that across the healthy skin model.

Table 3: The E-PABA steady-state flux across the model membranes with their SD, the wavenumber at 10 °C and midpoint temperatures of the orthorhombic-hexagonal phase transition ($T_{M,OR-HEX}$) in mixtures with protiated CERs and FFA chains and the ordered to disordered phase transition ($T_{M,HEX-LIQ}$) of the v_sCH_2 mode and v_sCD_2 mode in mixtures with protiated CER chains and deuterated FFA chains.

Lipid model	Steady-state flux ($\mu\text{g}/\text{cm}^2/\text{h}$)	wavenumber (cm^{-1})	$T_{M,OR-HEX}$ ($^{\circ}\text{C}$)	v_sCH_2 mode $T_{M,HEX-LIQ}$ ($^{\circ}\text{C}$)	v_sCD_2 mode $T_{M,HEX-LIQ}$ ($^{\circ}\text{C}$)
(D-)Healthy	11.8 ± 2.7	2848.7 ± 0.2	28.0 ± 1.7	67.1 ± 1.5	66.9 ± 2.5
(D-)Dis-CER _{ch}	16.4 ± 2.3	2848.8 ± 0.2	27.1 ± 0.8	65.9 ± 1.4	64.9 ± 2.5
(D-)Dis-CER _{ch-sbC}	20.0 ± 3.6	2848.6 ± 0.2	27.6 ± 0.9	63.1 ± 2.4	62.2 ± 1.7
(D-)Dis-FFA _{ch}	28.7 ± 11.6	2849.0 ± 0.4	24.9 ± 1.3	62.8 ± 0.7	63.7 ± 0.2
(D-)Dis-Combi	30.8 ± 5.0	2849.3 ± 0.3	Undefined	62.9 ± 1.1	63.2 ± 0.1

Changes in lipid composition resulted in increased TEWL in AD patients' skin models

TEWL is often monitored to measure the inside-out skin barrier function in clinical studies. For this reason, TEWL was also used to detect whether selected changes in CERs and FFAs composition resulted in an increased TEWL indicating a reduced lipid barrier. The TEWL values of Healthy, DIS-CER_{ch-sbC}, and Dis FFA_{ch} are plotted in figure 3C. The diseased model membranes show higher TEWL values than the healthy skin model indicating reduced barrier capability. The TEWL value of DIS-CER_{ch-sbC} was 1.2 times higher than that of the healthy skin model and not statistically significant. In contrast, DIS-FFA_{ch} resulted in significantly higher TEWL values, exceeding that of the healthy skin model by 2.8 times. This finding is consistent with the results of the E-PABA permeation study.

Increased levels of short-chain FFAs resulted in lower conformational ordering and significantly lower OR-HEX phase transition temperature

The lateral organization and conformational ordering of the lipids in the healthy and diseased skin models were examined using FTIR. Information about the conformational ordering and packing of lipid chains are provided by the $\nu_s\text{CH}_2$ and δCH_2 frequencies respectively. Low $\nu_s\text{CH}_2$ frequency below 2850 cm^{-1} is characteristic of highly ordered hydrocarbon chains typically packed either in the orthorhombic or hexagonal lateral phase. The thermotropic response of the $\nu_s\text{CH}_2$ mode in the healthy and diseased skin models are presented in figure 4. The average $\nu_s\text{CH}_2$ frequencies for the various models at $10\text{ }^\circ\text{C}$ are presented in Table 3. Dis-Combi exhibits the highest wavenumber indicating a lower conformational ordering compared to the other models. However, the difference was not significant. As the temperature increases, an approximate 1 cm^{-1} rise in the wavenumber occurs between 20 and $40\text{ }^\circ\text{C}$ indicative of an OR-HEX phase transition. The midpoint temperatures of the OR-HEX phase transition ($T_{M,OR-HEX}$) are presented in Table 3. The $T_{M,OR-HEX}$ of Dis-FFA_{ch} is significantly lower than that of the healthy skin model. The $T_{M,OR-HEX}$ of Dis-Combi was not defined indicating that the lipid chains were primarily in the hexagonal phase at the initial temperature.

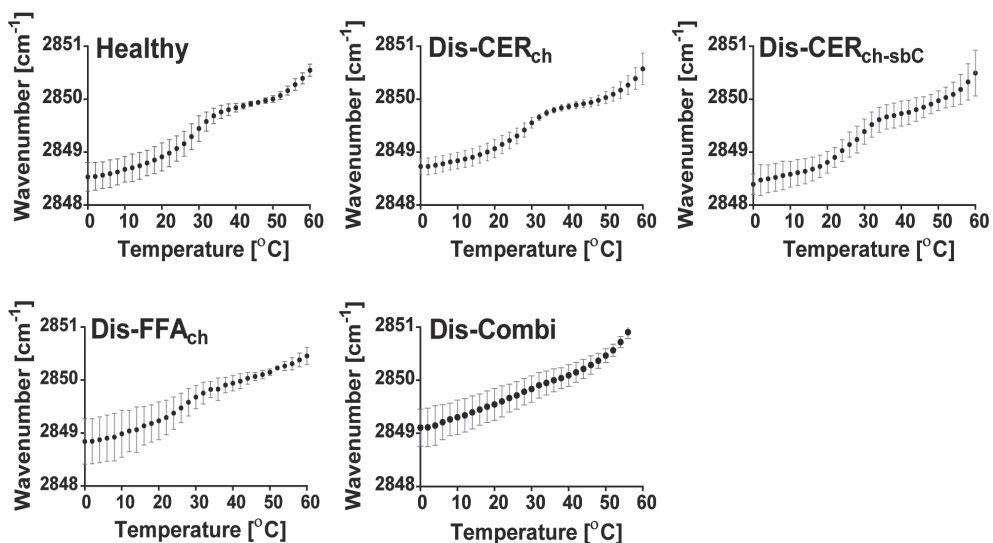


Figure 4: The thermotropic response of the $\nu_s\text{CH}_2$ modes of the lipid models.

The $\nu_s\text{CH}_2$ modes of all models showing frequencies between 0 and $60\text{ }^\circ\text{C}$. The wavenumber at $10\text{ }^\circ\text{C}$ is higher in the Dis-FFA_{ch} and Dis-Combi compared to the healthy skin model indicating the highest conformational ordering in the latter. The midpoint temperature of the OR-HEX phase transition is significantly lower in Dis-FFA_{ch} compared to the healthy skin model while the transition is undefined in Dis-Combi. Data presented as the means \pm SD, $n \geq 3$.

Increased level of short-chain FFAs induced hexagonal lateral packing at physiological temperature

In addition to the ρCH_2 mode, the δCH_2 and δCD_2 modes are affected by the packing arrangements in ordered phases. Broadening or splitting of the scissoring contour signifies an orthorhombic packing. In contrast, hexagonal packing is characterized by a single peak located at $\sim 1467\text{ cm}^{-1}$. The thermotropic response of the δCH_2 frequencies is provided in figure 5. The contour of the δCH_2 modes of the healthy skin model at $10\text{ }^\circ\text{C}$ is split into a strong doublet located at ~ 1462 and 1473 cm^{-1} indicating orthorhombic lateral packing. At $32\text{ }^\circ\text{C}$, the δCH_2 mode of the healthy skin model displayed a weaker doublet with a peak shift in the lower frequency component to $\sim 1467\text{ cm}^{-1}$ indicating a co-existence

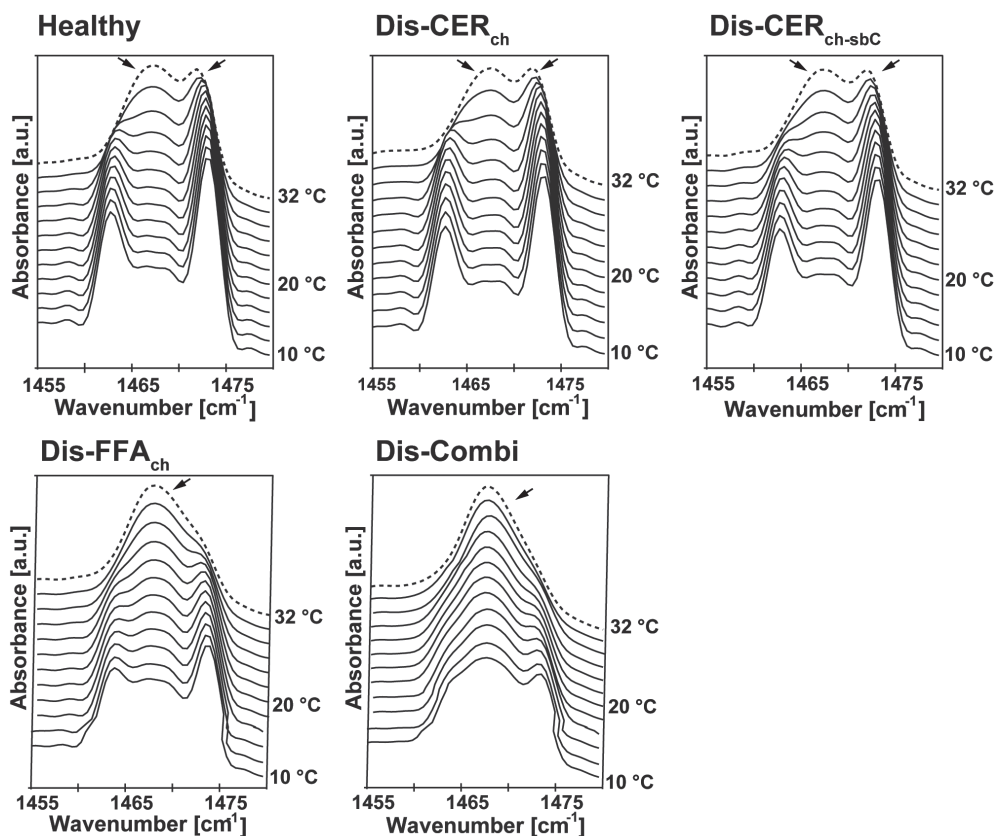


Figure 5: The thermotropic response of the δCH_2 modes of the healthy and diseased skin models.

At $32\text{ }^\circ\text{C}$, the modes of Healthy, Dis-CER_{ch} and Dis-CER_{ch-sbC} display two peaks at $\sim 1467\text{ cm}^{-1}$ and 1473 cm^{-1} indicated by two arrows, showing co-existence of orthorhombic and hexagonal lateral packing while those of Dis-FFA_{ch} and Dis-combi display a single peak located at $\sim 1467\text{ cm}^{-1}$ indicated by single arrows representing hexagonal phase.

with a hexagonal phase. A similar profile was observed in the δCH_2 modes of Dis-CER_{ch} and Dis-CER_{ch-sbC}. In contrast, the δCH_2 mode of Dis-FFA_{ch} displayed a weak doublet at 10 °C indicating a substantially lower proportion of lipids in an orthorhombic phase already at low temperatures. The δCH_2 mode of Dis-combi at 10 °C displays a strong central peak located at $\sim 1467\text{ cm}^{-1}$ and a weak peak at $\sim 1473\text{ cm}^{-1}$ showing that the lipids form predominantly a hexagonal phase. At 32 °C, the δCH_2 mode of Dis-FFA_{ch} and Dis-combi display a single peak at $\sim 1467\text{ cm}^{-1}$ indicating the lipids exist predominantly in the hexagonal phase.

Changes in CER composition reduced the mixing of CERs and FFAs at low temperature

By substituting the FFAs with their deuterated counterparts, the phase transition of the CER and DFFA chains can be monitored simultaneously since the frequencies of vibrational modes of protonated and deuterated acyl chains appear at different positions in the IR spectrum. The $T_{M, \text{HEX-LIQ}}$ of the $\nu_5\text{CH}_2$ and $\nu_5\text{CD}_2$ modes are presented in table 3. In all the models, the CERs and DFFA chains melted in the same temperature range (not shown) indicating the mixing of the CER and DFFA chains. To obtain detailed information on the mixing of protonated and deuterated chains, we examined the δCH_2 and δCD_2 modes. When CER and DFFA chains mix in the same orthorhombic lattice and are thus adjacent to each other, the δCH_2 and δCD_2 vibrational frequencies are sufficiently different in energy to preclude the short-range vibrational coupling between the chains thereby precluding the mode splitting characteristic of orthorhombic packing. Consequently, only a single peak is observed in the δCH_2 and δCD_2 modes. The δCD_2 modes of the healthy and diseased skin models are displayed in figure 6. At 10 °C, the δCD_2 mode from the DFFAs in D-Healthy, D-Dis-CER_{ch'} and D-Dis-CER_{ch-sbC} are split into weak doublets indicating coupling of adjacent DFFA chains. A fraction of the DFFA chains were still able to interact as they are located at neighbouring positions in the orthorhombic lattice [38]. The magnitude of the band splitting is indicative of the degree of inter-chain interactions and the size of the domains with an orthorhombic organization [12, 37, 39]. The splitting values in the δCD_2 mode of the samples were 3.1 ± 0.2 , 3.5 ± 0.2 , and $4.2 \pm 0.5\text{ cm}^{-1}$ for D-Healthy, D-Dis-CER_{ch'} and D-Dis-CER_{ch-sbC} respectively. The mixing of the CERs and DFFA chains was more enhanced in the healthy compared with the diseased skin models as indicated by the lower splitting value and shallower minima between the δCD_2 peaks in the spectrum. D-Dis-CER_{ch-sbC} exhibited the highest splitting value and deepest minima between the δCD_2 peaks indicating the most CD_2 - CD_2 interaction. Upon further increase in temperature, the splitting collapse into single peaks in all the models at $\sim 25\text{ °C}$ resulting from

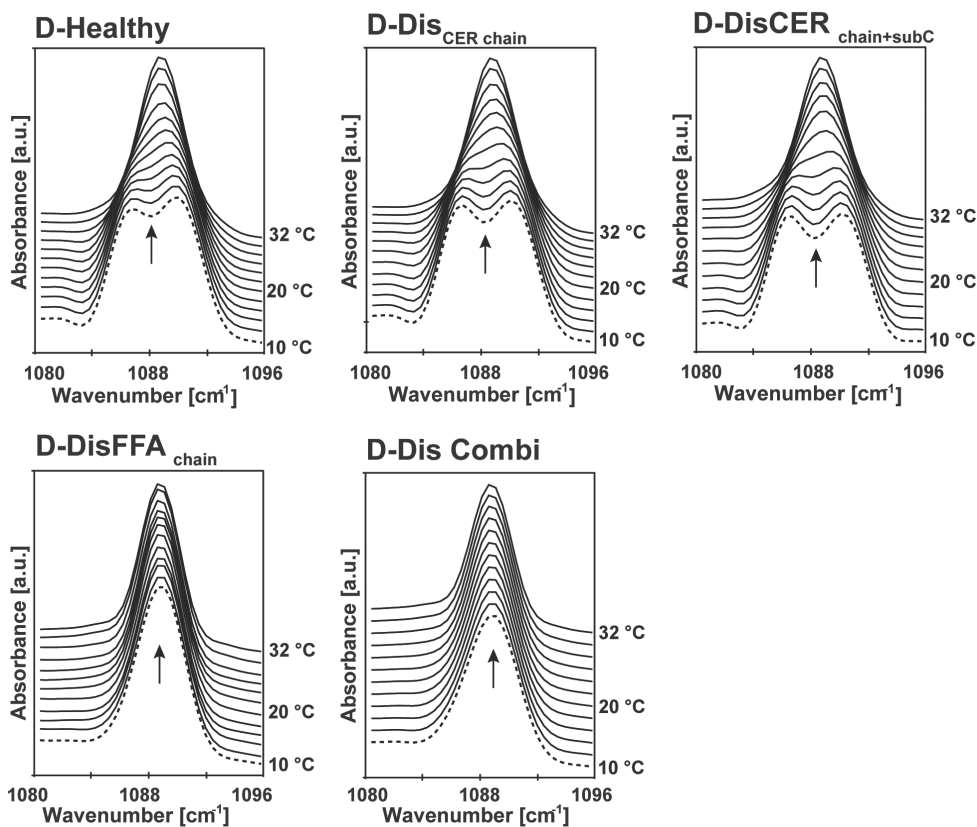


Figure 6: δCD_2 modes of the lipid models.

D-Dis-CER_{ch-sbC} δCD_2 mode doublets displayed the deepest minima at 10 °C when compared with D-Dis-CER_{ch} and D-Healthy indicating the greatest interaction between DFFA chains in the former, while D-Dis-FFA_{ch} and D-Dis-combi displayed single peaks since the chains pack predominantly in a hexagonal phase.

a combined effect of mixing of the CERs and DFFA chains and transition to the hexagonal phase. The δCD_2 modes of D-Dis-FFA_{ch} and Dis-combi at 10 °C exhibit a single central peak since the chains pack predominantly in a hexagonal phase as shown in the corresponding protonated mixtures.

Short-chain CERs present in diseased models are less ordered than the physiological chain length CERs

Another application of selective lipid deuteration is monitoring the individual acyl chain of CER NS conformational ordering in the $\nu_s\text{CD}_2$ mode of mixtures. For these measurements, the deuterated acyl chain in either CER NS (C16) or CER NS (C24) in the Dis-CER_{ch} model was selected. We compared the conformational ordering of the long and short chains in Dis CER_{ch}. The compositions of both

models are presented in table 1 and their $\nu_5\text{CD}_2$ wavenumbers are shown in figure 7. The $\nu_5\text{CD}_2$ wavenumber of $\text{Dis-CER}_{\text{ch-D-NS (C16)}}$ at 10 °C is $2089.9 \pm 0.4 \text{ cm}^{-1}$ being significantly higher than $2088.4 \pm 0.04 \text{ cm}^{-1}$ in $\text{Dis-CER}_{\text{ch-D-NS (C24)}}$ ($n = 3, p < 0.01$) indicating lower conformational ordering in the former.

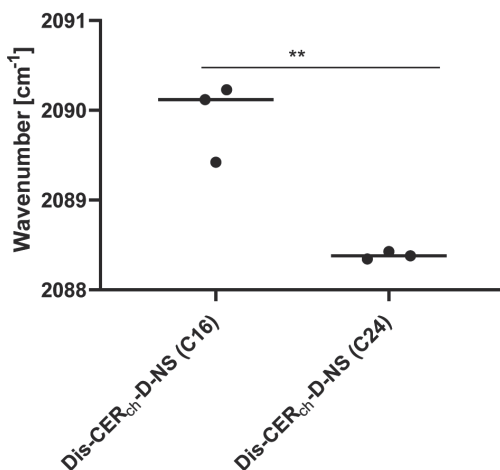


Figure 7: $\nu_5\text{CD}_2$ wavenumber at 10 °C.

The average peak position of the $\nu_5\text{CD}_2$ curve for $\text{Dis-CER}_{\text{ch-D-NS (C16)}}$ and $\text{Dis-CER}_{\text{ch-D-NS (C24)}}$. $\text{Dis-CER}_{\text{ch-D-NS (C16)}}$ wavenumber is significantly higher than that of $\text{Dis-CER}_{\text{ch-D-NS (C24)}}$ indicating more disordering of the lipid chains in the former $n = 3, ** p < 0.01$

Changes in CER composition affects the lamellar organization in skin lipid models

The influence of the changes in lipid composition in the diseased model on the lamellar organization was examined by SAXD. The SAXD profile of the healthy skin model is shown earlier in figure 2A while those of the diseased models are provided in figure 8. Both the healthy and the diseased skin models revealed a number of diffraction peaks attributed to the LPP and the SPP with repeat distances of $\sim 12.8 \text{ nm}$ and 5.4 nm respectively. The diffraction pattern of $\text{Dis-CER}_{\text{ch}}$ displayed an extra peak at $q = 1.5 \text{ nm}^{-1}$ that did not match the spacing of either the LPP or SPP, suggesting the presence of an additional phase. When focusing on $\text{Dis-CER}_{\text{ch-sbC}}$ the LPP formation was drastically reduced compared to the healthy skin model. Meanwhile, the diffraction pattern of $\text{Dis-FFA}_{\text{ch}}$ did not markedly differ from that of $\text{Dis-CER}_{\text{ch}}$. The diffraction pattern of Dis-combi was similar to the $\text{Dis-CER}_{\text{ch-sbC}}$ model aside from an extra peak at $q = 1.3 \text{ nm}^{-1}$ in the diffraction profile of the former. All the SAXD profiles studied revealed the presence of a peak related to a spacing of 3.4 nm attributed to crystalline domains of phase-separated CHOL.

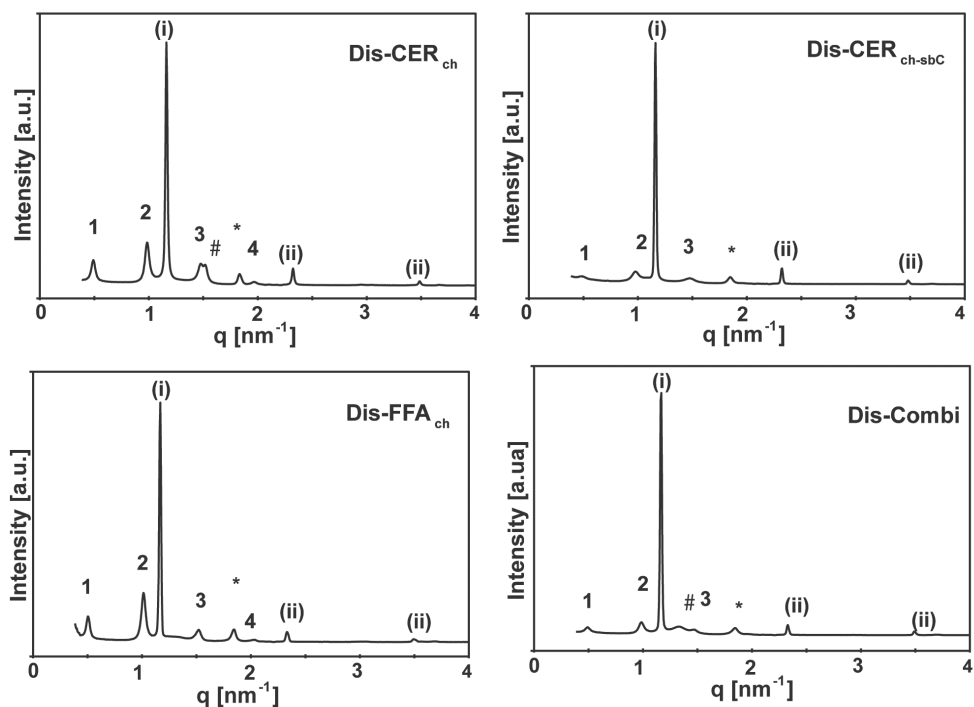


Figure 8: SAXD profile of the diseased skin models at 25 °C.

The arabic numbers (1, 2, 3,4) indicate the 1st, 2nd, 3rd, and 4th order diffraction peaks of the LPP respectively, while the roman numbers (i, ii, iii) indicate the diffraction orders of the SPP. In the diffraction profile of Dis-CER_{ch}, the peak positions at $q = 0.48, 0.97, 1.45,$ and 1.92 nm^{-1} are attributed to the LPP with a repeat distance of 12.9 nm. While in Dis-CER_{ch-sbC} diffraction profile, the peak positions at $q = 0.49, 0.98,$ and 1.47 nm^{-1} are attributed to the LPP with a repeat distance of 12.8 nm. In the diffraction pattern of Dis-FFA_{ch}, the reflections at $q = 0.49, 0.99, 1.48,$ and 1.96 nm^{-1} are attributed to the LPP with a repeat distance of 12.7 nm. Finally, the Dis-Combi diffraction profile is characterized by a series of sequential peaks positioned at $q = 0.48, 0.97,$ and 1.47 nm^{-1} attributed to the LPP with a repeat distance of 12.9 nm. In addition, an extra peak indicated by # is located at $q=1.3$. In all the models, the series of diffraction peaks positioned at $q = 1.16, 2.3,$ and 3.48 nm^{-1} indicate the 1st, 2nd, and 3rd diffraction orders attributed to the SPP with a repeat distance of 5.4 nm and the peaks attributed to crystalline CHOL located at $q = 1.83 \text{ nm}^{-1}$ are indicated by an asterisk (*).

In addition to the lamellar organization, X-ray diffraction provides information about lateral packing of lipid chains. Hexagonal lateral packing is characterized by a single $\sim 0.41 \text{ nm}$ peak, while orthorhombic packing is characterized by two peaks at ~ 0.41 and $\sim 0.37 \text{ nm}$. We examined the changes in lamellar and lateral lipid organization simultaneously. A temperature range from 25 to 85 °C was chosen. We selected three models; Healthy, along with Dis-CER_{ch-sbC} and Dis-FFA_{ch}, which exhibited pronounced alterations in the lamellar and lateral lipid organization respectively. Sequential SAXD and WAXD plots as a function of

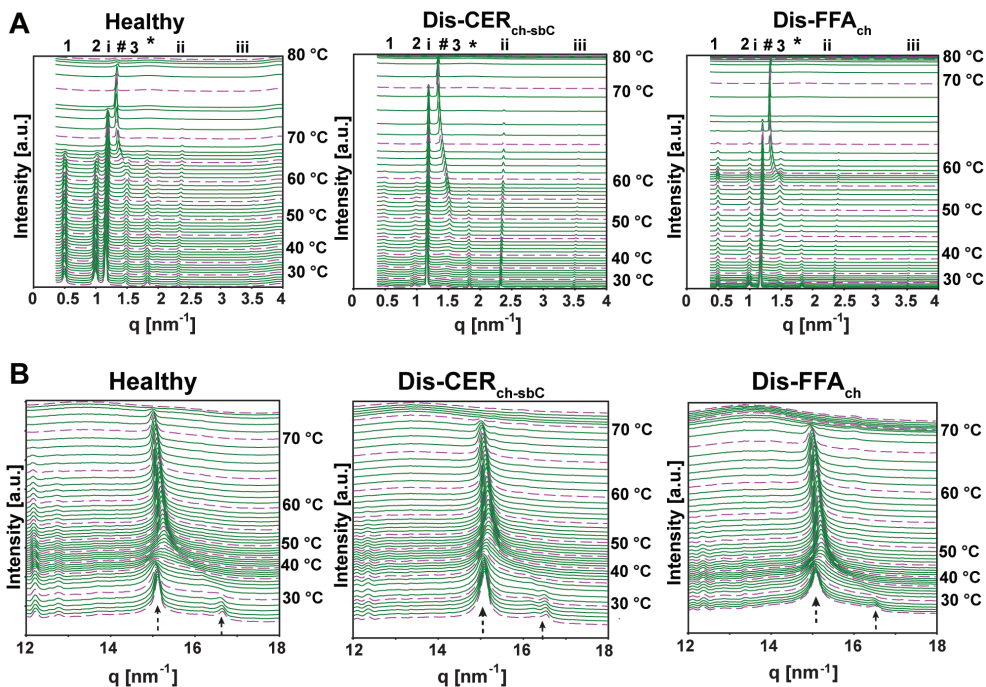


Figure 9: X-ray diffraction profile of the healthy and diseased skin lipid models 25 to 85 °C.

A) SAXD profile showing the changes in the lamellar organization with increasing temperature. The arabic numbers (1, 2, 3) indicate the diffraction orders of the LPP. The roman numbers (i, ii, iii) indicate the diffraction orders of the SPP. * and # indicate phase-separated CHOL and additional phase respectively. B) WAXD showing the changes in the lateral packing with increasing temperature. The arrows show the 0.41 and 0.37 nm peaks located at $q = \sim 15.20$ and 16.7 nm^{-1} respectively.

temperature are presented in figures 9A and B respectively, while a summary of the phase changes in the various models is provided in Table 4. In all three models, the SPP is generally more thermostable than the LPP and the collapse of the SPP coincides with the disappearance of the hexagonal phase. Focusing on the WAXD profile, the intensity of the 0.41 nm peak in the models decreases with increasing temperature, shifts slightly to the right before finally disappearing marking the collapse of the hexagonal phase. Dis-CER_{ch-sbC} LPP was the least thermostable, while Dis-FFA_{ch} exhibited the least thermostable orthorhombic and hexagonal phases. In the SAXD profile, the 3.4 nm reflections attributed to CHOL also disappear at 70 °C, 60 °C, and 57 °C in Healthy, Dis-CER_{ch-sbC}, and Dis-FFA_{ch} respectively. After the disappearance of the CHOL peaks, a broad 3.4 nm peak indicated by # appear in the models, shifting to lower q-values and increasing in intensity with increasing temperature, remaining present till 85 °C.

Table 4: Summary of phase changes on temperature increase.

Model	Temperature at phase disappearance (°C)			
	LPP	SPP	OR phase	HEX phase
Healthy	70	74	38	74
Dis-CER _{ch-sbc}	63	72	37	71
Dis-FFA _{ch}	68	68	33	68

DISCUSSION

Though several studies have reported the association of filaggrin deficiency with AD and ichthyosis vulgaris [40-44], the role of filaggrin gene mutation in barrier function impairment of AD patients remains contentious [16, 22, 45], suggesting other factors also play a role. Some studies have reported a strong correlation between altered lipid composition and TEWL in the skin of AD patients [23, 26, 46]. As CERs and FFAs have a common synthetic pathway [47, 48], changes in their composition were observed simultaneously in AD patients' skin including reduction in chain length of CERs and FFAs and changes in CER subclass composition. However, it is not yet known which changes in the lipid composition impact most on the skin barrier in AD, as multiple compositional changes occur simultaneously. Therefore, we have investigated the contribution of various abnormalities common to the lipid matrix of AD patients' skin using model membrane systems. This allows us to systematically study the impact of each of these changes on the lipid barrier [49].

For a model membrane to be used as a substitute for the native skin, preferably the lipid composition and organization should be similar. In the present study, we developed a model membrane mimicking the CER composition of human SC as closely as possible taking into account, the commercially available synthetic CER subclasses. A previous study from our group employed a model based on pig CER composition, as when the model was developed most of the CER subclasses in pigskin were available [35]. The pig CER model differs from the human CER model by the presence of short-chain CERs (particularly CER NP (C16)) and the presence of an abundant amount of CER NS at the expense of the more hydrophilic subclasses. When comparing the human lipid model with that of the previous pig CER model, there was hardly any difference in the lipid organization in the models. In both models, the lipids assembled in the two characteristic lamellar phases and adopted orthorhombic lateral packing. However, the LPP repeat distance was slightly longer in the human CER model, thereby more closely resembling that of the native human skin.

Changes in the CER profile altered the lamellar organization in model SC

Changes in the CER subclass distribution, as well as a reduction in the chain length, occur in the skin of AD patients. In a previous report, the level of CER NS (C16) was shown to correlate strongly with the TEWL values in AD patients' skin [23]. Subsequently, an excellent correlation was demonstrated between CER chain length reduction and barrier function impairment in AD patients [26]. In the current study, we show that the inclusion of CERs NS(C16) and AS (C16) in the SC model membrane (Dis-CER_{ch}) results in a slightly higher permeability compared to the healthy skin model. By selective deuteration of either the C16 fatty acid acyl chain of CER NS (C16) or the C24 fatty acid acyl chain of CER NS (C24) in Dis-CER_{ch}, we demonstrated that shorter chain length CERs are less conformationally ordered than the long physiological acyl chain length CERs. This is a plausible explanation for the slight increase in the permeability of Dis-CER_{ch} compared to the healthy skin model. Previous studies reported significantly higher permeability in model membranes with the CER fraction made up of short-chain length CERs with fatty acid acyl chain length C4-C8 as opposed to physiological chain length CERs [50, 51]. While the substitution of CER NS/AS (C24) in the healthy skin model by their C16 CER counterparts in Dis-CER_{ch} is substantial, the permeability difference between the models was not significant. This indicates that although a strong correlation was observed between the skin barrier and the presence of CER NS (C16) in the clinical studies, this might not be the prime underlying factor for an impaired skin barrier.

For a comprehensive representation of the CER profile of AD patients, we made additional changes in CER composition, thereby mimicking the CER subclass composition more closely as found in SC of AD patients. The levels of sphingosine-based CERs AS and NS were increased at the expense of CER NP and CER EOS fractions. These simultaneous changes in the CER chain length and subclass (Dis-CER_{ch-sbC}) resulted in a further increase in permeability, but not yet significant. The compositional change resulted in a drastic reduction of the lipid fraction forming the LPP, mainly attributed to the reduction in CER EOS level as reported in the literature. For instance, in a lipid mixture based on human isolated CERs, predominantly the SPP was formed at the expense of the LPP when CER EOS was excluded from the mixture [52]. In addition, model mixtures based on synthetic lipids formed exclusively the short phase when CER EOS was excluded and showed a reduced lipid barrier [53-56]. Furthermore, a reduced level of CER NP is also expected to contribute to a reduced lipid barrier, as recently it was reported that a higher permeability was observed in sphingosine-based CERs membranes compared to their phytosphingosine counterparts [34]. Although

a further increase in permeability was observed, our results indicate that a change in ceramide subclass composition is not a major underlying factor for the increased permeability of the skin in AD patients.

Increased level of short-chain length FFAs reduced the packing density and conformational ordering in model SC

While maintaining the CER composition of the healthy skin, an increased fraction of short-chain FFAs (Dis-FFA_{ch}), as reported in lesional skin of AD patients [27], resulted in a significant increase in permeability compared with the healthy skin model and the changes in permeability were more pronounced than induced by the changes in CER profile. By calculating the average carbon chain length in the diseased skin models relative to the healthy skin model, we deduced that increased levels of short-chain FFAs (mostly C16 and C18) decreased the average FFA chain length by 2.4 carbon atoms in Dis-FFA_{ch}. While increased levels of CERs NS and AS (C16) at the expense of their C24 counterparts resulted in a 1.0 carbon atom reduction in Dis-CER_{ch}. Interestingly, a greater reduction in carbon atoms (3.8) was obtained in Dis-CER_{ch-sbC}, attributed to the reduced concentration of the exceptionally long CER EOS. The compositional changes in CERs composition had more consequences on the carbon chain length than compositional changes in the FFAs and therefore the FFAs did not have a stronger reduction in chain length that could account for the higher impact on the barrier function.

In a previous study, it was shown that shorter FFA chain lengths resulted in an increased conformational disordering and a reduced barrier [57], but in addition to this change in conformational ordering, the reduction in FFA chain length in the present study resulted also in a reduced lipid fraction assembled in the orthorhombic phase. This change in lateral packing was not observed by reducing the average chain length of the CERs and may therefore explain the higher permeability in the Dis-FFA_{ch} model. Our results agree with those of previous studies that reported an increased permeability of model membranes as a consequence of reduced packing density [35, 58]. A reduced lateral packing density was also observed in AD skin in comparison with healthy skin model and may be caused by the shorter FFA rather than the shorter CER chains in AD [25, 26, 59]. Thus, the reduction in FFA chain length can result in the reduced conformational ordering of lipid chains observed in AD patients' skin, compared to healthy skin model [26].

There was extensive mixing of the CER and FFA chains in the models studied since no domains of phase-separated FFA were identified in the δCD_2 modes of the models. As previously reported, the δCD_2 of pure DFFA mixture is

characterized by large splitting, measuring 7.2 cm^{-1} and remaining present till $72\text{ }^{\circ}\text{C}$ [34]. The introduction of C16 acyl chain length CERs NS and AS in D-DIS CER_{ch} resulted in slightly less miscibility of the CER and FFA chains compared to the healthy skin model at the low temperature indicated by the slight increase in splitting value of the δCD_2 mode. Further increase in splitting value was recorded after modulations in the CER subclass fractions. Our data suggest that a lower level of CER EOS may reduce the miscibility of CERs and FFA as we observed that the absence of CER EOS reduced the miscibility of CERs and FFAs (unpublished work).

Previous FTIR studies of ternary SC model mixtures (CER NS (C24)/CHOL/FFA (C16) or (C24)) reported phase separation when FFA (C16) was incorporated into the SC model mixture and was homogeneously mixed on the incorporation of C24 chain length FFA [36, 60, 61]. Separate domains of FFA occurred in CER NS (C24)/CHOL/FFA (C16) as the short-chain length FFA did not fit with the long-chain CER. The reason for the extensive mixing of the CERs and FFA chains in D-DIS CER_{ch} irrespective of the introduction of short-chain length CERs may be the variety in FFA chain lengths in the present mixture. Despite the simultaneous reduction of CER EOS in Dis-CER_{ch-sbC}, CER C16 still fitted in the lamellar structure. This is evident by the absence of phase-separated CER in the CH_2 mode of D-Dis-CER_{ch-sbC} (not shown). The absence of phase separation was also reported in complex SC models containing CER (C24)/CHOL/FFAs (C16-C24) and our pig SC models [36, 62]. A previous study reported that such FFA chain length distribution in the SC may be required for the coexistence of a proportion of solid lipids and fluid domains, which is suggested to be important for normal skin barrier function [63]. Complex SC model mixtures with a variety of CER subclasses and FFAs chain length as employed in the current study, appear to be resilient to phase separation even when the level of short acyl chain lengths are increased. CER headgroup diversity and FFA chain length distribution may provide robustness to the barrier necessary for withstanding challenges in the environment.

SUMMARY AND CONCLUSIONS

The changes in the lipid composition of model membranes that mimic the changes observed in AD patients resulted in a reduced barrier capability. Modulations in CER composition altered the lamellar organization, while changes in FFAs composition induced the phase transition from the dense orthorhombic to the less dense hexagonal packing. The present study shows

that FFA compositional changes in AD skin has a greater impact on the barrier function than changes in the CER profile most likely due to a change in packing density, which does not occur when shortening the CER chain length. These findings are highly suggestive that AD therapies that target the normalization of the FFA composition are at least as important as the normalization of CER composition.

ACKNOWLEDGEMENTS

We are grateful to the company Evonik for the donation of CERs. We also acknowledge the staff at the DUBBLE beamline 26B at the ESRF, Grenoble, France who assisted with the X-ray diffraction measurements.

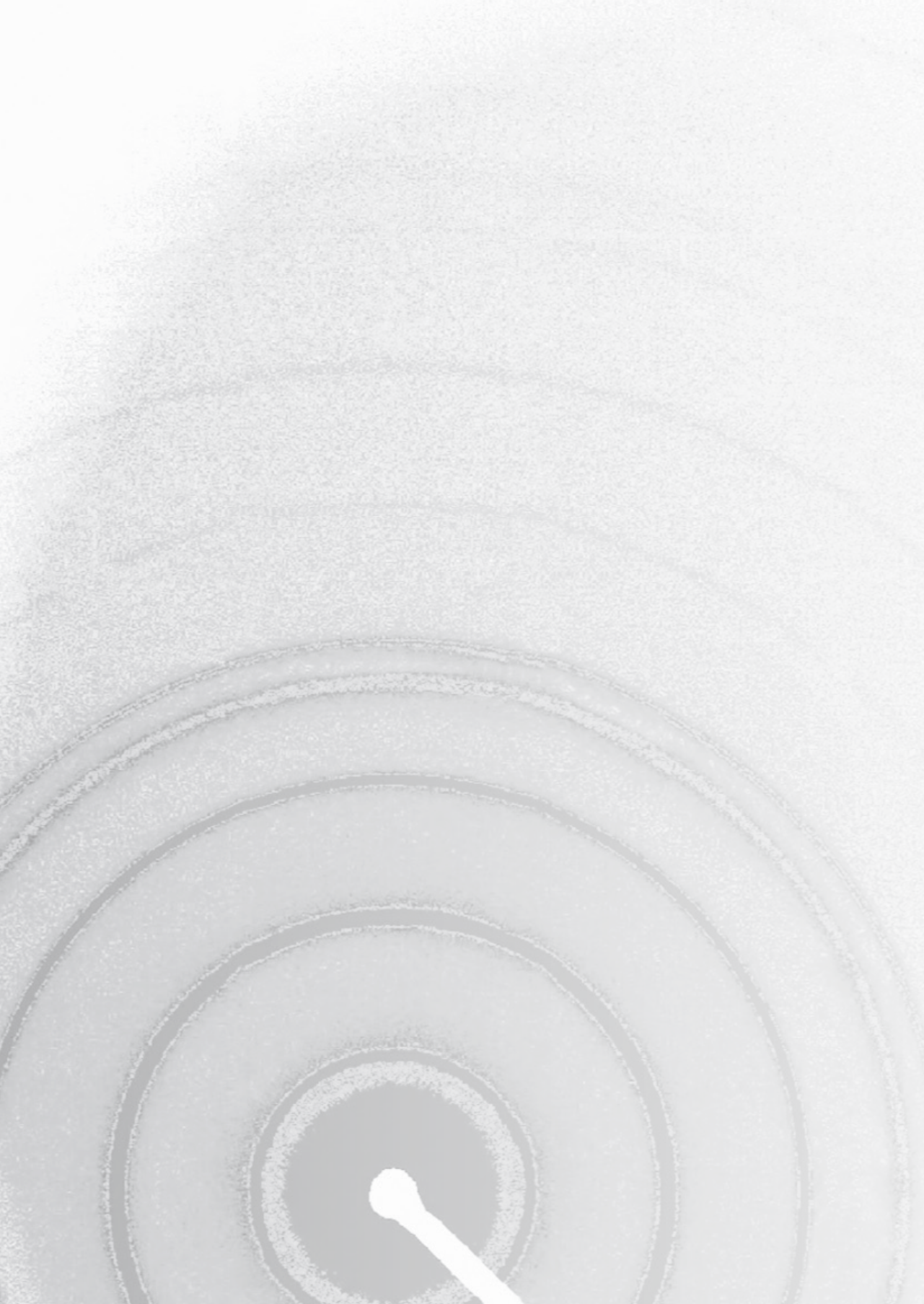
REFERENCES

1. Hannun, Y. A., Functions of ceramide in coordinating cellular responses to stress. *Science* **1996**, 274 (5294), 1855-9.
2. Brasaemle, D. L., Thematic review series: adipocyte biology. The perilipin family of structural lipid droplet proteins: stabilization of lipid droplets and control of lipolysis. *J. Lipid Res.* **2007**, 48 (12), 2547-59.
3. van Blitterswijk, W. J.; van der Luit, A. H.; Veldman, R. J.; Verheij, M.; Borst, J., Ceramide: second messenger or modulator of membrane structure and dynamics? *Biochem. J.* **2003**, 369 (Pt 2), 199-211.
4. Wang, X., Lipid signaling. *Curr. Opin. Plant Biol.* **2004**, 7 (3), 329-336.
5. Quinn, P. J., Structure of sphingomyelin bilayers and complexes with cholesterol forming membrane rafts. *Langmuir* **2013**, 29 (30), 9447-56.
6. Gonzalez-Ramirez, E. J.; Artetxe, I.; Garcia-Arribas, A. B.; Goni, F. M.; Alonso, A., Homogeneous and heterogeneous bilayers of ternary lipid compositions containing equimolar ceramide and cholesterol. *Langmuir* **2019**, 35 (15), 5305-5315.
7. Weerheim, A.; Ponec, M., Determination of stratum corneum lipid profile by tape stripping in combination with high-performance thin-layer chromatography. *Arch. Dermatol. Res.* **2001**, 293 (4), 191-199.
8. Mendelsohn, R.; Flach, C. R.; Moore, D. J., Determination of molecular conformation and permeation in skin via IR spectroscopy, microscopy, and imaging. *Biochim. Biophys. Acta* **2006**, 1758 (7), 923-933.
9. Bouwstra, J. A.; Gooris, G. S.; van der Spek, J. A.; Bras, W., Structural investigations of human stratum corneum by small-angle X-ray scattering. *J. Invest. Dermatol.* **1991**, 97 (6), 1005-12.
10. White, S. H.; Mirejovsky, D.; King, G. I., Structure of lamellar lipid domains and corneocyte envelopes of murine stratum corneum. An X-ray diffraction study. *Biochemistry* **1988**, 27 (10), 3725-32.
11. Bouwstra, J.; Gooris, G.; Ponec, M., The lipid organisation of the skin barrier: Liquid and crystalline domains coexist in lamellar phases. *Journal of biological physics* **2002**, 28 (2), 211-223.
12. Boncheva, M.; Damien, F.; Normand, V., Molecular organization of the lipid matrix in intact stratum corneum using ATR-FTIR spectroscopy. *Biochim. Biophys. Acta* **2008**, 1778 (5), 1344-55.
13. Norlen, L.; Nicander, I.; Lundsjo, A.; Cronholm, T.; Forslind, B., A new HPLC-based method for the quantitative analysis of inner stratum corneum lipids with special reference to the free fatty acid fraction. *Arch. Dermatol. Res.* **1998**, 290 (9), 508-16.
14. van Smeden, J.; Boiten, W. A.; Hankemeier, T.; Rissmann, R.; Bouwstra, J. A.; Vreeken, R. J., Combined LC/MS-platform for analysis of all major stratum corneum lipids, and the profiling of skin substitutes. *Biochim. Biophys. Acta* **2014**, 1841 (1), 70-79.
15. t'Kindt, R.; Jorge, L.; Dumont, E.; Couturon, P.; David, F.; Sandra, P.; Sandra, K., Profiling and characterizing skin ceramides using reversed-phase liquid chromatography-quadrupole time-of-flight mass spectrometry. *Anal. Chem.* **2012**, 84 (1), 403-411.
16. van Smeden, J.; Bouwstra, J. A., Stratum corneum lipids: Their role for the skin barrier function in healthy subjects and atopic dermatitis patients. *Curr. Probl. Dermatol.* **2016**, 49, 8-26.
17. Wertz, P. W.; Miethke, M. C.; Long, S. A.; Strauss, J. S.; Downing, D. T., The composition of the ceramides from human stratum corneum and from comedones. *J. Invest. Dermatol.* **1985**, 84 (5), 410-2.

18. Motta, S.; Monti, M.; Sesana, S.; Caputo, R.; Carelli, S.; Ghidoni, R., Ceramide composition of the psoriatic scale. *Biochim. Biophys. Acta* **1993**, *1182* (2), 147-51.
19. Alanne, S.; Nermes, M.; Soderlund, R.; Laitinen, K., Quality of life in infants with atopic dermatitis and healthy infants: a follow-up from birth to 24 months. *Acta Paediatr.* **2011**, *100* (8), e65-70.
20. Proksch, E.; Folster-Holst, R.; Jensen, J. M., Skin barrier function, epidermal proliferation and differentiation in eczema. *J. Dermatol. Sci.* **2006**, *43* (3), 159-69.
21. Jensen, J. M.; Folster-Holst, R.; Baranowsky, A.; Schunck, M.; Winoto-Morbach, S.; Neumann, C.; Schutze, S.; Proksch, E., Impaired sphingomyelinase activity and epidermal differentiation in atopic dermatitis. *J. Invest. Dermatol.* **2004**, *122* (6), 1423-31.
22. Jakasa, I.; Koster, E. S.; Calkoen, F.; Irwin McLean, W. H.; Campbell, L. E.; Bos, J. D.; Verberk, M. M.; Kezic, S., Skin Barrier Function in Healthy Subjects and Patients with Atopic Dermatitis in Relation to Filaggrin Loss-of-Function Mutations. *J. Invest. Dermatol.* **2011**, *131* (2), 540-542.
23. Ishikawa, J.; Narita, H.; Kondo, N.; Hotta, M.; Takagi, Y.; Masukawa, Y.; Kitahara, T.; Takema, Y.; Koyano, S.; Yamazaki, S.; Hatamochi, A., Changes in the ceramide profile of atopic dermatitis patients. *J. Invest. Dermatol.* **2010**, *130* (10), 2511-4.
24. Di Nardo, A.; Wertz, P.; Giannetti, A.; Seidenari, S., Ceramide and cholesterol composition of the skin of patients with atopic dermatitis. *Acta Derm-Venereol.* **1998**, *78* (1), 27-30.
25. Imokawa, G.; Abe, A.; Jin, K.; Higaki, Y.; Kawashima, M.; Hidano, A., Decreased level of ceramides in stratum corneum of atopic dermatitis: an etiologic factor in atopic dry skin? *J. Invest. Dermatol.* **1991**, *96* (4), 523-6.
26. Janssens, M.; van Smeden, J.; Gooris, G. S.; Bras, W.; Portale, G.; Caspers, P. J.; Vreeken, R. J.; Hankemeier, T.; Kezic, S.; Wolterbeek, R.; Lavrijsen, A. P.; Bouwstra, J. A., Increase in short-chain ceramides correlates with an altered lipid organization and decreased barrier function in atopic eczema patients. *J. Lipid Res.* **2012**, *53* (12), 2755-66.
27. van Smeden, J.; Janssens, M.; Kaye, E. C.; Caspers, P. J.; Lavrijsen, A. P.; Vreeken, R. J.; Bouwstra, J. A., The importance of free fatty acid chain length for the skin barrier function in atopic eczema patients. *Exp. Dermatol.* **2014**, *23* (1), 45-52.
28. Elias, P. M., Primary role of barrier dysfunction in the pathogenesis of atopic dermatitis. *Exp. Dermatol.* **2018**, *27* (8), 847-851.
29. Cork, M. J.; Danby, S. G.; Vasilopoulos, Y.; Hadgraft, J.; Lane, M. E.; Moustafa, M.; Guy, R. H.; MacGowan, A. L.; Tazi-Ahnini, R.; Ward, S. J., Epidermal Barrier Dysfunction in Atopic Dermatitis. *J. Invest. Dermatol.* **2009**, *129* (8), 1892-1908.
30. Wertz, P.W.; Dowing, D.T., *Physiology, biochemistry and molecular biology of the skin*. second ed.; Oxford University Press: New York, 1991; Vol. 1, p 205-236.
31. Schmitt, T.; Lange, S.; Sonnenberger, S.; Dobner, B.; Demé, B.; Neubert, R. H. H.; Gooris, G.; Bouwstra, J. A., Determination of the influence of C24 D/(2R)- and L/(2S)-isomers of the CER[AP] on the lamellar structure of stratum corneum model systems using neutron diffraction. *Chemistry and Physics of Lipids* **2017**, *209*, 29-36.
32. International Conference on Harmonization (ICH) Q2 (R1), Validation of analytical procedures: Text and Methodology. 2005.
33. European Pharmacopoeia. 8 ed.; European Directorate for the quality of medicines & healthcare. Strasbourg, 2014; Vol. 1.
34. Uche, L. E.; Gooris, G. S.; Beddoes, C. M.; Bouwstra, J. A., New insight into phase behavior and permeability of skin lipid models based on sphingosine and phytosphingosine ceramides. *Biochim. Biophys. Acta* **2019**, *1861* (7), 1317-1328.
35. Mojumdar, E. H.; Helder, R. W.; Gooris, G. S.; Bouwstra, J. A., Monounsaturated fatty acids reduce the barrier of stratum corneum lipid membranes by enhancing the formation of a hexagonal lateral packing. *Langmuir* **2014**, *30* (22), 6534-43.

36. Oguri, M.; Gooris, G. S.; Bito, K.; Bouwstra, J. A., The effect of the chain length distribution of free fatty acids on the mixing properties of stratum corneum model membranes. *Biochim. Biophys. Acta* **2014**, *1838* (7), 1851-1861.
37. Mendelsohn, R.; Liang, G. L.; Strauss, H. L.; Snyder, R. G., IR spectroscopic determination of gel state miscibility in long-chain phosphatidylcholine mixtures. *Biophys. J.* **1995**, *69* (5), 1987-1998.
38. Groen, D.; Gooris, G. S.; Bouwstra, J. A., Model membranes prepared with ceramide EOS, cholesterol, and free fatty acids form a unique lamellar phase. *Langmuir* **2010**, *26* (6), 4168-75.
39. Snyder, R. G.; Goh, M. C.; Srivatsavoy, V. J. P.; Strauss, H. L.; Dorset, D. L., Measurement of the growth-kinetics of microdomains in binary N-alkane solid-solutions by infrared-spectroscopy. *J. Phys. Chem-US* **1992**, *96* (24), 10008-10019.
40. Rodriguez, E.; Illig, T.; Weidinger, S., Filaggrin loss-of-function mutations and association with allergic diseases. *Pharmacogenomics* **2008**, *9* (4), 399-413.
41. Gruber, R.; Elias, P. M.; Crumrine, D.; Lin, T. K.; Brandner, J. M.; Hachem, J. P.; Presland, R. B.; Fleckman, P.; Janecke, A. R.; Sandilands, A.; McLean, W. H.; Fritsch, P. O.; Mildner, M.; Tschachler, E.; Schmuth, M., Filaggrin genotype in ichthyosis vulgaris predicts abnormalities in epidermal structure and function. *Am. J. Pathol.* **2011**, *178* (5), 2252-63.
42. Irvine, A. D.; McLean, W. H.; Leung, D. Y., Filaggrin mutations associated with skin and allergic diseases. *N. Engl. J. Med.* **2011**, *365* (14), 1315-27.
43. Hudson, T. J., Skin barrier function and allergic risk. *Nat. Genet.* **2006**, *38* (4), 399-400.
44. McGrath, J. A., Filaggrin and the great epidermal barrier grief. *Australas J. Dermatol.* **2008**, *49* (2), 67-73; quiz 73-4.
45. Danso, M.; Boiten, W.; van Drongelen, V.; Gmelig Meijling, K.; Gooris, G.; El Ghalbzouri, A.; Absalah, S.; Vreeken, R.; Kezic, S.; van Smeden, J.; Lavrijsen, S.; Bouwstra, J., Altered expression of epidermal lipid bio-synthesis enzymes in atopic dermatitis skin is accompanied by changes in stratum corneum lipid composition. *J. Dermatol. Sci.* **2017**, *88* (1), 57-66.
46. Janssens, M.; van Smeden, J.; Gooris, G. S.; Bras, W.; Portale, G.; Caspers, P. J.; Vreeken, R. J.; Kezic, S.; Lavrijsen, A. P.; Bouwstra, J. A., Lamellar lipid organization and ceramide composition in the stratum corneum of patients with atopic eczema. *J. Invest. Dermatol.* **2011**, *131* (10), 2136-8.
47. van Smeden, J.; Janssens, M.; Boiten, W. A.; van Drongelen, V.; Furio, L.; Vreeken, R. J.; Hovnanian, A.; Bouwstra, J. A., Intercellular skin barrier lipid composition, and organization in Netherton syndrome patients. *J. Invest. Dermatol.* **2014**, *134* (5), 1238-1245.
48. Kihara, A., Synthesis and degradation pathways, functions, and pathology of ceramides and epidermal acylceramides. *Prog. Lipid Res.* **2016**, *63*, 50-69.
49. Kováčik, A.; Pullmannová, P.; Maixner, J.; Vávrová, K., Effects of ceramide and dihydroceramide stereochemistry at C-3 on the phase behavior and permeability of skin lipid membranes. *Langmuir* **2018**, *34* (1), 521-529.
50. Skolova, B.; Janusova, B.; Zbytovska, J.; Gooris, G.; Bouwstra, J.; Slepicka, P.; Berka, P.; Roh, J.; Palat, K.; Hrabalek, A.; Vavrova, K., Ceramides in the skin lipid membranes: length matters. *Langmuir* **2013**, *29* (50), 15624-33.
51. Janusova, B.; Zbytovska, J.; Lorenc, P.; Vavrysova, H.; Palat, K.; Hrabalek, A.; Vavrova, K., Effect of ceramide acyl chain length on skin permeability and thermotropic phase behavior of model stratum corneum lipid membranes. *Biochim. Biophys. Acta* **2011**, *1811* (3), 129-37.
52. Bouwstra, J. A.; Gooris, G. S.; Dubbelaar, F. E.; Ponec, M., Phase behavior of lipid mixtures based on human ceramides: coexistence of crystalline and liquid phases. *J. Lipid Res.* **2001**, *42* (11), 1759-70.

53. Groen, D.; Gooris, G. S.; Barlow, D. J.; Lawrence, M. J.; van Mechelen, J. B.; Deme, B.; Bouwstra, J. A., Disposition of ceramide in model lipid membranes determined by neutron diffraction. *Biophys. J.* **2011**, *100* (6), 1481-1489.
54. Mojumdar, E. H.; Groen, D.; Gooris, G. S.; Barlow, D. J.; Lawrence, M. J.; Deme, B.; Bouwstra, J. A., Localization of cholesterol and fatty acid in a model lipid membrane: a neutron diffraction approach. *Biophys. J.* **2013**, *105* (4), 911-8.
55. de Jager, M.; Groenink, W.; Bielsa i Guivernau, R.; Andersson, E.; Angelova, N.; Ponec, M.; Bouwstra, J., A novel in vitro percutaneous penetration model: evaluation of barrier properties with p-aminobenzoic acid and two of its derivatives. *Pharm. Res.* **2006**, *23* (5), 951-60.
56. Opalka, L.; Kovacik, A.; Maixner, J.; Vavrova, K., Omega-O-Acylceramides in skin lipid membranes: effects of concentration, sphingoid base, and model complexity on microstructure and permeability. *Langmuir* **2016**, *32* (48), 12894-12904.
57. Uchiyama, M.; Oguri, M.; Mojumdar, E. H.; Gooris, G. S.; Bouwstra, J. A., Free fatty acids chain length distribution affects the permeability of skin lipid model membranes. *Biochim. Biophys. Acta* **2016**, *1858* (9), 2050-9.
58. Skolova, B.; Jandovska, K.; Pullmannova, P.; Tesar, O.; Roh, J.; Hrabalek, A.; Vavrova, K., The role of the trans double bond in skin barrier sphingolipids: permeability and infrared spectroscopic study of model ceramide and dihydroceramide membranes. *Langmuir* **2014**, *30* (19), 5527-35.
59. Pilgram, G. S. K.; Vissers, D. C. J.; van der Meulen, H.; Koerten, H. K.; Pavel, S.; Lavrijsen, S. P. M.; Bouwstra, J. A., Aberrant lipid organization in stratum corneum of patients with atopic dermatitis and lamellar ichthyosis. *J. Invest. Dermatol.* **2001**, *117* (3), 710-717.
60. Paz Ramos, A.; Lafleur, M., Chain length of free fatty acids influence the phase behavior of stratum corneum model membranes. *Langmuir* **2015**, *31* (42), 11621-11629.
61. Skolova, B.; Hudska, K.; Pullmannova, P.; Kovacik, A.; Palat, K.; Roh, J.; Fleddermann, J.; Estrela-Lopis, I.; Vavrova, K., Different phase behavior and packing of ceramides with long (C16) and very long (C24) acyls in model membranes: infrared spectroscopy using deuterated lipids. *J Phys Chem-Us* **2014**, *118* (35), 10460-70.
62. de Jager, M. W.; Gooris, G. S.; Ponec, M.; Bouwstra, J. A., Lipid mixtures prepared with well-defined synthetic ceramides closely mimic the unique stratum corneum lipid phase behavior. *J. Lipid Res.* **2005**, *46* (12), 2649-2656.
63. Chen, X.; Kwak, S.; Lafleur, M.; Bloom, M.; Kitson, N.; Thewalt, J., Fatty acids influence "solid" phase formation in models of stratum corneum intercellular membranes. *Langmuir* **2007**, *23* (10), 5548-56.



3

High concentration of the ester-linked -hydroxy ceramide increases the permeability in skin lipid model membranes

3

Authors and affiliations:

Lorretta.E. Uche¹, Gerrit.S. Gooris¹, Joke.A. Bouwstra¹ and Charlotte.M. Beddoes¹

¹Division of Drug Delivery Technology, Cluster BioTherapeutics, Leiden Academic Centre for Drug Research, Leiden University, Netherlands

Adapted from: *Biochimica et Biophysica Acta (BBA) - Biomembranes*, 2021. **1863**(1): p. 183487-183497.

ABSTRACT

The ester-linked ω -hydroxy acyl chain linked to a sphingosine base referred to as CER EOS is essential for the skin barrier lipid organization. While the majority of the skin lipids form a dense, crystalline structure, associated with low permeability, the unsaturated moiety of CER EOS, (either the linoleate or the oleate chain) exists in a liquid phase at the skin's physiological temperature. Thus, the relationship between CER EOS and barrier function is not entirely comprehended. We studied the permeability and lipid organization in skin lipid models, gradually increasing in CER EOS concentration, mixed with non-hydroxy sphingosine-based ceramide (CER NS) in an equimolar ratio of CERs, cholesterol, and free fatty acids (FFAs) mimicking the ratio in the native skin. A significant increase in the orthorhombic-hexagonal phase transition temperature was recorded when CER EOS concentration was raised to 70 mol% of the total CER content and higher, rendering a higher fraction of lipids in the orthorhombic phase at the expense of the hexagonal phase at physiological temperature. The model's permeability did not differ when CER EOS concentration ranged between 10 to 30% but increased significantly at 70% and higher. Using CER EOS with a perdeuterated oleate chain, it was shown that the fraction of lipids in a liquid phase increased with CER EOS concentration, while the neighboring CERs and FFAs remained in a crystalline state. The increased fraction of the liquid phase therefore, had a stronger effect on permeability than the increased fraction of lipids forming an orthorhombic phase.

Keywords:

Intercellular lipid; Stratum corneum; Infrared spectroscopy; X-ray diffraction; Long periodicity phase; Sphingolipids.

INTRODUCTION

The skin protects the body from the invasion of pathogens and other harmful substances in the external environment, as well as preventing desiccation from within. This skin's barrier function is ascribed to its thin outermost layer known as the stratum corneum (SC) [1-3]. The SC comprises of keratin-filled, flattened dead cells referred to as corneocytes, embedded in a lipid matrix. The corneocytes show a reduced permeability by the presence of a densely cross-linked protein envelope thereby redirecting the permeation of substances along the intercellular lipid matrix [4-6]. Consequently, the composition and organization of the SC lipids are essential to the barrier function.

The SC lipids are arranged into intercellular lamellae aligned approximately parallel to the cell surface [7]. Two distinct lamellar phases, the long periodicity phase (LPP) and the short periodicity phase (SPP) are detected by X-ray diffraction studies [8, 9]. The LPP is exclusively present in the SC and is considered to be important for the skin barrier function [10, 11]. X-ray and neutron diffraction revealed that the LPP is a trilayer structure [12, 13]. Perpendicular to the basal layer of the lamellae, the lipids adopt predominantly the dense orthorhombic lateral packing. This packing plays a role in the low permeability of the skin barrier [14].

The SC intercellular lipid domains are primarily composed of approximately an equimolar ratio of cholesterol (CHOL), free fatty acids (FFAs), and ceramides (CERs) [15, 16]. The FFAs are predominantly saturated and display a chain length distribution between 12 and 30 carbon atoms [17, 18]. CERs are a structurally heterogeneous group of sphingolipids, comprising of a sphingoid base linked to an acyl chain via an amide bond. Currently, at least 18 CER subclasses have been identified in human SC [19-23]. Four of the subclasses often referred to as acylCERs, constitute of an ultra-long ω -hydroxy acyl chain, which contains up to 30-34 carbon atoms, ester-linked to an unsaturated fatty acid (usually linoleic acid) and amide-linked to one of the various sphingoid bases. These acyl CERs are only present in the SC and their concentration is reduced in skin diseases such as atopic dermatitis, psoriasis, Netherton syndrome, and autosomal recessive congenital ichthyosis, but also in dry skin [24-30]. Consequently, their role in barrier function has attracted attention [10, 31, 32]. The relative abundance of the acylCERs is ~8-13 mol% of the total CERs in the human SC [33, 34]. The most abundant acylCER is the subclass with a sphingosine (S) base referred to as CER EOS [33]. Using lipid models prepared with both isolated [35-38] and synthetic CER mixtures [31, 39], it was shown that CER EOS is efficient in enhancing the

formation of the LPP. Previous FTIR and NMR studies reported that the linoleate moiety of CER EOS linoleate (CER EOS-L) (Fig. 1A) exists in a disordered fluid phase in a crystalline environment of the SC model [40, 41]. In the present study, a similar behavior was reported for the oleate moiety of CER EOS oleate (CER EOS-O) (Fig. 1B), which is in agreement with another recent study using FTIR, Raman spectroscopy, and NMR techniques [42]. Another NMR study showed that concerning the linoleate chain, the fluidity is primarily located in the middle and end segment of the chain [40]. With regards to the effect of CER EOS on barrier function, SC model membranes prepared with synthetic CERs, that mimicked the composition in pig SC, showed a two-fold increase in permeability of ethyl para-aminobenzoic acid when CER EOS was excluded from the lipid composition [10]. In another study, incorporation of 10% CER EOS resulted in an increase in permeability of theophylline and indomethacin across a simple SC model compared to that in the absence of CER EOS, but the permeability reduced as CER EOS concentration was increased up to 30% [31]. Opalka et al. further reported that the permeability of a complex lipid model was not improved when the content of either an individual acylCER or an acylCER mixture was increased above the physiological concentration to 30% [43]. However, the barrier function in relation to the fraction of lipids forming co-existing crystalline and liquid phases was not studied, neither was the effect of concentrations of CER EOS beyond 30% investigated.

Therefore, in the present study, we aimed to determine the effect of increasing the concentration of CER EOS on the lipid phase behavior and barrier function. To achieve our purpose, SC models were used with a composition that systematically increased in CER EOS concentration between 10-90% mol of the total CER content. We incorporated CER NS in the models since SC

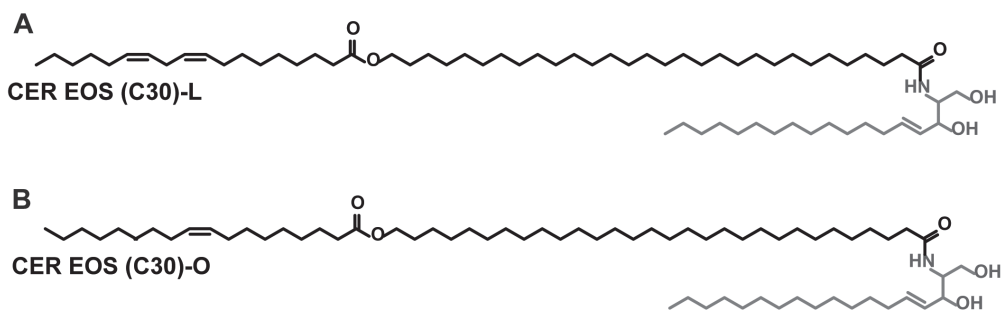


Fig. 1: Molecular structure of the acylCERs used in the study.

The CERs consist of an unsaturated fatty acid esterified to an ω -hydroxy fatty acid acyl chain (black), which is linked to a sphingoid base (grey) via an amide bond. The unsaturated fatty acid is either A) linoleic acid (CER EOS (C30)-L) or B) oleic acid (CER EOS (C30)-O).

models prepared with CER NS easily formed the LPP [44-46]. Furthermore, this composition allowed us to use deuterated CERs, which provide more detailed insight into the lipid phase behavior. Small-angle X-ray diffraction (SAXD) and Fourier transform infrared spectroscopy (FTIR) were used to study the lipid arrangement and phase behavior of the models. The barrier function of the models was assessed by carrying out permeation studies and transepidermal water loss (TEWL) measurements.

EXPERIMENTAL SECTION

Materials

The synthetic CERs used in the study: i) N-(tetracosanoyl)-sphingosine (CER NS C24), ii) CER NS C24 with a deuterated fatty acid chain denoted as D-NS, iii) N-(30-Linoleoyloxy-triacontanoyl)-sphingosine (CER EOS (C30)-L), and iv) CER EOS (C30)-O with deuterated oleate chain denoted as D-EOS, were generously donated by Evonik (Essen, Germany). The CERs had a purity of $\geq 90\%$ (as determined by mass spectrometry). Using mass spectrometry method for CER analysis [47], the CERs had a purity of $\geq 98\%$. CHOL, ethyl-p-aminobenzoate (E-PABA), acetate buffer salts, and the FFAs: palmitic acid (C16), stearic acid (C18), arachidic acid (C20), behenic acid (C22), and lignoceric acid (C24), were purchased from Sigma-Aldrich Chemie GmbH (Schnelldorf, Germany). The perdeuterated FFAs (DFFAs) with chain lengths of C18 and C20 were obtained from Cambridge Isotope Laboratories (Andover, Massachusetts). The DFFAs with chain lengths of C16 and C22 were purchased from Larodan (Malmö, Sweden). The DFFA with a chain length of C24 was obtained from Arc Laboratories B.V. (Apeldoorn, The Netherlands). All organic solvents were of analytical grade. The water was of Millipore quality, obtained through a Milli-Q Integral water purification system with a resistivity of 18 M Ω cm at 25°C (Millipore, Bedford, MA). Nucleopore polycarbonate filter disks (pore size 0.05 μ m) were purchased from Whatman (Kent, UK).

Composition of the model lipid mixtures

SC lipid models were prepared as equimolar mixtures of CER, CHOL, and FFAs. The FFA component comprised of C16, C18, C20, C22, and C24 at relative molar percentages of 1.8, 4.0, 7.6, 47.8, and 38.8 respectively, a composition adapted from the FFA composition in the native SC [17]. The CER fraction of the models differed by the CER EOS concentration (10/30/50/70/90 mol%) and was

counterbalanced with CER NS. The resulting lipid models are named EOS-10, EOS-30, EOS-50, EOS-70, and EOS-90. Secondly, similar models were prepared but with the FFAs replaced by their deuterated counterparts (CER EOS/CER NS/CHOL/DFFAs) denoted by -DFFA as a suffix to the model name. In the third set of models, the fatty acid acyl chain of CER NS was replaced with the deuterated chain (CER EOS/CER D-NS/CHOL/FFAs), resulting in the models identified by the suffix -D-NS. Finally, since CER EOS with deuterated linoleate chain, is not available, the oleate counterpart was used in the preparation of the fourth set of models (CER D-EOS/CER NS/CHOL/FFAs). Therein, the oleate moiety of CER EOS oleate was substituted with the deuterated counterpart and the resulting models are denoted by D- as a prefix to the model name. CER EOS linoleate and oleate are structural analogues (Fig. 1) and have a similar influence on lipid phase behavior in SC models both resulting in similar phase transition temperatures and leading to the formation of LPP in SC models [37, 48]. The composition of the models are shown in table 1.

Table 1: Composition of the various models used in this study. CER:CHOL:FFA mixture is prepared as equimolar. For clarification, the CER EOS concentration in this study refers to the percentage of CER EOS relative to the CER fraction, not the total lipid content.

Lipid model name	Composition and molar ratio (1:1:1)
EOS-10	[EOS(C30)-L 10% + NS(C24) 90%]: CHOL: FFAs
EOS-30	[EOS(C30)-L 30% + NS(C24) 70%]: CHOL: FFAs
EOS-50	[EOS(C30)-L 50% + NS(C24) 50%]: CHOL: FFAs
EOS-70	[EOS(C30)-L 70% + NS(C24) 30%]: CHOL: FFAs
EOS-90	[EOS(C30)-L 90% + NS(C24) 60%]: CHOL: FFAs
EOS-10-DFFA	[EOS(C30)-L 10% + NS(C24) 90%]: CHOL: DFFAs
EOS-30-DFFA	[EOS(C30)-L 30% + NS(C24) 70%]: CHOL: DFFAs
EOS-50-DFFA	[EOS(C30)-L 50% + NS(C24) 50%]: CHOL: DFFAs
EOS-70-DFFA	[EOS(C30)-L 70% + NS(C24) 30%]: CHOL: DFFAs
EOS-90-DFFA	[EOS(C30)-L 90% + NS(C24) 60%]: CHOL: DFFAs
EOS-10-D-NS	[EOS(C30)-L 10% + D-NS(C24) 90%]: CHOL: FFAs
EOS-30-D-NS	[EOS(C30)-L 30% + D-NS(C24) 70%]: CHOL: FFAs
EOS-70-D-NS	[EOS(C30)-L 70% + D-NS(C24) 30%]: CHOL: FFAs
D-EOS-10	[D-EOS(C30)-O 10% + NS(C24) 90%]: CHOL: FFAs
D-EOS-30	[D-EOS(C30)-O 30% + NS(C24) 70%]: CHOL: FFAs
D-EOS-70	[D-EOS(C30)-O 70% + NS(C24) 30%]: CHOL: FFAs

Preparation of samples for permeability studies, X-ray diffraction, and FTIR spectroscopy

For the permeability and X-ray diffraction studies, 0.9mg of the appropriate lipid composition was dissolved in 200 μl hexane:ethanol (2:1) solution, to a final concentration of 4.5 mg/ml. For FTIR spectroscopy, 1.5 mg of the applicable lipid composition was dissolved in chloroform:methanol (2:1) to a concentration of 5 mg/ml. Using a Linomat IV device (Camag, Muttenz, Switzerland) the solution was sprayed on a suitable substrate (nucleopore polycarbonate filter disk with 0.05 μm pore size for the permeability and X-ray studies, and AgBr window for FTIR spectroscopy). It was necessary to use hexane:ethanol as solvent for spraying on the polycarbonate membrane since this membrane is not resistant to chloroform [49]. However, this did not cause any difference in phase behaviour. Spraying was performed at the rate of 14 $\mu\text{l}/\text{sec}$, over an area of 10 x 10 mm^2 , under a gentle stream of nitrogen. An approximate distance of 1 mm was maintained between the nozzle and the spraying surface. The samples were equilibrated at 85 $^{\circ}\text{C}$ for 30 min, which was sufficient to ensure that the lipid mixtures had fully melted, and then gradually cooled to room temperature. Finally, the samples for X-ray studies were hydrated over 27% NaBr in milli-Q water (water vapour) for at least 15 h. While FTIR samples were hydrated in deuterated acetate buffer (pH 5.0) and incubated at 37 $^{\circ}\text{C}$ for at least 15 h to ensure that the samples were fully hydrated. The membranes used in permeability studies were thus hydrated with phosphate-buffered saline inside the flow-through diffusion cell to mimic the in-vivo situation as much as possible [49].

Permeability studies

Permegear in-line diffusion cells (Bethlehem PA, USA) with a diffusion area of 0.28 cm^2 were used for the *in-vitro* permeation studies. The model membranes were mounted in the diffusion cells and hydrated for an hour with the acceptor phase consisting of phosphate-buffered saline (PBS 0.1 M solution: NaCl, Na_2HPO_4 , KH_2PO_4 , and KCl in milli-Q water with a concentration of 8.13, 1.14, 0.20, and 0.19 g/l respectively) at pH 7.4 prior to the experiment. Before use, the PBS was filtered and degassed. The donor compartment consisted of 1400 μl of a saturated E-PABA (0.65mg/ml) in acetate buffer solution (pH 5) and was sealed with an adhesive tape to prevent solvent evaporation. The acceptor phase was constantly stirred and perfused at a flow rate of 2 ml/h through an in-line degasser to remove air bubbles that may form during the experiment. The temperature of the membranes was maintained at 32 $^{\circ}\text{C}$. The acceptor fluid was collected over 15 h at 1-hour intervals. At the end of the diffusion study, the volume per collected

fraction of PBS was determined by weight and the concentration of E-PABA was determined by ultra performance liquid chromatography (UPLC). The flux of E-PABA was calculated using Fick's first law of diffusion [50]. Permeation of multiple samples of each composition was analyzed, $n > 4$. The steady-state flux values were calculated using a time interval between the 5th and 15th hour.

UPLC analysis

UPLC was run with Acquity UPLC systems (Waters Co., Milford, MA, USA) for the analysis of E-PABA. The UPLC systems consisted of a quaternary solvent manager (a high-pressure pump), a tunable ultraviolet/visible absorbance detector, and a sample manager. The stationary phase consisted of a UPLC special analytical column packed with 1.7 μm , bridged, ethyl siloxane, hybrid particles. The column temperature was set at 40 °C. The mobile phase was composed of a mixture of 0.1% trifluoroacetic acid in acetonitrile: milli-Q water at 40:60 (v/v) ratio. The flow rate of the mobile phase was 1 ml/min. 10 μl of the sample was injected on the column. The detector wavelength was set at 286 nm. Data were collected and processed by MassLynx and TargetLynx software V4.1 SCN951 (Waters Co., Milford, USA).

The standard stock solution of E-PABA, 0.5 mg/ml was prepared in a 1:1 solution of methanol and milli-Q. Ten different concentrations were prepared by serial dilutions from the stock, with milli-Q water, to plot the standard curve. The linearity of the relationship was evaluated in a concentration range between 0.1 -10 $\mu\text{g/ml}$ covering the range of concentrations obtained when analyzing the concentration of E-PABA permeating the model membranes. The calibration curves were obtained using least square linear regression fitting and the linearity was confirmed with the R^2 values. R^2 value very close to 1 indicates excellent linearity.

The UPLC method was previously validated for E-PABA analysis as per ICH (International conference on harmonization) guidelines concerning linearity, precision, limit of detection (LOD), and limit of quantification (LOQ) [46, 51, 52].

TEWL measurements

An AquaFlux (AF200, Biox Systems Ltd., London, UK) was used to measure the water loss from the lipid models. The measurement has been previously described elsewhere [50]. Briefly, the sprayed membranes were mounted in flow-through diffusion cells, which were subsequently filled with milli-Q water. The cells were left to hydrate for at least 30min before measuring. The TEWL device was then coupled vertically with the donor compartment of the diffusion

cell using a special measurement cap (Biox Systems Limited, UK) in order to seal the compartment and ensure vapour tight connectivity. The TEWL values for the models studied were recorded for 30 min. The final 10 min of the measurement was used to calculate the TEWL value, $n = 7$.

Data analysis for the permeability and TEWL measurements.

One-way ANOVA with Bonferroni's multiple comparison test was performed to analyze the permeability and TEWL data. Differences in mean are considered statistically significant when $P < 0.05$.

FTIR measurements

FTIR spectra were acquired on a Varian 670-IR spectrometer (Agilent Technologies, Inc., Santa Clara, CA) equipped with a broad-band mercury cadmium telluride detector, cooled by liquid nitrogen. The sample was kept under a continuous dry air purge, starting 30 min before data acquisition. The spectra were generated in the transmission mode by the coaddition of 256 interferograms, at a resolution of 1 cm^{-1} , collected over 4 min. To determine the phase transitions in relation to the temperature, the spectra were collected between $0 - 100 \text{ }^\circ\text{C}$ at a heating rate of $0.25 \text{ }^\circ\text{C}/\text{min}$, resulting in a $1 \text{ }^\circ\text{C}$ temperature rise per recorded spectrum. Samples were measured over a range of $600-4000 \text{ cm}^{-1}$. The spectra were deconvoluted using a half-width of 4 cm^{-1} , and an enhancement factor of 1.6. The software used was Agilent resolution pro (Agilent Technologies, Palo Alto CA, USA). The conformational ordering and phase transition of the lipid chains were obtained by examination of the protiated methylene symmetric stretching modes observed at $\sim 2850 \text{ cm}^{-1}$ and the deuterated symmetric stretching modes at $\sim 2090 \text{ cm}^{-1}$, referred to as $\nu_s\text{CH}_2$ and $\nu_s\text{CD}_2$ modes respectively. The linear regression curve fitting method was used to determine the mid-transition temperature as described previously [53]. The CH_2 scissoring mode (δCH_2), $1462-1473 \text{ cm}^{-1}$ and CD_2 scissoring mode (δCD_2), $1085-1095 \text{ cm}^{-1}$ were analyzed to evaluate the lateral packing and mixing properties of the lipid chains respectively. Multiple samples of each composition were measured, $n > 2$.

SAXD studies

To determine the long-range ordering, SAXD experiments were conducted at the European Synchrotron Radiation Facility (ESRF, Grenoble) at station BM26B. The X-ray wavelength (λ) was 0.1033 nm and the sample-to-detector distance was 2.1 m . Diffraction patterns were recorded using a Pilatus 1M detector. The spatial calibration of the detector was performed using silver behenate. Samples were

measured for 90 s. The scattering intensity (I) was measured as a function of the scattering vector (q) which is proportional to the scattering angle (θ) according to the equation, defined as $q = \frac{4\pi \sin \theta}{\lambda}$. From the positions of a series of equidistant peaks (q_h), the periodicity of a lamellar phase was calculated using the equation $d = \frac{2h\pi}{q_h}$ in which h is the order of the diffraction peak. Samples were prepared and measured in triplicate. The peak intensities attributed to the LPP were determined from the SAXD patterns, fitted with a Voigt function in the software Fityk [54].

RESULTS

A high concentration of CER EOS increases the permeability of the SC model membranes

To evaluate the effect of CER EOS concentration on the permeability of the model membranes, we compared their permeability to E-PABA. The average fluxes of E-PABA across the models with a gradual increase in CER EOS concentration are displayed in Fig. 2A. The E-PABA average steady-state flux values are plotted in Fig. 2B. Increasing the CER EOS concentration from 10 to 30% of the total CER fraction in the model membrane resulted in no significant difference in permeability (7.8 ± 2.9 to $8.2 \pm 4.8 \mu\text{g}/\text{cm}^2/\text{h}$). On further increase in CER EOS concentration to 50, 70, and 90%, the permeability increased (14.5 ± 8.6 , 22.2 ± 5.0 and $25.2 \pm 3.3 \mu\text{g}/\text{cm}^2/\text{h}$ respectively), with EOS-70 and EOS-90 being significantly more permeable than EOS-10 and EOS-30.

Water transport was also monitored by performing TEWL measurements. The water loss across EOS-90 and EOS-70 was 3.5 ± 0.2 and $2.9 \pm 0.5 \mu\text{g}/\text{m}^2/\text{h}$ respectively, both significantly higher than that across EOS-30 ($1.8 \pm 0.2 \mu\text{g}/\text{m}^2/\text{h}$). See Fig. 2C.

The phase transition temperature and packing density of the lipid chains are higher with increasing CER EOS concentration

The packing density of the lipids is important for understanding the changes in permeability at increasing CER EOS content. In the FTIR spectrum, $\nu_s\text{CH}_2$ and δCH_2 frequencies provide information about lipid chain conformational ordering and packing density [55-57]. The thermotropic response of the $\nu_s\text{CH}_2$ modes of EOS-10 and EOS-90 are plotted in Fig. 3A. The initial wavenumber of the fully protiated models appeared below 2850 cm^{-1} indicating highly ordered hydrocarbon chains [56, 58]. EOS-90 $\nu_s\text{CH}_2$ wavenumber was higher than that of EOS-10 suggesting lower conformational ordering of the lipid chains, but the

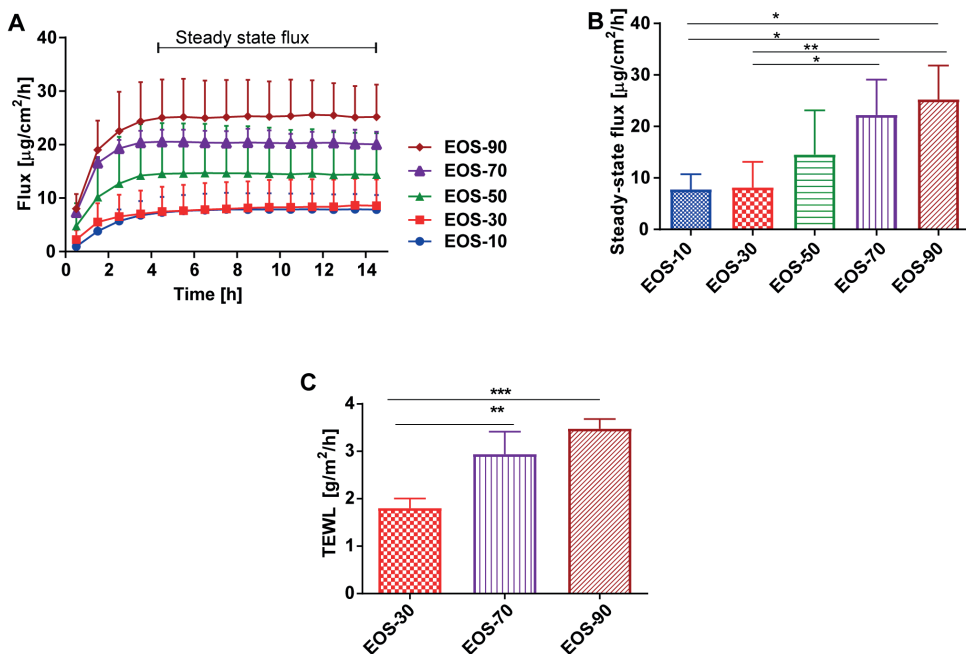


Fig. 2: Permeability of the model membranes.

A) Average flux of E-PABA across the model membranes over 15 h. B) The average steady-state flux of E-PABA across the model membranes (5-15 h). Data presented as the mean \pm SD, $n \geq 4$. E-PABA steady-state flux was significantly higher in EOS-70 and EOS-90. C) TEWL across the model membranes, EOS-70 and EOS-90 showing significantly higher permeability compared to EOS-30, $n \geq 3$, [$*P < 0.05$, $**P < 0.01$, $***P < 0.001$].

difference was not significant. The increase in temperature between 20 and 40 $^{\circ}\text{C}$ resulted in an approximate 1 cm^{-1} rise in the wavenumber, representing the orthorhombic-hexagonal phase transition. Further increase in temperature resulted in a larger wavenumber shift of 3-4 cm^{-1} between 60 and 80 $^{\circ}\text{C}$. This indicates the transition from a hexagonal to the disordered liquid phase [59, 60]. The midpoint temperatures of the orthorhombic-hexagonal phase transition ($T_{\text{M,OR-HEX}}$) in the various fully protiated models are presented in Fig. 3B. The $T_{\text{M,OR-HEX}}$ increased gradually with increasing CER EOS concentration.

Concerning the lateral packing of the lipid chains, the δCH_2 mode was split into two peaks, centered at $\sim 1462 \text{ cm}^{-1}$ and 1473 cm^{-1} signifying an orthorhombic packing [59, 61]. This doublet is a direct result of short-range coupling between adjacent hydrocarbon chains of the same isotope [61]. While the δCH_2 mode of the less dense hexagonal packing is characterized by a singlet positioned at $\sim 1467 \text{ cm}^{-1}$ in the spectrum. The δCH_2 modes of the various models at 10 $^{\circ}\text{C}$

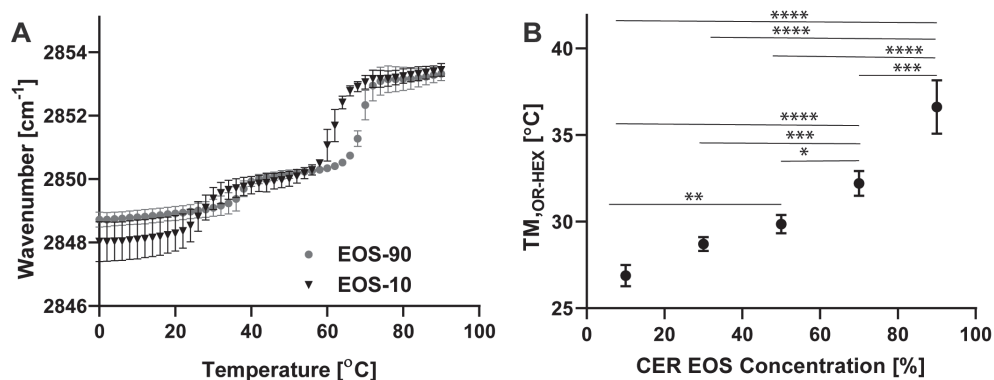


Fig. 3: The thermotropic response of the $\nu_s\text{CH}_2$ modes and midpoint temperatures of the orthorhombic-hexagonal phase transition ($T_{M,OR-HEX}$).

A) The initial wavenumber is higher in the EOS-90 than EOS-10 suggesting lower conformational ordering of the lipid chains in EOS-10. B) The $T_{M,OR-HEX}$ increases with CER EOS concentration. Differences between EOS 10 and 30, and between EOS 30 and 50 were not significant, while differences between EOS 10 and 50, EOS 10 and 70, EOS 10 and 90, EOS 30 and 70, EOS 30 and 90, EOS 50 and 70, EOS 50 and 90, and EOS 70 and 90 were significant. $n \geq 3$, [* $P < 0.05$, ** $P < 0.01$, *** $P < 0.001$, **** $P < 0.0001$].

and 32 °C are presented in Fig. 4A and B respectively. At 10 °C, the δCH_2 modes of all protiated models displayed two strong peaks typical of orthorhombic packing. At 32 °C, the δCH_2 modes in the spectrum of EOS-10, EOS-30, and EOS-50 exhibited strong central asymmetric peaks positioned at $\sim 1467\text{ cm}^{-1}$ indicating an increased fraction of lipids adopting a hexagonal lateral packing at the expense of the fraction of lipids forming an orthorhombic packing (Fig. 4B). In contrast, EOS-70 and EOS-90 δCH_2 modes retained the two characteristic peaks attributed to orthorhombic packing.

The proportion of the liquid phase increases with CER EOS concentration

In a lipid mixture, selective deuteration of the various components enables the simultaneous monitoring of the conformational ordering and phase behavior of individual species [56]. This is because the vibrational energy of protiated and deuterated chains is sufficiently different when detected in the infrared spectrum. We deuterated the FFA chains in the various models. The compositions of the resulting samples are shown in table 1. The $\nu_s\text{CD}_2$ and $\nu_s\text{CH}_2$ peak positions attributed to DFFA and CER chains respectively were analyzed in the temperature range between 0 to 90 °C (Fig. 5A). At the initial temperature, $\nu_s\text{CD}_2$ peak positions were consistent with previous reports of high conformational ordering of the

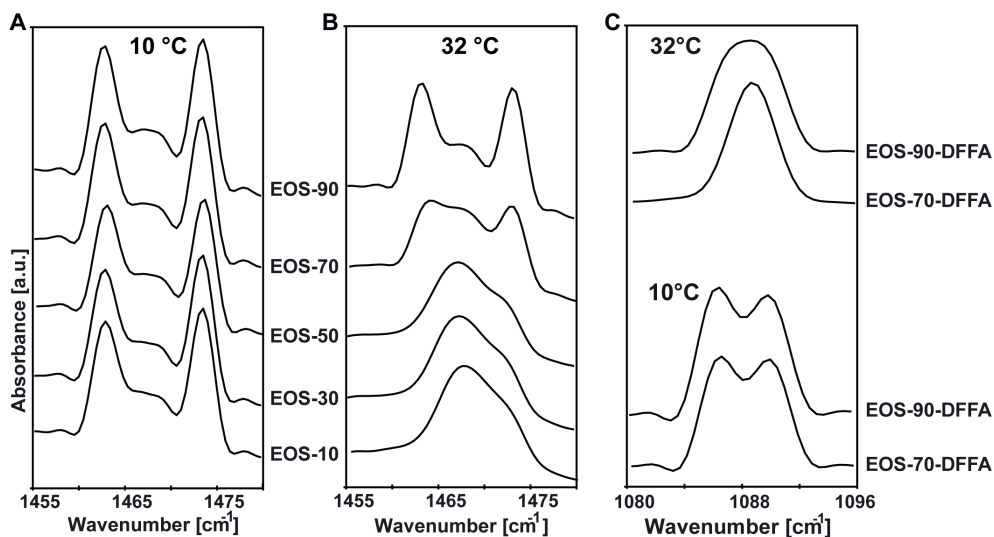


Fig. 4: δCH_2 and δCD_2 modes of the fully protiated and deuterated lipid models.

A) The δCH_2 frequencies at 10 °C display two distinct bands at approximately 1462 cm^{-1} and 1473 cm^{-1} indicating an orthorhombic lateral packing. B) At 32 °C (physiological temperature), EOS-10, 30, and 50 display a strong central peak indicating that a significant proportion of the lipids adopt the hexagonal phase. C) At 10 °C, EOS-70-DFFA and EOS-90 DFFA δCD_2 mode display weak splitting compared with the strong splitting of the δCD_2 mode of DFFA mixture [46] and transformed into single peaks at 32 °C, indicating that the FFAs are not phase separated.

methylene chains [46] indicating that the DFFA chains were highly crystalline, even at high CER EOS level. The $\nu_s\text{CH}_2$ mode of EOS-10-DFFA and EOS-30-DFFA revealed rearrangement of the protiated chain just before the hexagonal-liquid phase transition (between 60 and 80 °C), attributed to a high concentration of CER NS, as reported previously [46]. As the continued presence of orthorhombic packing in EOS-70 and EOS-90 at 32 °C in the fully protiated mixtures (Fig. 4B) could result from phase-separated FFA, we analyzed the δCH_2 and δDH_2 modes of the CER EOS/CER NS/CHOL/DFFAs mixtures. When deuterated and protiated chains are mixed in an orthorhombic lattice, the short-range coupling and peak splitting described in section 3.4 are eliminated as adjacent δCH_2 and δDH_2 modes will not interact due to differences in vibrational energy. Analysis of the CD_2 modes of EOS-70-DFFA and EOS-90-DFFA at 10 °C (Fig. 4C) showed significantly reduced peak splitting width compared with the maximum peak splitting in a fully deuterated environment that has been previously determined [46], indicating extensive mixing of the CERs and DFFA chains. At 32 °C, the CD_2 modes of EOS-70-DFFA and EOS-90-DFFA transformed to single peaks. This indicates that the orthorhombic packing at elevated temperatures cannot be due to phase-separated FFA.

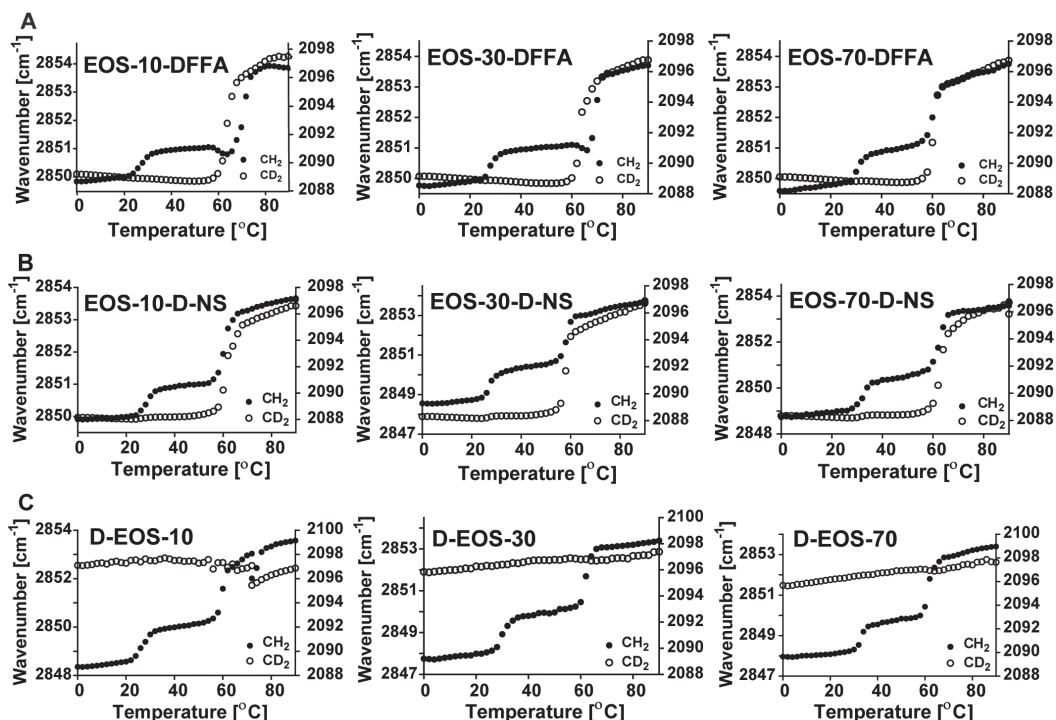


Fig. 5: Thermotropic response of the $\nu_5\text{CH}_2$ and $\nu_5\text{CD}_2$ modes of the partially deuterated lipid models.

The CH_2 (filled circle) and the CD_2 (open circle) peak positions are plotted on the primary y-axis and secondary y-axis respectively. The phase transition temperatures of the protiated and deuterated chains in the lipid models are displayed. A) FFA chains were deuterated. B) CER NS with deuterated C24 acyl chain. C) Deuterated oleate chain of CER EOS.

Lipid mixtures including CER NS with a deuterated C24 acyl chain were also examined. The $\nu_5\text{CD}_2$ modes of EOS-10 D-NS, EOS-30 D-NS, and EOS-70 D-NS were located initially at $\sim 2088\text{ cm}^{-1}$ (Fig. 5B) indicating that CER NS chains are highly conformationally ordered in the lipid models, even at high CER EOS concentration. As the temperature increased, the order-disorder transition of the protiated chains and the deuterated CER NS chains occurred in the same temperature range. Finally, we analyzed the spectra of the lipid mixtures in which the linoleate moiety of CER EOS was replaced by deuterated oleate. The thermotropic response of the $\nu_5\text{CH}_2$ and $\nu_5\text{CD}_2$ modes of D-EOS-10, D-EOS-30, and D-EOS70 are displayed in Fig. 5C.

In the models with deuterated oleate chains, the $\nu_5\text{CD}_2$ mode was located at a higher wavenumber, $\sim 2097\text{ cm}^{-1}$ from 0 until $90\text{ }^\circ\text{C}$, indicating that the oleate chains were disordered across the temperature range. Analysis of the $\nu_5\text{CD}_2$ peak

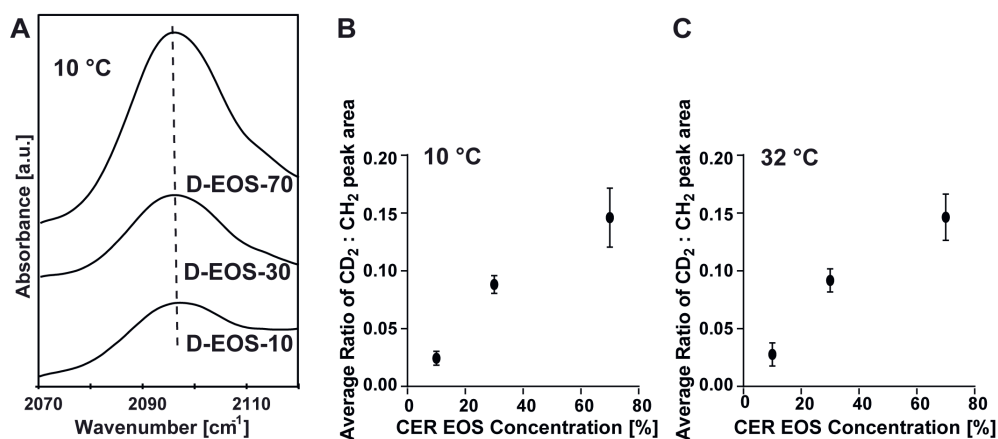


Fig. 6: Peak position of $\nu_s\text{CD}_2$, peak area ratio of $\nu_s\text{CD}_2$ to $\nu_s\text{CH}_2$, and correlation to permeability.

A) Mixtures with deuterated oleate chains of CER EOS show no shift in peak positions with increasing CER EOS concentration. B) and C) The average ratio of CD_2 (attributed to the disordered oleate) to CH_2 symmetric stretching peak area at 10 and 32 °C indicates an increase in the proportion of lipid fraction in the liquid phase with CER EOS concentration.

position at 10 °C revealed no shift in peak positions with increasing CER EOS-O concentration (Fig. 6A).

To evaluate the proportion of the liquid phase in the models, we compared the ratio of $\nu_s\text{CD}_2$ peak area (disordered) to $\nu_s\text{CH}_2$ peak area (crystalline) in the mixtures with deuterated oleate chains at 10 and 32 °C (Fig. 6B and C). There was a gradual increase in the ratio of the liquid/crystalline symmetric stretching peak area with increasing CER EOS-O content.

CER EOS concentration affects the LPP repeat distance

The influence of CER EOS concentration on the lamellar phase behavior of SC lipid models was studied. The SAXD profiles of the models with a gradual increase in CER EOS content are displayed in Fig. 7A-E. In CER EOS-10, the lipids form both the SPP and LPP with repeat distances of 5.4 and 12.2 nm respectively. Increasing the concentration of CER EOS from 10 to 30% resulted in the disappearance of the SPP. No significant difference in LPP repeat distance was observed between EOS-10 and EOS-30. Further increase in CER EOS concentration to 50, 70, and 90%, resulted in a gradual increase in LPP repeat distance (Fig. 7F) and the intensity ratio between the 2nd and 1st order of the LPP decreased concurrently. The diffraction curve of CER EOS-90, showed the 6th order to be absent, while the 1st order intensity surpassed the 2nd order, thus deviating from the characteristic

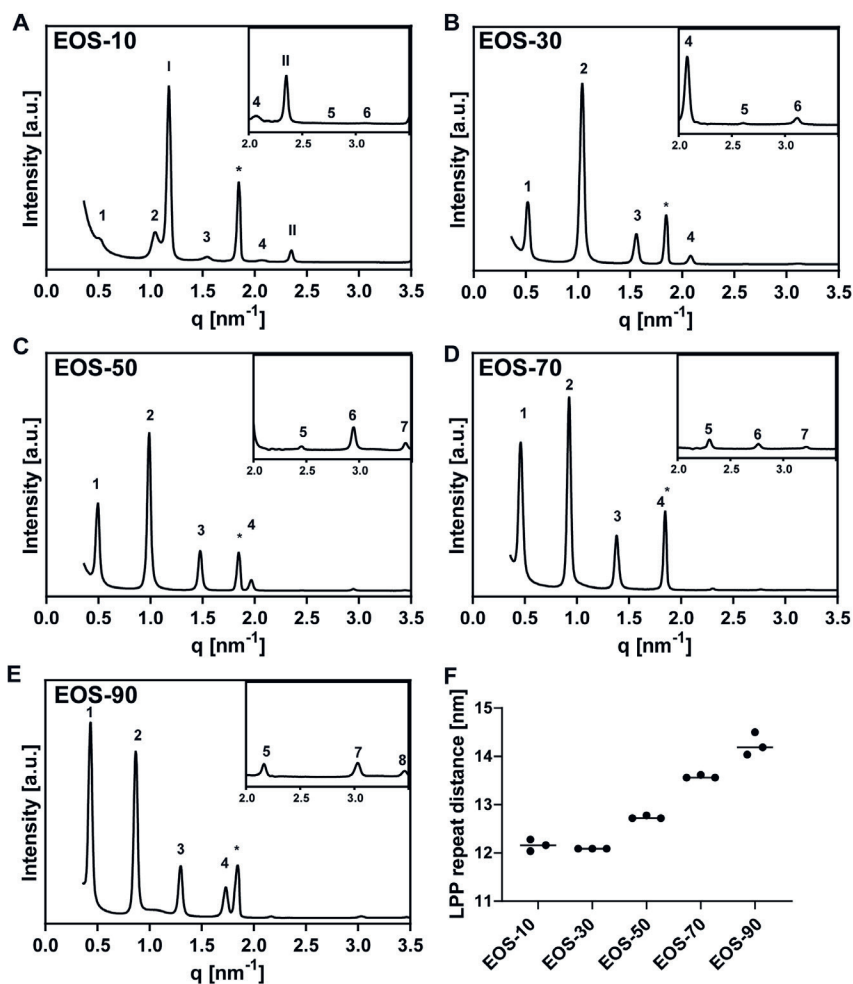


Fig. 7: X-ray diffraction profile of the lipid models.

The arabic numbers 1-8 indicate the diffraction orders of the LPP, while the roman numbers I and II indicate the diffraction orders of the SPP. A) In the diffraction profile of EOS-10, a series of diffraction peaks positioned at $q = 0.52, 1.04, 1.52, 2.09, 2.53,$ and 3.03 nm^{-1} indicate the 1st, 2nd, 3rd, 4th, 5th, and 6th diffraction orders attributed to the LPP with a repeat distance of 12.2 nm and peaks positioned at $q = 1.17$ and 2.34 nm^{-1} indicate the 1st and 2nd diffraction orders attributed to the SPP with a repeat distance of 5.4 nm. B) In the diffraction profile of EOS-30, the peak positions at $q = 0.52, 1.03, 1.56, 2.07, 2.60,$ and 3.11 nm^{-1} indicate the 1st-6th diffraction orders attributed to the LPP with a repeat distance of 12.2 nm. C) In the diffraction pattern of EOS-50, the peak positions at $q = 0.49, 0.99, 1.48, 1.97, 2.46, 2.95,$ and 3.45 nm^{-1} are attributed to 1st-7th diffraction orders of the LPP with a repeat distance of 12.7 nm. D) In the diffraction pattern of EOS-70, the reflections at $q = 0.46, 0.92, 1.38, 1.84$ (overlapping the CHOL peak), $2.3, 2.76,$ and 3.22 nm^{-1} are attributed to the 1st-7th diffraction orders of the LPP with a repeat distance of 13.6 nm. E) In the diffraction pattern of EOS-90, the peak positions at $q = 0.43, 0.87, 1.31, 1.73, 2.16, 3.02,$ and 3.46 nm^{-1} are attributed to 1st, 2nd, 3rd, 4th, 5th, 7th, and 8th diffraction orders of the LPP with a repeat distance of 14.4 nm. The 6th order peak was absent, The reflections at $q = 1.85 \text{ nm}^{-1}$ indicated by * in all the models are attributed to phase-separated CHOL. F) Graph showing an increase of LPP repeat distance with CER EOS concentration.

LPP intensity distribution (2nd order peak taller than 1st and 3rd order peaks), which has been described previously [46, 62].

DISCUSSION

For the first time, the influence of a gradual increase of CER EOS over a wide range of concentrations, namely from 10 % to 90% of the CER fraction of SC models was investigated. Despite the crucial role of CER EOS in the LPP formation, its influence on lipid phase behavior and barrier function are not entirely comprehended. To understand the skin barrier thoroughly, knowledge of the molecular arrangement of the lamellar unit cell is vital [12]. Previous experiments have identified that the linoleate chain of CER EOS is located in the inner head group regions and in the central region of the trilayer LPP, while the C(30) acyl chain extends from the borders of the unit cell towards the central layer [12, 63]. It has been suggested that the linoleate/oleate moiety in the matrix could be a key element contributing to the SC impermeability by acting as an obstacle for the diffusion of hydrophilic compounds through the SC and traps for the apolar species [42]. The results from the current study have shown that this hypothesis does not hold when CER EOS concentration is $\geq 70\%$.

The SC lipid matrix is endowed with a characteristic composition and organization required for the barrier function. The physiological concentration of CER EOS in the SC is associated with low permeability indicating good barrier function. Data from our study shows that the barrier capability of the SC model is maintained somewhat up to a 50% increase in CER EOS concentration. Such robustness is an advantage to withstand the numerous challenges faced by the body due to the external environment.

Effect of CER EOS concentration on barrier function

In SC lipid model systems, CER EOS induces a co-existence of crystalline and disordered liquid domains. We examined the impact of increasing CER EOS concentration on the permeability of the SC lipid models. The results show that the permeability of the membrane to E-PABA did not differ when CER EOS concentration was raised from 10 to 30% of the total CER content. Similarly, it was reported that the permeability of indomethacin and theophylline through a complex lipid model was not improved when the concentration of either individual acylCER or an acylCER mixture was raised above the physiological concentration to 30% [43]. In contrast, a previous study demonstrated that the

permeability of a SC model prepared with pig CERs with CER EOS concentration of 14% was reduced when an additional 20% mol CER EOS was incorporated [64]. However, in this case, the difference is not solely due to the difference in the acylCER content as isolated pig CERs were used, which contain a wide distribution in chain lengths, while the additional synthetic CER EOS had only a single-chain length. Thus a change in chain length distribution might also have affected the permeability as demonstrated previously [64]. Opalka et al. also reported a reduction in the permeability of a simple SC model membrane when the concentration of CER EOS was increased from 10 to 30% [31]. In their study, there was also a reduction in the LPP repeat distance when increasing the CER EOS content from 10 to 30%, while we observed no difference. The LPP peak intensity distribution in their study also differed from ours, signifying a different structure.

In the present study, E-PABA steady-state flux only increased when CER EOS concentration was raised to 50%, becoming significantly higher when raised to $\geq 70\%$. This finding was corroborated by the TEWL values, which were also significantly higher for EOS-70 and EOS-90.

Effect of CER EOS concentration on lateral lipid organization

Several studies have associated a higher lipid chain packing density with reduced permeability of SC model membranes [32, 64, 65]. This relationship was not observed in the current study. The remarkably high permeability of EOS-70 and EOS-90 was irrespective of the presence of a high concentration of lipids forming an orthorhombic phase at 32 °C, the physiological temperature at which the permeation studies were carried out. Analysis of the FTIR data showed that the increased permeability was not due to phase separation as the hexagonal-liquid phase transition of FFA and CERs occurred in the same temperature range and the scissoring vibrations demonstrated mixing of the CERs and FFA chains in the EOS-70 and EOS-90 models. Thus, the delayed orthorhombic-hexagonal phase transition observed in the δCD_2 modes of EOS-70 and EOS-90 may be attributed to the increased level of the exceptionally long acyl chain of CER EOS.

To study the behavior of the unsaturated C18 acyl chain moiety of CER EOS, we used mixtures in which the oleate moiety of CER EOS-O was deuterated (Table 1). Several studies have reported a similar phase behavior for CER EOS-L and CER EOS-O containing mixtures. de Sousa et al. [48] analyzed equimolar mixtures of CERs, CHOL, and FFAs. The CER fraction contained either 30 mol% CER EOS-L or 30 mol% CER EOS-O. The results showed that the model prepared

with CER EOS-L and that prepared with the oleate analogue have a similar lipid phase behavior, both resulting in similar phase transition temperatures and leading to exclusive formation of the LPP with similar repeat distance. Bouwstra et al. [37] reported similar phase behavior in model mixtures with human CERs containing either synthetic CER EOS-L or synthetic CER EOS-O. In both mixtures, the LPP, as well as the SPP with very similar repeat distances, were formed. In addition using CER EOS-L, with the linoleate chain deuterated, Janssens et al. [41] determined that the linoleate moiety of CER EOS-L was already disordered at 20 °C indicated by the high δCD_2 wavenumber of 2099 cm^{-1} , which were very similar values as that of the deuterated oleate chain of CER EOS in this present study. Based on these studies we conclude that CER EOS linoleate and CER EOS oleate are very similar as far as the conformational ordering and the phase behavior is concerned, which are the properties we focused on in the present study.

In the spectrum of CER D-EOS-O/CER NS/CHOL/FFAs mixtures, the deuterated oleate chains were in the liquid phase in the entire temperature range studied (0-100°C). Despite increasing CER EOS concentration, there was no increasing shift in the $\nu_5\text{CD}_2$ frequencies of the deuterated oleate chains to indicate any further degree of disordering. In mixtures with the deuterated oleate the $\text{CD}_2:\text{CH}_2$ peak area ratio is an indication of the proportion of the liquid phase; an increase in this ratio with CER EOS concentration is observed.

Based on the carbon number in the model mixtures, the total fraction of CER moiety that is liquid in EOS-10 is 2.7% of the total CER volume and 1% of the total lipid volume given the equimolar ratio of CERs, FFAs, and CHOL. Likewise, the liquid fraction of the total lipids in EOS-30 and EOS-70 are 2.7% and 6.4% respectively. At very high CER EOS concentration ($\geq 70\%$), the disordered linoleate located in the inner head group regions and the central layer of the LPP probably can no longer act as isolated fluid droplets that trap materials. Rather, there is a sufficient fraction of the disordered phase to increase the transport of substances along the inner headgroup region through the SC model membrane. Thus, the increased permeability of the SC models when CER EOS concentration is increased may be attributed to the increased proportion of the liquid phase. Our data demonstrate that the contribution of the increased fraction of lipids forming a disordered phase impacted more the barrier than the higher fraction of lipids forming the orthorhombic phase.

Effect of CER EOS concentration on lamellar organization

To gain insight into the relationship between SC lipid composition and lipid organization, SC model systems based on either isolated CERs or synthetic CERs are used [32, 50, 62, 66]. The SAXD peaks' position and their intensity can provide information about the lamellar structure within a sample [67]. In the present study, a two CER subclass model, EOS-10, which contained near physiological acylCER concentration formed both the SPP and LPP, mimicking the lamellar organization found in the extracellular lipid of native human SC. A previous study also reported the presence of the SPP and LPP in a simple five-component SC model (CER EOS/CER NS/CHOL/FFA(C24)/CHOL sulphate) with CER EOS also constituting 10% of the CER content [31]. In that same study, a more complex SC model (with a higher number of CERs and FFAs subclasses) also containing 10% CER EOS did not exhibit the formation of the LPP. Only when a mixture of acylCERs with different sphingoid bases was incorporated in the complex model could both the SPP and LPP be formed. In contrast, other complex SC models mimicking porcine [50, 62, 66] or human SC [32] CER composition incorporating a single acylCER subclass (15% CER EOS) or even 7% CER EOS in diseased skin model [32], resulted in the formation of both the SPP and LPP. The difference in the lipid organization obtained for SC models containing single acylCER may be due to the differences in the preparation method as previously reported [46]. The model prepared with an acylCER mixture may be less sensitive to such differences in the preparation method as seen by its formation of both the SPP and LPP.

When we increased CER EOS concentration from 10 to 30%, only the LPP was present. Exclusive formation of the LPP has been associated with a high content of CER EOS in SC models containing 30-40% CER EOS in their CER fraction [31, 44, 45, 62, 68]. The LPP diffraction peaks of EOS-10 and EOS-30 exhibited the intensity distribution corresponding to that in the unit cell of a complex SC model and the native SC LPP (2nd order peak more intense than 1st and 3rd order peaks) as described previously [46, 62] indicating similarity in the basic LPP structure. This finding supports the use of simple models with fewer components for a more detailed evaluation of the effect of individual lipid components on the lipid organization of SC models. Simple SC models modified in composition to form exclusively the LPP have been employed for a detailed study of the LPP structure, lipid arrangement, and molecular interaction within the LPP [12, 42, 45, 46, 68]. However, when CER EOS concentration was raised to 90 mol% the LPP intensity distribution deviated. The 1st order LPP peak became more intense than the 2nd. Together with the very long repeat distance (14.4 nm), this demonstrates that the lipids form a different molecular organization than the typical SC's LPP structure.

CONCLUSIONS

In the present paper, we have advanced the previously reported studies of disordered lipid domains in the crystalline SC model, attributed to the unsaturated fatty acid moiety of CER EOS. Increasing CER EOS concentration induced a higher fraction of lipids forming orthorhombic and liquid phases at the expense of the hexagonal phase. Only when CER EOS concentration was raised to $\geq 70\%$, did the permeability of the SC model increase significantly. This could be attributed to the increased fraction of lipids forming a liquid phase. Such sturdiness contributes to the skin's primary function which is to protect the body from the invasion of pathogens and other harmful substances in the external environment as well as preventing uncontrolled loss of fluid from the body.

ACKNOWLEDGEMENTS

We thank the company Evonik for the donation of several CER subclasses. We also acknowledge the staff at the DUBBLE beamline 26B at the ESRF, Grenoble, France for assisting with the X-ray diffraction measurements.

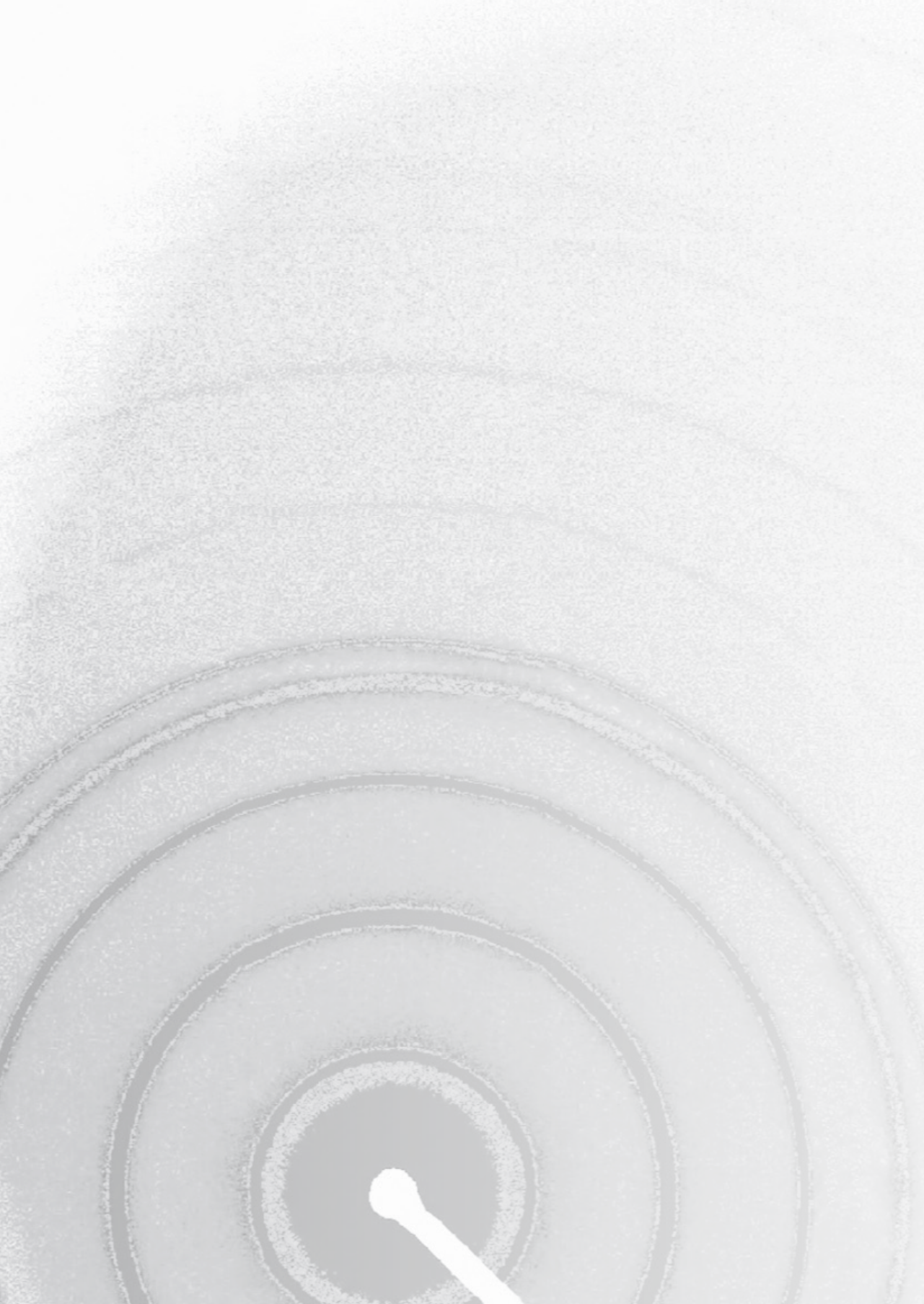
REFERENCES

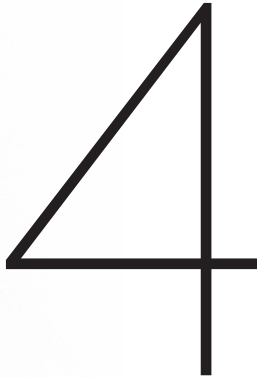
1. Elias, P. M., Stratum corneum defensive functions: an integrated view. *J. Invest. Dermatol.* **2005**, *125* (2), 183-200.
2. Baroni, A.; Buommino, E.; De Gregorio, V.; Ruocco, E.; Ruocco, V.; Wolf, R., Structure, and function of the epidermis related to barrier properties. *Clin. Dermatol.* **2012**, *30* (3), 257-62.
3. Madison, K. C., Barrier function of the skin: "la raison d'être" of the epidermis. *J. Invest. Dermatol.* **2003**, *121* (2), 231-41.
4. Bodde, H. E.; Kruithof, M. A. M.; Brussee, J.; Koerten, H. K., Visualization of normal and enhanced HgCl₂ transport through human-skin invitro. *Int. J. Pharm.* **1989**, *53* (1), 13-24.
5. Talreja, P. S.; Kleene, N. K.; Pickens, W. L.; Wang, T. F.; Kasting, G. B., Visualization of the lipid barrier and measurement of lipid pathlength in human stratum corneum. *AAPS Pharmsci.* **2001**, *3* (2), art. no. 13.
6. Proksch, E.; Brandner, J. M.; Jensen, J. M., The skin: an indispensable barrier. *Exp. Dermatol.* **2008**, *17* (12), 1063-72.
7. Wickert, R. R.; Visscher, M. O., Structure and function of the epidermal barrier. *Am J Infect Control* **2006**, *34* (10), S98-S110.
8. Bouwstra, J. A.; Gooris, G. S.; van der Spek, J. A.; Bras, W., Structural investigations of human stratum corneum by small-angle X-ray scattering. *J. Invest. Dermatol.* **1991**, *97* (6), 1005-12.
9. White, S. H.; Mirejovsky, D.; King, G. I., Structure of lamellar lipid domains and corneocyte envelopes of murine stratum corneum. An X-ray diffraction study. *Biochemistry* **1988**, *27* (10), 3725-32.
10. de Jager, M.; Groenink, W.; Bielsa i Guivernau, R.; Andersson, E.; Angelova, N.; Ponec, M.; Bouwstra, J., A novel in vitro percutaneous penetration model: evaluation of barrier properties with p-aminobenzoic acid and two of its derivatives. *Pharm. Res.* **2006**, *23* (5), 951-60.
11. Groen, D.; Poole, D. S.; Gooris, G. S.; Bouwstra, J. A., Is an orthorhombic lateral packing and a proper lamellar organization important for the skin barrier function? *Biochim. Biophys. Acta* **2011**, *1808* (6), 1529-1537.
12. Mojumdar, E. H.; Gooris, G. S.; Groen, D.; Barlow, D. J.; Lawrence, M. J.; Deme, B.; Bouwstra, J. A., Stratum corneum lipid matrix: Location of acyl ceramide and cholesterol in the unit cell of the long periodicity phase. *Biochim. Biophys. Acta* **2016**, *1858* (8), 1926-34.
13. Madison, K. C.; Swartzendruber, D. C.; Wertz, P. W.; Downing, D. T., Presence of intact intercellular lipid lamellae in the upper layers of the stratum corneum. *J. Invest. Dermatol.* **1987**, *88* (6), 714-8.
14. Damien, F.; Boncheva, M., The extent of orthorhombic lipid phases in the stratum corneum determines the barrier efficiency of human skin in vivo. *J. Invest. Dermatol.* **2010**, *130* (2), 611-614.
15. Weerheim, A.; Ponec, M., Determination of stratum corneum lipid profile by tape stripping in combination with high-performance thin-layer chromatography. *Arch. Dermatol. Res.* **2001**, *293* (4), 191-199.
16. Coderch, L.; López, O.; de la Maza, A.; Parra, J. L., Ceramides and Skin Function. *Am. J. Clin. Dermatol.* **2003**, *4* (2), 107-129.
17. Wertz, P.W.; Downing, D.T., *Physiology, biochemistry and molecular biology of the skin.* second ed.; Oxford University Press: New York, 1991; Vol. 1, p 205-236.

18. Norlen, L.; Nicander, I.; Lundsjo, A.; Cronholm, T.; Forslind, B., A new HPLC-based method for the quantitative analysis of inner stratum corneum lipids with special reference to the free fatty acid fraction. *Arch. Dermatol. Res.* **1998**, *290* (9), 508-16.
19. Masukawa, Y.; Narita, H.; Shimizu, E.; Kondo, N.; Sugai, Y.; Oba, T.; Homma, R.; Ishikawa, J.; Takagi, Y.; Kitahara, T.; Takema, Y.; Kita, K., Characterization of overall ceramide species in human Stratum corneum. *J. Lipid Res.* **2008**, *49* (7), 1466-1476.
20. Rabionet, M.; Gorgas, K.; Sandhoff, R., Ceramide synthesis in the epidermis. *Biochim. Biophys. Acta* **2014**, *1841* (3), 422-34.
21. Robson, K. J.; Stewart, M. E.; Michelsen, S.; Lazo, N. D.; Downing, D. T., 6-Hydroxy-4-sphingenine in human epidermal ceramides. *J. Lipid Res.* **1994**, *35* (11), 2060-8.
22. Stewart, M. E.; Downing, D. T., A new 6-hydroxy-4-sphingenine-containing ceramide in human skin. *J. Lipid Res.* **1999**, *40* (8), 1434-9.
23. van Smeden, J.; Hoppel, L.; van der Heijden, R.; Hankemeier, T.; Vreeken, R. J.; Bouwstra, J. A., LC/MS analysis of stratum corneum lipids: ceramide profiling and discovery. *J. Lipid Res.* **2011**, *52* (6), 1211-21.
24. Janssens, M.; van Smeden, J.; Gooris, G. S.; Bras, W.; Portale, G.; Caspers, P. J.; Vreeken, R. J.; Kezic, S.; Lavrijzen, A. P.; Bouwstra, J. A., Lamellar lipid organization and ceramide composition in the stratum corneum of patients with atopic eczema. *J. Invest. Dermatol.* **2011**, *131* (10), 2136-8.
25. van Smeden, J.; Janssens, M.; Boiten, W. A.; van Drongelen, V.; Furio, L.; Vreeken, R. J.; Hovnanian, A.; Bouwstra, J. A., Intercellular skin barrier lipid composition, and organization in Netherton syndrome patients. *J. Invest. Dermatol.* **2014**, *134* (5), 1238-1245.
26. Schreiner, V.; Gooris, G. S.; Pfeiffer, S.; Lanzendorfer, G.; Wenck, H.; Diembeck, W.; Proksch, E.; Bouwstra, J., Barrier characteristics of different human skin types investigated with X-ray diffraction, lipid analysis, and electron microscopy imaging. *J. Invest. Dermatol.* **2000**, *114* (4), 654-60.
27. J.A. Bouwstra, E. H. M., *Cosmetic formulation principles and practice*. CRC Press: Boca Raton, 2019.
28. Crumrine, D.; Khnykin, D.; Krieg, P.; Man, M.-Q.; Celli, A.; Mauro, T. M.; Wakefield, J. S.; Menon, G.; Mauldin, E.; Miner, J. H.; Lin, M.-H.; Brash, A. R.; Sprecher, E.; Radner, F. P. W.; Choate, K.; Roop, D.; Uchida, Y.; Gruber, R.; Schmuth, M.; Elias, P. M., Mutations in Recessive Congenital Ichthyoses Illuminate the Origin and Functions of the Corneocyte Lipid Envelope. *J. Invest. Dermatol.* **2019**, *139* (4), 760-768.
29. Eckl, K.-M.; Tidhar, R.; Thiele, H.; Oji, V.; Hausser, I.; Brodesser, S.; Preil, M.-L.; Önal-Akan, A.; Stock, F.; Müller, D.; Becker, K.; Casper, R.; Nürnberg, G.; Altmüller, J.; Nürnberg, P.; Traupe, H.; Futerman, A. H.; Hennies, H. C., Impaired Epidermal Ceramide Synthesis Causes Autosomal Recessive Congenital Ichthyosis and Reveals the Importance of Ceramide Acyl Chain Length. *J. Invest. Dermatol.* **2013**, *133* (9), 2202-2211.
30. Motta, S.; Monti, M.; Sesana, S.; Caputo, R.; Carelli, S.; Ghidoni, R., Ceramide composition of the psoriatic scale. *Biochim. Biophys. Acta* **1993**, *1182* (2), 147-51.
31. Opalka, L.; Kovacik, A.; Maixner, J.; Vavrova, K., Omega-O-Acylceramides in skin lipid membranes: effects of concentration, sphingoid base, and model complexity on microstructure and permeability. *Langmuir* **2016**, *32* (48), 12894-12904.
32. Uche, L. E.; Gooris, G. S.; Bouwstra, J. A.; Beddoes, C. M., Barrier Capability of Skin Lipid Models: Effect of Ceramides and Free Fatty Acid Composition. *Langmuir* **2019**, *35* (47), 15376-15388.
33. t'Kindt, R.; Jorge, L.; Dumont, E.; Couturon, P.; David, F.; Sandra, P.; Sandra, K., Profiling and characterizing skin ceramides using reversed-phase liquid chromatography-quadrupole time-of-flight mass spectrometry. *Anal. Chem.* **2012**, *84* (1), 403-411.

34. van Smeden, J.; Bouwstra, J. A., Stratum corneum lipids: Their role for the skin barrier function in healthy subjects and atopic dermatitis patients. *Curr. Probl. Dermatol.* **2016**, *49*, 8-26.
35. McIntosh, T. J.; Stewart, M. E.; Downing, D. T., X-ray diffraction analysis of isolated skin lipids: reconstitution of intercellular lipid domains. *Biochemistry* **1996**, *35* (12), 3649-53.
36. Bouwstra, J. A.; Gooris, G. S.; Dubbelaar, F. E.; Ponec, M., Phase behavior of lipid mixtures based on human ceramides: coexistence of crystalline and liquid phases. *J. Lipid Res.* **2001**, *42* (11), 1759-70.
37. Bouwstra, J. A.; Gooris, G. S.; Dubbelaar, F. E.; Ponec, M., Phase behavior of stratum corneum lipid mixtures based on human ceramides: the role of natural and synthetic ceramide 1. *J. Invest. Dermatol.* **2002**, *118* (4), 606-17.
38. Bouwstra, J. A.; Gooris, G. S.; Dubbelaar, F. E.; Weerheim, A. M.; Ijzerman, A. P.; Ponec, M., Role of ceramide 1 in the molecular organization of the stratum corneum lipids. *J. Lipid Res.* **1998**, *39* (1), 186-96.
39. de Jager, M. W.; Gooris, G. S.; Ponec, M.; Bouwstra, J. A., Lipid mixtures prepared with well-defined synthetic ceramides closely mimic the unique stratum corneum lipid phase behavior. *J. Lipid Res.* **2005**, *46* (12), 2649-2656.
40. Pham, Q. D.; Mojumdar, E. H.; Gooris, G. S.; Bouwstra, J. A.; Sparr, E.; Topgaard, D., Solid and fluid segments within the same molecule of stratum corneum ceramide lipid. *Quarterly Reviews of Biophysics* **2018**, *51*.
41. Janssens, M.; Gooris, G. S.; Bouwstra, J. A., Infrared spectroscopy studies of mixtures prepared with synthetic ceramides varying in head group architecture: coexistence of liquid and crystalline phases. *Biochim. Biophys. Acta* **2009**, *1788* (3), 732-742.
42. Paz Ramos, A.; Gooris, G.; Bouwstra, J.; Lafleur, M., Evidence of hydrocarbon nanodrops in highly ordered stratum corneum model membranes. *J. Lipid Res.* **2018**, *59* (1), 137-143.
43. Opalka, L.; Kovacik, A.; Pullmannova, P.; Maixner, J.; Vavrova, K., Effects of omega-O-acylceramide structures and concentrations in healthy and diseased skin barrier lipid membrane models. *J. Lipid Res.* **2020**, *61* (2), 219-228.
44. Gooris, G. S.; Kamran, M.; Kros, A.; Moore, D. J.; Bouwstra, J. A., Interactions of dipalmitoylphosphatidylcholine with ceramide-based mixtures. *Biochim. Biophys. Acta* **2018**, *1860* (6), 1272-1281.
45. Beddoes, C. M.; Gooris, G. S.; Bouwstra, J. A., Preferential arrangement of lipids in the long-periodicity phase of a stratum corneum matrix model. *J. Lipid Res.* **2018**, *59* (12), 2329-2338.
46. Uche, L. E.; Gooris, G. S.; Beddoes, C. M.; Bouwstra, J. A., New insight into phase behavior and permeability of skin lipid models based on sphingosine and phytosphingosine ceramides. *Biochim. Biophys. Acta* **2019**, *1861* (7), 1317-1328.
47. Boiten, W.; Absalah, S.; Vreeken, R.; Bouwstra, J.; van Smeden, J., Quantitative analysis of ceramides using a novel lipidomics approach with three dimensional response modelling. *Biochim. Biophys. Acta* **2016**, *1861* (11), 1652-1661.
48. de Sousa Neto, D.; Gooris, G.; Bouwstra, J., Effect of the omega-acylceramides on the lipid organization of stratum corneum model membranes evaluated by X-ray diffraction and FTIR studies (Part I). *Chem. Phys. Lipids* **2011**, *164* (3), 184-95.
49. de Jager, M.; Groeninck, W.; van der Spek, J.; Janmaat, C.; Gooris, G.; Ponec, M.; Bouwstra, J., Preparation and characterization of a stratum corneum substitute for in vitro percutaneous penetration studies. *Biochim. Biophys. Acta* **2006**, *1758* (5), 636-44.
50. Mojumdar, E. H.; Helder, R. W.; Gooris, G. S.; Bouwstra, J. A., Monounsaturated fatty acids reduce the barrier of stratum corneum lipid membranes by enhancing the formation of a hexagonal lateral packing. *Langmuir* **2014**, *30* (22), 6534-43.

51. International Conference on Harmonization (ICH) Q2 (R1), Validation of analytical procedures: Text and Methodology. 2005.
52. European Pharmacopoeia. . 8 ed.; European Directorate for the quality of medicines & healthcare. Strasbourg, 2014; Vol. 1.
53. Oguri, M.; Gooris, G. S.; Bito, K.; Bouwstra, J. A., The effect of the chain length distribution of free fatty acids on the mixing properties of stratum corneum model membranes. *Biochim. Biophys. Acta* **2014**, *1838* (7), 1851-1861.
54. Wojdyr, M., Fityk: a general-purpose peak fitting program. *J Appl Crystallogr* **2010**, *43*, 1126-1128.
55. Snyder, R. G.; Liang, G. L.; Strauss, H. L.; Mendelsohn, R., IR spectroscopic study of the structure and phase behavior of long-chain diacylphosphatidylcholines in the gel state. *Biophys. J.* **1996**, *71* (6), 3186-98.
56. Mendelsohn, R.; Moore, D. J., Vibrational spectroscopic studies of lipid domains in biomembranes and model systems. *Chem. Phys. Lipids* **1998**, *96* (1-2), 141-57.
57. Mendelsohn, R.; Flach, C. R.; Moore, D. J., Determination of molecular conformation and permeation in skin via IR spectroscopy, microscopy, and imaging. *Biochim. Biophys. Acta* **2006**, *1758* (7), 923-933.
58. Mendelsohn, R.; Moore, D. J., Infrared determination of conformational order and phase behavior in ceramides and stratum corneum models. *Methods Enzymol.* **2000**, *312*, 228-47.
59. Gooris, G. S.; Bouwstra, J. A., Infrared spectroscopic study of stratum corneum model membranes prepared from human ceramides, cholesterol, and fatty acids. *Biophys. J.* **2007**, *92* (8), 2785-95.
60. Mendelsohn, R.; Liang, G. L.; Strauss, H. L.; Snyder, R. G., IR spectroscopic determination of gel state miscibility in long-chain phosphatidylcholine mixtures. *Biophys. J.* **1995**, *69* (5), 1987-1998.
61. Moore, D. J.; Rerek, M. E., Insights into the molecular organization of lipids in the skin barrier from infrared spectroscopy studies of stratum corneum lipid models. *Acta Derm-Venereol.* **2000**, 16-22.
62. Groen, D.; Gooris, G. S.; Bouwstra, J. A., New insights into the stratum corneum lipid organization by X-ray diffraction analysis. *Biophys. J.* **2009**, *97* (8), 2242-2249.
63. Mojumdar, E. H.; Gooris, G. S.; Barlow, D. J.; Lawrence, M. J.; Deme, B.; Bouwstra, J. A., Skin lipids: localization of ceramide and fatty acid in the unit cell of the long periodicity phase. *Biophys. J.* **2015**, *108* (11), 2670-2679.
64. Mojumdar, E. H.; Kariman, Z.; van Kerckhove, L.; Gooris, G. S.; Bouwstra, J. A., The role of ceramide chain length distribution on the barrier properties of the skin lipid membranes. *Biochim Biophys Acta* **2014**, *1838* (10), 2473-2483.
65. Skolova, B.; Jandovska, K.; Pullmannova, P.; Tesar, O.; Roh, J.; Hrabalek, A.; Vavrova, K., The role of the trans double bond in skin barrier sphingolipids: permeability and infrared spectroscopic study of model ceramide and dihydroceramide membranes. *Langmuir* **2014**, *30* (19), 5527-35.
66. de Jager, M. W.; Gooris, G. S.; Dolbnya, I. P.; Bras, W.; Ponec, M.; Bouwstra, J. A., Novel lipid mixtures based on synthetic ceramides reproduce the unique stratum corneum lipid organization. *J. Lipid Res.* **2004**, *45* (5), 923-32.
67. Wess, T. J.; Drakopoulos, M.; Snigirev, A.; Wouters, J.; Paris, O.; Fratzl, P.; Collins, M.; Hiller, J.; Nielsen, K., The use of small-angle x-ray diffraction studies for the analysis of structural features in archaeological samples. *Archaeometry* **2001**, *43*, 117-129.
68. Pullmannova, P.; Ermakova, E.; Kovacic, A.; Opalka, L.; Maixner, J.; Zbytovska, J.; Kucerka, N.; Vavrova, K., Long and very long lamellar phases in model stratum corneum lipid membranes. *J. Lipid Res* **2019**, *60* (5), 963-971.





New insight into phase behavior
and permeability of skin lipid models
based on sphingosine and
phytosphingosine ceramides

Authors and affiliations:

Lorretta.E. Uche¹, Gerrit.S. Gooris¹, Joke.A. Bouwstra¹ and Charlotte.M. Beddoes¹

¹Division of Drug Delivery Technology, Cluster BioTherapeutics, Leiden Academic Centre for Drug Research, Leiden University, Netherlands

Adapted from: *Biochim. Biophys. Acta*, 2019. **1861**(7): p. 1317-1328.

ABSTRACT

The intercellular lipid matrix of the *stratum corneum* (SC), which consists mainly of ceramides (CERs), free fatty acids, and cholesterol, is fundamental to the skin barrier function. These lipids assemble into two lamellar phases, known as the long and short periodicity phases (LPP and SPP respectively). The LPP is unique in the SC and is considered important for the skin barrier function. Alterations in CER composition, as well as impaired skin barrier function, are commonly observed in diseased skin, yet the understanding of this relationship remains insufficient. In this study, we have investigated the influence of non-hydroxy and α -hydroxy sphingosine-based CERs and their phytosphingosine counterparts on the permeability and lipid organization of model membranes, which were adjusted in composition to enhance formation of the LPP. The permeability was compared by diffusion studies using ethyl-p-aminobenzoate as a model drug, and the lipid organization was characterized by X-ray diffraction and infrared spectroscopy. Both the sphingosine- and phytosphingosine-based CER models formed the LPP, while the latter exhibited a longer LPP repeat distance. The ethyl-p-aminobenzoate flux across the sphingosine-based CER models was higher when compared to the phytosphingosine counterparts, contrary to the fact that the α -hydroxy phytosphingosine-based CER model had the lowest chain packing density. The unanticipated low permeability of the α -hydroxy phytosphingosine-based CER model is probably associated with a stronger headgroup hydrogen bonding network. Our findings indicate that the increased level of sphingosine-based CERs at the expense of phytosphingosine-based CERs, as observed in the diseased skin, may contribute to the barrier function impairment.

Keywords:

Skin barrier; Stratum corneum; Ceramides; Membrane permeability; Infrared spectroscopy; X-ray diffraction

INTRODUCTION

The skin is a large multilayered organ with the primary function of protecting the body from an influx of dust, pathogens, chemicals, ultraviolet radiation, and other unwanted substances in the external environment, while also preventing the excessive loss of fluids from the body [1]. The outermost layer of the skin, the *stratum corneum* (SC), is fundamental to the skin barrier function [2, 3]. It consists of keratin-filled dead cells, referred to as corneocytes, embedded in a highly organized lipid matrix [4]. The cornified cross-linked protein envelope encapsulates the corneocytes and renders them highly impermeable. Consequently, the tortuous intercellular pathway occupied by the lipid matrix is the preferred pathway for exogenous substance penetration through the skin [5, 6]. Thus, knowledge of the lipid composition and organization is crucial to understand the skin barrier function.

The major lipid classes in the SC are ceramides (CERs), cholesterol (CHOL), and free fatty acids (FFAs) [7-11]. These lipids are present in an approximately equimolar ratio in the human SC. As detected by X-ray diffraction, the SC lipids are assembled into either one of two coexisting crystalline lamellar phases with repeat distances of ~ 13 nm and ~ 6 nm referred to as the long and the short periodicity phases (LPP and SPP) respectively [12-14]. Within the lipid lamellae, the lipids can further assemble into various phases with distinct packing densities including the orthorhombic, hexagonal, and liquid/fluid phases. At physiological temperature, these lipids adopt predominantly a dense orthorhombic lateral packing, while a subpopulation of the lipids arranges to form lesser densely packed phases including the hexagonal and disordered liquid phase [15-18]. Both the lamellar organization and the lateral packing of the SC lipids are important for the skin barrier function [19].

The CERs, unlike the other major SC lipid classes, show great diversity in their headgroup architecture. Currently, eighteen CER subclasses have been identified in human SC [20-27]. Several studies have investigated the phase behavior of SC lipid mixtures prepared with isolated CERs, in order to gain insight into the processes and factors underlying the skin barrier function [28-30]. CERs isolated from skin lipids can form the characteristic LPP and SPP only when mixed with CHOL [31], while the further addition of FFAs increases the packing density [32]. Alternatively, synthetic lipid model systems can range from simple ternary component mixtures [33-35] to complex mixtures that contain a greater number of components [36-38] and have been utilized to study the contributions of the major lipid classes and subclasses to SC lipid organization. With the use of these

models, the CER EOS subclass, belonging to the group of ester-linked ω -hydroxy CERs (fig. 1A), has been identified as crucial for the formation of the LPP [32, 39-41]. The LPP is unique in the SC, which indicates its importance for the integrity of the skin barrier [42]. To investigate the influence of SC lipid composition and organization on barrier function, several studies have examined the influence of CER subclasses on the permeability of model SC membranes [42-46]. However, most of these studies were carried out in models containing either a single CER or a mixture of CERs, while lacking ester-linked ω -hydroxy CERs, so that the LPP was not formed. For a comprehensive understanding of the relationship between CER composition, lipid organization, and barrier function, it is necessary to investigate the influence of the CER headgroup structure on the formation of the LPP, molecular interactions, and lipid chain packing, as well as how these interactions can influence the SC lipid barrier function in models organized in the LPP. This is of special importance as variation in CER subclass composition has been reported in several diseased skin conditions including; atopic dermatitis [26] and psoriasis [47], which express among other anomalies, a reduction in ester-linked ω -hydroxy CERs level and thus a reduction in LPP formation, and an increase in sphingosine-based CER level at the expense of phytosphingosine-based CERs.

In the current work, we aimed to determine the influence of sphingosine- and phytosphingosine-based CERs on the permeability, lamellar organization, phase transitions, headgroup interactions, chain conformational ordering, lateral packing, and mixing properties in LPP lipid model systems. The level of CER EOS (molecular architecture, see figure 1) was increased to 40 mol% to avoid the formation of the SPP in the lipid model systems [48, 49]. The significance of our findings to impaired skin barrier function in inflammatory skin disease is discussed.

EXPERIMENTAL SECTION

Materials

Molecular structures of the five synthetic CER subclasses used to prepare the model mixtures are displayed in figure 1A-E. The synthetic CERs were kindly provided by Evonik (Essen, Germany). The CERs were of $\geq 90\%$ purity. The FFAs, Ethyl-p-aminobenzoate referred to as E-PABA (Figure 1F), CHOL, and acetate buffer salts were purchased from Sigma- Aldrich Chemie GmbH (Schnelldorf, Germany). The perdeuterated FFAs (DFFAs) with chain lengths of C18 and C20

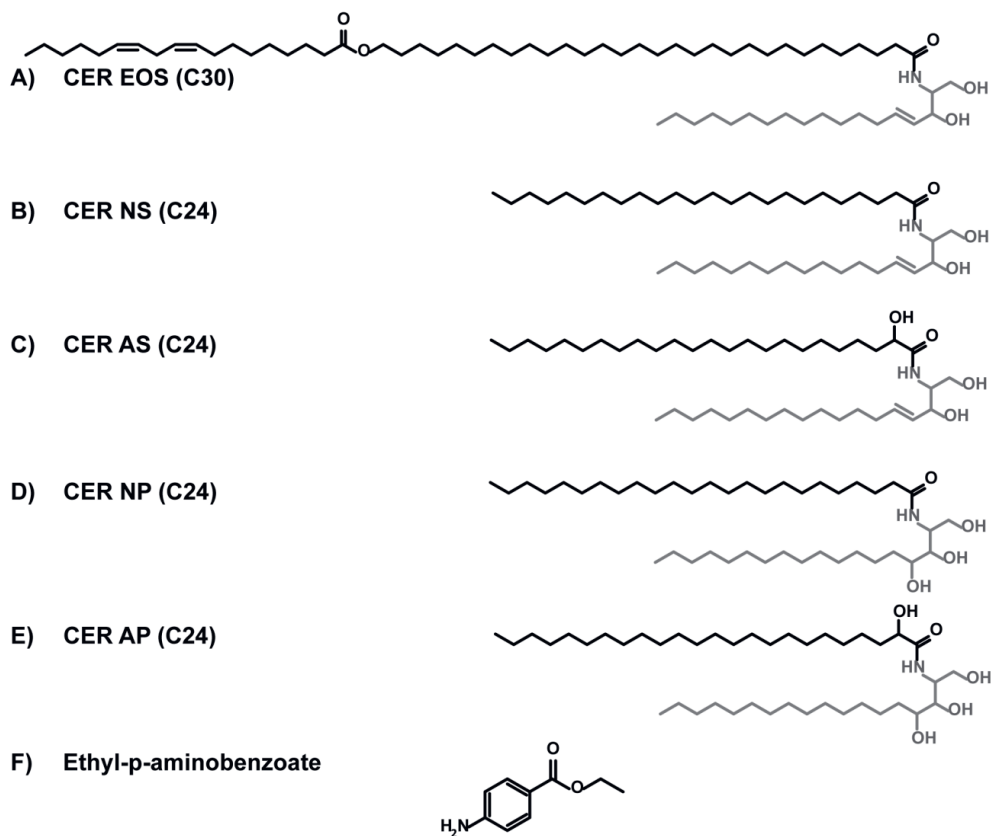


Figure 1: Molecular structure of the CER subclasses and ethyl-p-aminobenzoic acid used in the study.

The CERs consist of a fatty acid acyl chain {non-hydroxylated [N], α -hydroxylated [A] or ω -hydroxylated [O]} linked by an amide bond to a sphingoid base {sphingosine [S], or phytosphingosine [P] with 18 carbon atoms}. A) N-(30-Linoleoyloxy-triacontanoyl)-sphingosine: a linoleate esterified to an ω -hydroxylated acyl chain [EO], with a chain length of 30 carbon atoms (C30) linked to a [S] base, referred to as CER EOS (C30); B) N-(tetracosanoyl)-sphingosine: a [N] acyl chain (C24) linked to a [S] base, referred to as CER NS (C24); C) N-(2R-hydroxy-tetracosanoyl)-sphingosine: an [A] acyl chain (C24) linked to a [S] base, referred to as CER AS (C24); D) N-(tetracosanoyl)-phytosphingosine: a [N] acyl chain (C24) linked to a [P] base, referred to as CER NP (C24); and E) N-(2R-hydroxy-tetracosanoyl)-phytosphingosine: an [A] acyl chain (C24) linked to a [P] base referred to as CER AP (C24). The [P] based CERs, NP, and AP contain a C4 hydroxyl group on the base chain while [A] based CERs, AS, and AP contain a hydroxyl group on the fatty acid moiety. The CER fatty acid acyl chain and sphingoid base are depicted in black and grey respectively. F) Molecular structure of ethyl-p-aminobenzoate (E-PABA) used as a model drug for the permeability studies.

were obtained from Cambridge Isotope Laboratories (Andover, Massachusetts). The DFFAs with chain lengths of C16 and C22 were obtained from Larodan (Malmö, Sweden). The DFFA with a chain length of C24 was obtained from Arc Laboratories B.V. (Apeldoorn, The Netherlands). All organic solvents were purchased from Labscan Ltd. (Dublin, Ireland). All analytical solvents were HPLC grade or higher. The nucleopore polycarbonate filter disks, 0.05 μm pore size were purchased from Whatman (Kent, UK).

Preparation of the model lipid mixtures

SC lipid models were prepared as equimolar mixtures of CER, CHOL, and FFAs. The CER fraction is comprised of CER EOS (40 mol% of the total CER fraction) and either CER NS, CER AS, CER NP, or CER AP (60 mol% of the total CER fraction). The FFA content comprised of FFAs with the following composition: C16, C18, C20, C22, and C24 at relative molar percentages of 1.8, 4.0, 7.6, 47.8, and 38.8 respectively, a composition adapted from the FFA composition in the SC [50]. The resulting lipid models, whose compositions are presented in table 1, are denoted by CER EOS-NS, CER EOS-NP, CER EOS-AS, and CER EOS-AP. Additional models were prepared in which FFAs were replaced by their deuterated counterparts, denoted by CER EOS-NS-DFFA, CER EOS-NP-DFFA, CER EOS-AS-DFFA, and CER EOS-AP-DFFA.

Table 1: Composition of the various models used in the study.

Lipid model name	Composition and molar ratio (1:1:1)
CER EOS-NS	CER EOS(C30) 40% + NS(C24) 60%: CHOL: FFAs
CER EOS-AS	CER EOS(C30) 40% + AS(C24) 60%: CHOL: FFAs
CER EOS-NP	CER EOS(C30) 40% + NP(C24) 60%: CHOL: FFAs
CER EOS-AP	CER EOS(C30) 40% + AP(C24) 60%: CHOL: FFAs
CER EOS-NS-DFFA	CER EOS(C30) 40% + NS(C24) 60%: CHOL: DFFAs
CER EOS-AS-DFFA	CER EOS(C30) 40% + AS(C24) 60%: CHOL: DFFAs
CER EOS-NP-DFFA	CER EOS(C30) 40% + NP(C24) 60%: CHOL: DFFAs
CER EOS-AP-DFFA	CER EOS(C30) 40% + AP(C24) 60%: CHOL: DFFAs

Preparation of SC model membranes for permeability studies

To prepare the SC model membranes, 0.9 mg of the appropriate lipid composition was dissolved in 200 μl hexane:ethanol (2:1) solution, to a final concentration of 4.5 mg/ml. The solution was sprayed over an area of 10 x 10 mm², on a nucleopore polycarbonate filter disk with 0.05 μm pore size (Whatman, Kent, UK), using a

Linomat IV device with an extended y-axis arm (Camag, Muttenz, Switzerland) under a gentle stream of nitrogen. The spraying rate was set at 14 $\mu\text{l}/\text{sec}$ and an approximate distance of 1 mm was maintained between the nozzle and the spraying surface. The samples were equilibrated for 10 min at 85 $^{\circ}\text{C}$, which was sufficient to ensure that the lipid mixtures had fully melted and then gradually cooled to room temperature. The heating and cooling cycle was repeated once more.

Permeability studies

In vitro permeation studies were performed using Permegear in-line diffusion cells (Bethlehem PA, USA) with a diffusion area of 0.28 cm^2 . The model membranes prepared with the various lipid mixtures were mounted in the diffusion cells and hydrated for an hour with the acceptor phase consisting of phosphate buffered saline (PBS 0.1 M solution: NaCl, Na_2HPO_4 , KH_2PO_4 , and KCl in milli-Q water with a concentration of 8.13, 1.14, 0.20 and 0.19 g/l respectively) at pH 7.4 prior to the experiment. Before use, the PBS was filtered and degassed for 30 min under vacuum to remove the dissolved air. As a model drug, E-PABA was used, as it results in acceptor phase samples with sufficiently high concentrations that are measurable with the UPLC. The donor compartment was filled with 1400 μl of E-PABA in acetate buffer (pH 5) at a saturated concentration of 0.65 mg/ml. This concentration was used to enable the maximum thermodynamic activity. The acceptor phase was perfused at a flow rate of about 2 ml/h with an Ismatec IPC pump (IDEX Health & Science, Germany) through an in-line degasser (Biotech, Sweden) to remove air bubbles that may form during the experiment. The acceptor phase was stirred with a tico 731 magnetic stirrer (Hengstler, Germany) at 120 rpm. The experiment was performed under occlusive conditions, by closing the opening of the donor compartment with adhesive tape. The temperature of the membranes was maintained at 32 $^{\circ}\text{C}$. The acceptor fluid was collected over 15 h at 1-hour intervals. At the end of the diffusion study, the volume per collected fraction of PBS was determined by weight and the concentration of E-PABA was determined by UPLC (see below). During the steady-state conditions, the permeation of E-PABA across the model membrane can be described by Fick's first law of diffusion:

$$J_{ss} = \frac{K \cdot D \cdot C_d}{h}$$

J_{ss} represents the steady-state flux of E-PABA across the model membrane ($\mu\text{g}/\text{cm}^2/\text{h}$), while D is the diffusion coefficient of E-PABA in the model membrane

(cm²/h). K is the partition coefficient between the donor compartment and the lipid membrane. C_d is the drug concentration (µg/cm³), and h is the pathway length in the model membrane (cm). Permeation of multiple samples of each composition was analyzed, $n > 4$. The steady-state flux values were calculated at a time interval between the 9th and 15th hour from the plots of E-PABA flux values.

Ultra performance liquid chromatography (UPLC)

The analysis of E-PABA was carried out using Acquity UPLC systems (Waters Co., Milford, MA, USA). The Waters' Acquity UPLC systems consisted of a quaternary solvent manager (a high-pressure pump), tunable ultraviolet/visible absorbance detector controlled by MassLynx software application, and sample manager with flow-through needle. Specialized Acquity UPLC column packed with 1.7 µm, bridged, ethyl siloxane, hybrid particles, was used as the stationary phase. The column temperature was set at 40 °C. The mobile phase used for the UPLC analysis contained mixtures of 0.1% trifluoroacetic acid in acetonitrile: milli-Q water at 40:60 (v/v) ratio. The flow rate of the mobile phase was set at 1 ml/min. 10 µl of sample was injected on the column. A UV-detection wavelength of 286 nm was used for the detection of E-PABA. MassLynx software was used for the acquisition of data in chromatogram peaks resulting from the permeation samples. All UPLC data were analyzed and processed using MassLynx and TargetLynx software V4.1 SCN951 (Waters Co., Milford, USA).

The analytical method was validated as per ICH (International conference on harmonization) guidelines with respect to linearity, precision, limit of detection (LOD), and limit of quantification (LOQ) [51]. Calibration standards were prepared by serial dilutions of stock solution in order to evaluate the relationship between the area under the curve and the concentration of E-PABA. The solutions were prepared in 1:1 solution of methanol and milli-Q water. The linearity of the relationship was evaluated in a concentration range of 0.1 -10 µg/ml covering the range of concentrations obtained when analyzing the concentration of E-PABA permeating the model membranes. The calibration curves were obtained using ordinary least square linear regression and the linearity was confirmed with the R^2 values. A series of calibration samples were run together with the samples to quantify E-PABA. To assess the system precision, E-PABA standard solution was prepared and six replicate injections were injected into the UPLC system and the percentage relative standard deviation (% RSD) was determined. The limit of quantification (LOQ) and limit of detection (LOD) were used to evaluate the quantitative performance and sensitivity of the method for E-PABA analysis [51, 52].

Sample preparation for FTIR studies

1.5 mg of the appropriate lipid composition was dissolved in chloroform:methanol (2:1) to a concentration of 7.5 mg/ml and sprayed over an area of $10 \times 10 \text{ mm}^2$ on an AgBr window using a Linomat IV device (Camag, Muttentz, Switzerland) with an extended y-axis arm and equilibrated as described earlier (section 2.3). The samples were equilibrated at 85 °C. A higher equilibration temperature of 95 °C was used for CER EOS-NP-DFFA and CER EOS-AP-DFFA mixtures in order for the lipids to fully melt. Finally, the samples were hydrated in deuterated acetate buffer (pH 5.0) and incubated at 37 °C for at least 15 h to ensure that the samples were fully hydrated.

FTIR measurements

FTIR spectra were acquired on a Bio-Rad Excalibur series FTIR spectrometer (Cambridge, MA) equipped with a broad-band mercury cadmium telluride detector, cooled by liquid nitrogen. The sample was continuously dry air purged, starting 30 min prior to data acquisition. The spectra were generated in the transmission mode by the coaddition of 256 interferograms, collected at 1 cm^{-1} resolution over 4 min. In order to examine the thermotropic phase behavior, the sample was measured between 0 – 100 °C at a heating rate of 0.25 °C/min, resulting in a 1 °C temperature rise per recorded spectrum. The spectra were deconvoluted using a half-width of 4 cm^{-1} , and an enhancement factor of 1.7. The software used was Agilent resolution pro (Agilent Technologies, Palo Alto CA, USA). Samples were measured over a range of 600–4000 cm^{-1} . The CH_2 symmetric stretching modes (2845–2855 cm^{-1}) and CD_2 symmetric stretching modes (2080–2100 cm^{-1}), referred to as $\nu_s\text{CH}_2$ and $\nu_s\text{CD}_2$ modes respectively, were selected to examine the conformational ordering and phase transition of the lipid chains. The linear regression curve fitting method was used to determine the mid-transition temperature and the transition temperature range, as described elsewhere [53]. The CH_2 (1462–1473 cm^{-1}) and CD_2 (1085–1095 cm^{-1}) scissoring modes referred to as δCH_2 and δCD_2 modes respectively were analyzed to monitor the lateral packing and mixing properties of the lipid chains. The frequencies of the CER amide I (1610–1690 cm^{-1}) and amide II (1510–1560 cm^{-1}) modes were analyzed to investigate the headgroup interactions and peak positions determined from the second derivative spectra. Multiple measurements of the samples were made, $n > 2$.

Sample preparation for X-ray diffraction studies

Sample preparation was similar to that described for FTIR studies. 1.0 mg of

lipids in chloroform:methanol (2:1) solution was sprayed on a mica window at a concentration of 7.5 mg/ml. The samples were equilibrated for 10 min at 85 °C and were subsequently measured both dry and fully hydrated. The lipid organization was not influenced by the number of equilibrations (either single or double, figure S1).

X-ray diffraction studies

The diffraction measurements were performed at the European Synchrotron Radiation Facility (ESRF, Grenoble) at station BM26B. The small- and wide-angle X-ray diffraction (SAXD and WAXD) patterns were acquired simultaneously. SAXD images were collected using a Pilatus 1M detector with 981 x 1043 pixels of 172 μm spatial resolution while the WAXD patterns were collected using a 300K-W linear Pilatus detector with 1475 x 195 pixels of 172 μm spatial resolution. The spatial calibration of the detectors was performed using silver behenate for SAXD detector and the two strongest reflections of high-density polyethylene (HDPE) for the WAXD detector. The X-ray wavelength was set at 0.1033 nm. The sample-to-detector distances were 2.1 m and 0.308 m for SAXD and WAXD respectively. The samples were mounted in a sample holder with mica windows. Diffraction patterns of the lipid models were acquired at room temperature on two positions, at each position, the samples were measured for 90 seconds. SAXD was used to determine the long-range ordering in the samples. The scattering intensity (I) was measured as a function of the scattering vector q . The latter is defined as $q = \frac{4\pi \sin \theta}{\lambda}$, where θ is the scattering angle and λ is the wavelength. From the positions of a series of equidistant peaks (q_h), the periodicity of a lamellar phase was calculated using the equation $d = \frac{2h\pi}{q_h}$ in which h is the order of the diffraction peak. The one-dimensional intensity profiles used in these calculations were obtained by the reduction of the 2D SAXD pattern from Cartesian (x,y) to polar (ρ,θ) coordinates and integrated over an θ range. WAXD was used to obtain the diffraction patterns related to the lateral packing of lipids. Each sample was measured at least twice.

Data analysis

One-way ANOVA with Bonferroni's multiple comparison test was performed to analyze the permeability studies' data. The significance level for rejection of null hypothesis was set at $P < 0.05$ (*), $P < 0.01$ (**), $P < 0.001$ (***) and $P < 0.0001$ (****).

RESULTS

Phytosphingosine-based CER model membranes exhibit higher barrier capability than the sphingosine-based CER model membranes

The permeability of E-PABA through the model membranes was evaluated by *in-vitro* permeation studies. E-PABA was analyzed by means of the UPLC method. The calibration curve R^2 value was 0.9989 ± 0.0023 indicating excellent linearity. For assessment of the system precision, the RSD for the peak area obtained from six replicate injections was $9248.7 \pm 0.1\%$ (acceptance limit of NMT 2.0%) demonstrating high repeatability. The LOD and LOQ values were 0.10 ± 0.01 ng/ml and 0.51 ± 0.02 ng/ml respectively, demonstrating the high sensitivity and quantitative performance of the UPLC method for E-PABA analysis.

The E-PABA flux profiles are displayed in figure 2A. The bars of steady-state fluxes are shown in figure 2B, while the values are reported in Table 2. The steady-state flux of E-PABA was significantly lower in the phytosphingosine-based CER models compared to the sphingosine-based CER counterparts. In contrast, no significant difference in the E-PABA steady-state flux was observed between models prepared with non-hydroxy fatty acid based CERs and with their α -hydroxy fatty acid counterparts.

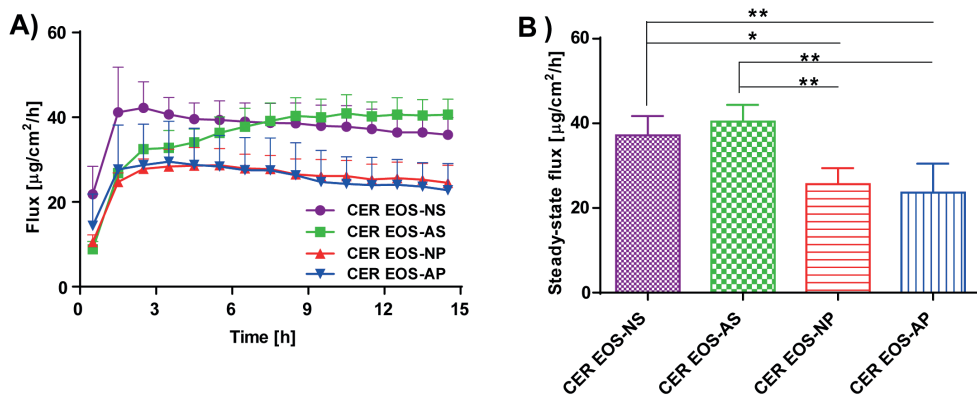


Figure 2: Permeability of the model membranes.

A) The flux of E-PABA across the model membranes over 15 h. B) The average steady-state flux of E-PABA across the model membranes (9-15 h). Data presented as the means \pm SD, $n \geq 4$. E-PABA steady-state flux was significantly lower in the phytosphingosine-based CER model compared to their sphingosine analogues, [** ($P < 0.01$), * ($P < 0.05$)].

Table 2: The E-PABA steady-state flux across the model membranes with their standard deviation, the midpoint temperatures of the orthorhombic-hexagonal phase transition ($T_{M,OR-HEX}$) and hexagonal-liquid phase transition ($T_{M,HEX-LIQ}$), the widths of the orthorhombic-hexagonal ($T_{W,OR-HEX}$), and hexagonal-liquid transition ($T_{W,HEX-LIQ}$).

Lipid model	Steady-state flux ($\mu\text{g}/\text{cm}^2/\text{hr}$)	$T_{M,OR-HEX}$ ($^{\circ}\text{C}$)	$T_{W,OR-HEX}$ ($^{\circ}\text{C}$)	$T_{M,HEX-LIQ}$ ($^{\circ}\text{C}$)	$T_{W,HEX-LIQ}$ ($^{\circ}\text{C}$)
CER EOS-NS	37.1 ± 4.5	38.5 ± 0.8	8.3	74.7 ± 3.2	9.1
CER EOS-AS	40.4 ± 3.9	34.5 ± 0.3	8.5	73.3 ± 0.3	8.1
CER EOS-NP	25.7 ± 3.8	41.7 ± 1.8	12.8	73.7 ± 1.5	19.4
CER EOS-AP	23.7 ± 6.8	28.7 ± 0.3	9.4	78.5 ± 1.6	18.7

Models prepared with phytosphingosine-based CERs undergo a gel to liquid phase transition over a wider temperature range compared to models prepared with sphingosine-based CERs

To probe the factors that dictate the difference in the observed permeability rates, the lateral lipid organization was examined by FTIR spectroscopy. The conformational ordering in the lipid models was examined using the $\nu_5\text{CH}_2$ frequencies. A $\nu_5\text{CH}_2$ frequency below 2850 cm^{-1} indicates the presence of primarily ordered lipid chains typical in a hexagonal and/or orthorhombic lateral packing [54]. The thermotropic response of the $\nu_5\text{CH}_2$ mode of the various lipid models are presented in figure 3. The $\nu_5\text{CH}_2$ frequencies in the spectra of the CER EOS-NS, CER EOS-AS, CER EOS-NP, and CER EOS-AP at $10\text{ }^{\circ}\text{C}$ appear at 2849.0 , 2849.7 , 2849.3 and 2849.3 cm^{-1} respectively, indicative of a high conformational hydrocarbon chain ordering in all of the models. When gradually increasing the temperature, the $\nu_5\text{CH}_2$ frequencies also gradually increased. The first shift in $\nu_5\text{CH}_2$ frequency, of approximately 1 cm^{-1} , indicates an orthorhombic-hexagonal phase transition. Differences in the shift magnitude are observed between the models. The $\nu_5\text{CH}_2$ frequency shift is more pronounced in the models containing non-hydroxy fatty acid based CERs compared to their α -hydroxy fatty acid based counterparts. When increasing the temperature further, a second major transition from a hexagonal to the liquid phase is observed. In the $\nu_5\text{CH}_2$ curve, this is seen as a wavenumber shift of $3\text{-}4\text{ cm}^{-1}$, which in our samples occur between 70 and $90\text{ }^{\circ}\text{C}$. In the sphingosine-based CER models, the hexagonal-liquid phase transitions occurred with an immediate sharp rise in wavenumber over a shorter temperature range (Fig. 3A and 3B). In contrast, in the phytosphingosine-based CER models, the hexagonal-liquid phase transition commenced gradually with a wavenumber increase of $\sim 0.5\text{ cm}^{-1}$ over $10\text{ }^{\circ}\text{C}$, followed by a sharper rise in $\nu_5\text{CH}_2$ wavenumber. When comparing models prepared with CERs, which differ in their fatty acid acyl chain e.g. CER

NS and AS, there is no difference between the hexagonal-liquid phase transition profile. From these thermotropic response curves, the midpoint temperatures of the orthorhombic-hexagonal phase transition ($T_{M,OR-HEX}$) and hexagonal-liquid phase transition ($T_{M,HEX-LIQ}$), the temperature widths of the orthorhombic-hexagonal ($T_{W,OR-HEX}$), and hexagonal-liquid transition ($T_{W,HEX-LIQ}$) were calculated. These values are presented in Table 2. The hexagonal-liquid phase transitions occurred over a wider temperature range in the phytosphingosine-based CER models when compared to their sphingosine counterparts. In CER EOS-NS, a comparatively high $T_{M,HEX-LIQ}$ standard deviation was observed as recrystallization occurred to different extents in replicate samples analyzed (see figure S2). When focusing on the midrange temperature (T_M), the CER EOS-AP had the highest $T_{M,HEX-LIQ}$ indicating increased thermostability.

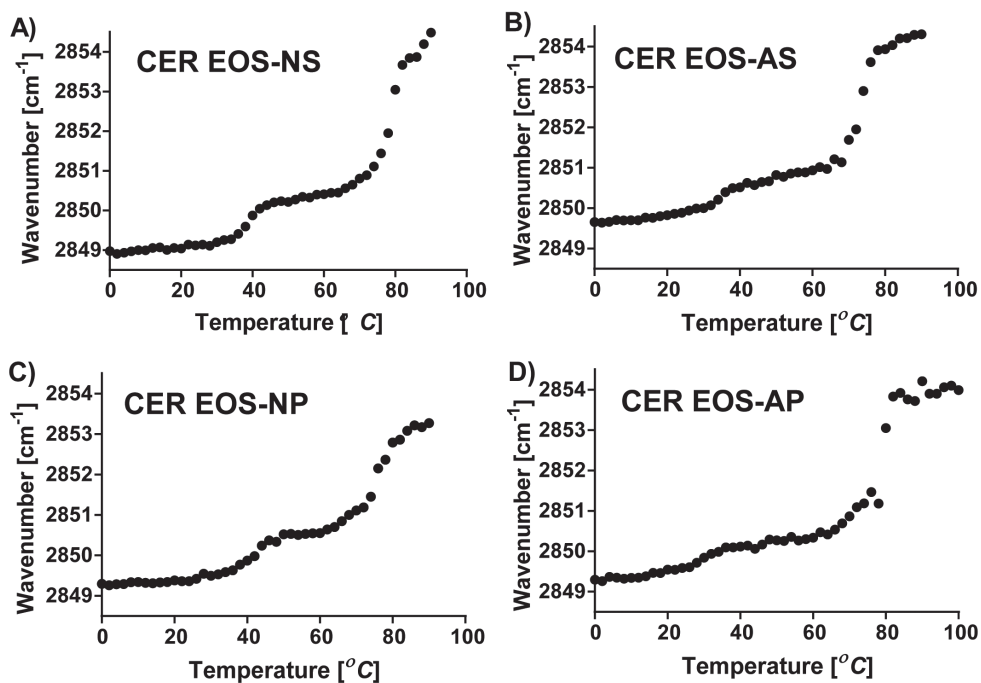


Figure 3: Thermotropic response of the $\nu_5\text{CH}_2$ modes of the lipid models.

The $\nu_5\text{CH}_2$ modes of all models showing frequencies below 2850 cm^{-1} at $10\text{ }^{\circ}\text{C}$, orthorhombic-hexagonal phase transition between 30 and $50\text{ }^{\circ}\text{C}$, and hexagonal-liquid phase transition between 70 and $90\text{ }^{\circ}\text{C}$.

CER EOS-AP exhibited the least proportion of orthorhombic packing at skin physiological temperature

When lipid chains adopt a dense orthorhombic lateral packing, two bands are observed in the IR spectrum of the δCH_2 mode. This doublet is due to short-range coupling between adjacent hydrocarbon chains of the same isotope and is distinct from the less dense hexagonal packing where only a single peak is observed in the δCH_2 mode. The magnitude of the band splitting is indicative of the degree of inter-chain interactions and the size of the domains with an orthorhombic organization [16, 55, 56]. The δCH_2 mode of the lipid models at 10 °C and 32 °C are provided in Figures 4A and 4B respectively. At 10 °C the δCH_2 mode of all lipid models are split into two bands centered at 1462 cm^{-1} and 1473 cm^{-1} , signifying orthorhombic packing. The δCH_2 mode of CER EOS-AP showed lower intensity peaks compared to the other compositions indicating a lower fraction of hydrocarbon chains in orthorhombic packing. At 32 °C, the δCH_2 modes of CER EOS-AP displayed a single broad peak with a weak shoulder indicating significant orthorhombic-hexagonal shift while the δCH_2 mode peaks of CER EOS-NS, CER EOS-AS, and CER EOS-NP remained doublets but reduced in peak intensity (figure 4B). As the temperature increased, a pronounced reduction in band splitting was obtained in all samples. The components collapse into a single peak at slightly different temperatures indicating the transition to a hexagonal packing (figure S3).

The CERs and FFAs undergo order to disorder phase transition in the same temperature range

If the structurally different lipids are fully mixed, the components will have the same melting temperature range. To determine whether the CERs and FFAs had completely mixed, the protiated FFAs were replaced by the DFFAs enabling the protiated CER and DFFA chains to be monitored both individually and simultaneously. The thermotropic response of the $\nu_s\text{CH}_2$ and $\nu_s\text{CD}_2$ modes of the various lipid models are presented in figure 5. In the FTIR spectrum of the CER EOS-NS-DFFA (Figure 5A), the $\nu_s\text{CD}_2$ mode revealed that the hexagonal-liquid phase transition of the deuterated chains commenced at 66 °C. The hexagonal-liquid phase transition of the CER chains also starts at a similar temperature, but the slight reduction in $\nu_s\text{CH}_2$ frequencies at 68 °C suggests that the protiated chains had recrystallized, thereby slightly delaying the transition. As the temperature was further increased, the ordered-disordered phase transition of the CER and DFFA chains concluded at the same temperature. A similar phase behavior was shown by CER EOS-AS-DFFA (figure 5B). In the FTIR spectrum of

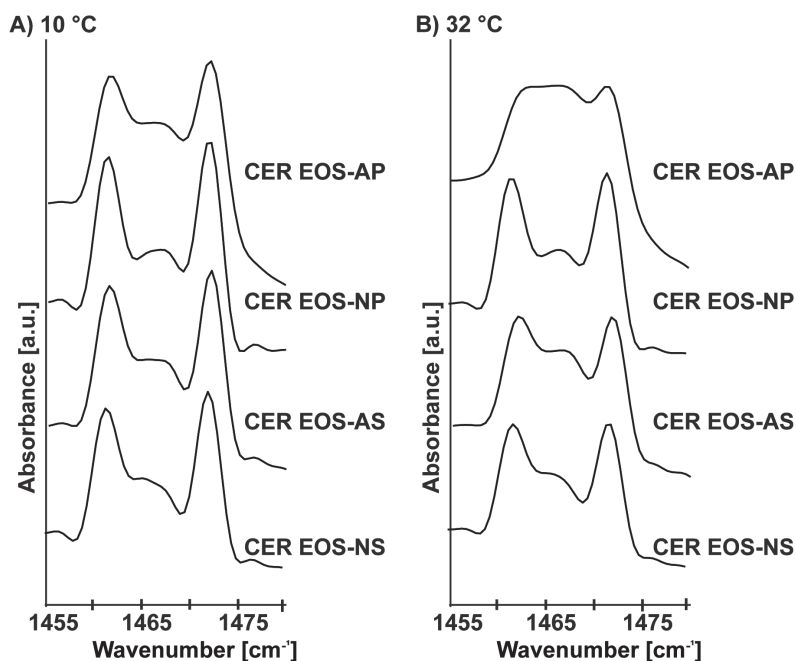


Figure 4: δCH_2 modes of the lipid models.

A) The curves at 10 °C display two distinct bands at approximately 1462 cm^{-1} and 1473 cm^{-1} indicating orthorhombic lateral packing. B) The curve at skin temperature (32 °C).

the CER EOS-NP-DFFA (Figure 5C), the different phase transition temperatures of the CER and DFFA chains suggests the existence of separate CER and DFFA domains. In the FTIR spectrum of CER EOS-AP-DFFA (Figure 5D), the $\nu_s\text{CD}_2$ mode revealed a slight upward shift in wavenumber between 66 °C and 76 °C. At higher temperatures, the thermotropic response of the DFFAs and CER chains underwent order to disorder phase transition in the same temperature range indicating mixing of the lipid chains. The hexagonal-liquid phase transition of the DFFA chains in CER EOS-AP-DFFA occurred at a higher temperature than in the other lipid models (figure 5E).

The CERs and FFAs participate in the same orthorhombic lattice at physiological temperature

When deuterated FFA and protiated CER chains participate in the same orthorhombic lattice, the adjacent CD_2 and CH_2 groups, being of different isotopes with different vibrational frequencies, cannot engage in a short-range coupling. As a consequence, when both isotopes are present in one lattice, only a single

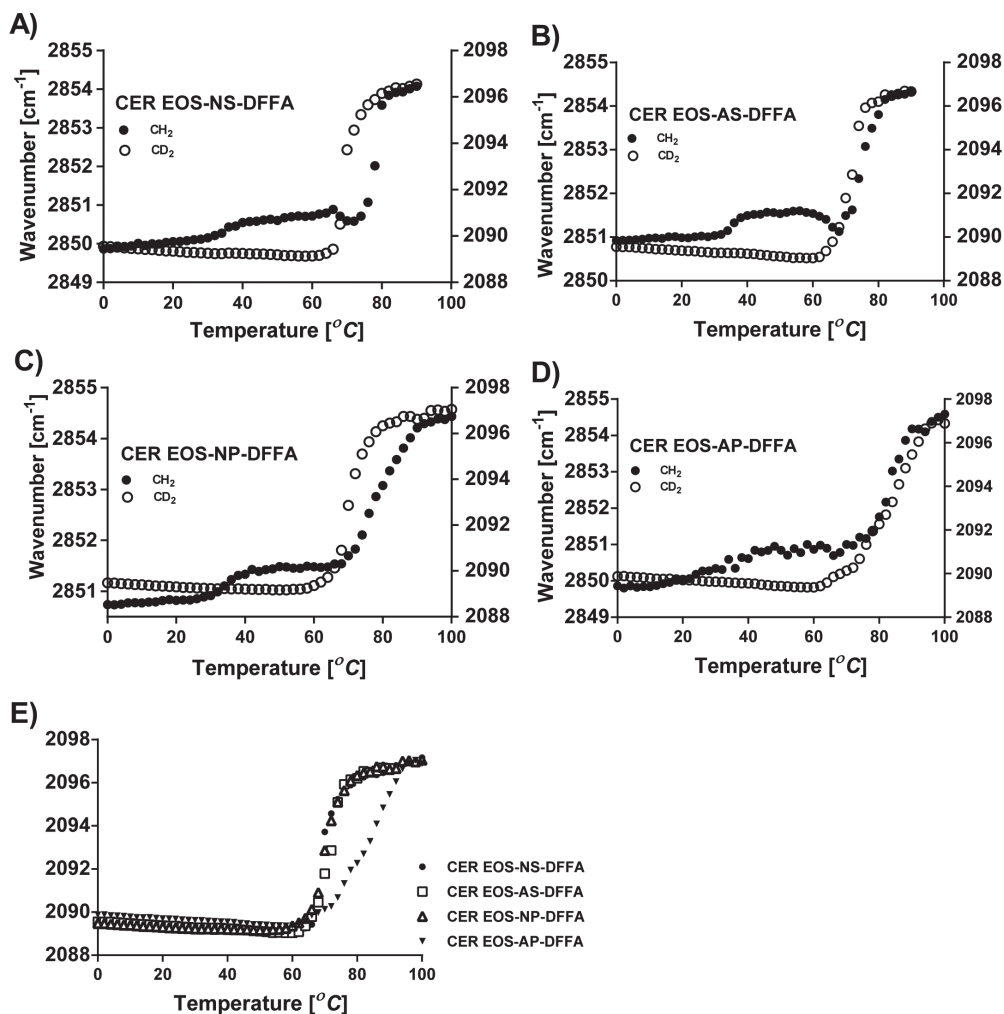


Figure 5: Thermotropic response of the $\nu_s\text{CH}_2$ and $\nu_s\text{CD}_2$ modes of the lipid models.

A-D) The CH_2 (filled circle) and the CD_2 (open circle) peak positions are plotted on the primary y-axis and secondary y-axis respectively displaying the phase transition temperatures of the CER and DFFA chains in the lipid models. E) $\nu_s\text{CD}_2$ modes of the lipid models showing the transition of the DFFA chains.

peak is observed in δCH_2 and δCD_2 modes while packed in the orthorhombic phase. The δCD_2 mode of the various models and DFFA mixture at 10 °C are displayed in figure 6A. The δCD_2 mode from the DFFAs in CER EOS-NS-DFFA, CER EOS-AS-DFFA, and CER EOS-NP-DFFA are split into two bands, indicating coupling of adjacent DFFA chains. In contrast, the δCD_2 mode of CER EOS-AP-DFFA exhibits an additional central peak, likewise observed in the δCH_2 mode at $\sim 1467\text{ cm}^{-1}$ (figure S4B), attributed to both a fraction of lipids in a hexagonal phase and the

presence of CD₂-CH₂ interaction. The size of the orthorhombic domain formed by the deuterated lipids was evaluated by measuring the magnitude of band splitting in the δCD₂ mode, in the region approximately 1080-1100 cm⁻¹ using the spectra collected at 10 °C. The magnitude of the band splitting of pure DFFA mixture was 7.2 cm⁻¹, which represents maximum CD₂-CD₂ peak splitting in a fully deuterated environment. The splitting values measured in the samples were 3.3, 4.1, and 3.9 cm⁻¹ for CER EOS-NS-DFFA, CER EOS-AS-DFFA, and CER EOS-NP-DFFA respectively. The reduction of the splitting and the shallower minima between the δCD₂ peaks in the spectrum of the various models compared to that of pure DFFA mixture represent reduced CD₂-CD₂ chain interaction and an increased CH₂-CD₂ chain interaction, indicating mixing of the deuterated and protiated chains. Evidently, due to the equimolar ratio of the lipid classes, a fraction of the DFFA chains in the lipid mixtures remain close enough to interact portrayed by the weak splitting. When increasing the temperature, the splitting of the δCD₂ mode of the various models collapse into single peaks (figure S4A). The δCD₂ mode of the various models and DFFA mixture at 32 °C are displayed in figure 6B. Only one peak or a weak split was detected in the spectra of all models. This

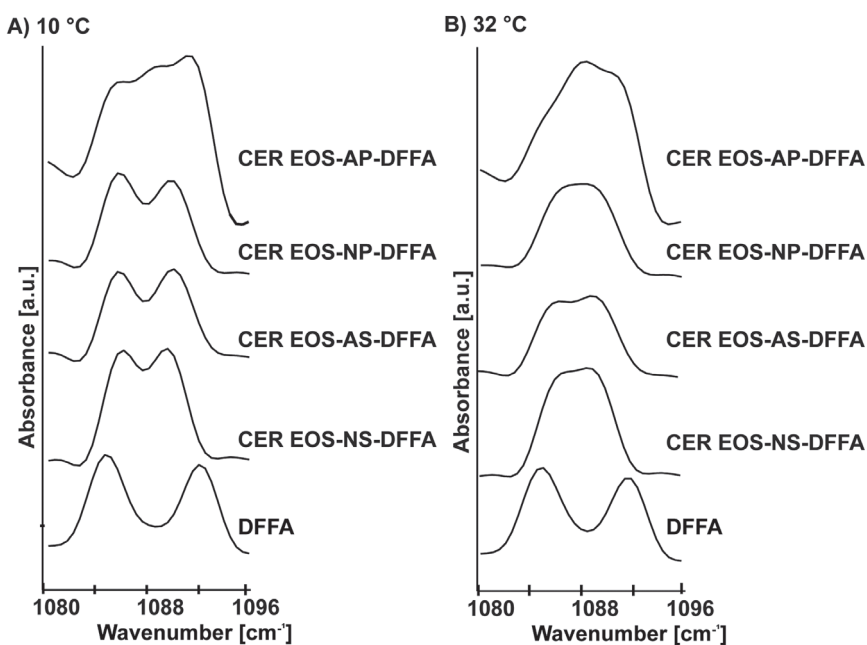


Figure 6: δCD₂ modes of the lipid models and DFFA.

A) The δCD₂ curves of the various lipid models at 10 °C displaying reduced splitting compared to DFFA. B) The δCD₂ modes of the various models and DFFA at skin physiological temperature (32 °C).

may be due to a mixed effect of increased CD₂-CH₂ interaction and a transition from orthorhombic to hexagonal packing. Similar behavior was displayed by the δCH₂ mode from the CER chains (figure S4B).

CER headgroup interactions differ in the various models

The content of free hydroxyl groups and an amide group enable CERs to act as both hydrogen bond donors and acceptors [57]. To investigate the hydrogen bonding in the headgroup regions, the CER amide I (~ 1650 cm⁻¹) and amide II (~ 1550 cm⁻¹) were examined by FTIR. The CER amide I band is related mainly to the C=O stretching vibration while amide II results primarily from the N-H bending vibration and the C-N stretching vibration. Lower amide I and higher amide II frequencies are consistent with stronger hydrogen bonding [58, 59]. The 1525-1675 cm⁻¹ spectral region for the lipid models at 10 °C are displayed in figure 7. Regarding amide I frequencies, CER EOS-NS amide I mode are split into two components centred at 1624.6 cm⁻¹ and 1641.1 cm⁻¹, attributed to intermolecular hydrogen bonding between two CER NS headgroups, similarly as reported in previous CER NS containing samples [59]. CER EOS-AS amide I mode shows an asymmetric peak centred at 1618.7 cm⁻¹ and shoulder at 1633.8 cm⁻¹. As a non-hydroxy and an α-hydroxy sphingosine-based CER are present in this mixture, both may contribute to the signal. In the spectrum of CER- EOS-NP in which two non-hydroxy CERs contribute to the amide 1 band, the mode is a doublet with a sharp peak positioned at 1639.6 cm⁻¹ and a broad shoulder on the left-hand side, positioned at 1618.8 cm⁻¹ being consistent with earlier reports [60]. Finally, in the spectrum of the CER EOS-AP, only one broad band at an amide I frequency of 1624.2 cm⁻¹ is present, which indicates the existence of strong hydrogen bonding interactions. The amide II bands are less complex. The single peaks are located at 1547.8 cm⁻¹, 1539.0 cm⁻¹, 1541.8 cm⁻¹ and 1551.3 cm⁻¹ in the spectrum of the CER EOS-NS, CER EOS-AS, CER- EOS-NP, and CER EOS-AP respectively. CER EOS-AP displayed a comparatively low amide I frequency and the highest amide II frequency indicating stronger hydrogen bonding compared to the other models.

CER headgroup affects the lamellar organization in the lipid models

The lamellar organization in the lipid models was examined by SAXD. This technique can provide information about the lamellar phases including their repeat distances. The X-ray diffraction profiles of the various models are provided in figure 8. CER EOS-NS and CER EOS-AS had similar diffraction curves with 4 diffraction peaks attributed to LPP with a repeat distance of 12.5 and 12.6 nm

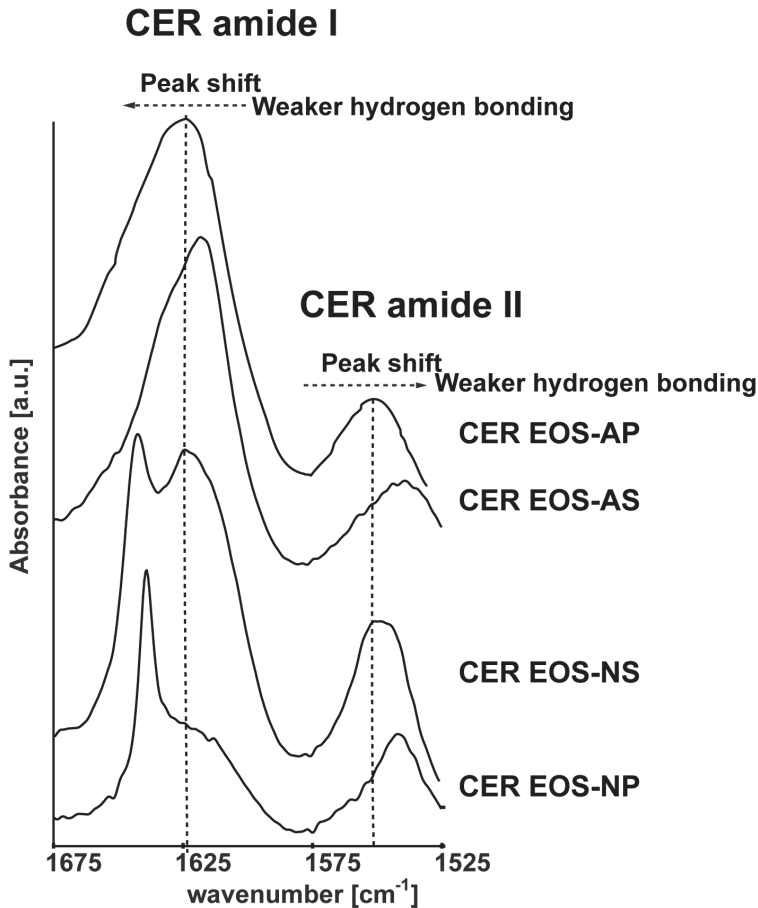


Figure 7: IR spectrum of the 1525-1675 cm^{-1} region of the lipid models at 10 °C.

CER EOS-NS amide I mode is split into 2 components. CER EOS-AS and CER EOS-NP amide I mode consist of a peak and a shoulder respectively, while CER EOS-AP amide I mode is not split. CER EOS-AP spectrum shows a comparatively low amide I frequency and the highest amide II frequency value indicating the strongest hydrogen bonding.

respectively. When focusing on the CER EOS-NP, the lipids also assembled in the LPP as is indicated by the 6 diffraction orders with a repeat distance of 13.3 nm. Besides the LPP, the peak at 3.7 nm ($q = 1.69 \text{ nm}^{-1}$) indicates the presence of phase-separated crystalline CER NP [61]. Finally, at $q = 1.1 \text{ nm}^{-1}$ (5.7 nm) a peak is present and no higher diffraction order could be identified. Consequently, this peak could not be assigned to a particular phase. Meanwhile, the diffraction pattern of CER EOS-AP model displayed 6 diffraction orders attributed to the LPP with a repeat distance of 13.4 nm. However, the 2nd and 3rd order peaks show

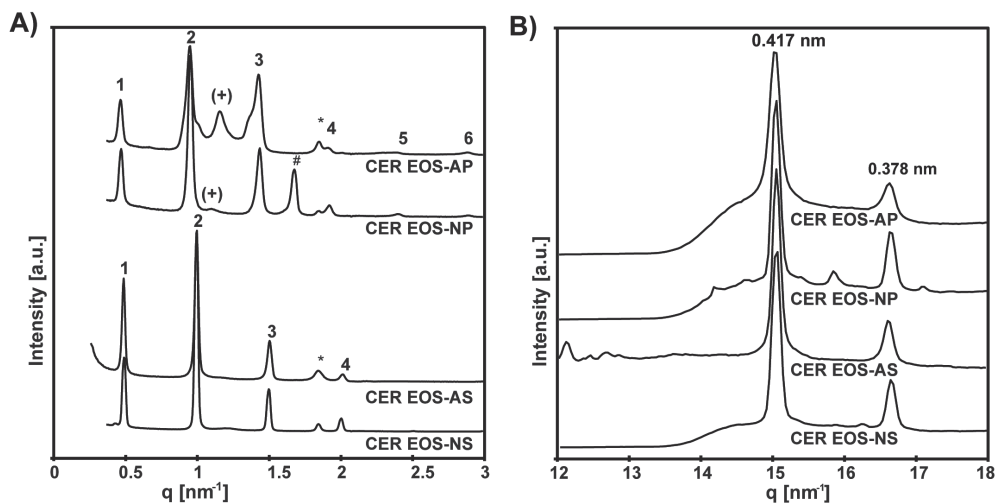


Figure 8: X-ray diffraction profile of the hydrated lipid models.

A) The SAXD profile of the lipid models. The arabic numbers 1, 2, 3 indicate the diffraction orders of the LPP. In the diffraction profile of CER EOS-NS, a series of diffraction peaks positioned at $q = 0.50, 1.00, 1.51, 2.01 \text{ nm}^{-1}$ indicate the 1st, 2nd, 3rd, and 4th diffraction orders attributed to the LPP with a repeat distance of 12.5 nm. In the diffraction profile of CER EOS-AS, the peak positions at $q = 0.49, 0.99, 1.52, \text{ and } 1.98 \text{ nm}^{-1}$ indicate the 1st, 2nd, 3rd, and 4th diffraction orders attributed to the LPP with a repeat distance of 12.6 nm. In the diffraction pattern of CER EOS-NP, the peak positions at $q = 0.48, 0.96, 1.45, 1.94$ (a shoulder) $2.41, \text{ and } 2.90 \text{ nm}^{-1}$ are attributed to 1st, 2nd, 3rd, 4th, 5th, and 6th diffraction orders of the LPP with a repeat distance of 13.3 nm. The reflection denoting crystalline CER NP is indicated by #. In the diffraction pattern of CER EOS-AP, the reflections at $q = 0.47, 0.96, 1.43, 1.93$ (a shoulder), $2.40, 2.89 \text{ nm}^{-1}$ are attributed to the 1st, 2nd, 3rd, 4th, 5th, and 6th diffraction orders attributed to the LPP with a repeat distance of 13.4 nm. The reflections at $q = 1.12 \text{ nm}^{-1}$ in CER EOS-NP and 1.16 nm^{-1} in CER EOS-AP are indicated by (+) and represent an unknown phase. The peaks attributed to crystalline CHOL are indicated by asterisk *. B) WAXD profile of the lipid models displaying two peaks, the 0.417 and the 0.378 nm peaks, located at $q \sim 15.2 \text{ and } 16.7 \text{ nm}^{-1}$ respectively. CER EOS-AP showed the lowest intensity 0.378 nm peak, indicating the lowest proportion of orthorhombic phase.

a shoulder, indicating additional phases. The strong shoulder at the 3rd order peak is most probably the reason why the intensity of this order diffraction peak is somewhat higher in this diffraction profile compared with the 3rd order peak intensity in the pattern of the other systems. Similar to CER EOS-NP, an additional peak of 5.4 nm was detected. All SAXD profiles revealed the presence of a peak related to a spacing of 3.4 nm attributed to crystalline domains of phase-separated CHOL. In summary, in all systems, the LPP was formed. In the sphingosine-based CER models besides the LPP, only phase-separated CHOL was present. In contrast, phytosphingosine-based systems formed the LPP, phase-separated CHOL, and additional phases.

Besides the SAXD studies, the WAXD pattern of the models was measured to obtain information on the lateral packing of the lipid chains. The WAXD profiles are shown in figure 8B. All the models display two reflections, ~ 0.417 and 0.378 nm located at $q = \sim 15.20$ and 16.7 nm^{-1} respectively. While the 0.417 nm peak can be attributed to the orthorhombic and hexagonal packing, the 0.378 nm peak is only attributed to the orthorhombic packing. CER EOS-AP has the lowest intensity 0.378 nm peak indicating the smallest proportion of lipids forming an orthorhombic phase. These findings are in agreement with our FTIR result.

DISCUSSION

CER headgroup affects the skin barrier function

The composition and organization of intercellular lipids of the SC are important for the skin barrier function. Changes in SC lipid composition have been reported in several inflammatory skin diseases [26, 62-64], as well as in human skin equivalents [65, 66] and regenerated SC after tape-stripping [67]. In these examples, the levels of CER AS and CER NS were increased at the expense of the level of CER NP. The exchange of CER subclasses contributed to a compromised skin barrier, as illustrated by increased values of transepidermal water loss (TEWL) [62]. However, studying whether a change in the ratio between these lipid classes is an underlying factor for an impaired barrier function is not possible in intact SC as there are always other associated changes in the lipid or protein composition, and lipids cannot be extracted selectively from SC. Therefore to study the relationship between lipid composition, lipid organization, and barrier function, lipid model membranes were developed [42, 68].

The aim of the present study was to examine the effect of CER headgroup architecture, particularly focusing on the comparison between sphingosine and phytosphingosine-based CER compositions, on the permeability and phase behavior of lipid models. Lipid model systems of an equimolar mixture of CERs, CHOL, and FFAs were employed, in a similar molar ratio as is present in human SC [10]. The CER fraction of the lipid mixture comprised of 60% of either CER NS, AS, NP, or AP with a single chain length and 40% CER EOS in order to form an LPP model system. Our purpose was to study primarily the formation of the LPP. To form only a single LPP structure and avoid the formation of the SPP, the CER EOS level was increased beyond the approximate 10 mol% reported in the human SC [27]. Our results demonstrate that membranes containing CERs with the phytosphingosine subclass exhibited a stronger lipid barrier. These findings

indicate that increased levels of CER NS and reduced level of CER NP as observed in atopic dermatitis patients [69], psoriatic scale [47], and compromised tape-stripped skin [67] may contribute to the impaired barrier function. In contrast, it was previously shown that CER NP encouraged higher permeability through the model membrane when compared to CER NS [43]. In that study, no CER EOS was incorporated in the mixtures, thus, the lipids assembled in the SPP rather than the LPP as in the present study. Furthermore, we observed that CER EOS enhances the miscibility between the different lipid components (unpublished results), which may explain the difference in result. In another study, no difference in permeability was observed between model membranes of the same FFA composition containing either CER NS or a CER mixture incorporating sphingosine and phytosphingosine CERs [45]. However, this difference may be due to i) a lower concentration of phytosphingosine CERs that was replaced by the sphingosine counterpart in the CER mixture, ii) a simultaneous change in CER chain length distribution, in which CERs with C16 acyl chain were replaced by CERs with a C24 acyl chain in the present study and iii) the absence of CER EOS. The CER NS model membrane in that study, despite lacking CER EOS, resulted in an E-PABA flux value similar to that of CER EOS-NS model in the current study. However, as these are different experiments and small differences in temperature of the membranes substantially affect the flux [45], this may play a role. Furthermore, although low levels of CER EOS may reduce the permeability, high levels of CER EOS may affect the flux in a different way due to a higher level of liquid domains [37].

When comparing the E-PABA flux of lipid models prepared with non-hydroxy fatty acid-based CERs to the models prepared with α -hydroxy fatty acid-based CERs with the same sphingoid base (e.g. CER NS and AS), there was no significant difference in permeability. The phytosphingosine CERs which resulted in significantly lower membrane permeability do not possess a 4,5 trans double bond present in the sphingosine CERs but rather, contain an additional hydroxyl group on C4 position on the base chain. Thus, the position of the hydroxyl group in the CER headgroup and probably the presence or absence of the trans double bond influenced the permeability of the model membrane.

CER headgroup affects the lipid phase behavior, chain, and headgroup interactions in model SC

A wider ordered-disordered phase transition temperature range was observed in the phytosphingosine-based CER models. This may be due to either a combined effect of differences in headgroup interactions and/or the presence of the

multiple phases. The CER headgroup did not have an effect on the domain size of the lipids forming an orthorhombic packing since all the models exhibited large interpeak distance approaching the maximum value, indicating large orthorhombic domain sizes at 10 °C. However, when comparing the intensities of the characteristic orthorhombic peaks, which relate directly to the proportion of the orthorhombic phase [70], CER EOS-AP exhibited the least proportion of lipids in an orthorhombic phase. This was confirmed by the wide-angle X-ray diffraction pattern of CER-EOS-AP. Our results are in agreement with a previous infrared study of ternary SC models reporting that phytosphingosine-based CERs adopt a hexagonal chain packing [71], while sphingosine-based CERs adopt an orthorhombic chain packing [33]. The higher fraction of lipids forming a hexagonal packing in CER EOS-AP may be due to a larger interfacial area per headgroup of the phytosphingosine CERs than the sphingosine analogues, which allows more space and optimal geometry for hydrogen bonding [72].

In previous studies, it has been observed that an increase in the fraction of lipids forming a hexagonal packing results in an increase in permeability [73]. On the contrary, CER EOS-AP, which contained the highest proportion of the hexagonal phase, resulted in the lowest permeability. Our study indicates strong hydrogen bonding within the CER EOS-AP model. In this particular case, the effect of increased hydrogen bonding in the headgroup region seems to overrule the reduced inter-chain van der Waals interactions resulting in a reduced permeability. A previous infrared study of individual CERs also reported stronger hydrogen bonding and hexagonal lateral packing in phytosphingosine CERs and weaker hydrogen bonding and orthorhombic packing in their analogous sphingosine CERs [60]. CER EOS-NP displayed a low amide II frequency and an orthorhombic lateral packing, which are characteristic of sphingosine CERs. This may be caused by the presence of 40% CER EOS that contributed to the molecular interactions observed in the models in the current study. In addition, the resilient orthorhombic phase of CER EOS-NP evinced by its indisputably high $T_{M,OR-HEX}$ contributed to its low permeability.

Focusing on the mixing property of the lipid chains, CERs and DFFAs chains were mixed with each other in all models as indicated by the weak split in the δCD_2 modes of the models compared to the strong split in DFFA. The transition of the CER and FFA chain in CER EOS-NP does not occur in exactly the same temperature range. This may be due to the presence of CER and FFA rich regions within the orthorhombic lattice or to phase-separated CER NP. Since recrystallization of only the CER chains occurred in CER EOS-NS-DFFA, the recrystallization observed in CER EOS-NS δCH_2 mode was thus due to the

CERs. It is also remarkable that a modification in CER EOS-NS model, by spraying the lipid mixture at a lower concentration, of less than 5 mg/ml resulted in the disappearance of CER chain recrystallization (figure S5). Considering the v_sCD_2 modes, the DFFAs in the CER EOS-AP-DFFA underwent an ordered-disordered phase transition at a higher temperature than in the other models implying a stronger cohesive bond. This may be attributed to the stronger headgroup hydrogen bonding interaction in CER EOS-AP.

CER headgroup affect the lamellar organization in lipid model mixtures

In-depth knowledge of the lipid organization within the unit cell of the lamellar phases is important for understanding the skin barrier function. In the present study we observed that in all four systems an LPP can be formed, irrespective of the choice of CER NS, AS, NP or AP. However, in CER EOS-NS and CER EOS-AS systems, the LPP is formed without additional phases, except for phase-separated crystalline CHOL. These results indicate that it is easier for CER EOS combined with CER NS or AS, to exclusively form the LPP than when combined with CER AP or NP. Furthermore, when forming the LPP, the characteristic intensity distribution of the 1st (weaker intensity), 2nd (stronger intensity), and 3rd (weaker intensity) order peak is observed (for additional information see next section), signifying that the LPP has been formed. The LPP in phytosphingosine-based CER models had longer periodicities than those of their sphingosine counterparts. In contrast, the non-hydroxy or α -hydroxy CER models with the same sphingoid base (e.g. CER NS and AS), did not show significant differences in their LPP repeat distance. Possible explanations for the longer repeat distance experienced by the phytosphingosine-based CER model are i) the presence of additional water molecules in the headgroup region that would cause swelling in the lamellar. However, this is unlikely as fully hydrated and dry mixtures result in similar repeat distance (figure S6); ii) the presence of additional phases. In the diffraction pattern of the CER EOS-NP, a strong reflection at 1.7 nm^{-1} is attributed to crystalline CER NP [61]. As a consequence, the LPP contained a higher proportion of CER EOS, which induced an increase in the periodicity (unpublished data). This would also explain the similarity in repeat distances of non-hydroxy and α -hydroxy based sphingoid bases, as in these models no additional phases had formed; iii) a difference in the headgroup orientation at the basal plane of the lamellar phase. This change in orientation may be related to the presence/absence of 4,5 trans double bond, number and position of hydroxyl groups in the CER species as is observed for the air-water interface [74]

or iv) a difference in the arrangement of the CERs, namely, linear versus hairpin arrangement.

The formation of the LPP in SC and lipid mixtures.

Using X-ray diffraction, the LPP has been identified not only in human SC [75] but also in murine [14, 76], porcine skin [12], and human skin equivalents [65]. In all these cases, the repeat distance of the LPP was reported to be approximately 13 nm. By examining CERs isolated from porcine [31] or human SC [41], mixed with cholesterol and FFAs, both the LPP and SPP were reproduced all with repeat distance very similar to that in native SC. In subsequent studies, synthetic CERs were used as this allowed a more detailed analysis of the interactions between the individual lipids. It was reported that after incorporating acyl CERs in the synthetic CER mixtures, the lipids assembled in the LPP and SPP, although the repeat distance of the LPP was somewhat shorter [36]. This could be expected as the chain lengths of the natural lipids are longer than those of the synthetic CERs: the mean total CER chain length (sphingoid base + acyl chain) in SC of human skin is approximately 47 C atoms [77], while in the lipid model system used in these studies the CERs have a mean chain length of 45.2 C atoms (calculated from the CER subclass composition) [36]. In addition, the choice of the headgroup may also contribute to a difference in repeat distance, as is reported in the present paper. Therefore, differences in lamellar repeat distance in synthetic mixtures compared to that in native SC can be explained without assuming different lipid arrangements in the unit cell as was suggested recently [78]. In fact, the similarity in the lipid arrangement in the LPP in mixtures prepared from synthetic [36], and isolated CERs [69, 79], but also in SC of mice skin [76] and human skin equivalents [65] (In both SC, the lipids form primarily an LPP) has been demonstrated by the characteristic intensity distribution of the various diffraction peaks attributed to the LPP: the 1st and 3rd order diffraction peaks have a lower intensity than the 2nd order diffraction peak. This intensity distribution is a reflection of the electron density profile in the unit cell of a lamellar phase. Therefore, all these systems do have a similar unit cell electron density profile, and thus the arrangement of the lipids appears to be very similar. The latter has also been demonstrated by the similarity in the structure factors of the LPP in SC and those of the LPP in synthetic and isolated CER mixtures [49]. These structure factors are the basis for calculating the electron density profile of the unit cell.

It is important to realize, especially when using synthetic CERs, after the proper composition, the choice of the spraying method and the temperature of annealing are both crucial for the LPP formation, which has been discussed previously [78].

Setting the equilibration temperature too high or too low can be detrimental to the LPP formation [80]. Furthermore, the distance between the nozzle and the spraying surface, and the gas flow are crucial parameters. Differences in the choice of these parameters may be a reason why phases with the characteristic LPP intensity distribution are sometimes not formed even with a proper choice of the CER composition [46], while a very similar lipid composition does result in the exclusive formation of the LPP [48]. In contrast, to current literature [78], an increase in the level of CER EOS results in an increase in the fraction of lipids forming the LPP at the expense of the lipids forming the SPP, keeping the characteristic intensity distribution of diffraction peaks of the LPP very similar [38, 48]. As the intensity distribution is directly related to the electron density profile, this demonstrates that by increasing the CER EOS level, there is no substantial change in the LPP electron density profile and therefore the basic structure in the unit cell remains the same. Finally, the absence of the LPP in systems in which the CER EOS is replaced by a CER EOS with a saturated but branched C18-acyl chain is most likely due to a reduction of a fluid phase as has been shown by NMR studies [81]. This is in agreement with a previous publication demonstrating that the presence of a fluid phase is an absolute necessity for the formation of the LPP [82].

CONCLUSION

CER headgroup architecture influences the permeability, lipid phase behavior, and molecular interactions of lipid models. In the presence of CER EOS, the majority of lipid population in all the models assembled in the LPP. When focusing on the interactions in the systems, we have shown that due to distinct phase behavior, lipid chain packing, and headgroup interactions, sphingosine-based CER model membranes resulted in a higher permeability than the phytosphingosine-based models. This is an important observation for understanding the effect of changes in CER subclass composition on the skin barrier function in diseased skin, which is paramount to the optimization and targeting of therapies.

ACKNOWLEDGEMENTS

We thank the company Evonik for the donation of CERs. We also acknowledge the staff at the DUBBLE beamline 26B at the ESRF, Grenoble, France who assisted with the X-ray diffractions measurements.

REFERENCES

1. Blank, I. H., Cutaneous barriers. *J. Invest. Dermatol.* **1965**, *45* (4), 249-256.
2. Madison, K. C., Barrier function of the skin: "la raison d'être" of the epidermis. *J. Invest. Dermatol.* **2003**, *121* (2), 231-41.
3. Feingold, K. R., Thematic review series: skin lipids. The role of epidermal lipids in cutaneous permeability barrier homeostasis. *J. Lipid Res.* **2007**, *48* (12), 2531-46.
4. Elias, P. M., Epidermal barrier function - Intercellular lamellar lipid structures, origin, composition, and metabolism. *J. Control. Release* **1991**, *15* (3), 199-208.
5. Talreja, P. S.; Kleene, N. K.; Pickens, W. L.; Wang, T. F.; Kasting, G. B., Visualization of the lipid barrier and measurement of lipid pathlength in human stratum corneum. *AAPS Pharmsci.* **2001**, *3* (2), art. no. 13.
6. Bodde, H. E.; Kruithof, M. A. M.; Brussee, J.; Koerten, H. K., Visualization of normal and enhanced Hgcl2 transport through human-skin invitro. *Int. J. Pharm.* **1989**, *53* (1), 13-24.
7. Gray, G. M.; Yardley, H. J., Lipid compositions of cells isolated from pig, human, and rat epidermis. *J. Lipid Res.* **1975**, *16* (6), 434-440.
8. Elias, P. M.; Goerke, J.; Friend, D. S., Mammalian epidermal barrier layer lipids: composition and influence on structure. *J. Invest. Dermatol.* **1977**, *69* (6), 535-46.
9. Elias, P. M., Epidermal lipids, membranes, and keratinization. *Int. J. Dermatol.* **1981**, *20* (1), 1-19.
10. Weerheim, A.; Ponec, M., Determination of stratum corneum lipid profile by tape stripping in combination with high-performance thin-layer chromatography. *Arch. Dermatol. Res.* **2001**, *293* (4), 191-199.
11. Wertz, P. W.; van den Bergh, B., The physical, chemical and functional properties of lipids in the skin and other biological barriers. *Chem. Phys. Lipids* **1998**, *91* (2), 85-96.
12. Bouwstra, J. A.; Gooris, G. S.; Bras, W.; Downing, D. T., Lipid organization in pig stratum-corneum. *J. Lipid Res.* **1995**, *36* (4), 685-695.
13. Hill, J. R.; Wertz, P. W., Molecular models of the intercellular lipid lamellae from epidermal stratum corneum. *Biochim. Biophys. Acta* **2003**, *1616* (2), 121-6.
14. White, S. H.; Mirejovsky, D.; King, G. I., Structure of lamellar lipid domains and corneocyte envelopes of murine stratum corneum. An X-ray diffraction study. *Biochemistry* **1988**, *27* (10), 3725-32.
15. Damien, F.; Boncheva, M., The extent of orthorhombic lipid phases in the stratum corneum determines the barrier efficiency of human skin in vivo. *J. Invest. Dermatol.* **2010**, *130* (2), 611-614.
16. Boncheva, M.; Damien, F.; Normand, V., Molecular organization of the lipid matrix in intact stratum corneum using ATR-FTIR spectroscopy. *Biochim. Biophys. Acta* **2008**, *1778* (5), 1344-55.
17. Moore, D. J.; Rerek, M. E.; Mendelsohn, R., Lipid domains and orthorhombic phases in model stratum corneum: Evidence from Fourier transform infrared spectroscopy studies. *Biochemical and Biophysical Research Communications* **1997**, *231* (3), 797-801.
18. Mendelsohn, R.; Rerek, M. E.; Moore, D. J., Infrared spectroscopy and microscopic imaging of stratum corneum models and skin. *Phys. Chem. Chem. Phys.* **2000**, *2* (20), 4651-4657.
19. Groen, D.; Poole, D. S.; Gooris, G. S.; Bouwstra, J. A., Is an orthorhombic lateral packing and a proper lamellar organization important for the skin barrier function? *Biochim. Biophys. Acta* **2011**, *1808* (6), 1529-1537.

20. Robson, K. J.; Stewart, M. E.; Michelsen, S.; Lazo, N. D.; Downing, D. T., 6-Hydroxy-4-sphinganine in human epidermal ceramides. *J. Lipid Res.* **1994**, *35* (11), 2060-8.
21. Stewart, M. E.; Downing, D. T., A new 6-hydroxy-4-sphinganine-containing ceramide in human skin. *J. Lipid Res.* **1999**, *40* (8), 1434-9.
22. Masukawa, Y.; Narita, H.; Shimizu, E.; Kondo, N.; Sugai, Y.; Oba, T.; Homma, R.; Ishikawa, J.; Takagi, Y.; Kitahara, T.; Takema, Y.; Kita, K., Characterization of overall ceramide species in human Stratum corneum. *J. Lipid Res.* **2008**, *49* (7), 1466-1476.
23. van Smeden, J.; Hoppel, L.; van der Heijden, R.; Hankemeier, T.; Vreeken, R. J.; Bouwstra, J. A., LC/MS analysis of stratum corneum lipids: ceramide profiling and discovery. *J. Lipid Res.* **2011**, *52* (6), 1211-21.
24. Rabionet, M.; Gorgas, K.; Sandhoff, R., Ceramide synthesis in the epidermis. *Biochim. Biophys. Acta* **2014**, *1841* (3), 422-34.
25. Wertz, P. W.; Miethke, M. C.; Long, S. A.; Strauss, J. S.; Downing, D. T., The Composition of the ceramides from human stratum-corneum and from comedones. *J. Invest. Dermatol.* **1985**, *84* (5), 410-412.
26. van Smeden, J.; Bouwstra, J. A., Stratum corneum lipids: Their role for the skin barrier function in healthy subjects and atopic dermatitis patients. *Curr. Probl. Dermatol.* **2016**, *49*, 8-26.
27. t'Kindt, R.; Jorge, L.; Dumont, E.; Couturon, P.; David, F.; Sandra, P.; Sandra, K., Profiling and characterizing skin ceramides using reversed-phase liquid chromatography–quadrupole time-of-flight mass spectrometry. *Anal. Chem.* **2012**, *84* (1), 403-411.
28. Gooris, G. S.; Bouwstra, J. A., Infrared spectroscopic study of stratum corneum model membranes prepared from human ceramides, cholesterol, and fatty acids. *Biophys. J.* **2007**, *92* (8), 2785-95.
29. Caussin, J.; Gooris, G. S.; Janssens, M.; Bouwstra, J. A., Lipid organization in human and porcine stratum corneum differs widely, while lipid mixtures with porcine ceramides model human stratum corneum lipid organization very closely. *Biochim. Biophys. Acta* **2008**, *1778* (6), 1472-1482.
30. McIntosh, T. J.; Stewart, M. E.; Downing, D. T., X-ray diffraction analysis of isolated skin lipids: reconstitution of intercellular lipid domains. *Biochemistry* **1996**, *35* (12), 3649-53.
31. Bouwstra, J. A.; Gooris, G. S.; Cheng, K.; Weerheim, A.; Bras, W.; Ponec, M., Phase behavior of isolated skin lipids. *J. Lipid Res.* **1996**, *37* (5), 999-1011.
32. Bouwstra, J. A.; Gooris, G. S.; Dubbelaar, F. E.; Ponec, M., Phase behavior of stratum corneum lipid mixtures based on human ceramides: the role of natural and synthetic ceramide 1. *J. Invest. Dermatol.* **2002**, *118* (4), 606-17.
33. Moore, D. J.; Rerek, M. E., Insights into the molecular organization of lipids in the skin barrier from infrared spectroscopy studies of stratum corneum lipid models. *Acta Derm-Venereol.* **2000**, 16-22.
34. Lafleur, M., Phase behaviour of model stratum corneum lipid mixtures: an infrared spectroscopy investigation. *Can. J. Chem.* **1998**, *76* (11), 1501-1511.
35. Thewalt, J.; Kitson, N.; Araujo, C.; Mackay, A.; Bloom, M., Models of Stratum-Corneum Intercellular Membranes - the Sphingolipid Headgroup Is a Determinant of Phase-Behavior in Mixed Lipid Dispersions. *Biochem. Biophys. Res. Co.* **1992**, *188* (3), 1247-1252.
36. de Jager, M. W.; Gooris, G. S.; Ponec, M.; Bouwstra, J. A., Lipid mixtures prepared with well-defined synthetic ceramides closely mimic the unique stratum corneum lipid phase behavior. *J. Lipid Res.* **2005**, *46* (12), 2649-2656.
37. Janssens, M.; Gooris, G. S.; Bouwstra, J. A., Infrared spectroscopy studies of mixtures prepared with synthetic ceramides varying in head group architecture: coexistence of liquid and crystalline phases. *Biochim. Biophys. Acta* **2009**, *1788* (3), 732-742.

38. de Jager, M.; Gooris, G.; Ponec, M.; Bouwstra, J., Acylceramide head group architecture affects lipid organization in synthetic ceramide mixtures. *J. Invest. Dermatol.* **2004**, *123* (5), 911-6.
39. Bouwstra, J. A.; Gooris, G. S.; Dubbelaar, F. E.; Weerheim, A. M.; Ijzerman, A. P.; Ponec, M., Role of ceramide 1 in the molecular organization of the stratum corneum lipids. *J. Lipid Res.* **1998**, *39* (1), 186-96.
40. Groen, D.; Gooris, G. S.; Bouwstra, J. A., Model membranes prepared with ceramide EOS, cholesterol, and free fatty acids form a unique lamellar phase. *Langmuir* **2010**, *26* (6), 4168-75.
41. Bouwstra, J. A.; Gooris, G. S.; Dubbelaar, F. E.; Ponec, M., Phase behavior of lipid mixtures based on human ceramides: coexistence of crystalline and liquid phases. *J. Lipid Res.* **2001**, *42* (11), 1759-70.
42. de Jager, M.; Groenink, W.; Bielsa i Guivernau, R.; Andersson, E.; Angelova, N.; Ponec, M.; Bouwstra, J., A novel in vitro percutaneous penetration model: evaluation of barrier properties with p-aminobenzoic acid and two of its derivatives. *Pharm. Res.* **2006**, *23* (5), 951-60.
43. Skolova, B.; Kovacik, A.; Tesar, O.; Opalka, L.; Vavrova, K., Phytosphingosine, sphingosine and dihydrosphingosine ceramides in model skin lipid membranes: permeability and biophysics. *Biochim. Biophys. Acta* **2017**, *1859* (5), 824-834.
44. Skolova, B.; Jandovska, K.; Pullmannova, P.; Tesar, O.; Roh, J.; Hrabalek, A.; Vavrova, K., The role of the trans double bond in skin barrier sphingolipids: permeability and infrared spectroscopic study of model ceramide and dihydroceramide membranes. *Langmuir* **2014**, *30* (19), 5527-35.
45. Uchiyama, M.; Oguri, M.; Mojumdar, E. H.; Gooris, G. S.; Bouwstra, J. A., Free fatty acids chain length distribution affects the permeability of skin lipid model membranes. *Biochim. Biophys. Acta* **2016**, *1858* (9), 2050-9.
46. Opalka, L.; Kovacik, A.; Maixner, J.; Vavrova, K., Omega-O-Acylceramides in skin lipid membranes: effects of concentration, sphingoid base, and model complexity on microstructure and permeability. *Langmuir* **2016**, *32* (48), 12894-12904.
47. Motta, S.; Monti, M.; Sesana, S.; Caputo, R.; Carelli, S.; Ghidoni, R., Ceramide composition of the psoriatic scale. *Biochim. Biophys. Acta* **1993**, *1182* (2), 147-51.
48. Gooris, G. S.; Kamran, M.; Kros, A.; Moore, D. J.; Bouwstra, J. A., Interactions of dipalmitoylphosphatidylcholine with ceramide-based mixtures. *Biochim. Biophys. Acta* **2018**, *1860* (6), 1272-1281.
49. Groen, D.; Gooris, G. S.; Bouwstra, J. A., New insights into the stratum corneum lipid organization by X-ray diffraction analysis. *Biophys. J.* **2009**, *97* (8), 2242-2249.
50. Wertz, P.W.; Downing, D.T., *Physiology, biochemistry and molecular biology of the skin*. second ed.; Oxford University Press: New York, 1991; Vol. 1, p 205-236.
51. International Conference on Harmonization (ICH) Q2 (R1), Validation of analytical procedures: Text and Methodology. 2005.
52. European Pharmacopoeia. 8 ed.; European Directorate for the quality of medicines & healthcare. Strasbourg, 2014; Vol. 1.
53. Oguri, M.; Gooris, G. S.; Bito, K.; Bouwstra, J. A., The effect of the chain length distribution of free fatty acids on the mixing properties of stratum corneum model membranes. *Biochim. Biophys. Acta* **2014**, *1838* (7), 1851-1861.
54. Mendelsohn, R.; Moore, D. J., Infrared determination of conformational order and phase behavior in ceramides and stratum corneum models. *Methods Enzymol.* **2000**, *312*, 228-47.

55. Snyder, R. G.; Goh, M. C.; Srivatsavoy, V. J. P.; Strauss, H. L.; Dorset, D. L., Measurement of the growth-kinetics of microdomains in binary N-alkane solid-solutions by infrared-spectroscopy. *J. Phys. Chem-US* **1992**, *96* (24), 10008-10019.
56. Mendelsohn, R.; Liang, G. L.; Strauss, H. L.; Snyder, R. G., IR spectroscopic determination of gel state miscibility in long-chain phosphatidylcholine mixtures. *Biophys. J.* **1995**, *69* (5), 1987-1998.
57. Pascher, I., Molecular arrangements in sphingolipids. Conformation and hydrogen bonding of ceramide and their implication on membrane stability and permeability. *Biochim. Biophys. Acta* **1976**, *455* (2), 433-51.
58. Moore, D. J.; Rerek, M. E.; Mendelsohn, R., FTIR spectroscopy studies of the conformational order and phase behavior of ceramides. *J Phys Chem-Us* **1997**, *101* (44), 8933-8940.
59. Moore, D. J.; Rerek, M. E.; Mendelsohn, R., Role of ceramides 2 and 5 in the structure of the stratum corneum lipid barrier. *Int. J. Cosmet. Sci.* **1999**, *21* (5), 353-68.
60. Rerek, M. E.; Chen, H. C.; Markovic, B.; Van Wyck, D.; Garidel, P.; Mendelsohn, R.; Moore, D. J., Phytosphingosine and sphingosine ceramide headgroup hydrogen bonding: structural insights through thermotropic hydrogen/deuterium exchange. *J Phys Chem-Us* **2001**, *105* (38), 9355-9362.
61. de Jager, M. W.; Gooris, G. S.; Dolbnya, I. P.; Ponec, M.; Bouwstra, J. A., Modelling the stratum corneum lipid organisation with synthetic lipid mixtures: the importance of synthetic ceramide composition. *Biochim. Biophys. Acta* **2004**, *1664* (2), 132-140.
62. Ishikawa, J.; Narita, H.; Kondo, N.; Hotta, M.; Takagi, Y.; Masukawa, Y.; Kitahara, T.; Takema, Y.; Koyano, S.; Yamazaki, S.; Hatamochi, A., Changes in the ceramide profile of atopic dermatitis patients. *J. Invest. Dermatol.* **2010**, *130* (10), 2511-4.
63. Danso, M.; Boiten, W.; van Drongelen, V.; Gmelig Meijling, K.; Gooris, G.; El Ghalbzouri, A.; Absalah, S.; Vreeken, R.; Kezic, S.; van Smeden, J.; Lavrijsen, S.; Bouwstra, J., Altered expression of epidermal lipid bio-synthesis enzymes in atopic dermatitis skin is accompanied by changes in stratum corneum lipid composition. *J. Dermatol. Sci.* **2017**, *88* (1), 57-66.
64. Di Nardo, A.; Wertz, P.; Giannetti, A.; Seidenari, S., Ceramide and cholesterol composition of the skin of patients with atopic dermatitis. *Acta Derm-Venereol.* **1998**, *78* (1), 27-30.
65. Thakoersing, V. S.; Gooris, G. S.; Mulder, A.; Rietveld, M.; El Ghalbzouri, A.; Bouwstra, J. A., Unraveling barrier properties of three different in-house human skin equivalents. *Tissue Eng. Pt. C-Me.* **2012**, *18* (1), 1-11.
66. Danso, M. O.; van Drongelen, V.; Mulder, A.; van Esch, J.; Scott, H.; van Smeden, J.; El Ghalbzouri, A.; Bouwstra, J. A., TNF-alpha, and Th2 cytokines induce atopic dermatitis-like features on epidermal differentiation proteins and stratum corneum lipids in human skin equivalents. *J. Invest. Dermatol.* **2014**, *134* (7), 1941-1950.
67. Boiten, W. A.; Berkers, T.; Absalah, S.; van Smeden, J.; Lavrijsen, A. P. M.; Bouwstra, J. A., Applying a vernix caseosa based formulation accelerates skin barrier repair by modulating lipid biosynthesis. *J. Lipid Res.* **2018**, *59* (2), 250-260.
68. de Jager, M.; Groenink, W.; van der Spek, J.; Janmaat, C.; Gooris, G.; Ponec, M.; Bouwstra, J., Preparation and characterization of a stratum corneum substitute for in vitro percutaneous penetration studies. *Biochim. Biophys. Acta* **2006**, *1758* (5), 636-44.
69. Janssens, M.; van Smeden, J.; Gooris, G. S.; Bras, W.; Portale, G.; Caspers, P. J.; Vreeken, R. J.; Kezic, S.; Lavrijsen, A. P.; Bouwstra, J. A., Lamellar lipid organization and ceramide composition in the stratum corneum of patients with atopic eczema. *J. Invest. Dermatol.* **2011**, *131* (10), 2136-8.
70. Berkers, T.; van Dijk, L.; Absalah, S.; van Smeden, J.; Bouwstra, J. A., Topically applied fatty acids are elongated before incorporation in the stratum corneum lipid matrix in compromised skin. *Exp. Dermatol.* **2017**, *26* (1), 36-43.

71. Rerek, M. E.; Van Wyck, D.; Mendelsohn, R.; Moore, D. J., FTIR spectroscopic studies of lipid dynamics in phytosphingosine ceramide models of the stratum corneum lipid matrix. *Chem. Phys. Lipids* **2005**, *134* (1), 51-8.
72. Lunden, B. M.; Lofgren, H.; Pascher, I., Accommodation of hydroxyl groups and their hydrogen bond system in a hydrocarbon matrix. *Chem. Phys. Lipids* **1977**, *20* (4), 263-71.
73. Mojumdar, E. H.; Helder, R. W.; Gooris, G. S.; Bouwstra, J. A., Monounsaturated fatty acids reduce the barrier of stratum corneum lipid membranes by enhancing the formation of a hexagonal lateral packing. *Langmuir* **2014**, *30* (22), 6534-43.
74. Lofgren, H.; Pascher, I., Molecular arrangements of sphingolipids. The monolayer behaviour of ceramides. *Chem. Phys. Lipids* **1977**, *20* (4), 273-84.
75. Bouwstra, J. A.; Gooris, G. S.; Vanderspek, J. A.; Bras, W., Structural Investigations of human stratum-corneum by small-angle X-ray-scattering. *J. Invest. Dermatol.* **1991**, *97* (6), 1005-1012.
76. Bouwstra, J. A.; Gooris, G. S.; van der Spek, J. A.; Lavrijsen, S.; Bras, W., The lipid and protein structure of mouse stratum corneum: a wide and small angle diffraction study. *Biochim. Biophys. Acta* **1994**, *1212* (2), 183-92.
77. Janssens, M.; van Smeden, J.; Gooris, G. S.; Bras, W.; Portale, G.; Caspers, P. J.; Vreeken, R. J.; Hankemeier, T.; Kezic, S.; Wolterbeek, R.; Lavrijsen, A. P.; Bouwstra, J. A., Increase in short-chain ceramides correlates with an altered lipid organization and decreased barrier function in atopic eczema patients. *J. Lipid Res.* **2012**, *53* (12), 2755-66.
78. Schmitt, T.; Lange, S.; Sonnenberger, S.; Dobner, B.; Deme, B.; Langner, A.; Neubert, R. H. H., The long periodicity phase (LPP) controversy part I: the influence of a natural-like ratio of the CER[EOS] analogue [EOS]-br in a CER[NP]/[AP] based stratum corneum modelling system: a neutron diffraction study. *Biochim. Biophys. Acta* **2019**, *1861* (1), 306-315.
79. Bouwstra, J. A.; Gorris, G. S.; Cheng, K.; Weerheim, A.; Bras, W.; Ponec, M., Phase behavior of isolated skin lipids. *J. Lipid Res.* **1996**, *37* (5), 999-1011.
80. de Jager, M. W.; Gooris, G. S.; Dolbnya, I. P.; Bras, W.; Ponec, M.; Bouwstra, J. A., Novel lipid mixtures based on synthetic ceramides reproduce the unique stratum corneum lipid organization. *J. Lipid Res.* **2004**, *45* (5), 923-32.
81. Eichner, A.; Stahlberg, S.; Sonnenberger, S.; Lange, S.; Dobner, B.; Ostermann, A.; Schrader, T. E.; Hauss, T.; Schroeter, A.; Huster, D.; Neubert, R. H. H., Influence of the penetration enhancer isopropyl myristate on stratum corneum lipid model membranes revealed by neutron diffraction and H-2 NMR experiments. *Biochim. Biophys. Acta* **2017**, *1859* (5), 745-755.
82. Bouwstra, J. A.; Gooris, G. S.; Dubbelaar, F. E. R.; Ponec, M., Phase behavior of stratum corneum lipid mixtures based on human ceramides: The role of natural and synthetic ceramide 1. *J. Invest. Dermatol.* **2002**, *118* (4), 606-617.

SUPPLEMENTARY INFORMATION

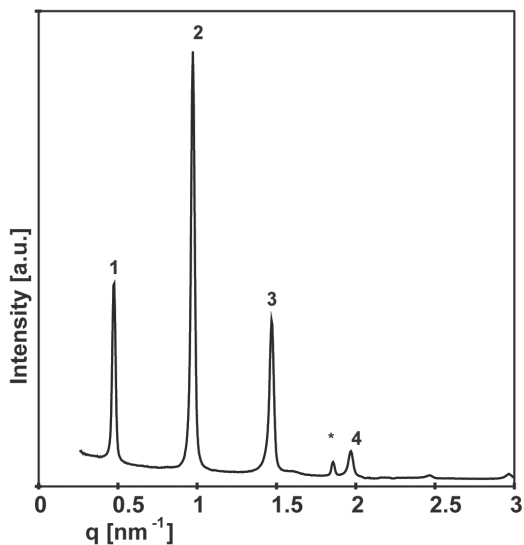


Figure S1: SAXD profile of CER EOS-NS subjected to double equilibration.

Double equilibrated CER EOS-NS showing a similar diffraction pattern as single equilibrated CER EOS-NS.

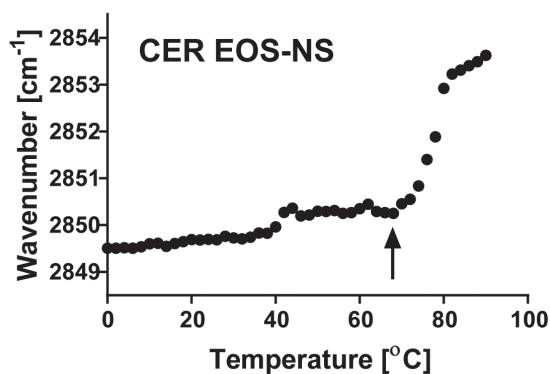


Figure S2: Thermotropic response of the $\nu_3\text{CH}_2$ mode of CER EOS-NS.

The $\nu_3\text{CH}_2$ modes of CER EOS-NS showing recrystallization between 62 and 70 °C (highlighted by arrow).

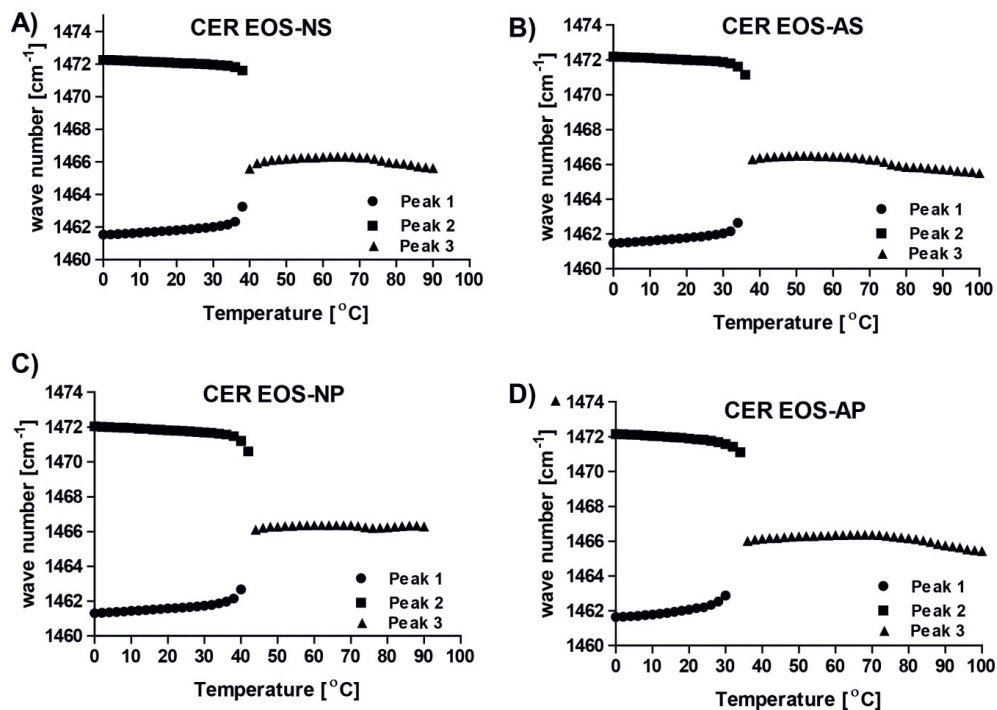


Figure S3: The thermotropic response of the δCH_2 frequencies.

The splitting of the δCH_2 modes into two components positioned at $\sim 1462 \text{ cm}^{-1}$ (peak 1) and 1473 cm^{-1} (peak 2), indicative of orthorhombic packing. As the temperature increased, a pronounced reduction in band splitting was obtained in all samples. The components collapsed into a single peak positioned at $\sim 1467 \text{ cm}^{-1}$ (peak 3) at slightly different temperatures indicating the transition to a hexagonal packing.

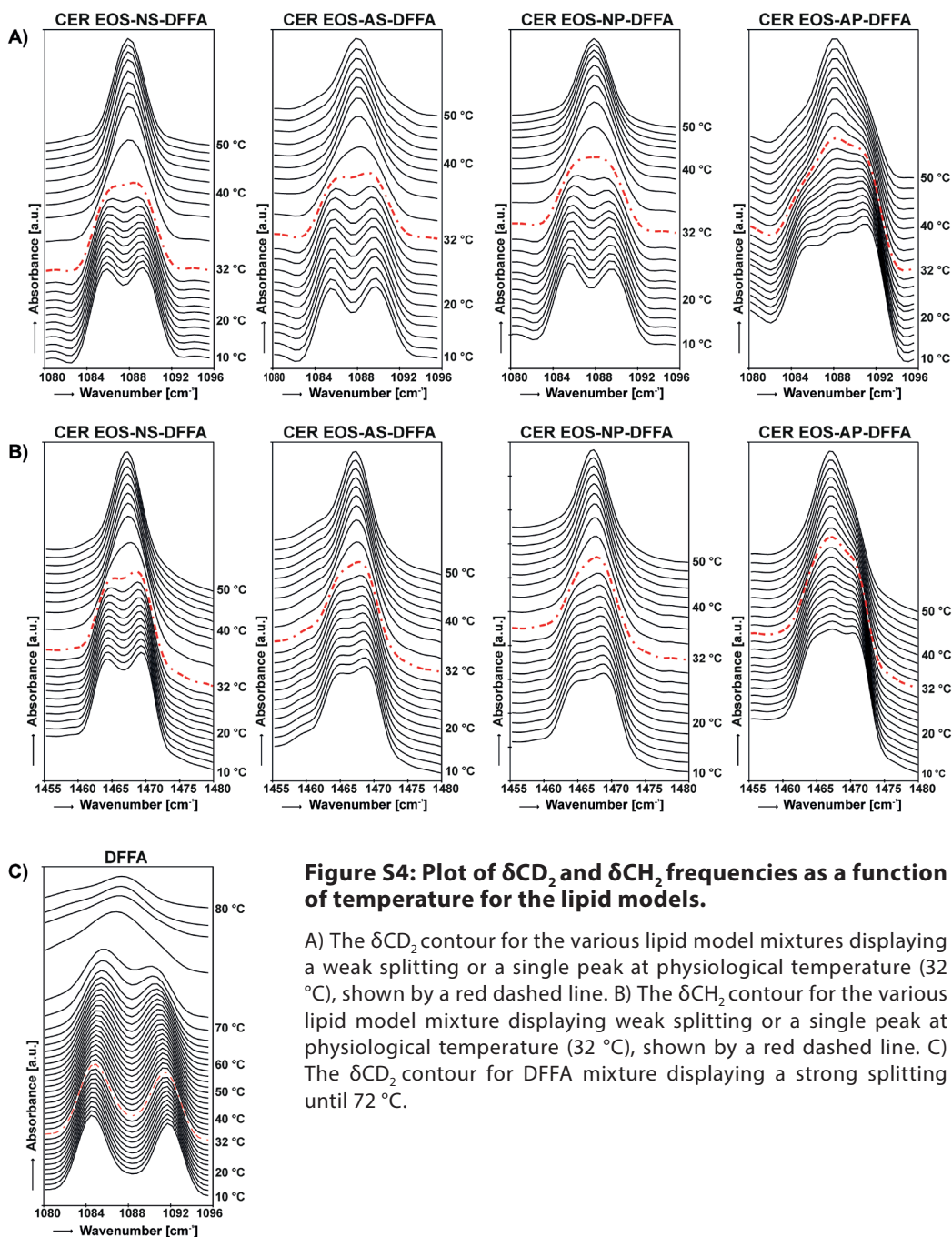


Figure S4: Plot of δCD_2 and δCH_2 frequencies as a function of temperature for the lipid models.

A) The δCD_2 contour for the various lipid model mixtures displaying a weak splitting or a single peak at physiological temperature (32 °C), shown by a red dashed line. B) The δCH_2 contour for the various lipid model mixture displaying weak splitting or a single peak at physiological temperature (32 °C), shown by a red dashed line. C) The δCD_2 contour for DFFA mixture displaying a strong splitting until 72 °C.

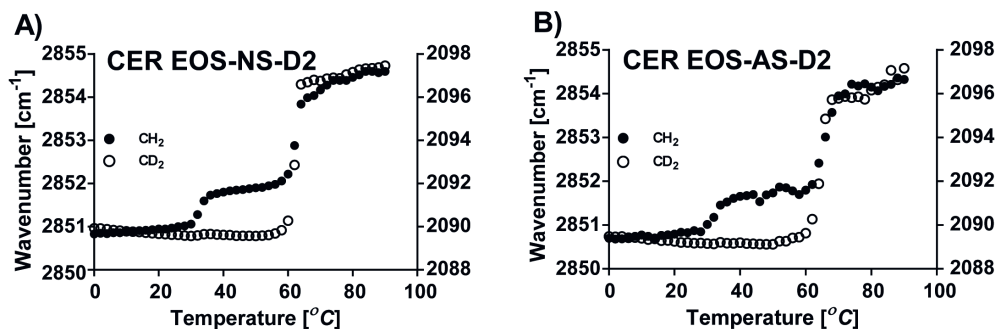


Figure S5: Thermotropic response of the $v_s\text{CH}_2$ and $v_s\text{CD}_2$ modes of the lipid models sprayed at a low concentration.

The CH_2 (filled circle) and the CD_2 (open circle) peak positions are plotted as a function of temperature. On the left y-axis the CH_2 wavenumber and on the secondary y-axis the CD_2 wavenumbers. A) CER EOS-NS-DFFA2 and B) CER EOS-AS-DFFA2 sprayed at concentrations below 5 mg/ml, no recrystallization of the CER chains was observed, evident by the similar transition temperature range of the CER and DFFAs chains.

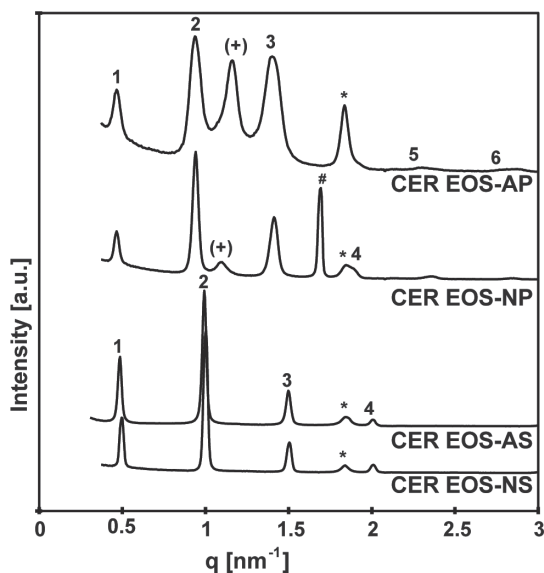
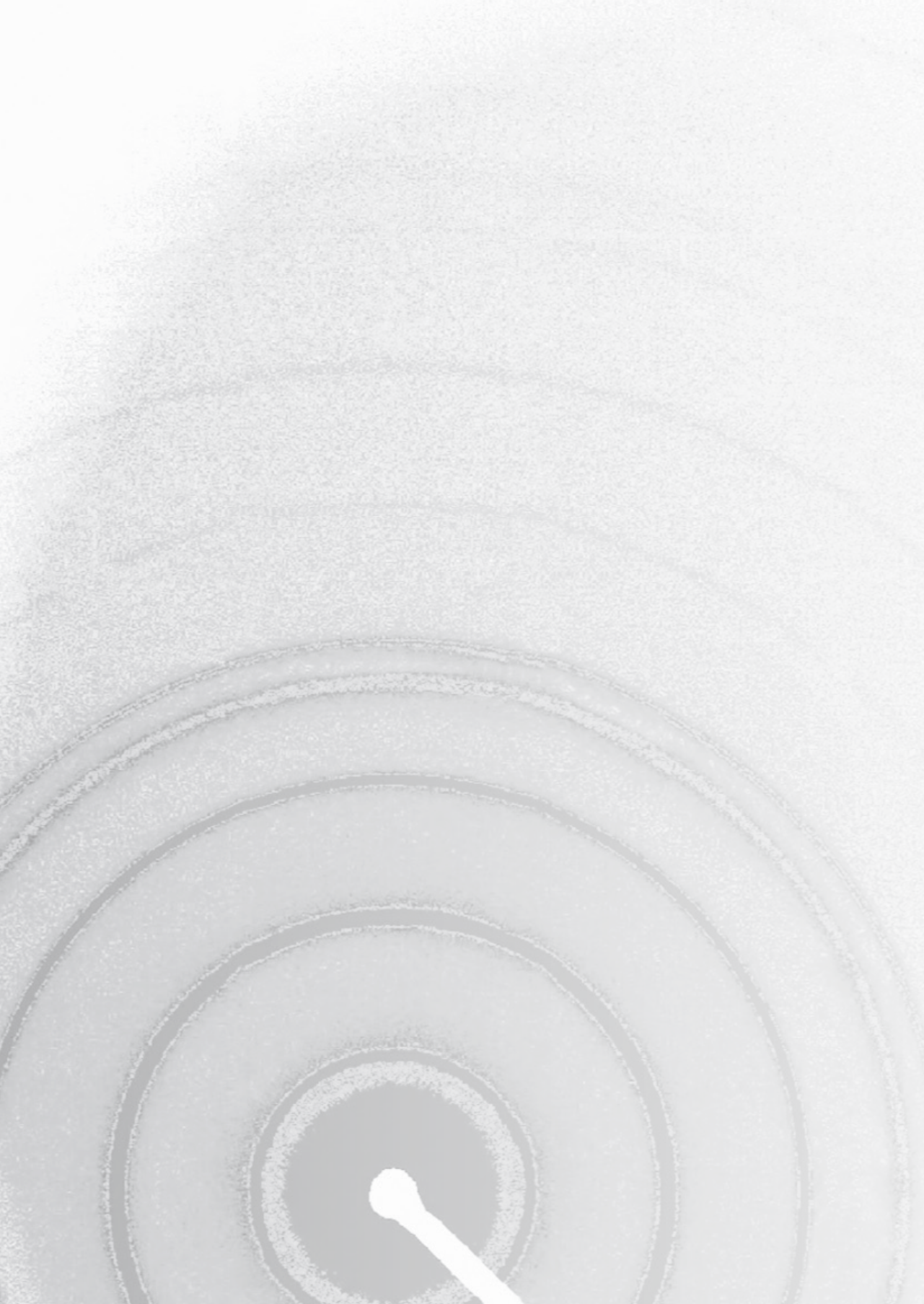


Figure S6: SAXD profile of the non-hydrated lipid models.

The LPP repeat distances are 12.5, 12.6, 13.4, and 13.4 cm^{-1} in CER EOS-NS, CER EOS-AS, CER EOS-NP, and CER EOS-AP respectively. The non-hydrated lipid models measured, show similar reflections and LPP repeat distance as the hydrated samples.



5

Increased levels of short-chain ceramides modify the lipid organization and reduce the lipid barrier of skin model membrane

5

Authors and affiliations:

Lorretta.E. Uche¹, Gerrit.S. Gooris¹, Joke.A. Bouwstra¹ and Charlotte.M. Beddoes¹

¹Division of Drug Delivery Technology, Cluster BioTherapeutics, Leiden Academic Centre for Drug Research, Leiden University, Netherlands

Adapted from: *Langmuir* **2021**, 37 (31), 9478-9489.

ABSTRACT

The skin barrier function is attributed to the stratum corneum (SC) intercellular lipid matrix, which is composed primarily of ceramides (CERs), free fatty acids, and cholesterol. These lipids are organized in two lamellar phases: the short and long periodicity phases (SPP and LPP), respectively. The LPP is considered important for the skin barrier function. High levels of short-chain CERs are observed in various inflammatory skin diseases and have been correlated with barrier dysfunction. In this research, we investigated how the increase in the fraction of the short-chain CER with a non-hydroxy C16 acyl chain linked to a C18 sphingosine base CER NS(C16) at the expense of the physiological chain-length CER NS with a C24 acyl chain (CER NS(C24)) impacts the microstructure and barrier function of a lipid model that mimicked certain characteristics of the SC lipid organization. The permeability and lipid organization of the model membranes were compared with that of a control model without CER NS(C16). The permeability increased significantly when $\geq 50\%$ CER NS(C24) was substituted with CER NS(C16). Employing biophysical techniques, we showed that the lipid packing density reduced with an increasing proportion of CER NS(C16). Substitution of 75% of CER NS(C24) by CER NS(C16) resulted in the formation of phase-separated lipid domains and alteration of the LPP structure. Using deuterium-labeled lipids enabled simultaneous characterization of the C24 and C16 acyl chains in the lipid models, providing insight into the mechanisms underlying the reduced skin barrier function in diseased skin.

Keywords:

Ceramide; chain length; inflammatory skin diseases; Infrared spectroscopy; Permeability; Stratum corneum; X-ray scattering.

INTRODUCTION

Ceramides (CERs) are one of the main lipid classes present in the intercellular regions of the stratum corneum (SC), which is the outermost layer of the skin. They belong to the lipid class referred to as sphingolipids, which are important components of biological membranes and are involved in several biological processes including apoptosis, inflammation, cell proliferation, and differentiation [1-5]. Together with cholesterol (CHOL) and free fatty acids (FFAs), CERs form a crystalline lipid matrix in the SC [6-10] that creates a barrier against the permeation of pathogenic organisms and other hazardous materials into the body and preventing excessive water loss from inside the body [8, 11-16]. In healthy skin, the SC lipids are organized in two lamellar phases with a repeat distance of approximately 6 and 13 nm referred to as the short and long periodicity phases (SPP and LPP), respectively [17-19].

The structure of the CERs in SC is unusual as it contains a long-chain fatty acid (FA) linked by an amide bond to a sphingoid base with a chain length of predominantly 18 carbon atoms [20, 21]. Diversity in the CER headgroup manifests as variations in the type and degree of hydroxylation and saturation. CERs also vary in the acyl chain length and to a lesser extent in the sphingoid base chain length. These variations result in the heterogeneity of the CERs and hence the numerous CER subclasses in the skin barrier [21-29]. Healthy human skin contains predominantly long acyl chain length CERs of > 22 carbon chain length [30].

Alterations of the CER subclass composition and CER chain length have been reported in SC of patients of several inflammatory skin diseases including atopic dermatitis (AD), lamellar ichthyosis, Netherton syndrome, psoriasis, and autosomal recessive congenital ichthyosis [31-42]. With regard to chain length variation, a reduction in long-chain CER levels was reported in diseased skin. CERs with a total chain length of 34 carbon atoms increased significantly in Netherton syndrome and AD patients when compared with healthy individuals [31, 34, 37, 43]. Since several alterations in the lipid composition occur simultaneously in these patients, the isolated single effect of shortened CER chain length on SC lipid organization and barrier function cannot be determined in clinical studies. To combat such challenges, model lipid membranes based on synthetic lipids were developed and employed to study the relationship between specific lipid compositional changes, lipid organization, and barrier function [44-47]. This is attractive because the composition of the lipid model prepared with synthetic lipids is well defined and can be altered on demand to simulate the desired

conditions. To acquire more detailed information on the lipid arrangement, we minimized the number of lipids. The CER subclasses used in this study are CER EOS and CER NS. In previous studies, it was reported that the use of these CER subclasses resulted in a lipid phase behavior mimicking important aspects of the lipid organization in SC, such as the formation of the LPP with a primarily orthorhombic packing [48-52]. The molecular structures and acronyms used to denote the lipids are provided in Figure S1.

Previous investigations reported that model membranes prepared with short-chain CERs exhibited higher permeability compared with their counterparts containing the physiological acyl chain-length CER NS(C24) [53, 54] and thus mimic similar consequences that are seen with diseased skin. The lower permeability of the SC models containing CER NS(C24) compared with that of the counterparts containing short-chain CERs was attributed to the higher packing density of the former as determined by Fourier transformed infrared spectroscopy (FTIR) [53]. In another study that employed ^2H NMR spectroscopy, CER NS(C24) containing model also exhibited a more dense orthorhombic packing while the short-chain CER counterpart was mostly in the less dense hexagonal phase at the skin temperature [55]. The models employed in the above mentioned studies contained entirely long or short acyl chain CER NS, while the diseased skin contains varying proportions of CERs with shorter acyl chains and CERs with a long acyl chain [43]. Thus, the studies did not consider differences in the proportions of the short-chain CERs, which may contribute to the severity of barrier dysfunction. Furthermore, the lipid model mixtures used in the previous studies did not contain the acylCERs such as N-(30-Linoleoyloxy-triacontanoyl)-sphingosine (CER EOS(C30)). These acylCERs are essential for the formation of the LPP, which is a unique trilayer lamellar structure only present in the SC and considered important for the barrier function of the skin [56-60]. Within the lamellae, the lipids form predominantly the dense orthorhombic packing contributing to the permeability barrier of the SC [61, 62]. Understanding the interactions of lipids within this unique lamellar phase is therefore essential to unravel the mechanisms and processes underlying the barrier function in both healthy and diseased skin.

In this research, we aimed to systematically investigate how the inclusion of various proportions of CER with a non-hydroxy C16 acyl chain linked to a C18 sphingosine base (total chain length 34 carbon atoms) referred to as CER NS(C16) will impact the microstructure and barrier function within the SC lipid model. We hypothesize that the extent of the change in lipid composition and organization contributes to the severity of barrier dysfunction. For our study,

we prepared SC models gradually increasing in concentration of CER NS(C16) at the expense of CER NS with an acyl chain of 24 carbon atoms (NS (C24)), and a total chain length of 42 carbon atoms. Besides CER NS, CER EOS was also present together with CHOL and FA(C24), one of the most prevalent FFAs in the SC [63]. The effect of the short-chain CER NS on the barrier function was evaluated by permeation studies. While the lipid phase behavior was examined by small-angle X-ray diffraction (SAXD) and Fourier transformed infrared spectroscopy (FTIR). Deuterium-labeled lipids were used to provide more detailed information on the interactions between the various molecules, including phase separation.

EXPERIMENTAL SECTION

Materials

N-(30-Linoleoyloxy-triacontanoyl)-sphingosine (CEREOS C30), N-(tetracosanoyl)-sphingosine (CER NS (C24)), CER NS(C24) with deuterated fatty acid moiety (D-CER NS(C24)) were gifted by Evonik (Essen, Germany). N-(palmitoyl)-sphingosine (CERs NS(C16)) and CER NS(C16) with deuterated fatty acid moiety (D-CER NS(C16)) were purchased from Avanti. Lignoceric acid (FA (C24)), CHOL, ethyl-p-aminobenzoate (E-PABA), and acetate buffer salts were obtained from Sigma-Aldrich Chemie GmbH (Schnelldorf, Germany). FA(C24) with the acyl chain deuterated (DFA(C24)) was purchased from Arc Laboratories B.V. (Apeldoorn, The Netherlands). Nucleopore polycarbonate filter disks (pore size 0.05 μm) were ordered from Whatman (Kent, UK). All organic solvents were of analytical or high-performance liquid chromatography grade. Ultrapure water was obtained through a Milli-Q integral water purification system with a resistivity of 18 M Ω cm at 25°C (Millipore, Bedford, MA).

Composition of the model lipid mixtures

SC lipid models were prepared from CERs, CHOL, and FA(C24) in an equimolar ratio. The CER composition in the control model consisted of CER EOS (40 mol% of the total CER fraction) and 60 mol% CER NS(C24). The composition with CER EOS at 40 mol% was selected to ensure that only the LPP was formed [48-51, 64, 65]. The model was denoted as NS(C16)-0 indicating the absence of CER NS (C16). Other models were prepared in which, 25, 50, and 75% of the total amount of CER NS(C24) were replaced with CER NS(C16), referred to as NS(C16)-25, NS(C16)-50, and NS(C16)-75 respectively, see table 1. Analogous models were prepared but with FA(C24) substituted with the deuterated counterpart denoted by -DFA

as a suffix to the model name. Next, a set of models were prepared in which the fatty acid chain of CER NS(C24)/CER NS(C16) in NS(C16)-50 was substituted with the deuterated chain resulting in the models identified by the prefix D24/16-NS. Finally, both CER NS (C24)/CER NS (C16) acyl chain and FA(C24) in NS(C16)-50 were deuterated resulting in the next set of models denoted by D24/16-NS as prefix and DFA as the suffix. The composition of the models used in the present study is shown in table 1.

Table 1: Composition of all of the models used in the study.

Lipid model name	CER composition in a CER:CHOL:FA (C24) equimolar ratio (1:1:1)
NS(C16)-0 (control)	[CER EOS(C30) 0.4 + CER NS(C24) 0.6]: CHOL: FA(C24)
NS(C16)-25	[CER EOS(C30) 0.4 + CER NS(C24) 0.45 + CER NS(C16) 0.15]: CHOL: FA(C24)
NS(C16)-50	[CER EOS(C30) 0.4 + CER NS(C24) 0.3 + CER NS(C16) 0.3]: CHOL: FA(C24)
NS(C16)-75	[CER EOS(C30) 0.4 + CER NS(C24) 0.15 + CER NS(C16) 0.45]: CHOL: FA(C24)
NS(C16)-0-DFA	[CER EOS(C30) 0.4 + CER NS(C24) 0.6]: CHOL: DFA(C24)
NS(C16)-25-DFA	[CER EOS(C30) 0.4 + CER NS(C24) 0.45 + CER NS(C16) 0.15]: CHOL: DFA(C24)
NS(C16)-50-DFA	[CER EOS(C30) 0.4 + CER NS(C24) 0.3 + CER NS(C16) 0.3]: CHOL: DFA(C24)
NS(C16)-75-DFA	[CER EOS(C30) 0.4 + CER NS(C24) 0.15 + CER NS(C16) 0.45]: CHOL: DFA(C24)
D24-NS(C16)-50	[CER EOS(C30) 0.4 + D-CER NS(C24) 0.3 + CER NS(C16) 0.3]: CHOL: FA(C24)
D16-NS(C16)-50	[CER EOS(C30) 0.4 + CER NS(C24) 0.3 + D-CER NS(C16) 0.3]: CHOL: FA(C24)
D24-NS(C16)-0-DFA	[CER EOS(C30) 0.4 + D-CER NS(C24) 0.6]: CHOL: DFA(C24)
D24-NS(C16)-50-DFA	[CER EOS(C30) 0.4 + D-CER NS(C24) 0.3 + CER NS(C16) 0.3]: CHOL: DFA(C24)
D16-NS(C16)-50-DFA	[CER EOS(C30) 0.4 + CER NS(C24) 0.3 + D-CER NS(C16) 0.3]: CHOL: DFA(C24)

Permeability studies

To prepare the model mixtures for permeability studies, the proper amount of the required lipids, amounting to 0.9 mg were dissolved in hexane:ethanol (2:1) to a concentration of 4.5 mg/ml. Using a Linomat IV device, the solution was sprayed at a rate of 14 $\mu\text{l}/\text{sec}$ on nucleopore polycarbonate membranes over an area of 10 x 10 mm^2 , under a gentle flow of nitrogen, resulting in an $\sim 12 \mu\text{m}$ -thick lipid layer [44]. The samples were equilibrated at 90 °C for 30 min, and then slowly cooled to room temperature.

In-vitro permeation studies were carried out using PermeGear in-line diffusion cells (Bethlehem PA, USA) with a diffusion area of 0.28 cm^2 . The model membranes were fixed in the diffusion cells and hydrated for an hour with the acceptor phase, phosphate-buffered saline (PBS 0.1 M solution: NaCl, Na_2HPO_4 , KH_2PO_4 , and KCl in milli-Q water with a concentration of 8.13, 1.14, 0.20, and 0.19 g/l respectively)

at pH 7.4 before the experiment. The PBS was filtered and degassed before use. The donor compartment was filled with 1400 μl of a saturated E-PABA (0.65 mg/ml) in acetate buffer solution (pH 5). The permeation experiment was performed under occlusive conditions to prevent solvent evaporation. The acceptor phase was perfused at a flow rate of 2 ml/h. To homogenize the acceptor phase constant stirring was performed. An in-line degasser was incorporated to trap air bubbles that could obstruct the flow. The temperature of the membranes was kept constant at skin temperature (32 °C). The acceptor fluid was collected at 1-hour intervals, over 15 h. After the diffusion experiment, the volume per collected fraction of the acceptor phase was determined by weighing. Using ultra performance liquid chromatography (UPLC), the concentration of E-PABA was determined. Fick's first law of diffusion was employed for the calculation of E-PABA flux values [46]. E-PABA steady-state flux values were calculated at time intervals between the 10th and 15th hour. Permeation of several samples of each condition was analyzed $n > 3$, where n is the number of repeats.

UPLC analysis

UPLC was performed using Acquity UPLC systems described previously [50]. The mobile phase comprised of a mixture of 0.1% trifluoroacetic acid in acetonitrile: milli-Q water at 40:60 (v/v) ratio and the flow rate was 1 ml/min. The stationary phase comprised of a 1.7 μm particle-packed column with the temperature set at 40 °C. The injection volume of 10 μl was used for the samples and solutions for the calibration curve described previously [49]. The wavelength of the detector was set at 286 nm and the data were acquired and processed by MassLynx and TargetLynx software [50].

Data analysis

Statistical analysis was performed using GraphPad Prism 7 (GraphPad Software Inc., CA, USA) to analyze the permeability and FTIR data. Statistically significant differences between two groups were determined by two-tailed, unpaired t-tests, while differences among groups, with each group compared to a control column, were determined using One-way ANOVA with Dunnett's multiple comparison test. Data are presented as mean \pm standard deviation (SD). Differences in mean are considered statistically significant when $P < 0.05$.

FTIR measurements

1.5 mg of the appropriate lipid composition was dissolved in chloroform:methanol (2:1) to a concentration of 5 mg/ml and sprayed on a AgBr window. Spraying

was performed using a Linomat IV device (Camag, Muttenz, Switzerland). The solution was sprayed at a rate of 14 $\mu\text{l}/\text{sec}$, over an area of $10 \times 10 \text{ mm}^2$, under a gentle flow of nitrogen. The samples were equilibrated at $90 \text{ }^\circ\text{C}$ for 30 min, ensuring the complete melting of the lipid mixtures, and then slowly cooled to room temperature. The samples were hydrated in deuterated acetate buffer (pH 5.0) and incubated at $37 \text{ }^\circ\text{C}$ for at least 15 h to ensure that the samples were fully hydrated.

FTIR spectra were acquired with a Varian 670-IR spectrometer (Agilent Technologies, Inc., Santa Clara, CA) equipped with a broad-band mercury cadmium telluride detector. Spectra were collected in transmission mode and generated from 256 co-added interferograms collected over 4 min at a 1 cm^{-1} resolution and analyzed using the software Agilent resolution pro (Agilent Technologies, Palo Alto CA, USA). The sample was kept under a continuous dry air purge, starting 30 min before data collection, and measured over a wavenumber range of $600\text{--}4000 \text{ cm}^{-1}$. To determine the phase transitions in relation to the temperature, the spectra were acquired between $0\text{--}90 \text{ }^\circ\text{C}$ at a heating rate of $0.25 \text{ }^\circ\text{C}/\text{min}$. Deconvolution of the spectra was executed using a half-width of 4 cm^{-1} ; an enhancement factor of 1.6 and was processed with the Agilent resolution pro (Agilent Technologies, Palo Alto CA, USA). Due to a closely overlapping peak, the enhancement factor was adjusted to 1.2 in the range of the rocking frequencies. To evaluate the conformational disordering and lateral organization, five different regions of specific vibrations on the infrared spectrum were analyzed i) $2840\text{--}2860 \text{ cm}^{-1}$: CH_2 symmetric stretching ($\nu_s\text{CH}_2$); ii) $2080\text{--}2100 \text{ cm}^{-1}$: CD_2 symmetric stretching ($\nu_s\text{CD}_2$); iii) $700\text{--}750 \text{ cm}^{-1}$: CH_2 rocking mode (ρCH_2); iv) $1455\text{--}1480 \text{ cm}^{-1}$: CH_2 scissoring mode (δCH_2); v) $1080\text{--}1096 \text{ cm}^{-1}$: CD_2 scissoring mode (δCD_2). Using the linear regression curve fitting method, the mid-transition temperature was determined as described previously [66]. Each composition was measured, $n > 2$.

SAXD studies

SAXD was employed to examine the lamellar organization. To prepare the mixtures, 0.9 mg of the required lipid composition were dissolved in hexane:ethanol (2:1) to a concentration of 4.5 mg/ml. The lipid solution was sprayed over an area of $1 \times 3 \text{ mm}^2$ on a nucleopore polycarbonate membrane under a gentle flow of nitrogen at a rate of $14 \mu\text{l}/\text{sec}$ using a Linomat IV device (Camag, Muttenz, Switzerland). The samples were equilibrated at $90 \text{ }^\circ\text{C}$ for 30 min, ensuring the complete melting of the lipid mixtures, and then slowly cooled to room temperature. The samples were hydrated in an oxygen-free,

84% relative humidity environment for 5 days at room temperature prior to data acquisition.

The SAXD measurements were undertaken at the NCD-SWEET beamline at the ALBA synchrotron (Barcelona, Spain). The X-ray wavelength (λ) and the sample-to-detector distances were 0.999 Å and 2.148 m, respectively. The diffraction patterns were collected using a Pilatus 1M detector that had a pixel array of 981 x 1043, with each pixel being 172 x 172 μm^2 . Silver behenate was used for the calibration of the detector. The samples were measured for 20 s at 23 °C. X-ray intensity scattered by the sample (I) was measured as a function of the scattering vector (q), which is proportional to the angle of scattering (θ) according to the equation $q = \frac{4\pi \sin \theta}{\lambda}$. A lamellar phase is identified by a series of peaks with the same interpeak distance. The repeat distance (d) of the lamellar phase was determined from the peak positions using the equation $d = \frac{2h\pi}{q_h}$. The order of the diffraction peak is denoted by h . The one-dimensional intensity profiles were integrated from the beam center over a 90° segment, centered at the beam center. The peak parameters were obtained from the SAXD patterns, fitted with a Pearson 7 function in the software Fityk [67]. Each composition was measured, $n > 2$.

RESULTS AND DISCUSSION

Permeability of the model membrane increases with the proportion of short-chain CERs

To evaluate the impact of the increasing proportion of short acyl chain length CERs on barrier function, we examined the effect of the gradual substitution of CER NS(C24) by CER NS(C16) on the permeability of the SC model membrane. *In-vitro* permeation studies were performed with E-PABA as the model drug. The plot of E-PABA flux values for the various membranes is displayed in Figure 1A, while the average steady-state flux values are presented in table 2. The average steady-state E-PABA flux was lowest across the control model NS(C16)-0 indicating good barrier capability. As the proportion of short-chain CER NS(C16) was increased at the expense of CER NS(C24), the permeability of the model membrane gradually increased. NS(C16)-50 and NS(C16)-75 E-PABA flux values were significantly higher than that of the control, being ~ 3.5 and 6 times higher respectively (Figure 1B).

In our previous study using a complex SC model mimicking the CER composition of the native human skin, partial substitution of CER NS(C24) with

CER NS(C16), which constituted 13% of the total CER fraction, did not result in a significant increase in permeability [68]. Interestingly, the simple SC model, NS(C16)-25 in which CER NS(C16) constituted 15% of the total CER fraction (table 2), did also not lead to a significant increase in permeability compared with the control. Another study reported that in a SC model membranes containing CER NS of varying acyl chain lengths (C2-C24), the entire substitution of C24 with C4 or C6 CER resulted in a significant increase in permeability while no significant difference was obtained with C2, C8, C12, or C18 CER substitution [53]. In another report, SC models prepared with CER NS(C16) were significantly more permeable than their counterparts containing CER NS(C24) [54]. However, there was a 100% substitution from CER NS(C24) to CER NS(C16) and an absence of CER EOS in these models and thus no formation of the LPP, which is characteristic of the lipid organization in the skin barrier. Our findings show that an increased level of CER C34 which correlated with an increase in transepidermal water loss (TEWL) in AD patients' skin, contributes to the barrier dysfunction [31, 34]. Our results further showed that the proportion of short-chain CERs at the expense of CER NS(C24) dictated the extent of barrier dysfunction in our model systems.

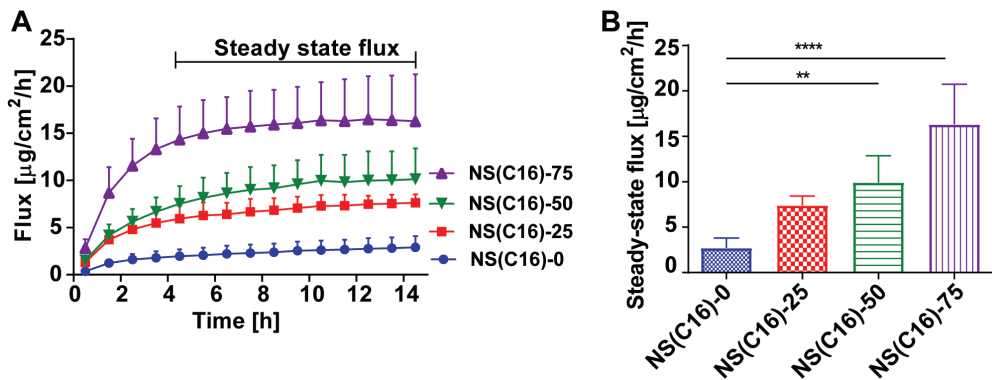


Figure 1: Permeability of the model membranes.

A) Flux of E-PABA across the model membranes over 15 h. The average steady-state flux of E-PABA was calculated from the flux values between 10 and 15 h. B) Average steady-state flux values. Data presented in both plots are the mean values \pm SD, $n \geq 3$. E-PABA steady-state flux was significantly higher in NS(C16)-50 and NS(C16)-75 compared to that of NS(C16)-0 (control), ** ($P < 0.01$), **** ($P < 0.0001$).

Table 2: The E-PABA steady-state flux across the model membranes, the LPP repeat distance, the midpoint temperatures of the orthorhombic-hexagonal phase transition ($T_{M,OR-HEX}$), the ratio of the 730-720 cm^{-1} rocking peak intensity, and the length of the δCD_2 modes peak splitting (cm^{-1})^a.

Lipid model (Fully protiated)	Steady-state flux ($\mu\text{g}/\text{cm}^2/\text{hr}$)	LPP repeat distance (nm)	$T_{M,OR-HEX}$ ($^{\circ}\text{C}$)	730:720 cm^{-1} peak intensity ratio (10 $^{\circ}\text{C}$)	730:720 cm^{-1} peak intensity ratio (32 $^{\circ}\text{C}$)	δCD_2 modes peak splitting distance (cm^{-1})
NS(C16)-0	2.7 \pm 1.1	12.7 \pm 0.0	35.6 \pm 1.1	0.67 \pm 0.08	0.53 \pm 0.07	3.4 \pm 0.2
NS(C16)-25	7.3 \pm 1.0	12.8 \pm 0.1	37.2 \pm 1.2	0.53 \pm 0.08	0.40 \pm 0.10	4.1 \pm 0.2
NS(C16)-50	9.9 \pm 2.9	13.0 \pm 0.0	38.9 \pm 0.5	0.48 \pm 0.14	0.36 \pm 0.17	4.5 \pm 0.2
NS (C16)-75	16.3 \pm 4.4	13.5 \pm 0.0	39.1 \pm 1.3	0.44 \pm 0.06	0.30 \pm 0.12	6.7 \pm 0.5
FA(C24)	-	-	-	0.92 \pm 0.05	-	-

^a The δCD_2 mode's peak splitting distance was obtained from the counterparts of the fully protiated models with the FA chains deuterated (-DFA). The error was calculated as the SD.

An increasing proportion of short-chain CERs results in an altered lamellar organization

Since the lipid organization of the SC intercellular lipid matrix is important for the skin barrier function, we utilized the SAXD technique to provide information about large structural units, including the repeat distances of the lamellar phases in our models. The X-ray diffraction profiles of the lipid mixtures are displayed in Figure 2, while the repeat distances are presented in table 2. All the models formed predominantly the LPP attributed to the high content of CER EOS. This is in agreement with previously investigated model lipid mixtures containing 30% CER EOS and higher [48-51, 64, 65, 69-71]. The LPP repeat distance increased with the proportion of CER NS(C16). The diffraction profile of NS(C16)-75 differed remarkably from the control. Besides the increased LPP repeat distance, the 3rd order peak in NS(C16)-75 was broad, especially at the base, and had a higher intensity than the 2nd order peak, thereby deviating from the characteristic LPP intensity distribution of the diffraction peaks [49, 72]. This may indicate an additional structure with a first-order peak at a similar peak position as the LPPs 3rd order peak. The presence of phase-separated lipids is also indicated by the small peak positioned at $q = 1.2 \text{ nm}^{-1}$ denoted by #. This peak may be attributed to the 1st order diffraction = peak of pure FA(C24) by virtue of its position (Figure S2). The additional phases in the diffraction profile of NS(C16)-75 may contain CER NS(C16), which would result in a higher concentration of CER EOS within the LPP, explaining the increased repeat distance in NS(C16)-75: a recent study showed that the LPP repeat distance increased with the CER EOS concentration [50]. All SAXD profiles revealed the presence of a peak $q = 1.85 \text{ nm}^{-1}$ attributed

to crystalline domains of phase-separated CHOL. In the NS(C16)-75 model the 4th order and CHOL are at the same position and thus probably overlapping.

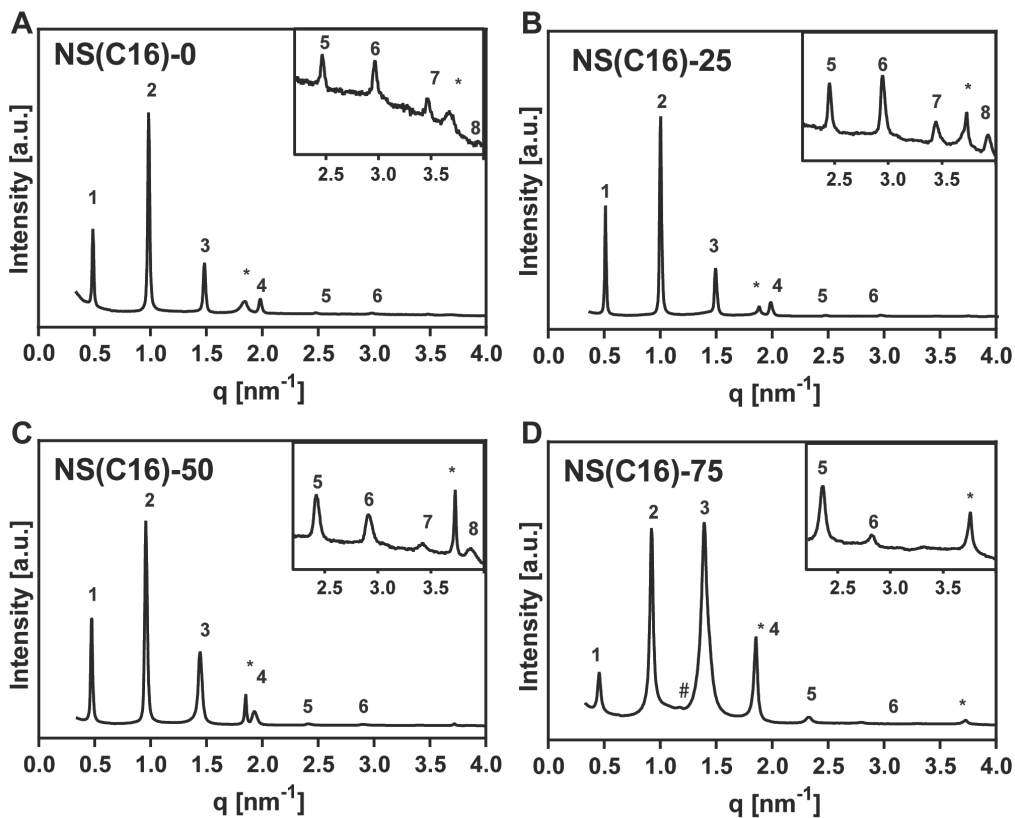


Figure 2: X-ray diffraction profile of the lipid models.

The arabic numbers 1-8 indicate the diffraction orders of the LPP. A) Repeat distance of the LPP in NS(C16) is 12.7 ± 0.04 nm, which is calculated from the reflections at $q = 0.50, 1.00, 1.49, 1.99, 2.50, 3.00, 3.49,$ and 3.97 nm^{-1} . This represents the 1st-8th diffraction orders, respectively. B) The repeat distance of the LPP in NS(C16)-25 is 12.8 ± 0.05 nm, calculated from the reflections at $q = 0.49, 0.99, 1.48, 1.97, 2.46, 2.97, 3.46,$ and 3.94 nm^{-1} . This represents the 1st-8th diffraction orders respectively. C) The repeat distance of the LPP in NS(C16)-50 is 13.0 ± 0.0 nm, calculated from the reflection at $q = 0.48, 0.97, 1.45, 1.94, 2.41, 2.90, 3.39$ and 3.85 nm^{-1} . This represents the 1st-8th diffraction orders respectively. D) The repeat distance of the LPP in NS(C16)-75 model is 13.5 ± 0.03 nm, calculated from the reflections at $q = 0.46, 0.93, 1.39, 1.86, 2.33,$ and 2.80 nm^{-1} . This represents the 1st-6th diffraction orders respectively. The low-intensity peak designated by # positioned at $q = 1.2$ nm^{-1} in the diffraction profile of NS(C16)-75 might be attributed to phase-separated FA(C24). The reflections at $q = 1.85$ nm^{-1} indicated by * in all the models are attributed to phase-separated CHOL and are at the same position as the 4th order diffraction peak in the diffraction profile of NS(C16)-75.

An increased level of short-chain CERs increases the phase transition temperatures in the lipid models

To investigate the reason for the increased permeability of the model membranes with increasing levels of short-chain CER NS(C16), we also examined the lateral lipid organization in the various models. Information about the conformational ordering and phase transition of lipid chains is provided by the position of the $\nu_5\text{CH}_2$ frequencies in the infrared spectrum [73]. Figure 3 shows the thermotropic behavior of $\nu_5\text{CH}_2$ vibration. At 10 °C, the $\nu_5\text{CH}_2$ frequencies in all the models appeared at a low wavenumber, below 2850 cm^{-1} , indicating that the lipid chains are ordered [73, 74]. As the temperature increased, a gradual increase in the wavenumber of the stretching vibration by approximately 1 cm^{-1} was observed between 34 and 44 °C representing orthorhombic-hexagonal phase transition. The mid temperature of the transition ($T_{\text{M,OR-HEX}}$) obtained for the various models is presented in table 2. $T_{\text{M,OR-HEX}}$ increased with the increase of the proportion of CER NS(C16). $T_{\text{M,OR-HEX}}$ for NS(C16)-50 and NS(C16)-75 were significantly higher than that of the control model.

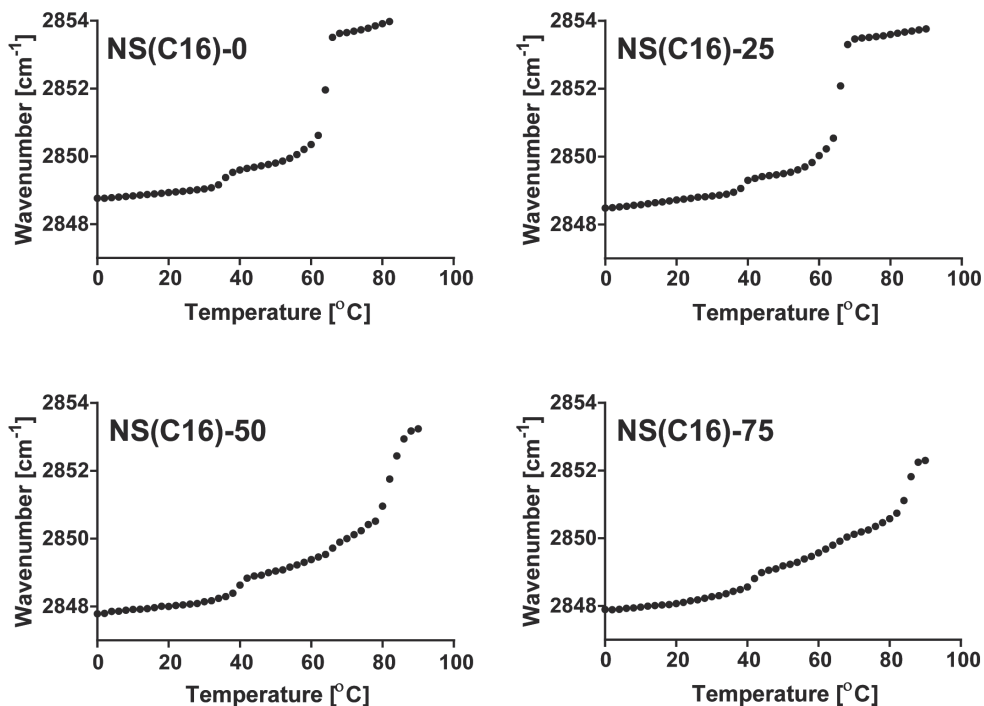


Figure 3: Temperature dependence of the $\nu_5\text{CH}_2$ mode frequency of the lipid mixtures.

The $\nu_5\text{CH}_2$ modes of all models between 0 – 90 °C, showing initial frequencies below 2850 cm^{-1} and two distinct phase transitions as temperature increases. Depending on the composition $T_{\text{M,OR-HEX}}$ was between 34 and 44 °C, and $T_{\text{M,HEX-LIQ}}$ between 60 and 86 °C.

A further temperature increase encountered a second major transition from an ordered to disordered phase, indicated by a large wavenumber increase of 3-4 cm^{-1} observed in the $\nu_3\text{CH}_2$ curves of the various models. The lipid chains in NS(C16)-0 and NS(C16)-25 melted over a narrow temperature range from ~ 60 to 68 $^\circ\text{C}$. In contrast, NS(C16)-50 and NS(C16)-75 melted in two steps, with a wider transition that started at ~ 66 and was completed at around 86 $^\circ\text{C}$. The multiple steps suggest the melting of multiple phases. Although the transition temperature of CERs increased with a longer acyl chain [75], increasing the level of short-chain CERs in the lipid model shifted the phase transitions of the lipid chains towards higher values in the present study. The mismatch of the short and long acyl chains is expected to influence the packing and mixing of the CERs with CHOL and/or FFA.

The packing density of lipid chains reduce as the level of short-chain CERs increases

The packing density of lipid chains is important for the skin barrier function [46, 47, 62, 76]. Analysis of the ρCH_2 modes of the infrared spectrum reveals the chain packing properties in lipid mixtures. A hexagonal lateral organization is characterized by a single peak positioned at ~ 720 cm^{-1} while the presence of two peaks positioned at ~ 720 and 730 cm^{-1} indicate that the lipid chains are packed in the more dense orthorhombic lattice [77, 78]. The ρCH_2 peaks at 10 and 32 $^\circ\text{C}$ for all the investigated systems are split into two strong peaks positioned at ~ 720 and 730 cm^{-1} . The modes at 32 $^\circ\text{C}$ are shown in Figure 4A. The ratio of the intensity of the peaks at 730 cm^{-1} and 720 cm^{-1} is an indication of the proportion of lipids adopting an orthorhombic phase [79, 80]. The $730:720$ cm^{-1} peak intensity ratio for the models is presented in table 2. At 10 $^\circ\text{C}$, the ratio was significantly lower in NS(C16)-50 and NS(C16)-75 compared with that of the control ($P < 0.05$), indicating that a lower proportion of the lipids pack in the orthorhombic phase.

Though primarily orthorhombic, the co-existence of the hexagonal phase, cannot be ruled out from the lipid lateral organization in the control model. To examine this we compared the ρCH_2 mode of FA(C24) at 10 $^\circ\text{C}$, representing the interaction in a system with chains adopting solely orthorhombic packing [80, 81], with that of the control, NS(C16)-0. In FA(C24) ρCH_2 mode, the $730:720$ cm^{-1} peak intensity ratio was practically equal to 1, characterizing a purely orthorhombic system. In contrast, NS(C16)-0, the 730 cm^{-1} peak was less intense than the 720 cm^{-1} peak (~ 0.70), indicating that a small fraction of the lipids adopts the hexagonal phase at the expense of the orthorhombic phase. The

slight reduction in the 730: 720 cm^{-1} peak intensity ratio at 32 °C in all the models indicates a gradual reduction in the proportion of the orthorhombic phase with increasing temperature. Though of lower proportion, NS(C16)-75 orthorhombic phase was more thermostable than that of the control indicated by the prominent 730 cm^{-1} peak still present at 40 °C (Figure 4B), suggesting some phase separation. This may explain why the $T_{\text{M,OR-HEX}}$ was higher as CER NS(C16) content increased. Though several studies have shown a direct relationship between the proportion of the orthorhombic phase and barrier function [46, 47, 76], other factors may also play a role here.

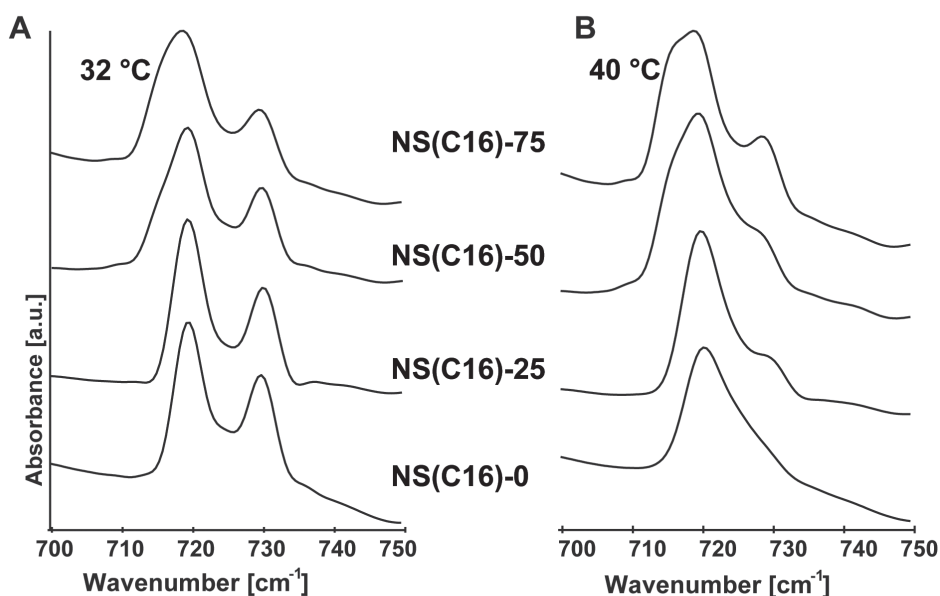


Figure 4: ν_{CH_2} mode of the fully protiated models.

The curves at A) 32 °C display two distinct bands positioned at approximately 730 cm^{-1} and 720 cm^{-1} . B) 40 °C, NS(C16)-75 ν_{CH_2} mode display a prominent 730 cm^{-1} indicating a thermostable orthorhombic phase. All curves are stacked.

Short-chain CERs reduce the miscibility of CERs and FFA chains

In a lipid mixture, selective chain deuteration allows for the behavior of different chains to be monitored separately within the same experiment. The vibrations of the methylene chain (protiated) and the deuterated counterpart occur at different regions in the infrared spectrum [80]. We analyzed the $\nu_{\text{s}}\text{CH}_2$ vibrations from the CER chains and $\nu_{\text{s}}\text{CD}_2$ vibrations from the deuterated FA(C24). The plot

of the thermotropic response of the $\nu_s\text{CH}_2$ and $\nu_s\text{CD}_2$ vibrations is displayed in Figure 5. The CERs and FA(C24) chains undergo an order-disorder phase transition at the same temperature range in NS(C16)-0-DFA, NS(C16)-25-DFA, and NS(C16)-50-DFA. Therefore considering the stretching frequencies there is no indication that the CER and FFA chains in these models phase separate. In contrast, the CERs and FA(C24) chains in NS(C16)-75-DFA did not melt simultaneously, but the FA(C24) melted at temperatures $\sim 12\text{ }^\circ\text{C}$ higher than the CER chains indicating segregation of the two lipid classes. Furthermore, the melting of the FA chains in NS(C16)-75-DFA was sharp and occurred between 80 and 86 $^\circ\text{C}$, which is in the same temperature range as the melting of pure DFA(C24), see Figure S3. Regarding the $\nu_s\text{CH}_2$ curves, as CERs and CHOL are protiated, the absence of noticeable phase transition from orthorhombic to hexagonal in NS(C16)-75-DFA $\nu_s\text{CH}_2$ thermotropic response curve strongly indicates phase separation between CERs and FFA since in general the addition of FFA to mixtures with CERs and CHOL induces an orthorhombic packing [82].

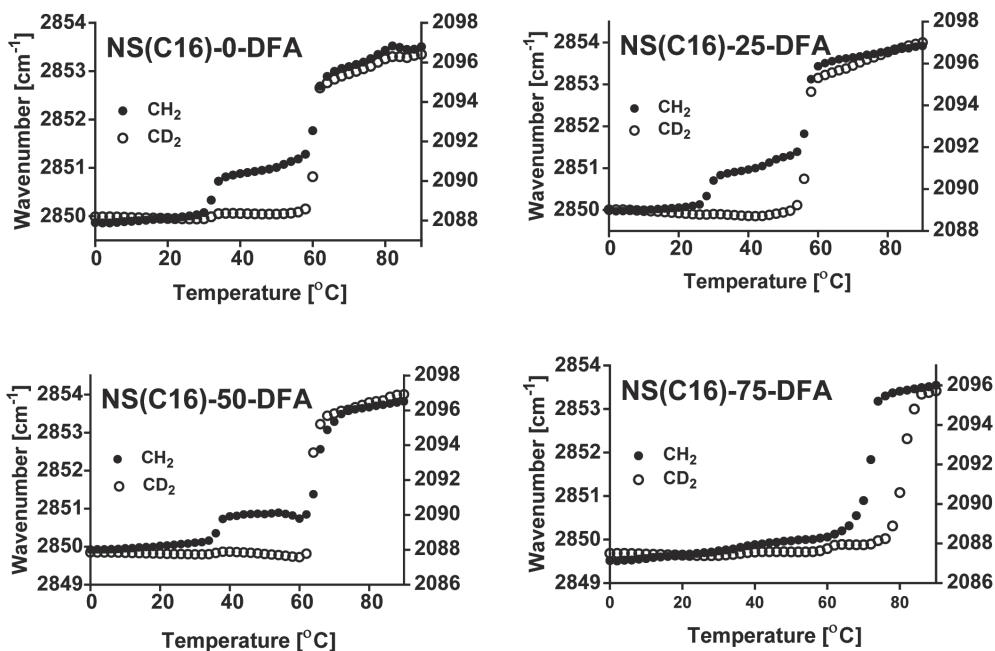


Figure 5: Thermotropic response of the $\nu_s\text{CH}_2$ and $\nu_s\text{CD}_2$ modes of the lipid models.

The CH_2 (filled circle) and the CD_2 (open circle) peak positions are plotted on the primary y-axis and secondary y-axis respectively displaying the phase transition temperatures of the CERs and DFA(C24) in the lipid models.

We analyzed the miscibility of the CERs and FA chains in more detail using the scissoring vibrations. When CER chains and deuterated FFA chains are mixed in an orthorhombic lattice, adjacent protiated CER and deuterated FFA chains cannot engage in short-range coupling due to the differences in vibrational energy [81]. As a consequence, the peak splitting, observed when chains from the same isotope are neighboring each other, is eliminated [80]. Thus, a single peak is displayed in the δCD_2 and δCH_2 modes. A plot of the δCD_2 modes of the various models and pure DFA(C24) mixture at 10 and 32 °C are displayed in Figures 6A and B respectively. At 10 °C, the δCD_2 bands in all models are split into two components. The size of the orthorhombic domain formed by the deuterated lipids was analyzed by measuring the magnitude of peak splitting [81]. A larger split corresponds to a larger domain size [83].

The splitting values are reported in Table 2. The splitting length increases with increasing proportion of short-chain CER NS(C16). The splitting length was small in NS(C16)-0-DFA and NS(C16)-25-DFA indicating a limited interaction of like deuterated chains and thus mixing of the protiated and deuterated chains. While the larger splitting value is measured in NS(C16)-50-DFA with a strong increase in NS(C16)-75-DFA. The latter approaches the maximum value as seen

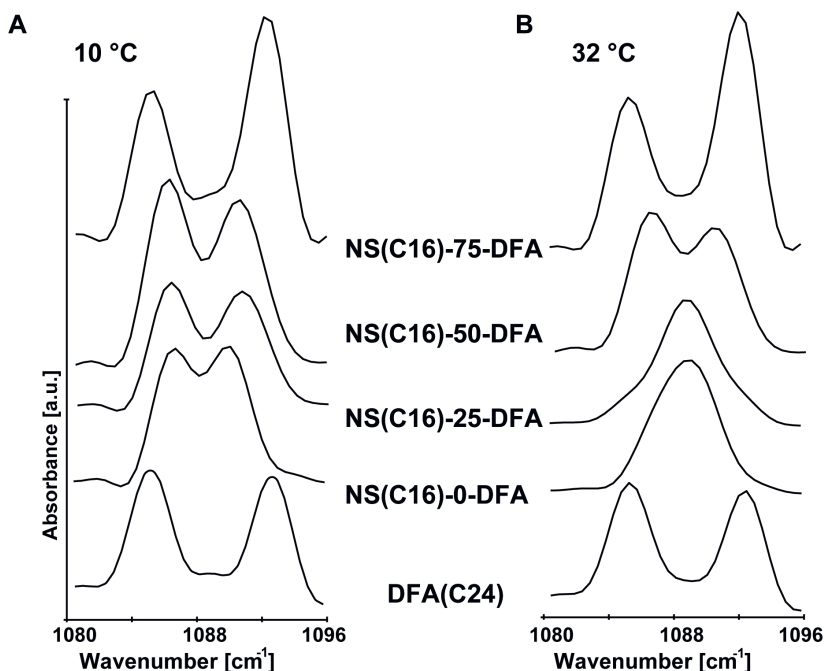


Figure 6: δCD_2 modes of the lipid models with FA(C24) chain deuterated.

The δCD_2 curves of the different lipid models at A) 10 °C B) and at 32 °C.

in pure DFA(C24) with a splitting distance of 7.5 cm^{-1} . This suggests the presence of large DFA(C24) rich domains. The extensive miscibility of the control model is attributed to an optimized hydrophobic match between FA(C24) with CER NS(C24) leading to strong Van der Waals inter-chain interaction. Miscibility of the CERs and the DFA(C24) chains reduced with an increasing proportion of CER NS(C16). At $32\text{ }^{\circ}\text{C}$, the δCD_2 modes of NS(C16)-0-DFA, and NS(C16)-25-DFA collapsed into single peaks while those of NS(C16)-50-DFA and NS(C16)-75-DFA remained split, collapsing into single peaks at $38\text{ }^{\circ}\text{C}$ and $84\text{ }^{\circ}\text{C}$, respectively (Figures S4A and B). The split of NS(C16)-75-DFA δCD_2 mode collapsed at the melting temperature of pure DFA(C24) indicating the presence of separate large crystalline domains containing pure DFA. The existence of phase-separated FA(C24) is also shown by the presence of an additional peak in the SAXD pattern of NS(C16)-75. Probably phase separation of FFA contributed to the increased permeability of NS(C16)-75.

Short-chain CERs are less ordered than long-chain CERs in SC models

To gain more insight into the effect of the different CER NS chain lengths on the phase behavior of the SC model, either the C24 or C16 acyl chains in NS(C16)-50, which contain equal proportions of CERs NS (C24) and (C16), were selectively deuterated. The detailed composition of D24-NS(C16)-50 and D16-NS(C16)-50 are presented in Table 1, while their corresponding $\nu_s\text{CH}_2$ and $\nu_s\text{CD}_2$ wavenumbers at $10\text{ }^{\circ}\text{C}$ are shown in Figures 7A and B, respectively. The $\nu_s\text{CH}_2$ and $\nu_s\text{CD}_2$ modes of the lipid models were well ordered at low temperatures. The $10\text{ }^{\circ}\text{C}$ wavenumber in the $\nu_s\text{CD}_2$ mode of D24-NS(C16)-50 appeared at $2088.2 \pm 0.0\text{ cm}^{-1}$, while that of D16-NS(C16)-50 appeared at a comparatively higher wavenumber $2089.1 \pm 0.1\text{ cm}^{-1}$ (Figure 7A) indicating less conformation by the short-chain CER NS(C16). This is similar as observed in a previous study with models containing CER composition that mimics that in human skin [68]. Regarding the $\nu_s\text{CH}_2$ modes, the $10\text{ }^{\circ}\text{C}$ wavenumber of D24-NS(C16)-50 and D16-NS(C16)-50 appeared at 2849.2 ± 0.1 and $2848.5 \pm 0.3\text{ cm}^{-1}$ respectively demonstrating highly ordered methylene chains (Figure 7B). The differences in the $\nu_s\text{CH}_2$ and $\nu_s\text{CD}_2$ modes can be explained by the C16 acyl chain being in a higher conformational disorder than the C24 acyl chain. The high mobility of the short-chain CERs in the lipid layers may contribute to the impaired lipid barrier function.

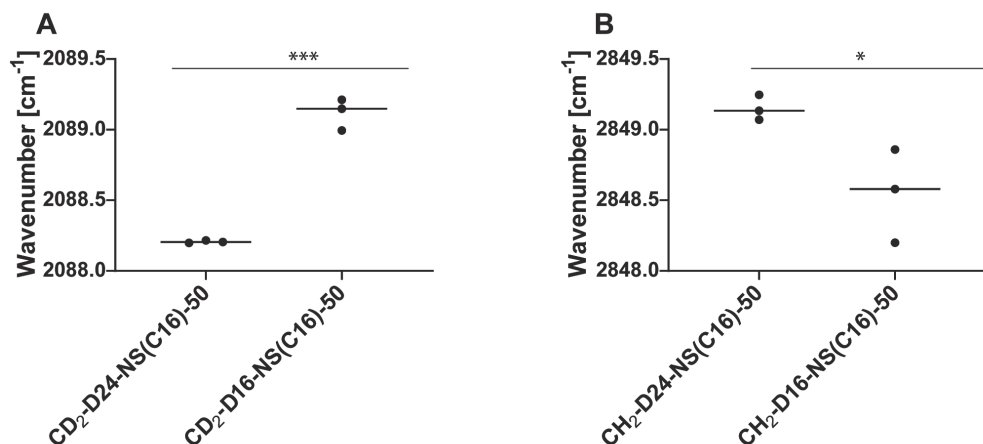


Figure 7: Thermotropic response of NS(C16)-50 vs ν_{CH_2} and ν_{CD_2} frequencies when either C16 or C24 chains are deuterated and the wavenumbers at 10 °C.

A) Wavenumbers at 10 °C for CD₂-D24-NS(C16)-50 and CD₂-D16-NS(C16)-50 with C24 and C16 acyl chains deuterated respectively. The wavenumber of the CER NS(C16) chain is significantly higher than that of the CER NS(C24) chain. B) Wavenumbers at 10 °C for CH₂-D24-NS(C16)-50 (arising from protiated chains when only NS(C24) acyl chains are deuterated) and CH₂-D16-NS(C16)-50 mode (arising from protiated chains when only when NS(16) acyl chains are deuterated). Wavenumber of CH₂-D24-NS(C16)-50 containing the protiated CER NS(C16) chain is significantly higher than that of the CH₂-D16-NS(C16)-50 mode in which CER NS(C24) chains were protiated.

CER NS(C16) and CER NS(C24) acyl chains are present in the central and outer layers of the LPP

Previous studies reported that the majority of CER NS (C24) acyl chain and the FA(C24) are co-localized with one another within the central region of the trilayer LPP structure, with CER NS(C24) in an extended conformation, encouraging tighter chain packing, favorable for a proper barrier function [65, 69, 84] (Figure 8).

To examine the influence of short-chain CERs on the lipid arrangement within the LPP, we analyzed the interaction in SC lipid models containing an equal proportion of NS(C24) and CER NS(C16) in their CER fraction, with the acyl chain of either CER NS(16) or CER NS(24) and FA(C24) deuterated. These models are referred to as D24-NS(C16)-50-DFA and D16-NS(C16)-50-DFA. As control model D24-NS(C16)-0-DFA was used. The detailed composition of the models is presented in Table 1, while their δCD_2 and δCH_2 contours are displayed in figures 9A and B respectively.

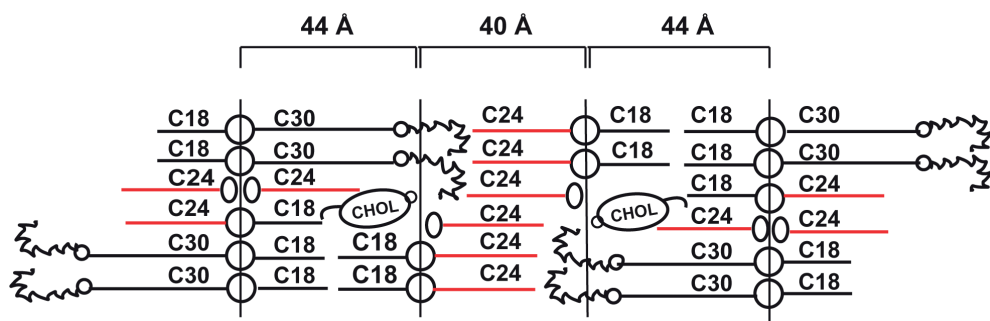


Figure 8: The molecular model proposed for the unit cell of the LPP is based on the determined location of lipids in a neutron diffraction experiment (Mojumdar et al.) [69]

The deuterated acyl chains are marked in red. The ovals, big and small circles represent the FA headgroups, CER headgroups, and ester-linkages respectively. FA(C24) and CER NS (C24) acyl chains are co-localized in the central layer of the LPP but smaller fractions are also present in the outer layers with CHOL, CER EOS (C30) acyl chain, and CER EOS and CER NS sphingosine chains. The figure is adapted from Mojumdar et al.[69].

In control model D24-NS(C16)-0-DFA, the δCD_2 mode was split into two strong peaks attributed to the interaction of the deuterated CER NS(C24) acyl chain and DFA(C24). The large split value of $6.4 \pm 0.1 \text{ cm}^{-1}$ together with a low minimum in between the peaks indicates that there is limited $\text{CH}_2\text{-CD}_2$ interaction. Thus the deuterated chains did not interact to a great extent with the protiated components, which include the CER EOS, sphingosine chains of CER NS(C24), and CHOL. Since FA(C24) and CER NS(C24) do not phase separate as shown in the partially deuterated mixture (Figure 6), the sphingosine chain and the acyl chain of CER NS (C24) must occupy different positions within the LPP. This is in agreement with an extended arrangement of CER NS, with the acyl and sphingosine chains in different layers of the LPP as reported previously [65, 85], and is shown in a schematic image of the lipid arrangement in the LPP [69] (Figure 8). The δCH_2 mode of D24-NS(C16)-0-DFA exhibited a single peak suggesting limited interaction between the protiated chains. Though the deuterated FA(C24) and CER NS(C24) acyl chains are located mainly in the middle layer of the LPP, a fraction of the chains was shown to be present in the outer layer of the LPP as well [65, 69, 85, 86], probably disrupting the $\text{CH}_2\text{-CH}_2$ interaction in the boundary layer and inducing $\text{CH}_2\text{-CD}_2$ interaction. $\text{CH}_2\text{-CH}_2$ interaction might also be limited when lipid chains adopt the less dense hexagonal packing. Though predominantly orthorhombic, the co-existence of a subpopulation of lipids adopting the hexagonal phase in D24-NS(C16)-0-DFA is indicated by the lower 730: 720 cm^{-1} peak intensity ratio of the fully protiated

counterpart NS(C16)-0 compared to that of the fully orthorhombic FA(C24) (Table 2). The single peak observed in D24-NS(C16)-0-DFA δCH_2 mode at 10 °C is probably due to a combined effect of the presence of hexagonal phase and FA(C24) and CER NS(C24) acyl chain in the outer layer of the LPP.

In D24-NS(C16)-50-DFA, the δCD_2 vibration arises from the interaction of DFA(C24) and D-CER NS(C24) acyl chain. The δCD_2 mode displayed a strong splitting measuring $6.1 \pm 0 \text{ cm}^{-1}$ indicating large orthorhombic domains. In the D24-NS(C16)-50-DFA, CD_2 peak intensities, and splitting length was only slightly less than that in the spectrum of D-NS(C16)-0-DFA. This indicates large domains of deuterated lipids, despite the presence of protiated CER NS(C16) in the mixture, which suggests that the NS(C16) acyl chains are not primarily distributed between the deuterated chains of DFA(C24) and D-CER NS(C24) in the central layer of the unit cell of the LPP. As the minimum between the peaks of δCD_2 mode is higher than observed in the spectrum of D24-NS(C16)-0-DFA, there may be some regions with $\text{CH}_2\text{-CD}_2$ interactions in D24-NS(C16)-50-DFA, that could be attributed to a small fraction of protiated C16 acyl chain of CER NS(C16) in the LPP's central layer. The δCH_2 vibrations in D24-NS(C16)-50-DFA arise from CERs NS(C16) and the remaining protiated chains. The δCH_2 peak is broader than that of D24-NS(C16)-0-DFA. The presence of a fraction of CER NS (C16) acyl in the outer layers of the LPP could explain the increased $\text{CH}_2\text{-CH}_2$ interaction compared to the control. An increased $\text{CH}_2\text{-CH}_2$ interaction could also suggest phase separation. However, this is not likely as neither phase-separated FA(C24) nor CER (NS) C16/C24 domains were detected when the mixing properties of the lipid chains in NS(C24)-50 were monitored by selective deuteration.

The spectrum of the D16-NS(C16)-50-DFA δCD_2 mode was also split into two peaks. The splitting length, being $4.1 \pm 0.1 \text{ cm}^{-1}$ was significantly less than that of D24-NS(C16)-0-DFA indicating smaller deuterated chain domains (Figure 9A). The shallower minimum means a higher proportion of $\text{CH}_2\text{-CD}_2$ interactions, showing that the protiated C24 acyl chain of CER NS(C24) mixes more extensively with DFA(C24) than the protiated C16 acyl chains of CER(C16) with the DFA chains in the D24-NS(C16)-50-DFA. The protiated lipids in D16-NS(C16)-50-DFA include CERs EOS, NS(C24), CHOL, and sphingosine chains of CER NS(C16). The CH_2 mode displays two distinct peaks indicating more $\text{CH}_2\text{-CH}_2$ chain interaction than in D24-NS(C16)-50-DFA and D24-NS(C16)-0-DFA. The increased interaction may result from some protiated NS(C24) chains at the same region with the rest of the protiated chains in the boundary layers of the LPP. This is consistent with the single peak of the protiated chains in the spectrum of the D24-NS(C16)-0-DFA.

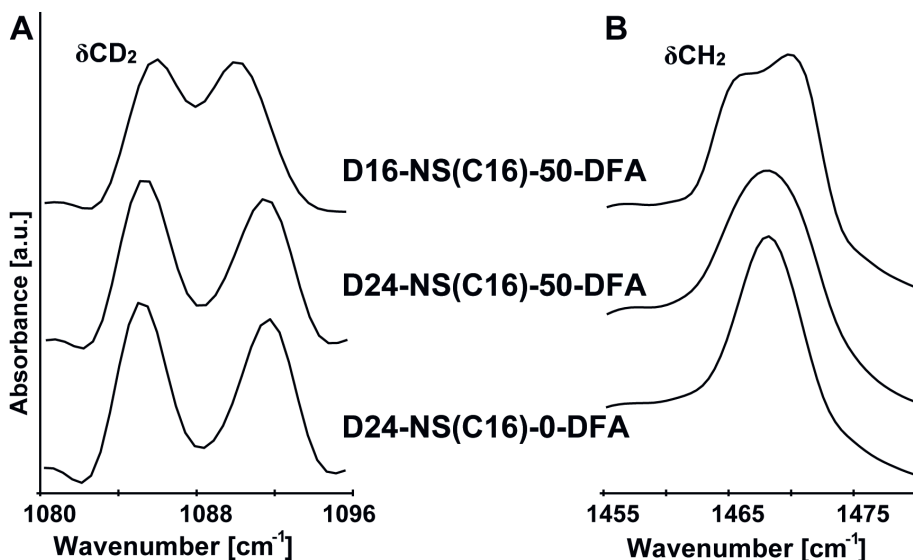


Figure 9: SC Models with CER NS acyl chains and FA(C24) chains deuterated at 10 °C.

A) δCD_2 mode; Strong peak splitting indicates strong CD_2 - CD_2 interaction while weak splitting indicates extensive CD_2 - CH_2 B) δCH_2 modes of the models; Single peak implies limited CH_2 - CH_2 interaction while increased peak width indicate greater CH_2 - CH_2 interaction.

CONCLUSION

SC lipid models enabled a detailed examination of the effect of the proportion of the short-chain CER NS(C16) on the permeability of the simple SC model membrane. The weakest barrier was obtained in the SC model when 75% of the CER NS(24) was substituted with CER NS(C16) resulting in the formation of separate domains, especially FA(C24), as could be deduced from the SAXD and FTIR studies. The proportion of the CER NS(C16) dictated the extent of the variation in lipid organization and barrier dysfunction in the SC model membrane. Relating these findings to diseased skin, the increased level of short-chain CERs reported in several inflammatory skin diseases including AD and Netherton syndrome contributes to the impaired barrier function.

Use of deuterated lipids afforded insight into the distribution of the C16 and C24 acyl chains within the trilayer LPP structure. We deduced that in the SC models containing both CER NS(C24) and CER NS(C16) as observed in diseased skin, the acyl chains of CER NS(C24) and the FA(C24) are mainly co-localized with one another within the central region of the trilayer LPP while CER NS(C16) acyl chains are not primarily distributed within this middle layer. The findings

in the present study contribute to our understanding of the contribution of CER compositional changes to barrier dysfunction in diseased skin, which is important for targeting treatment.

ACKNOWLEDGMENTS

We thank Evonik for donating several CER subclasses. We also express our gratitude to the ALBA Synchrotron facility, for awarding us time on the BL11-NCD-SWEET beamlines and providing assistance with X-ray scattering measurements.

REFERENCES

1. Hannun, Y. A., Functions of ceramide in coordinating cellular responses to stress. *Science* **1996**, 274 (5294), 1855-9.
2. van Blitterswijk, W. J.; van der Luit, A. H.; Veldman, R. J.; Verheij, M.; Borst, J., Ceramide: second messenger or modulator of membrane structure and dynamics? *Biochem. J.* **2003**, 369 (Pt 2), 199-211.
3. Wang, X., Lipid signaling. *Curr. Opin. Plant Biol.* **2004**, 7 (3), 329-336.
4. Taha, T. A.; Mullen, T. D.; Obeid, L. M., A house divided: Ceramide, sphingosine, and sphingosine-1-phosphate in programmed cell death. *Biochimica et Biophysica Acta* **2006**, 1758 (12), 2027-2036.
5. Kolesnick, R. N.; Goni, F. M.; Alonso, A., Compartmentalization of ceramide signaling: physical foundations and biological effects. *J. Cell Physiol.* **2000**, 184 (3), 285-300.
6. Weerheim, A.; Ponc, M., Determination of stratum corneum lipid profile by tape stripping in combination with high-performance thin-layer chromatography. *Arch. Dermatol. Res.* **2001**, 293 (4), 191-199.
7. Gray, G. M.; Yardley, H. J., Lipid compositions of cells isolated from pig, human, and rat epidermis. *J. Lipid Res.* **1975**, 16 (6), 434-440.
8. Elias, P. M.; Goerke, J.; Friend, D. S., Mammalian epidermal barrier layer lipids: composition and influence on structure. *J. Invest. Dermatol.* **1977**, 69 (6), 535-46.
9. Elias, P. M., Epidermal lipids, membranes, and keratinization. *Int. J. Dermatol.* **1981**, 20 (1), 1-19.
10. Wertz, P. W.; van den Bergh, B., The physical, chemical and functional properties of lipids in the skin and other biological barriers. *Chem. Phys. Lipids* **1998**, 91 (2), 85-96.
11. Blank, I. H., Cutaneous barriers. *J. Invest. Dermatol.* **1965**, 45 (4), 249-256.
12. Elias, P. M., Epidermal barrier function - Intercellular lamellar lipid structures, origin, composition, and metabolism. *J. Control. Release* **1991**, 15 (3), 199-208.
13. Lee, S. H.; Jeong, S. K.; Ahn, S. K., An update of the defensive barrier function of skin. *Yonsei Med J* **2006**, 47 (3), 293-306.
14. Proksch, E.; Brandner, J. M.; Jensen, J. M., The skin: an indispensable barrier. *Exp. Dermatol.* **2008**, 17 (12), 1063-72.
15. Wickett, R. R.; Visscher, M. O., Structure and function of the epidermal barrier. *Am J Infect Control* **2006**, 34 (10), S98-S110.
16. Feingold, K. R., The role of epidermal lipids in cutaneous permeability barrier homeostasis. *J. Lipid Res.* **2007**, 48 (12), 2531-2546.
17. Bouwstra, J. A.; Gooris, G. S.; Bras, W.; Downing, D. T., Lipid organization in pig stratum-corneum. *J. Lipid Res.* **1995**, 36 (4), 685-695.
18. Hill, J. R.; Wertz, P. W., Molecular models of the intercellular lipid lamellae from epidermal stratum corneum. *Biochim. Biophys. Acta* **2003**, 1616 (2), 121-6.
19. White, S. H.; Mirejovsky, D.; King, G. I., Structure of lamellar lipid domains and corneocyte envelopes of murine stratum corneum. An X-ray diffraction study. *Biochemistry* **1988**, 27 (10), 3725-32.
20. Schmitt, T.; Neubert, R. H. H., State of the art in Stratum Corneum research: The biophysical properties of ceramides. *Chem. Phys. Lipids* **2018**, 216, 91-103.
21. Masukawa, Y.; Narita, H.; Shimizu, E.; Kondo, N.; Sugai, Y.; Oba, T.; Homma, R.; Ishikawa, J.; Takagi, Y.; Kitahara, T.; Takema, Y.; Kita, K., Characterization of overall ceramide species in human Stratum corneum. *J. Lipid Res.* **2008**, 49 (7), 1466-1476.

22. Robson, K. J.; Stewart, M. E.; Michelsen, S.; Lazo, N. D.; Downing, D. T., 6-Hydroxy-4-sphingene in human epidermal ceramides. *J. Lipid Res.* **1994**, *35* (11), 2060-8.
23. Stewart, M. E.; Downing, D. T., A new 6-hydroxy-4-sphingene-containing ceramide in human skin. *J. Lipid Res.* **1999**, *40* (8), 1434-9.
24. van Smeden, J.; Hoppel, L.; van der Heijden, R.; Hankemeier, T.; Vreeken, R. J.; Bouwstra, J. A., LC/MS analysis of stratum corneum lipids: ceramide profiling and discovery. *J. Lipid Res.* **2011**, *52* (6), 1211-21.
25. Rabionet, M.; Gorgas, K.; Sandhoff, R., Ceramide synthesis in the epidermis. *Biochim. Biophys. Acta* **2014**, *1841* (3), 422-34.
26. Wertz, P. W.; Miethke, M. C.; Long, S. A.; Strauss, J. S.; Downing, D. T., The Composition of the ceramides from human stratum-corneum and from comedones. *J. Invest. Dermatol.* **1985**, *84* (5), 410-412.
27. van Smeden, J.; Bouwstra, J. A., Stratum corneum lipids: Their role for the skin barrier function in healthy subjects and atopic dermatitis patients. *Curr. Probl. Dermatol.* **2016**, *49*, 8-26.
28. t'Kindt, R.; Jorge, L.; Dumont, E.; Couturon, P.; David, F.; Sandra, P.; Sandra, K., Profiling and characterizing skin ceramides using reversed-phase liquid chromatography-quadrupole time-of-flight mass spectrometry. *Anal. Chem.* **2012**, *84* (1), 403-411.
29. Coderch, L.; López, O.; de la Maza, A.; Parra, J. L., Ceramides and Skin Function. *Am. J. Clin. Dermatol.* **2003**, *4* (2), 107-129.
30. Masukawa, Y.; Narita, H.; Sato, H.; Naoe, A.; Kondo, N.; Sugai, Y.; Oba, T.; Homma, R.; Ishikawa, J.; Takagi, Y.; Kitahara, T., Comprehensive quantification of ceramide species in human stratum corneum. *J. Lipid Res.* **2009**, *50* (8), 1708-19.
31. Ishikawa, J.; Narita, H.; Kondo, N.; Hotta, M.; Takagi, Y.; Masukawa, Y.; Kitahara, T.; Takema, Y.; Koyano, S.; Yamazaki, S.; Hatamochi, A., Changes in the ceramide profile of atopic dermatitis patients. *J. Invest. Dermatol.* **2010**, *130* (10), 2511-4.
32. Di Nardo, A.; Wertz, P.; Giannetti, A.; Seidenari, S., Ceramide and cholesterol composition of the skin of patients with atopic dermatitis. *Acta Derm-Venerol.* **1998**, *78* (1), 27-30.
33. Imokawa, G.; Abe, A.; Jin, K.; Higaki, Y.; Kawashima, M.; Hidano, A., Decreased level of ceramides in stratum corneum of atopic dermatitis: an etiologic factor in atopic dry skin? *J. Invest. Dermatol.* **1991**, *96* (4), 523-6.
34. Janssens, M.; van Smeden, J.; Gooris, G. S.; Bras, W.; Portale, G.; Caspers, P. J.; Vreeken, R. J.; Hankemeier, T.; Kezic, S.; Wolterbeek, R.; Lavrijsen, A. P.; Bouwstra, J. A., Increase in short-chain ceramides correlates with an altered lipid organization and decreased barrier function in atopic eczema patients. *J. Lipid Res.* **2012**, *53* (12), 2755-66.
35. Janssens, M.; van Smeden, J.; Gooris, G. S.; Bras, W.; Portale, G.; Caspers, P. J.; Vreeken, R. J.; Kezic, S.; Lavrijsen, A. P.; Bouwstra, J. A., Lamellar lipid organization and ceramide composition in the stratum corneum of patients with atopic eczema. *J. Invest. Dermatol.* **2011**, *131* (10), 2136-8.
36. Motta, S.; Monti, M.; Sesana, S.; Caputo, R.; Carelli, S.; Ghidoni, R., Ceramide composition of the psoriatic scale. *Biochim. Biophys. Acta* **1993**, *1182* (2), 147-51.
37. van Smeden, J.; Janssens, M.; Boiten, W. A.; van Drongelen, V.; Furio, L.; Vreeken, R. J.; Hovnanian, A.; Bouwstra, J. A., Intercellular skin barrier lipid composition, and organization in Netherton syndrome patients. *J. Invest. Dermatol.* **2014**, *134* (5), 1238-1245.
38. Crumrine, D.; Khnykin, D.; Krieg, P.; Man, M.-Q.; Celli, A.; Mauro, T. M.; Wakefield, J. S.; Menon, G.; Mauldin, E.; Miner, J. H.; Lin, M.-H.; Brash, A. R.; Sprecher, E.; Radner, F. P. W.; Choate, K.; Roop, D.; Uchida, Y.; Gruber, R.; Schmuth, M.; Elias, P. M., Mutations in Recessive Congenital Ichthyoses Illuminate the Origin and Functions of the Corneocyte Lipid Envelope. *J. Invest. Dermatol.* **2019**, *139* (4), 760-768.

39. Eckl, K.-M.; Tidhar, R.; Thiele, H.; Oji, V.; Hausser, I.; Brodesser, S.; Preil, M.-L.; Önal-Akan, A.; Stock, F.; Müller, D.; Becker, K.; Casper, R.; Nürnberg, G.; Altmüller, J.; Nürnberg, P.; Traupe, H.; Futerman, A. H.; Hennies, H. C., Impaired Epidermal Ceramide Synthesis Causes Autosomal Recessive Congenital Ichthyosis and Reveals the Importance of Ceramide Acyl Chain Length. *J. Investig. Dermatol.* **2013**, *133* (9), 2202-2211.
40. J.A. Bouwstra, E. H. M., *Cosmetic formulation principles and practice*. CRC Press: Boca Raton, 2019.
41. Farwanah, H.; Raith, K.; Neubert, R. H.; Wohlrab, J., Ceramide profiles of the uninvolved skin in atopic dermatitis and psoriasis are comparable to those of healthy skin. *Arch. Dermatol. Res.* **2005**, *296* (11), 514-21.
42. Eckl, K. M.; Tidhar, R.; Thiele, H.; Oji, V.; Hausser, I.; Brodesser, S.; Preil, M.; Önal-Akan, A.; Stock, F.; Müller, D., Impaired Epidermal Ceramide Synthesis Causes Autosomal Recessive Congenital Ichthyosis and Reveals the Importance of Ceramide Acyl Chain Length. *J. Invest. Dermatol.* **2013**, *133* (9), 2202-2211.
43. Boer, D. E. C.; van Smeden, J.; Al-Khakany, H.; Melnik, E.; van Dijk, R.; Absalah, S.; Vreeken, R. J.; Haenen, C. C. P.; Lavrijssen, A. P. M.; Overkleeft, H. S.; Aerts, J. M. F. G.; Bouwstra, J. A., Skin of atopic dermatitis patients shows disturbed β -glucocerebrosidase and acid sphingomyelinase activity that relates to changes in stratum corneum lipid composition. *Biochim. Biophys. Acta* **2020**, *1865* (6), 158673.
44. de Jager, M.; Groenink, W.; Bielsa i Guivernau, R.; Andersson, E.; Angelova, N.; Ponec, M.; Bouwstra, J., A novel in vitro percutaneous penetration model: evaluation of barrier properties with p-aminobenzoic acid and two of its derivatives. *Pharm. Res.* **2006**, *23* (5), 951-60.
45. Groen, D.; Berthaud, F.; Bouwstra, J. A.; Chapuis, C.; Gooris, G. S.; Boncheva, M., In vitro model systems for studying the impact of organic chemicals on the skin barrier lipids. *Biochim Biophys Acta* **2014**, *1838* (1), 310-318.
46. Mojumdar, E. H.; Helder, R. W.; Gooris, G. S.; Bouwstra, J. A., Monounsaturated fatty acids reduce the barrier of stratum corneum lipid membranes by enhancing the formation of a hexagonal lateral packing. *Langmuir* **2014**, *30* (22), 6534-43.
47. Skolova, B.; Jandovska, K.; Pullmannova, P.; Tesar, O.; Roh, J.; Hrabalek, A.; Vavrova, K., The role of the trans double bond in skin barrier sphingolipids: permeability and infrared spectroscopic study of model ceramide and dihydroceramide membranes. *Langmuir* **2014**, *30* (19), 5527-35.
48. Opalka, L.; Kovacik, A.; Maixner, J.; Vavrova, K., Omega-O-Acylceramides in skin lipid membranes: effects of concentration, sphingoid base, and model complexity on microstructure and permeability. *Langmuir* **2016**, *32* (48), 12894-12904.
49. Uche, L. E.; Gooris, G. S.; Beddoes, C. M.; Bouwstra, J. A., New insight into phase behavior and permeability of skin lipid models based on sphingosine and phytosphingosine ceramides. *Biochim. Biophys. Acta* **2019**, *1861* (7), 1317-1328.
50. Uche, L. E.; Gooris, G. S.; Bouwstra, J. A.; Beddoes, C. M., High concentration of the ester-linked ω -hydroxy ceramide increases the permeability in skin lipid model membranes. *Biochimica et Biophysica Acta* **2021**, *1863* (1), 183487-183497.
51. Pullmannova, P.; Ermakova, E.; Kovacik, A.; Opalka, L.; Maixner, J.; Zbytovska, J.; Kucerka, N.; Vavrova, K., Long and very long lamellar phases in model stratum corneum lipid membranes. *J. Lipid Res* **2019**, *60* (5), 963-971.
52. Beddoes, C. M.; Rensen, D. E.; Gooris, G. S.; Malfois, M.; Bouwstra, J. A., The Importance of Free Fatty Chain Length on the Lipid Organization in the Long Periodicity Phase. *Int. J. Mol. Sci.* **2021**, *22* (7), 3679.
53. Skolova, B.; Janusova, B.; Zbytovska, J.; Gooris, G.; Bouwstra, J.; Slepicka, P.; Berka, P.; Roh, J.; Palat, K.; Hrabalek, A.; Vavrova, K., Ceramides in the skin lipid membranes: length matters. *Langmuir* **2013**, *29* (50), 15624-33.

54. Pullmannová, P.; Pavlíková, L.; Kováčik, A.; Sochorová, M.; Školová, B.; Slepíčka, P.; Maixner, J.; Zbytovská, J.; Vávrová, K., Permeability and microstructure of model stratum corneum lipid membranes containing ceramides with long (C16) and very long (C24) acyl chains. *Biophys Chem* **2017**, *224*, 20-31.
55. Stahlberg, S.; Skolova, B.; Madhu, P. K.; Vogel, A.; Vavrova, K.; Huster, D., Probing the role of the ceramide acyl chain length and sphingosine unsaturation in model skin barrier lipid mixtures by (2)H solid-state NMR spectroscopy. *Langmuir* **2015**, *31* (17), 4906-15.
56. Bouwstra, J. A.; Gooris, G. S.; Dubbelaar, F. E.; Weerheim, A. M.; Ijzerman, A. P.; Ponec, M., Role of ceramide 1 in the molecular organization of the stratum corneum lipids. *J. Lipid Res.* **1998**, *39* (1), 186-96.
57. Bouwstra, J. A.; Gooris, G. S.; Dubbelaar, F. E.; Ponec, M., Phase behavior of stratum corneum lipid mixtures based on human ceramides: the role of natural and synthetic ceramide 1. *J. Invest. Dermatol.* **2002**, *118* (4), 606-17.
58. Groen, D.; Gooris, G. S.; Bouwstra, J. A., Model membranes prepared with ceramide EOS, cholesterol, and free fatty acids form a unique lamellar phase. *Langmuir* **2010**, *26* (6), 4168-75.
59. Bouwstra, J. A.; Gooris, G. S.; Dubbelaar, F. E.; Ponec, M., Phase behavior of lipid mixtures based on human ceramides: coexistence of crystalline and liquid phases. *J. Lipid Res.* **2001**, *42* (11), 1759-70.
60. McIntosh, T. J.; Stewart, M. E.; Downing, D. T., X-ray diffraction analysis of isolated skin lipids: reconstitution of intercellular lipid domains. *Biochemistry* **1996**, *35* (12), 3649-53.
61. Boncheva, M.; Damien, F.; Normand, V., Molecular organization of the lipid matrix in intact stratum corneum using ATR-FTIR spectroscopy. *Biochim. Biophys. Acta* **2008**, *1778* (5), 1344-55.
62. Damien, F.; Boncheva, M., The extent of orthorhombic lipid phases in the stratum corneum determines the barrier efficiency of human skin in vivo. *J. Invest. Dermatol.* **2010**, *130* (2), 611-614.
63. Wertz, P.W.; Downing, D.T, *Physiology, biochemistry and molecular biology of the skin*. second ed.; Oxford University Press: New York, 1991; Vol. 1, p 205-236.
64. Gooris, G. S.; Kamran, M.; Kros, A.; Moore, D. J.; Bouwstra, J. A., Interactions of dipalmitoylphosphatidylcholine with ceramide-based mixtures. *Biochim. Biophys. Acta* **2018**, *1860* (6), 1272-1281.
65. Beddoes, C. M.; Gooris, G. S.; Bouwstra, J. A., Preferential arrangement of lipids in the long-periodicity phase of a stratum corneum matrix model. *J. Lipid Res.* **2018**, *59* (12), 2329-2338.
66. Oguri, M.; Gooris, G. S.; Bito, K.; Bouwstra, J. A., The effect of the chain length distribution of free fatty acids on the mixing properties of stratum corneum model membranes. *Biochim. Biophys. Acta* **2014**, *1838* (7), 1851-1861.
67. Wojdyr, M., Fityk: a general-purpose peak fitting program. *J Appl Crystallogr* **2010**, *43*, 1126-1128.
68. Uche, L. E.; Gooris, G. S.; Bouwstra, J. A.; Beddoes, C. M., Barrier Capability of Skin Lipid Models: Effect of Ceramides and Free Fatty Acid Composition. *Langmuir* **2019**, *35* (47), 15376-15388.
69. Mojumdar, E. H.; Gooris, G. S.; Groen, D.; Barlow, D. J.; Lawrence, M. J.; Deme, B.; Bouwstra, J. A., Stratum corneum lipid matrix: Location of acyl ceramide and cholesterol in the unit cell of the long periodicity phase. *Biochim. Biophys. Acta* **2016**, *1858* (8), 1926-34.
70. Opalka, L.; Kovacik, A.; Pullmannova, P.; Maixner, J.; Vavrova, K., Effects of omega-O-acylceramide structures and concentrations in healthy and diseased skin barrier lipid membrane models. *J. Lipid Res.* **2020**, *61* (2), 219-228.

71. de Sousa Neto, D.; Gooris, G.; Bouwstra, J., Effect of the omega-acylceramides on the lipid organization of stratum corneum model membranes evaluated by X-ray diffraction and FTIR studies (Part I). *Chem. Phys. Lipids* **2011**, *164* (3), 184-95.
72. Groen, D.; Gooris, G. S.; Bouwstra, J. A., New insights into the stratum corneum lipid organization by X-ray diffraction analysis. *Biophys. J.* **2009**, *97* (8), 2242-2249.
73. Mendelsohn, R.; Moore, D. J., Vibrational spectroscopic studies of lipid domains in biomembranes and model systems. *Chem. Phys. Lipids* **1998**, *96* (1-2), 141-57.
74. Mendelsohn, R.; Flach, C. R.; Moore, D. J., Determination of molecular conformation and permeation in skin via IR spectroscopy, microscopy, and imaging. *Biochim. Biophys. Acta* **2006**, *1758* (7), 923-933.
75. Janusova, B.; Zbytovska, J.; Lorenc, P.; Vavrysova, H.; Palat, K.; Hrabalek, A.; Vavrova, K., Effect of ceramide acyl chain length on skin permeability and thermotropic phase behavior of model stratum corneum lipid membranes. *Biochim. Biophys. Acta* **2011**, *1811* (3), 129-37.
76. Mojumdar, E. H.; Kariman, Z.; van Kerckhove, L.; Gooris, G. S.; Bouwstra, J. A., The role of ceramide chain length distribution on the barrier properties of the skin lipid membranes. *Biochim Biophys Acta* **2014**, *1838* (10), 2473-2483.
77. Snyder, R. G.; Goh, M. C.; Srivatsavoy, V. J. P.; Strauss, H. L.; Dorset, D. L., Measurement of the growth-kinetics of microdomains in binary N-alkane solid-solutions by infrared-spectroscopy. *J. Phys. Chem-US* **1992**, *96* (24), 10008-10019.
78. Snyder, R. G., Vibrational Correlation Splitting and Chain Packing for the Crystalline N-Alkanes. *J. Chem. Phys.* **1979**, *71* (8), 3229-3235.
79. Berkers, T.; van Dijk, L.; Absalah, S.; van Smeden, J.; Bouwstra, J. A., Topically applied fatty acids are elongated before incorporation in the stratum corneum lipid matrix in compromised skin. *Exp. Dermatol.* **2017**, *26* (1), 36-43.
80. Mendelsohn, R.; Liang, G. L.; Strauss, H. L.; Snyder, R. G., IR spectroscopic determination of gel state miscibility in long-chain phosphatidylcholine mixtures. *Biophys. J.* **1995**, *69* (5), 1987-1998.
81. Gooris, G. S.; Bouwstra, J. A., Infrared spectroscopic study of stratum corneum model membranes prepared from human ceramides, cholesterol, and fatty acids. *Biophys. J.* **2007**, *92* (8), 2785-95.
82. Bouwstra, J. A.; Dubbelaar, F. E.; Gooris, G. S.; Ponec, M., The lipid organisation in the skin barrier. *Acta Derm-Venereol.* **2000**, *208*, 23-30.
83. Ramos, A. P.; Lafleur, M., Chain Length of Free Fatty Acids Influences the Phase Behavior of Stratum Corneum Model Membranes. *Langmuir* **2015**, *31* (42), 11621-9.
84. Mojumdar, E. H.; Gooris, G. S.; Barlow, D. J.; Lawrence, M. J.; Deme, B.; Bouwstra, J. A., Skin lipids: localization of ceramide and fatty acid in the unit cell of the long periodicity phase. *Biophys. J.* **2015**, *108* (11), 2670-2679.
85. Beddoes, C. M.; Gooris, G. S.; Foglia, F.; Ahmadi, D.; Barlow, D. J.; Lawrence, M. J.; Demé, B.; Bouwstra, J. A., Arrangement of Ceramides in the Skin: Sphingosine Chains Localize at a Single Position in Stratum Corneum Lipid Matrix Models. *Langmuir* **2020**, *36* (34), 10270-10278.
86. Mojumdar, E. H.; Groen, D.; Gooris, G. S.; Barlow, D. J.; Lawrence, M. J.; Deme, B.; Bouwstra, J. A., Localization of cholesterol and fatty acid in a model lipid membrane: a neutron diffraction approach. *Biophys. J.* **2013**, *105* (4), 911-8.

SUPPLEMENTARY INFORMATION

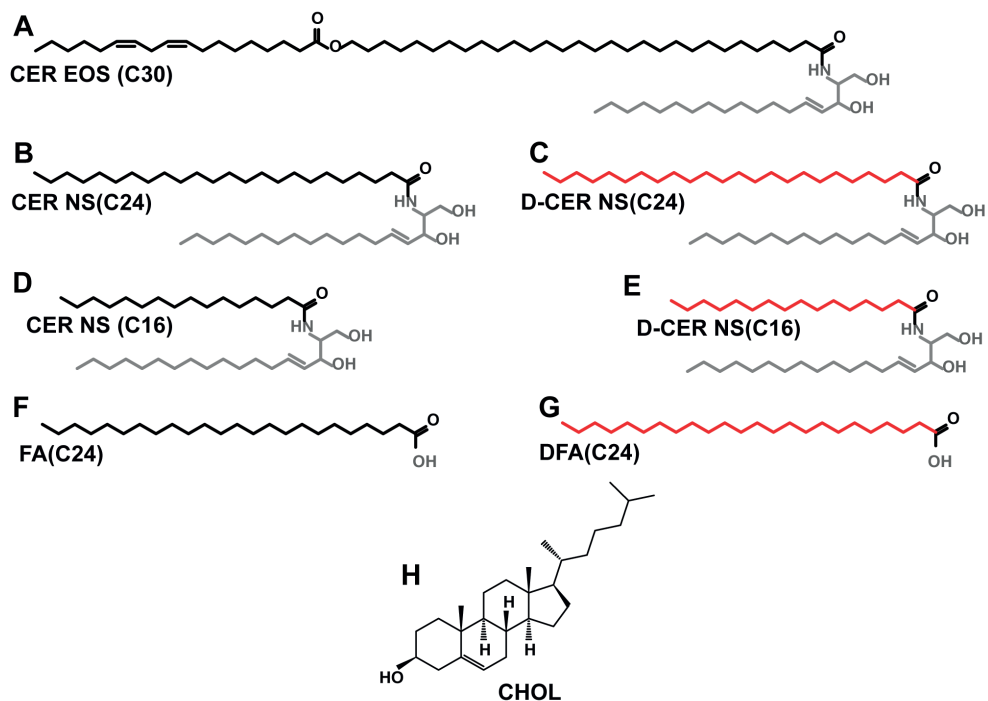


Figure S1: Molecular structure of the lipids used in the study.

A). CER EOS(C30): Linoleic acid esterified to an ω -hydroxylated acyl chain [EO], with a chain length of 30 carbon atoms (C30) linked by an amide bond to sphingosine base [S] B) CER NS(C24): Non-hydroxy [N] acyl chain of 24 carbon atoms (C24) linked to sphingosine C) D-CER NS(C24): CER NS(C24) with the acyl chain deuterated D) CER NS(C16): Non-hydroxy [N] acyl chain of 16 carbon atoms (C16) linked to sphingosine E) D-CER NS(C16): NS(C16) with the acyl chain deuterated F) FA(C24): Lignoceric acid G) DFA(C24): deuterated lignoceric acid H) CHOL: Cholesterol

The sphingosine base is marked in grey, while the protiated and the deuterated acyl chains are marked in black and red respectively.

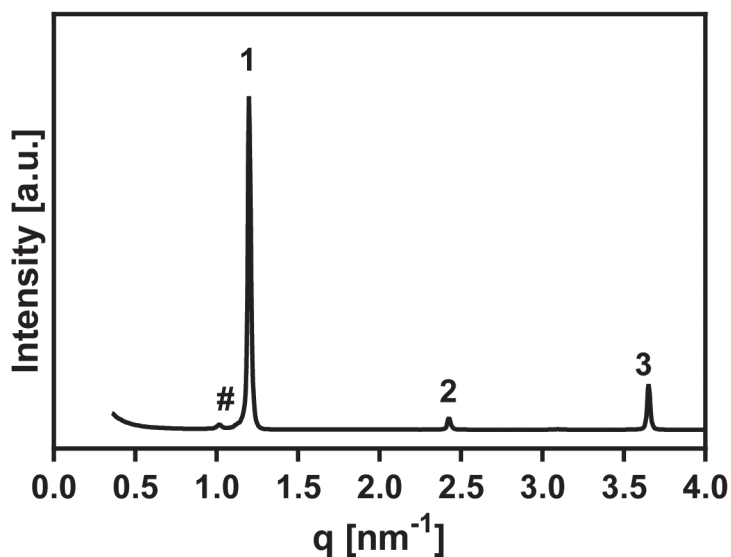


Figure S2: X-ray diffraction profile of FA(C24).

The arabic numbers (1, 2, 3) indicate the diffraction orders of the lamellar phase, $d = 5.2$, positioned at $q = 1.20, 2.41$ and 3.62 nm^{-1} . An extra peak indicated by # is located at $q=1.01$, which suggests the presence of an additional phase.

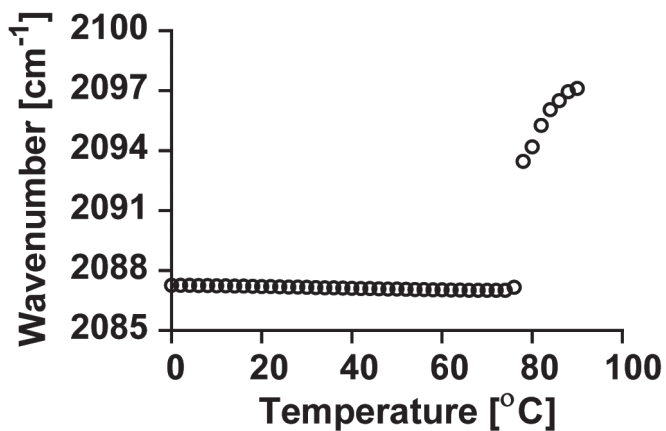


Figure S3: Plot of vCD2 frequencies as a function of temperature for DFA(C24).

The phase transition of DFA(C24) commenced at $80 \text{ }^\circ\text{C}$ and ended at $86 \text{ }^\circ\text{C}$.

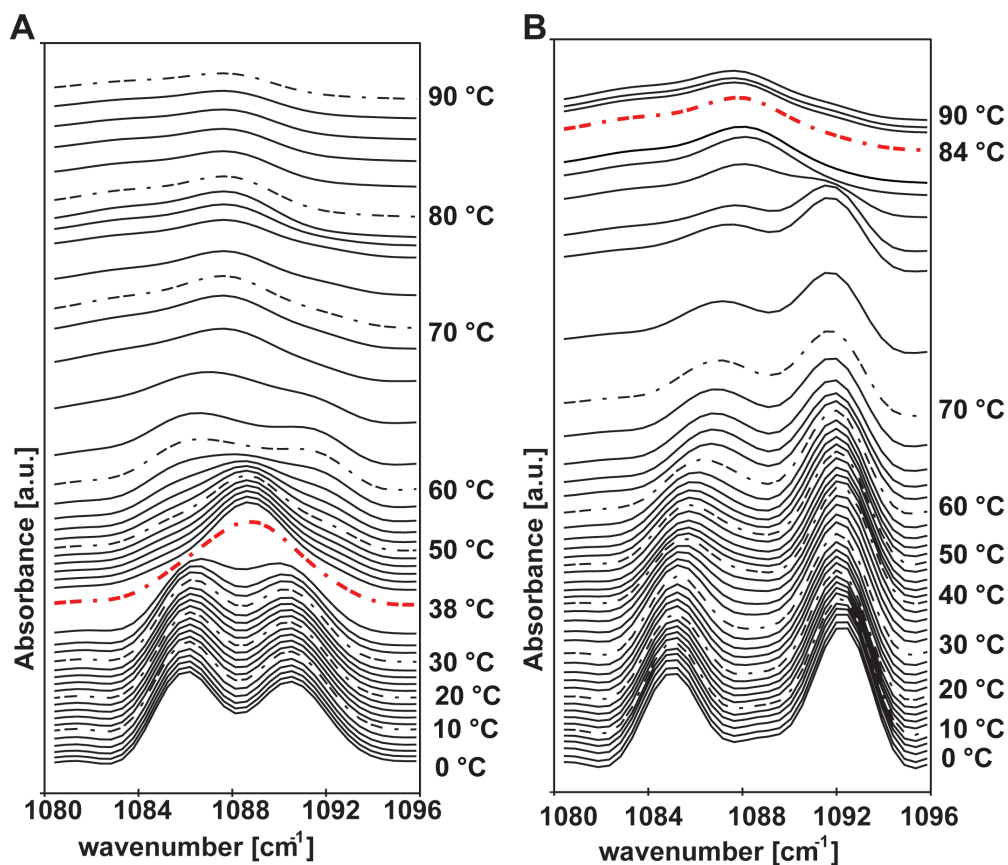
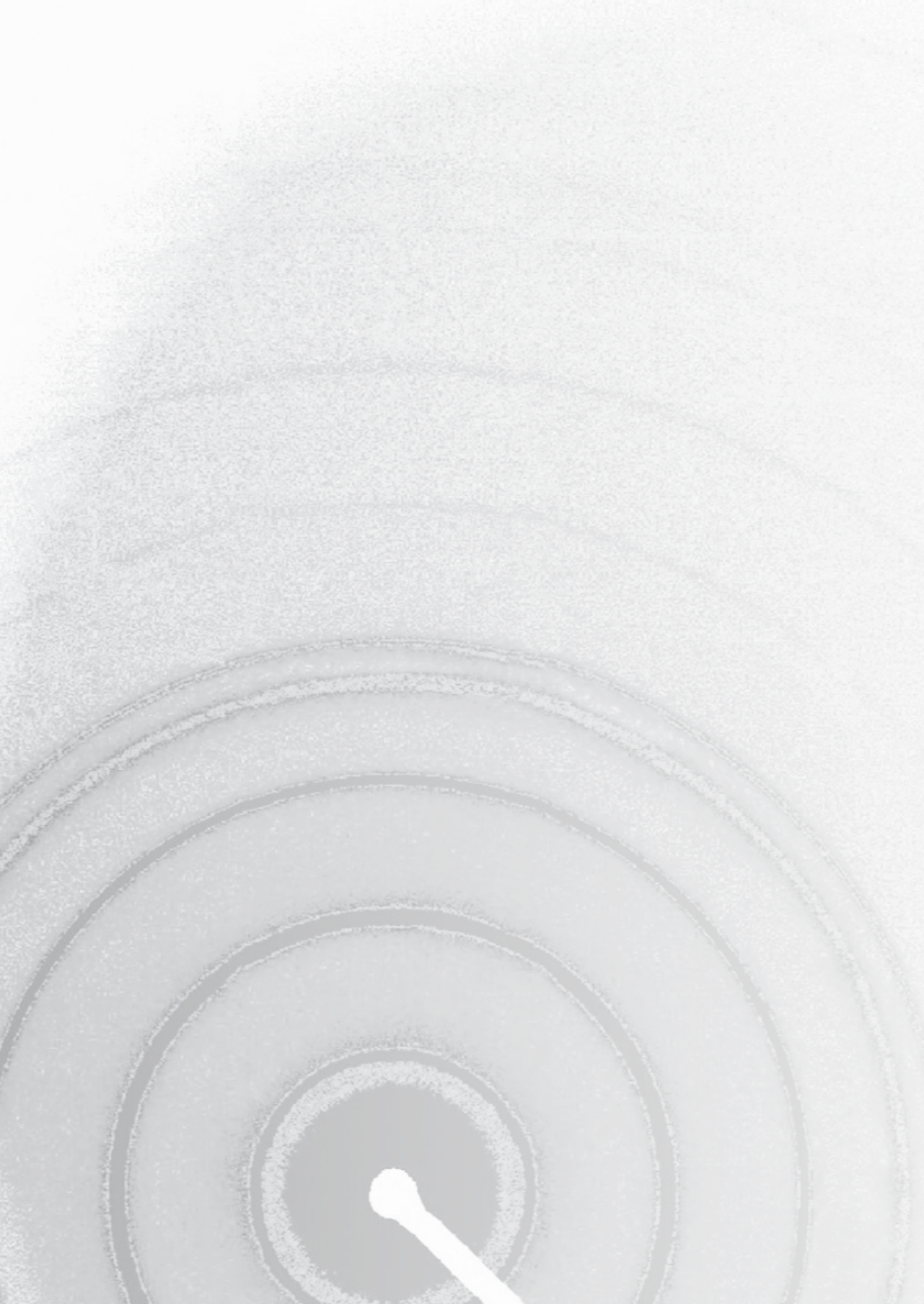


Figure S4: Plot of δ CD2 frequencies as a function of temperature for the lipid models with FA(C24) chains deuterated (0-90 °C).

The δ CD2 contour for A) NS(C16)-50-DFA B) NS(C16)-75-DFA displaying a strong splitting that collapsed into a single peak at ~ 84 °C, indicated by a red dashed line.



6

Summary and Perspectives

SUMMARY

Introduction

The skin protects the body from the invasion of pathogens and other inimical materials in the external environment, as well as preventing indiscriminate water loss from the body. This barrier function of the skin is attributed to its thin outermost layer known as the stratum corneum (SC) [1-3]. The SC comprises of keratin-filled, flattened dead cells referred to as corneocytes, embedded within a lipid matrix. The corneocytes are surrounded by a protein envelope that reduces the substance uptake. Consequently, the intercellular lipid matrix becomes the major pathway for substances permeating through the skin [4-6]. Thus, the composition and organization of the SC lipids are essential for the barrier function.

X-ray diffraction studies have shown that the intercellular lipids are assembled in two co-existing lamellar phases with periodicities of ~13 nm and ~6 nm known as the long and short periodicity phases (LPP and SPP), respectively [7, 8]. The LPP is a trilayer structure that is exclusively present in the SC and is considered to be important for the skin barrier function. Within the lamellae, the majority of the SC lipids preferably adopt a dense orthorhombic lateral packing at skin temperature (30-32 °C), while a portion of the lipids adopts the less dense hexagonal packing [9, 10]. This dense orthorhombic packing plays an important role in the low permeability of the skin barrier [11].

The major lipid classes found in the SC intercellular lipid domains are cholesterol (CHOL), free fatty acids (FFAs), and ceramides (CERs) [12, 13]. These lipids are present in an approximately equimolar ratio. The FFAs are mainly saturated, with their carbon chain lengths ranging between 12 and 30, the most common fatty acid chain length being 22, 24, or 26 carbon atoms [14-16]. The CERs have a diverse chemical structure. They comprise of a sphingoid base (sphingosine, phytosphingosine, 6-hydroxysphingosine, dihydrosphingosine, or dihydroxy dihydrosphingosine) linked to an acyl chain (Non-hydroxy, α -hydroxy or ω -hydroxy) via an amide bond. The CERs also show variation in their acyl chain length. The most abundant non-hydroxy or α -hydroxy acyl chain lengths are 24 and 26 carbon atoms. Four of the CER subclasses often referred to as acylCERs, constitute an ultra-long ω -hydroxy acyl chain, which contains up to 30-34 carbon atoms, ester-linked to an unsaturated fatty acid (usually linoleic acid) and amide-linked to one of the various sphingoid bases. These acylCERs are crucial for the formation of the LPP. At least 18 CER subclasses have been identified in human SC (Figure 1) [17-22].

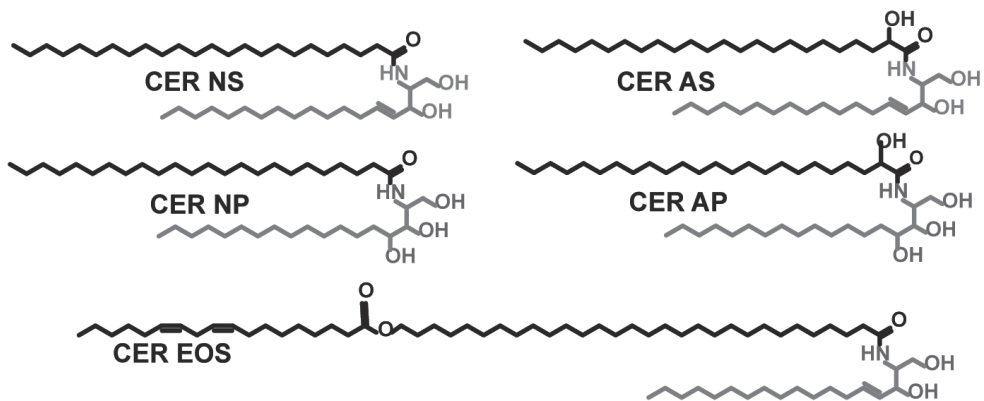


Figure 1: Some CER subclasses in the stratum corneum lipid matrix.

CERs consist of a sphingoid base linked to a FA chain. The acyl chain can either be nonhydroxylated (N), α -hydroxylated (A), or esterified ω -hydroxylated (EO), while the sphingoid base is either sphingosine (S) or phytosphingosine (P).

The composition of the SC lipids is altered in several inflammatory skin diseases including atopic dermatitis (AD), autosomal recessive congenital ichthyosis (ARCI), Netherton syndrome, and psoriasis [23-29]. Common to the skin of the patients of these diseases is barrier function impairment. Consequently, harmful substances gain access to the body. Aside from other factors such as reduced expression of the epidermal barrier proteins, several changes in SC lipid composition occur simultaneously in these patients. Therefore, although correlations between barrier function and change in lipid composition can be found *in vivo*, it is impossible to determine the effect of alterations in individual lipid classes on the SC lipid organization and skin barrier function in clinical studies. To determine the role of lipids in the impaired barrier properties in inflammatory skin diseases systematically, precluding any other interfering factors, model membrane systems based on synthetic lipids offer an excellent alternative.

The studies described in this thesis aimed to unravel the underlying factors and mechanisms for the impaired skin barrier function in inflammatory skin diseases, particularly focusing on AD, using model membrane systems mimicking the human SC lipid composition and organization.

Development of healthy human skin lipid model

As the composition can easily be modified in model membranes, lipid model

membranes offer the opportunity to mimic the lipid composition and organization in healthy as well as in diseased skin and thus allows for a detailed study of the relationship between lipid composition, molecular organization, and barrier function. In previous studies, the pigCER model comprising of synthetic CERs, CHOL, and FFAs in an equimolar ratio was used as a suitable model for healthy skin (control) to investigate the relationship between the altered lipid composition, lipid organization, and barrier function in psoriasis, Netherton syndrome, and X-linked lamellar ichthyosis skin model. However, the composition of the pigCER model is not fully representative of the CER composition in SC of healthy skin. The pigCER subclass composition is different from that in the human SC. Therefore, in **Chapter 2**, a lipid model membrane mimicking the human SC CER composition and organization was developed. The lipid organization and permeability of the lipid model membrane were compared with those of the human SC to establish the resemblance of the SC model to the native human SC. In subsequent studies, the lipid composition was modulated to mimic several aspects of the lipid composition of SC in AD skin. The changes in lipid composition investigated in this study include i) incorporation of short-chain length CERs with a total chain length of 34 C atoms ii) increased levels of CERs NS and AS, reduction in the level of CER NP iii) reduction in CER EOS concentration and iv) increased level of short-chain FFAs. To determine the effect of each of these alterations on the barrier function two complementary techniques were employed. *In-vitro* permeation study was carried out to measure the amount of a model drug ethyl-p-aminobenzoate (E-PABA) permeating the various membranes per unit area per unit time (flux) (outside-inside barrier), while transepidermal water loss (TEWL) measurements were performed to monitor the water loss across the models (inside-outside barrier). The effect of the various lipid compositional changes of AD skin on the lipid organization was analyzed.

From our result, the healthy skin model membrane properties were very similar to that of the lipid matrix in human SC, exhibiting 2 lamellar phases (SPP and LPP), orthorhombic lateral packing, and showed no significant difference in permeability to E-PABA when compared to the native skin. When the effect of individual changes in the lipid composition of AD skin on the barrier function was evaluated, the largest reduction in barrier function was observed in the model with an increased fraction of short-chain FFAs, attributed to the decrease in chain packing density deduced from the infrared spectrum. X-ray diffraction studies showed that reduction in the concentration of CER EOS resulted in a lower fraction of lipids forming the LPP. Our findings suggest that in the treatment of AD, focusing on the normalization of the FFA composition is at least as important as the normalization of CER composition.

Simple model systems for a detailed evaluation of the relationship between lipid composition, lipid organization, and barrier function

The interpretation of the interaction and lipid phase behaviour in simple systems is more detailed than in complex systems as interference from multiple lipid subclasses does not arise and more detailed information can be obtained using deuterated lipids. Consequently, simpler lipid models with a fewer number of components, prepared as an equimolar mixture of CERs, CHOL, and FFA were employed for a more detailed study of the relationship between changes in CER subclass chain length/composition and skin barrier function based on the changes in CER composition of AD patients' skin investigated in chapter 2.

Chapter 3 describes studies involving varying levels of CER EOS in the SC lipid model. As CER EOS concentration affects the formation of the LPP, simple SC models with gradually increasing levels of CER EOS (10/30/50/70/90) mol% were employed for a detailed investigation of the influence of CER EOS concentration on lamellar organization, LPP unit cell structure, lateral organization, and permeability of the model membrane. The results showed that the permeability of the model did not differ when CER EOS concentration ranged between 10 to 30% but increased significantly at 70% and higher concentrations despite the increased fraction of lipids forming an orthorhombic phase. Using CER EOS with an unsaturated deuterated C18 chain, it was determined that the fraction of lipids in a liquid phase increased. Most probably this contributes to the increased permeability with CER EOS concentration, while the surrounding CERs and FFAs remained in a crystalline orthorhombic state. The lamellar organization of the models was analyzed. At 10% CER EOS the model formed both the LPP and SPP similar to the native SC while increasing the concentration of CER EOS to 30% and higher resulted in the disappearance of the SPP. The LPP peak intensity distribution in the diffraction pattern was maintained somewhat up to 70% CER EOS concentration and corresponded to that in the unit cell of a complex SC model and the native SC LPP (2nd order peak more intense than 1st and 3rd order peaks) as described previously [30, 31] indicating similarity in the basic LPP structure. The lipid models used in the studies in chapters 4 and 5 were prepared as an equimolar mixture of CERs, CHOL, and FFA with the CER fraction containing 40% CER EOS. This was necessary to prepare models with lipids assembled in the LPP (hereafter referred to as LPP models) as part of the ongoing studies by our group to characterize the molecular interaction and arrangement of lipids within the trilayer LPP structure which until recently has not received much attention.

In **Chapter 4**, studies are described in which simple LPP models were employed for a more detailed study of the effect of different CER headgroups on

the lipid organization and barrier function of SC model membranes. The focus was on sphingosine-based CERs and phytosphingosine-based CERs as their levels are altered in the SC of AD and psoriasis patients. SC models containing CER EOS 40% and sphingosine-based CERs (CER NS or CER AS) as the CER fraction were compared with their counterparts containing phytosphingosine-based CERs (CER NP or CER AP). The permeability was compared by diffusion studies using E-PABA as a model drug, and the lipid organization was characterized by X-ray diffraction and infrared spectroscopy. Both the sphingosine- and phytosphingosine-based CER models formed the LPP, while the latter exhibited a longer LPP repeat distance and resulted also in additional phases. The E-PABA flux across the sphingosine-based CER models was higher when compared to the phytosphingosine counterparts, while the α -hydroxy phytosphingosine-based CER model had the lowest chain packing density. The unanticipated low permeability of the α -hydroxy phytosphingosine-based model is probably associated with a stronger headgroup hydrogen bonding network. Our findings indicate that the increased level of sphingosine-based CERs at the expense of phytosphingosine-based CERs, as observed in the diseased skin, possibly contribute to the barrier function impairment.

In **Chapter 5**, LPP models with varying levels of short-chain CERs were prepared for a detailed study of the effect of increased concentrations of short-chain CERs observed in SC of AD patients. The level of the long, physiological acyl chain length CER NS(C24) in the SC model membrane was gradually substituted by short-chain CER NS(C16) (0/25/50/75)% in a simple four-component skin lipid model. The effect of short-chain CERs on the permeability and phase behaviour of model membranes in the LPP models was systematically investigated. From our results, the weakest barrier was obtained in the SC model when 75% of the CER NS(24) was substituted with CER NS(C16) resulting in the formation of separate domains, especially of FA(C24) and a change in the LPP structure. This could be deduced from the SAXD and FTIR studies. Relating these findings to diseased skin, the increased level of C34 CERs reported in several inflammatory skin diseases including AD and Netherton syndrome contributes to the impaired barrier function.

CONCLUSION

Using a lipid model that mimics the human CER composition which was systematically altered to mimic various lipid compositional changes observed in

inflammatory skin disease, it was shown that the increased level of short-chain FFAs resulted in a greater reduction in barrier function than changes in the CER subclass/chain length. The former resulted in the reduction in the packing density of the lipid chains while modulations in the CER subclass composition impacted the lamellar organization and head group interactions.

The studies presented in this PhD thesis further show that simple models mimicking important aspects of the native SC lipid organization are suitable for a more detailed study and deeper understanding of the role of lipids in the changes in lipid organization as observed in inflammatory diseases. Thus, unraveling the factors and mechanism underlying the barrier function impairment which is paramount for appropriate targeting and optimization of therapy.

PERSPECTIVES

Further development of the skin lipid membrane model

Although the human skin lipid model presented in this project proved to be an effective tool for studying the effect of the altered lipid composition reported in AD patients' skin on the lipid organization and barrier function, certain improvements can be made for the model to resemble the native skin more closely. Although the CER composition contained the most prevalent CER subclasses, the model was limited as several subclasses were commercially not available. Therefore, it will be of interest to incorporate a wider range of CERs in the model as soon as these CER subclasses become available. The CER composition of the human skin model also differed from the native skin by having an almost uniform chain length: CER EOS ultra-long acyl chain contained 30 carbons, while the acyl chain of all the other CER subclasses contained 24 carbon atoms. Incorporation of a wider chain length distribution of CERs varying in acyl chain as well as sphingoid base chain length as present in the native skin should also be considered as chain length distribution affects the lipid barrier [32].

In addition to the major lipid classes, the SC lipid matrix contains a small amount of CHOL sulphate, which plays a crucial role in the desquamation process. Accumulation of CHOL sulphate was observed in the scale of X-linked ichthyosis patients [33, 34]. The human skin model prepared in this work did not contain CHOL sulphate but was effective for the study of AD since the concentration of CHOL sulphate is not affected in AD. In a previous study of SC models prepared with isolated CERs, CHOL, and FFAs, the lipid phase behavior was not affected

when CHOL sulphate was included in the lipid mixture, except that the solubility of CHOL increased [4, 35]. It would be of interest to examine the influence of CHOL sulphate in membranes based on synthetic CERs. The incorporation of CHOL sulphate 3.4% (of total lipid) in the lipid composition of the human skin model will increase its resemblance to the native skin lipid composition [34, 36] as well as increase its application.

The tortuous intercellular route filled by the lipid matrix, which is the main penetration pathway of substances into the body is not present in the lipid membranes as they do not contain corneocytes. Consequently, the thickness of the lipid membrane barrier is different from that of the SC. Abnormalities in the composition and formation of the bounds lipids linked to the cornified protein envelop surrounding the corneocyte are observed in AD and ARCI patients' skin [27, 37]. This could result in increased permeation through the corneocytes. It would be of interest to construct the tortuous intercellular permeation pathway in the skin model. This may be done by the introduction of synthetic corneocytes. The synthesis of corneocytes has been reported previously. This was done from hyperbranched polyglycerol hydrogel microparticles [38], covered with a monolayer of lipid (ω -hydroxyCER) on the membrane support. Subsequently, the lipid mixture mimicking the composition of the intercellular lipids is applied. By doing so, the permeation route of the native skin in healthy and diseased skin, as well as alterations in composition and structure of the cornified protein and lipid envelope can be mimicked.

Applications of the lipid model membrane

The SC lipid model can be of use for unraveling various factors underlying barrier dysfunction in inflammatory skin disease as well as treatment optimization study. In certain inflammatory skin diseases, the activity of enzymes involved in lipid metabolism is altered resulting in the impaired conversion of lipid precursors into CERs [39]. The activity of sphingomyelinase, which catalyzes the conversion of sphingomyelin to CER NS and CER AS was shown to be reduced in lesional and non-lesional AD skin, correlating with reduced SC CER content and barrier dysfunction. Therefore, it would be of interest to investigate the contribution of the altered sphingomyelinase activity to the reduced barrier in AD and its effect on lipid organization. Human SC models in which the CERs are gradually substituted with their precursor (sphingomyelin) can be used for these analyses. Similarly, the relationship between glucocerebrosidase deficiency observed in Gaucher's disease, SC lipid organization, and epidermal permeability barrier function can be studied using the SC lipid model. For the study, the CER

precursor, glucosylceramide could be incorporated in the skin model mixture at the expense of CERs.

Restoring skin barrier properties by the use of topical formulations aimed to improve the compromised barrier has been targeted in the treatment of skin barrier defects in AD patients [40, 41]. Understanding the action of the topical application, its interaction with the SC lipids, the effect on permeability is important for the preparation of an effective formulation. It will be of interest to study the interaction of the models with sebum, which is a natural moisturizer present on the body surface, comprising of a mixture of glycerides, FFAs, wax esters, squalene, CHOL esters, and CHOL. Skin barrier lipid components aimed to normalize the lipid composition can be systematically incorporated into the sebum lipid mixture resulting in various formulations. The effect of the formulations on the lipid organization and permeability of the model can then be investigated to select those components that normalize the skin barrier.

Due to the multifactorial nature of AD, the causes and severity of the disease can vary between patients. As there is a large variation in the CER and FFA composition of patients, one-size-fits-all treatment for different patients may not be ideal. The human skin model can offer the possibility of personalized medicine for AD patients. This is because individual patients' skin lipid composition can be directly mimicked and analyzed. A personalized treatment plan that will lead to optimal recovery of barrier function could then be established using the models, tailored to the individual patient's circumstance.

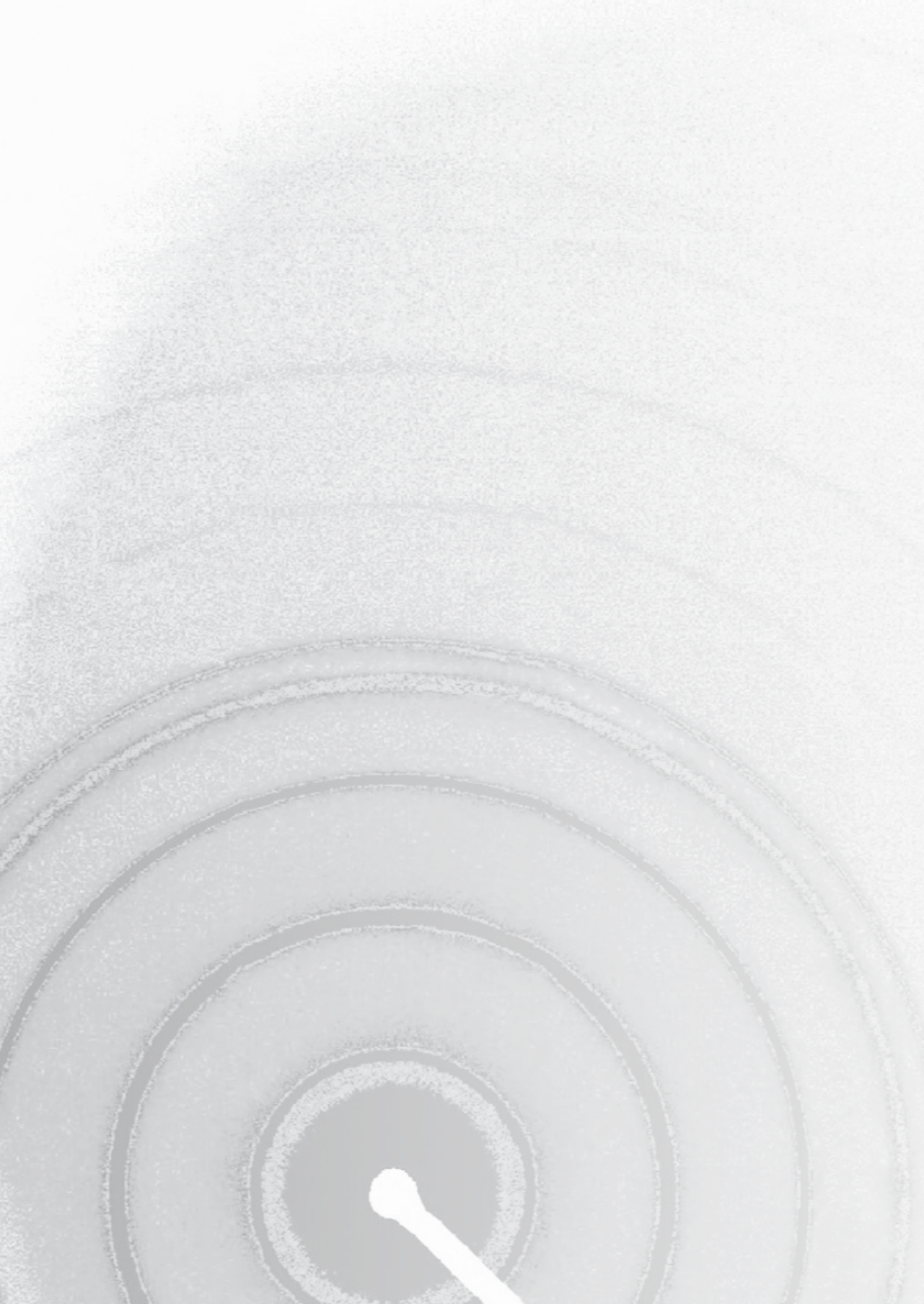
The human SC lipid model can be used for screening candidates for use as moisturizers, which are formulations applied for the treatment of dry skin. Their effectiveness in improving the barrier can be assessed. The use of the model membrane offers the opportunity to study the effect of the moisturizer on lipid organization and unravel the mechanism of action. Similarly, candidates for penetration enhancement, which are substances that increase the permeation of the skin can also be evaluated using the human skin model.

REFERENCES

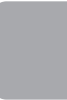
1. Elias, P. M., Stratum corneum defensive functions: an integrated view. *J. Invest. Dermatol.* **2005**, *125* (2), 183-200.
2. Baroni, A.; Buommino, E.; De Gregorio, V.; Ruocco, E.; Ruocco, V.; Wolf, R., Structure, and function of the epidermis related to barrier properties. *Clin. Dermatol.* **2012**, *30* (3), 257-62.
3. Madison, K. C., Barrier function of the skin: "la raison d'être" of the epidermis. *J. Invest. Dermatol.* **2003**, *121* (2), 231-41.
4. Bodde, H. E.; Kruithof, M. A. M.; Brussee, J.; Koerten, H. K., Visualization of normal and enhanced HgCl₂ transport through human-skin invitro. *Int. J. Pharm.* **1989**, *53* (1), 13-24.
5. Talreja, P. S.; Kleene, N. K.; Pickens, W. L.; Wang, T. F.; Kasting, G. B., Visualization of the lipid barrier and measurement of lipid pathlength in human stratum corneum. *AAPS Pharmsci.* **2001**, *3* (2), art. no. 13.
6. Proksch, E.; Brandner, J. M.; Jensen, J. M., The skin: an indispensable barrier. *Exp. Dermatol.* **2008**, *17* (12), 1063-72.
7. Bouwstra, J. A.; Gooris, G. S.; van der Spek, J. A.; Bras, W., Structural investigations of human stratum corneum by small-angle X-ray scattering. *J. Invest. Dermatol.* **1991**, *97* (6), 1005-12.
8. White, S. H.; Mirejovsky, D.; King, G. I., Structure of lamellar lipid domains and corneocyte envelopes of murine stratum corneum. An X-ray diffraction study. *Biochemistry* **1988**, *27* (10), 3725-32.
9. Bouwstra, J.; Gooris, G.; Ponec, M., The lipid organisation of the skin barrier: Liquid and crystalline domains coexist in lamellar phases. *Journal of biological physics* **2002**, *28* (2), 211-223.
10. Boncheva, M.; Damien, F.; Normand, V., Molecular organization of the lipid matrix in intact stratum corneum using ATR-FTIR spectroscopy. *Biochim. Biophys. Acta* **2008**, *1778* (5), 1344-55.
11. Damien, F.; Boncheva, M., The extent of orthorhombic lipid phases in the stratum corneum determines the barrier efficiency of human skin in vivo. *J. Invest. Dermatol.* **2010**, *130* (2), 611-614.
12. Weerheim, A.; Ponec, M., Determination of stratum corneum lipid profile by tape stripping in combination with high-performance thin-layer chromatography. *Arch. Dermatol. Res.* **2001**, *293* (4), 191-199.
13. Coderch, L.; López, O.; de la Maza, A.; Parra, J. L., Ceramides and Skin Function. *Am. J. Clin. Dermatol.* **2003**, *4* (2), 107-129.
14. Norlen, L.; Nicander, I.; Lundsjo, A.; Cronholm, T.; Forslind, B., A new HPLC-based method for the quantitative analysis of inner stratum corneum lipids with special reference to the free fatty acid fraction. *Arch. Dermatol. Res.* **1998**, *290* (9), 508-16.
15. van Smeden, J.; Boiten, W. A.; Hankemeier, T.; Rissmann, R.; Bouwstra, J. A.; Vreeken, R. J., Combined LC/MS-platform for analysis of all major stratum corneum lipids, and the profiling of skin substitutes. *Biochim. Biophys. Acta* **2014**, *1841* (1), 70-79.
16. P. W. Wertz, D. T. D., *Physiology, biochemistry and molecular biology of the skin*. second ed.; Oxford University Press: New York, 1991; Vol. 1, p 205-236.
17. Masukawa, Y.; Narita, H.; Shimizu, E.; Kondo, N.; Sugai, Y.; Oba, T.; Homma, R.; Ishikawa, J.; Takagi, Y.; Kitahara, T.; Takema, Y.; Kita, K., Characterization of overall ceramide species in human Stratum corneum. *J. Lipid Res.* **2008**, *49* (7), 1466-1476.

18. Rabionet, M.; Gorgas, K.; Sandhoff, R., Ceramide synthesis in the epidermis. *Biochim. Biophys. Acta* **2014**, *1841* (3), 422-34.
19. Robson, K. J.; Stewart, M. E.; Michelsen, S.; Lazo, N. D.; Downing, D. T., 6-Hydroxy-4-sphingenine in human epidermal ceramides. *J. Lipid Res.* **1994**, *35* (11), 2060-8.
20. Stewart, M. E.; Downing, D. T., A new 6-hydroxy-4-sphingenine-containing ceramide in human skin. *J. Lipid Res.* **1999**, *40* (8), 1434-9.
21. van Smeden, J.; Hoppel, L.; van der Heijden, R.; Hankemeier, T.; Vreeken, R. J.; Bouwstra, J. A., LC/MS analysis of stratum corneum lipids: ceramide profiling and discovery. *J. Lipid Res.* **2011**, *52* (6), 1211-21.
22. Boiten, W.; Absalah, S.; Vreeken, R.; Bouwstra, J.; van Smeden, J., Quantitative analysis of ceramides using a novel lipidomics approach with three dimensional response modelling. *Biochimica et Biophysica Acta (BBA) - Molecular and Cell Biology of Lipids* **2016**, *1861* (11), 1652-1661.
23. Janssens, M.; van Smeden, J.; Gooris, G. S.; Bras, W.; Portale, G.; Caspers, P. J.; Vreeken, R. J.; Kezic, S.; Lavrijsen, A. P.; Bouwstra, J. A., Lamellar lipid organization and ceramide composition in the stratum corneum of patients with atopic eczema. *J. Invest. Dermatol.* **2011**, *131* (10), 2136-8.
24. van Smeden, J.; Janssens, M.; Boiten, W. A.; van Drongelen, V.; Furio, L.; Vreeken, R. J.; Hovnanian, A.; Bouwstra, J. A., Intercellular skin barrier lipid composition, and organization in Netherton syndrome patients. *J. Invest. Dermatol.* **2014**, *134* (5), 1238-1245.
25. Schreiner, V.; Gooris, G. S.; Pfeiffer, S.; Lanzendorfer, G.; Wenck, H.; Diembeck, W.; Proksch, E.; Bouwstra, J., Barrier characteristics of different human skin types investigated with X-ray diffraction, lipid analysis, and electron microscopy imaging. *J. Invest. Dermatol.* **2000**, *114* (4), 654-60.
26. J.A. Bouwstra, E. H. M., *Cosmetic formulation principles and practice*. CRC Press: Boca Raton, 2019.
27. Crumrine, D.; Khnykin, D.; Krieg, P.; Man, M.-Q.; Celli, A.; Mauro, T. M.; Wakefield, J. S.; Menon, G.; Mauldin, E.; Miner, J. H.; Lin, M.-H.; Brash, A. R.; Sprecher, E.; Radner, F. P. W.; Choate, K.; Roop, D.; Uchida, Y.; Gruber, R.; Schmuth, M.; Elias, P. M., Mutations in Recessive Congenital Ichthyoses Illuminate the Origin and Functions of the Corneocyte Lipid Envelope. *J. Invest. Dermatol.* **2019**, *139* (4), 760-768.
28. Eckl, K.-M.; Tidhar, R.; Thiele, H.; Oji, V.; Hausser, I.; Brodesser, S.; Preil, M.-L.; Önal-Akan, A.; Stock, F.; Müller, D.; Becker, K.; Casper, R.; Nürnberg, G.; Altmüller, J.; Nürnberg, P.; Traupe, H.; Futerman, A. H.; Hennies, H. C., Impaired Epidermal Ceramide Synthesis Causes Autosomal Recessive Congenital Ichthyosis and Reveals the Importance of Ceramide Acyl Chain Length. *J. Invest. Dermatol.* **2013**, *133* (9), 2202-2211.
29. Motta, S.; Monti, M.; Sesana, S.; Caputo, R.; Carelli, S.; Ghidoni, R., Ceramide composition of the psoriatic scale. *Biochim. Biophys. Acta* **1993**, *1182* (2), 147-51.
30. Groen, D.; Gooris, G. S.; Bouwstra, J. A., New insights into the stratum corneum lipid organization by X-ray diffraction analysis. *Biophys. J.* **2009**, *97* (8), 2242-2249.
31. Uche, L. E.; Gooris, G. S.; Beddoes, C. M.; Bouwstra, J. A., New insight into phase behavior and permeability of skin lipid models based on sphingosine and phytosphingosine ceramides. *Biochim. Biophys. Acta* **2019**, *1861* (7), 1317-1328.
32. Mojumdar, E. H.; Kariman, Z.; van Kerckhove, L.; Gooris, G. S.; Bouwstra, J. A., The role of ceramide chain length distribution on the barrier properties of the skin lipid membranes. *Biochim Biophys Acta* **2014**, *1838* (10), 2473-2483.
33. Hamanaka, S.; Ujihara, M.; Serizawa, S.; Nakazawa, S.; Otsuka, F., A case of recessive X-linked ichthyosis: scale-specific abnormalities of lipid composition may explain the pathogenesis of the skin manifestation. *J. Dermatol. Sci.* **1997**, *24* (3), 156-60.

34. Elias, P. M.; Williams, M. L.; Maloney, M. E.; Bonifas, J. A.; Brown, B. E.; Grayson, S.; Epstein, E. H., Jr., Stratum corneum lipids in disorders of cornification. Steroid sulfatase and cholesterol sulfate in normal desquamation and the pathogenesis of recessive X-linked ichthyosis. *The Journal of clinical investigation* **1984**, *74* (4), 1414-21.
35. Bouwstra, J. A.; Gooris, G. S.; Dubbelaar, F. E.; Weerheim, A. M.; Ponc, M., pH, cholesterol sulfate, and fatty acids affect the stratum corneum lipid organization. *J. Invest. Dermatol. Symp. Proc.* **1998**, *3* (2), 69-74.
36. Elias, P. M., Epidermal lipids, membranes, and keratinization. *Int. J. Dermatol.* **1981**, *20* (1), 1-19.
37. Boiten, W.; van Smeden, J.; Bouwstra, J., The cornified envelope-bound ceramide fraction is altered in patients with atopic dermatitis. *J. Invest. Dermatol.* **2020**, *140* (5), 1097-1100.
38. Rissmann, R.; Oudshoorn, M. H.; Zwier, R.; Ponc, M.; Bouwstra, J. A.; Hennink, W. E., Mimicking vernix caseosa--preparation and characterization of synthetic biofilms. *Int. J. Pharm.* **2009**, *372* (1-2), 59-65.
39. van Smeden, J.; Bouwstra, J. A., Stratum corneum lipids: Their role for the skin barrier function in healthy subjects and atopic dermatitis patients. *Curr. Probl. Dermatol.* **2016**, *49*, 8-26.
40. Boiten, W. A.; Berkers, T.; Absalah, S.; van Smeden, J.; Lavrijsen, A. P. M.; Bouwstra, J. A., Applying a vernix caseosa based formulation accelerates skin barrier repair by modulating lipid biosynthesis. *J. Lipid Res.* **2018**, *59* (2), 250-260.41.
41. Hon, K. L.; Leung, A. K. C.; Barankin, B., Barrier Repair Therapy in Atopic Dermatitis: An Overview. *Am. J. Clin. Dermatol.* **2013**, *14* (5), 389-399.



Appendices



NEDERLANDSE SAMENVATTING

Introductie

De huid beschermt het lichaam tegen het binnen dringen van ziektekiemen en andere gevaarlijke substanties uit de omgeving en verhindert overmatig vochtverlies uit het lichaam. De barrièrefunctie van de huid wordt toegeschreven aan het buitenste laagje van de huid dat bekend staat als het stratum corneum (SC) [1-3]. Het SC bestaat uit met keratine gevulde dode cellen (corneocyten), die zijn ingebed in een lipiden matrix. De corneocyten worden begrensd door een dichte laag met aan elkaar gekoppelde eiwitten die de opname van stoffen in de corneocyten bemoeilijkt. Dit is de rede waarom de lipiden lagen tussen de cellen de belangrijkste penetratie route is voor stoffen door het SC [4-6]. De samenstelling en organisatie van de SC-lipiden zijn dus essentieel voor de barrièrefunctie.

Uit röntgendiffractie studies blijkt dat de lipiden tussen de cellen twee naast elkaar bestaande lamellaire fasen vormen met een repeterende eenheid van ~13 nm en ~6 nm, ook wel de lange en korte periodiciteitsfasen genoemd (LPP en SPP), respectievelijk [7, 8]. De LPP heeft een repeterende eenheid die bestaat uit 3 lipiden lagen. Deze lamellarie fase is uniek voor het SC en dat is de rede waarom deze fase belangrijk wordt geacht voor de huidbarrière. Bij de huidtemperatuur (ongeveer 30-32 °C) vormen de lipiden in de lamellen voornamelijk een dichte orthorombische pakking, terwijl een klein deel van de lipiden zich ordent in de minder compacte hexagonale pakking [9, 10]. Deze dichte orthorombische pakking speelt waarschijnlijk ook een belangrijke rol in de huidbarrièrefunctie [11].

De belangrijkste lipidenklassen in de lipiden matrix in het SC, zijn cholesterol (CHOL), vrije vetzuren (FFAs) en ceramiden (CERs) [12, 13]. Deze lipiden zijn aanwezig in een ongeveer equimolaire verhouding. De FFAs zijn overwegend verzadigd, met vetzuurketens variërend tussen de 12 en 30 koolstofatomen, waarbij de meest voorkomende FFAs een ketenlengte hebben van 22, 24 of 26 koolstofatomen [14-16]. De CERs vertonen een grote variatie in chemische structuur. Ze bestaan uit een sfingoïde base (sfingosine, fytosfingosine, 6-hydroxysfingosine, dihydrosfingosine of 2-hydroxysfingosine) gekoppeld aan een acylketen (non-hydroxy, α -hydroxy of ω -hydroxy) via een amidebinding. De CERs variëren ook in de lengte van hun vetzuur en sphingoïde keten. De meest voorkomende non-hydroxy- en α -hydroxy-acylketens zijn 24 of 26 koolstofatomen lang. Vier van de CER-subklassen, de zogenaamde acylCERs, hebben een ultralange ω -hydroxy-acylketen. De meest voorkomende acyl

ketenlengten zijn 30, 32 of 34 koolstofatomen. Deze acylketens zijn via een ester groep verbonden aan een onverzadigd vetzuur (meestal linolzuur) en via een amide gekoppeld aan één van de verschillende sfingoïde basen. Deze acylCERs zijn cruciaal voor de vorming van de LPP. De meest onderzochte acylCER is CER EOS met een sfingosine base. Op dit moment zijn 18 CER subklassen geïdentificeerd in het menselijk SC (Figuur 1) [17-22].

De samenstelling van de SC lipiden verandert bij inflammatoire huidziekten. Voorbeelden van inflammatoire huidziekten zijn constitutioneel eczeem (atopic dermatitis, (AD)), Netherton-syndroom, psoriasis en autosomaal recessieve congenitale ichthyosis (ARCI) [23-29]. De patiënten met deze huidziekten hebben een verstoorde huidbarrièrefunctie. Hierdoor krijgen schadelijke stoffen makkelijker toegang tot het lichaam. Hoewel in klinische studies correlaties tussen barrièrefunctie en verandering in lipiden samenstelling zijn vastgesteld is het niet mogelijk om het effect van veranderingen in individuele lipidenklassen op de SC lipidenorganisatie en huidbarrièrefunctie in klinisch onderzoek te ontrafelen. Om de rol van lipiden in de verminderde barrière-eigenschappen bij inflammatoire huidziekten in detail te bepalen, bieden modelmembraansystemen op basis van synthetische CERs een uitstekend alternatief, daar de membranen niet gevoelig zijn voor andere storende factoren en slechts één parameter veranderd kan worden.

De studies beschreven in dit proefschrift zijn gericht op het ontrafelen van de onderliggende factoren betreffende lipiden voor de verminderde huidbarrièrefunctie bij inflammatoire huidziekten. Hiertoe werden complexe en eenvoudige modelmembranen gebruikt.

Ontwikkeling van een lipiden modelmembraan voor de gezonde menselijke huid

Omdat de samenstelling in modelmembranen gemakkelijk kan worden gewijzigd, biedt het lipiden modelmembraan de mogelijkheid om de lipiden samenstelling en organisatie na te bootsen van zowel gezonde als zieke huid. Dit maakt het mogelijk gedetailleerder onderzoek uit te voeren naar de relatie tussen lipiden samenstelling, lipidenorganisatie, en barrièrefunctie. In eerdere studies werd het varkens CER-model bestaande uit een gelijke molaire verhouding van synthetische CERs, CHOL en FFAs gebruikt als een model. De samenstelling van het varkens CER-model is echter niet volledig representatief voor de CER samenstelling in SC van gezonde menselijke huid. Daarom is in het onderzoek beschreven in **Hoofdstuk 2** een membraan ontwikkeld dat de samenstelling en organisatie van de lipiden in het SC van menselijke huid nabootst. De

lipidenorganisatie en permeabiliteit van het lipiden modelmembraan werden vergeleken met die van het menselijke SC. In het daaropvolgende onderzoek werd de lipidsamenstelling gevarieerd om verschillende aspecten van de lipidsamenstelling van SC in AD patiënten na te bootsen. De volgende veranderingen in de lipidsamenstelling zijn onderzocht. i) Toevoeging van CERs met een korte totale ketenlengte van 34 koolstofatomen, ii) een afwijkende verhouding van de CER samenstelling, iii) een verlaging van de acylCER concentratie en iv) een verhoging van de concentratie van FFAs met een korte ketenlengte. Om het effect van elk van deze veranderingen op de barrièrefunctie te bepalen, werden twee complementaire technieken gebruikt. Een diffusiestudie werd uitgevoerd om de transportsnelheid van het modelgeneesmiddel ethyl-p-aminobenzoaat (E-PABA) te meten. Tevens werd de verdamping van water via het lipidenmembraan (TEWL-metingen) gemeten. Ook werd het effect van de verandering in lipidsamenstelling op de lipidenorganisatie geanalyseerd.

Uit de resultaten bleek dat de membraan eigenschappen van het gezonde huidmodel vergelijkbaar zijn met die van het menselijk SC. De lipiden in het membraan vormden de 2 lamellaire fasen (SPP en LPP), een orthorombische laterale pakking en ze vertoonden geen significant verschil in de permeabiliteit in vergelijking met menselijke SC. Het model werd dus goed genoeg bevonden om het effect van de afwijkende lipidsamenstellingen te onderzoeken. Uit deze onderzoeken bleek dat de sterkste vermindering van de barrièrefunctie werd waargenomen in het model met een verhoogde fractie FFAs met korte ketens. Deze verandering leidde tot een verlaagde dichtheid van de pakking van de ketens. Verder bleek dat verlaging van de concentratie acylCERs resulteerde in een sterk verlaagde fractie lipiden die de LPP vormden, maar dit had een kleiner effect op de permeabiliteit. Onze bevindingen suggereren dat bij de behandeling van AD, de normalisatie van de FFA-samenstelling minstens zo belangrijk is als de normalisatie van de CER-samenstelling.

Eenvoudige modelsystemen voor een gedetailleerde evaluatie van de relatie tussen lipidsamenstelling, lipidenorganisatie en barrièrefunctie.

De interpretatie van het fasegedrag van de lipiden in eenvoudige systemen is gedetailleerder dan in complexe systemen, aangezien wisselwerking van meerdere lipiden subklassen niet optreedt en er ook meer gedetailleerde informatie kan worden verkregen door gebruik te maken van gedeutereerde lipiden. Daarom werden lipiden modellen met een kleiner aantal componenten onderzocht, met steeds dezelfde molaire verhouding CERs, CHOL en FFAs. De relatie tussen

veranderingen in CER subklassen en de verandering in ketenlengte op de lipidenorganisatie en permeabiliteit kon zo in meer detail worden onderzocht.

Hoofdstuk 3 beschrijft studies met verschillende hoeveelheden CER EOS in het modelmembraan. Aangezien de CER EOS concentratie de vorming van de LPP beïnvloedt, werden eenvoudige modelmembranen met geleidelijk toenemende verhoudingen van CER EOS (10/30/50/70/90 mol% van de totale hoeveelheid CERs) gebruikt voor een gedetailleerd onderzoek naar de invloed van de CER EOS concentratie op zowel de lamellaire organisatie als op de laterale organisatie en permeabiliteit van het modelmembraan. Uit de resultaten bleek dat de permeabiliteit van het model niet veranderde wanneer de CER EOS concentratie tussen 10 en 30% van de totale CER concentratie lag, maar significant toenam bij 70% en hogere concentraties, terwijl de fractie van lipiden die een orthorombische fase vormden was toegenomen. Uit metingen van een lipidenamenstelling met CER EOS met een onverzadigde gedeutereerde C18-keten bleek dat de fractie lipiden in een vloeibare fase toenam wanneer de CER EOS concentratie toenam. Hoogstwaarschijnlijk draagt dit bij tot de verhoogde permeabiliteit bij een hogere CER EOS concentratie. De omringende CERs en FFAs vormden onafhankelijk van de hoeveelheid CER EOS onveranderd een kristallijne orthorombische fase. Ook werd de lamellaire organisatie van de modellen geanalyseerd. Bij 10% CER EOS vormde het model zowel de LPP als de SPP, dit is een vergelijkbare concentratie acylCERs als in menselijke huid, waar zowel de SPP en LPP aanwezig zijn. Bij een concentratie CER EOS van 30% en hoger werd alleen de LPP gevormd. Uit röntgendiffractie resultaten bleek dat de verhouding van de piekintensiteiten in het diffractiepatroon van de LPP gehandhaafd bleef bij mengsels tot 70% CER EOS-concentratie en kwam overeen met de verhouding van de diffractiepieken in het diffractiepatroon van het complex SC-model en van de LPP in humaan SC (2e-orde piek hogere intensiteit dan 1e en 3e-orde pieken), zoals eerder beschreven [30, 31]. Dit betekent dat de basis van de LPP structuur in modelmembranen met een verschillende samenstelling veel overeenkomst vertonen. De lipiden modelmembranen uit de studies in hoofdstuk 4 en 5, werden bereid met gelijke mol-verhouding CERs, CHOL en FFAs, waarbij de CER-fractie 40% CER EOS bevatte. Hiervoor werd gekozen omdat dit leidt tot modellen die alleen de LPP vormen en niet de SPP (hierna LPP-modellen genoemd). Deze twee onderzoeken zijn onderdeel van het lopende onderzoek binnen onze groep om de moleculaire interactie en rangschikking van lipiden binnen de LPP-structuur in detail te karakteriseren.

In **Hoofdstuk 4** worden studies beschreven waarin eenvoudige LPP modellen werden gebruikt om in meer detail het effect van verschillende CER kopgroepen

op de lipidenorganisatie en barrièrefunctie van SC modelmembranen te onderzoeken. De focus lag op zowel op sfingosine als op fytosfingosine gebaseerde CERs, aangezien de hoeveelheid van beide groepen verandert in het SC van AD en psoriasis patiënten. Modelmembranen met 40% CER EOS en op sfingosine gebaseerde CERs (CER NS of CER AS) werden vergeleken met modellen waarin hun tegenhangers de op fytosfingosine gebaseerde CERs (CER NP of CER AP) zijn geïncorporeerd. De permeabiliteit werd vergeleken door diffusiestudies met E-PABA als modelgeneesmiddel uit te voeren. Tevens werd de lipidenorganisatie onderzocht met röntgendiffractie en infraroodspectroscopie. Zowel de mengels met CERs gebaseerd op sfingosine als op fytosfingosine vormden de LPP. Echter mengels gebaseerd op fytosfingosine vormden een LPP met een langere periodiciteit en extra fasen. De E-PABA-flux door de sfingosine gebaseerde CER modellen was hoger dan door de modellen gebaseerd op fytosfingosine CERs. Belangrijk was de constatering dat het CER model gebaseerd op α -hydroxy-fytosfingosine (CER AP) de laagste pakkingsdichtheid had: voornamelijk een hexagonale pakking. De onverwachts lage permeabiliteit van dit model wordt waarschijnlijk veroorzaakt door de sterkere waterstofbrug binding tussen de kopgroepen van de lipiden. Uit onze bevindingen blijkt dat de verhoogde concentratie op sfingosine gebaseerde CERs (ten opzichte van de fytosfingosine), zoals waargenomen in zieke huid, mogelijk bijdraagt aan de verminderde barrièrefunctie.

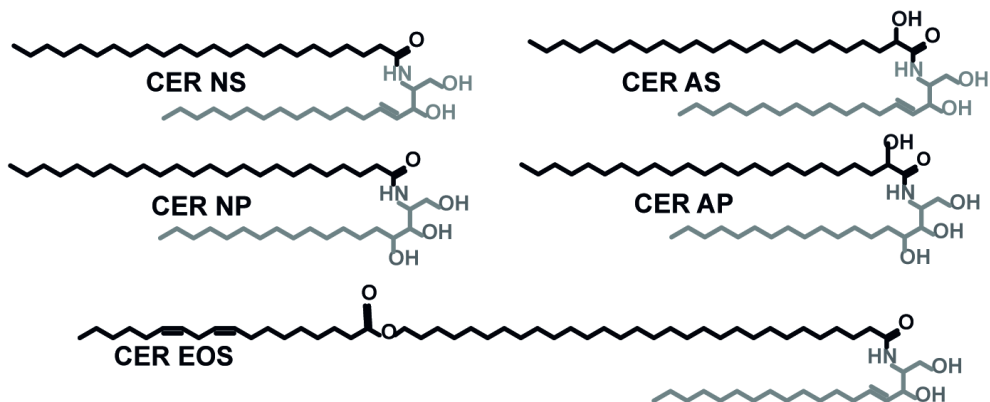
In het onderzoek beschreven in **Hoofdstuk 5** werden modellen waarin de lipiden alleen de LPP vormen met een systematische verhoging van C34 CERs (CERs met een totale ketenlengte van 34 koolstofatomen) onderzocht. Interessant, omdat een verhoogde concentratie C34 CERs ook is waargenomen in SC van AD huid. Het modelsysteem bestond uit slechts 4 componenten, CER EOS, CER NS, CHOL en FFA met 24 koolstofatomen (FAC24). In dit onderzoek werd de fysiologische acylketenlengte van CER NS (totaal aantal koolstof atomen in de keten 42) met 24 koolstofketens in de acylketen (CER NS(C24)) in het modelmembraan geleidelijk vervangen door C34 CER NS met 16 koolstofatomen in de acylketen CER NS(C16). Het effect van een systematische verhoging van de concentratie CER NS(C16) ten koste van CER NS(C24) op de permeabiliteit en het fasegedrag van de modelmembranen werd onderzocht. De zwakste barrière van het SC model werd waargenomen, wanneer 75 mol% van de CER NS (24) werd vervangen door CER NS (C16). Uit zowel de diffractie als infrarood experimenten bleek dat bij deze concentratie CER NS(C16) verschillende fasen gevormd werden, waarbij vooral de vetzuren uitkristalliseerden in aparte domeinen. Deze bevindingen dragen bij aan de mogelijke effecten die een verhoogde

concentratie C34 CER heeft op de lipidenorganisatie en barrierefunctie in inflammatoire huidziekten waaronder AD en Netherton-syndroom.

Conclusie

Er is een lipiden modelmembraan ontwikkeld dat de lipiden samenstelling, organisatie en permeabiliteit van menselijk SC nabootst. Door de samenstelling van dit model systematisch te veranderen is meer informatie verzameld over het effect van de verandering in de lipiden samenstelling in inflammatoire huidziekten. Uit het onderzoek bleek dat een verhoogde concentratie FFAs met korte ketens resulteerde in een sterke verminderde barrierefunctie. Veranderingen in de CER-subklassen samenstelling en ketenlengte hadden een veel kleiner effect. De verandering in de FFAs verlaagde de pakkingsdichtheid van de lipiden ketens, terwijl modulaties in de CER samenstelling de lamellaire organisatie en kopgroep interacties beïnvloedden.

Uit de studies beschreven in dit proefschrift bleek verder dat eenvoudige modellen die belangrijke aspecten van de menselijke SC lipidenorganisatie nabootsen, geschikt zijn voor gedetailleerde studies en tot een beter begrip leiden betreffende de rol van lipiden in de veranderingen in de lipidenorganisatie en barrierefunctie zoals waargenomen bij inflammatoire huidziekten. Het ontrafelen van de factoren en de mechanismes die ten grondslag liggen aan de verstoring van de barrierefunctie is van het grootste belang voor een doelmatige, optimale therapie.



Figuur 1: Sommige CER-subklassen in het lipidenstelsel van het stratum corneum.

CER's bestaan uit een sfingoïde basis gekoppeld aan een FA-keten. De acylketen kan ofwel niet-gehydroxyleerd (N), α-gehydroxyleerd (A), of veresterd ω-gehydroxyleerd (EO) zijn, terwijl de sfingoïde-base uit sfingosine (S), of fytosfingosine (P) bestaat.

REFERENCES

1. Elias, P. M., Stratum corneum defensive functions: an integrated view. *J. Invest. Dermatol.* **2005**, *125* (2), 183-200.
2. Baroni, A.; Buommino, E.; De Gregorio, V.; Ruocco, E.; Ruocco, V.; Wolf, R., Structure, and function of the epidermis related to barrier properties. *Clin. Dermatol.* **2012**, *30* (3), 257-62.
3. Madison, K. C., Barrier function of the skin: "la raison d'être" of the epidermis. *J. Invest. Dermatol.* **2003**, *121* (2), 231-41.
4. Bodde, H. E.; Kruithof, M. A. M.; Brussee, J.; Koerten, H. K., Visualization of normal and enhanced HgCl₂ transport through human-skin invitro. *Int. J. Pharm.* **1989**, *53* (1), 13-24.
5. Talreja, P. S.; Kleene, N. K.; Pickens, W. L.; Wang, T. F.; Kasting, G. B., Visualization of the lipid barrier and measurement of lipid pathlength in human stratum corneum. *AAPS Pharmsci.* **2001**, *3* (2), art. no. 13.
6. Proksch, E.; Brandner, J. M.; Jensen, J. M., The skin: an indispensable barrier. *Exp. Dermatol.* **2008**, *17* (12), 1063-72.
7. Bouwstra, J. A.; Gooris, G. S.; van der Spek, J. A.; Bras, W., Structural investigations of human stratum corneum by small-angle X-ray scattering. *J. Invest. Dermatol.* **1991**, *97* (6), 1005-12.
8. White, S. H.; Mirejovsky, D.; King, G. I., Structure of lamellar lipid domains and corneocyte envelopes of murine stratum corneum. An X-ray diffraction study. *Biochemistry* **1988**, *27* (10), 3725-32.
9. Bouwstra, J.; Gooris, G.; Ponec, M., The lipid organisation of the skin barrier: Liquid and crystalline domains coexist in lamellar phases. *Journal of biological physics* **2002**, *28* (2), 211-223.
10. Boncheva, M.; Damien, F.; Normand, V., Molecular organization of the lipid matrix in intact stratum corneum using ATR-FTIR spectroscopy. *Biochim. Biophys. Acta* **2008**, *1778* (5), 1344-55.
11. Damien, F.; Boncheva, M., The extent of orthorhombic lipid phases in the stratum corneum determines the barrier efficiency of human skin in vivo. *J. Invest. Dermatol.* **2010**, *130* (2), 611-614.
12. Weerheim, A.; Ponec, M., Determination of stratum corneum lipid profile by tape stripping in combination with high-performance thin-layer chromatography. *Arch. Dermatol. Res.* **2001**, *293* (4), 191-199.
13. Coderch, L.; López, O.; de la Maza, A.; Parra, J. L., Ceramides and Skin Function. *Am. J. Clin. Dermatol.* **2003**, *4* (2), 107-129.
14. Norlen, L.; Nicander, I.; Lundsjo, A.; Cronholm, T.; Forslind, B., A new HPLC-based method for the quantitative analysis of inner stratum corneum lipids with special reference to the free fatty acid fraction. *Arch. Dermatol. Res.* **1998**, *290* (9), 508-16.
15. van Smeden, J.; Boiten, W. A.; Hankemeier, T.; Rissmann, R.; Bouwstra, J. A.; Vreeken, R. J., Combined LC/MS-platform for analysis of all major stratum corneum lipids, and the profiling of skin substitutes. *Biochim. Biophys. Acta* **2014**, *1841* (1), 70-79.
16. P. W. Wertz, D. T. D., *Physiology, biochemistry and molecular biology of the skin*. second ed.; Oxford University Press: New York, 1991; Vol. 1, p 205-236.
17. Masukawa, Y.; Narita, H.; Shimizu, E.; Kondo, N.; Sugai, Y.; Oba, T.; Homma, R.; Ishikawa, J.; Takagi, Y.; Kitahara, T.; Takema, Y.; Kita, K., Characterization of overall ceramide species in human Stratum corneum. *J. Lipid Res.* **2008**, *49* (7), 1466-1476.

18. Rabionet, M.; Gorgas, K.; Sandhoff, R., Ceramide synthesis in the epidermis. *Biochim. Biophys. Acta* **2014**, *1841* (3), 422-34.
19. Robson, K. J.; Stewart, M. E.; Michelsen, S.; Lazo, N. D.; Downing, D. T., 6-Hydroxy-4-sphingenine in human epidermal ceramides. *J. Lipid Res.* **1994**, *35* (11), 2060-8.
20. Stewart, M. E.; Downing, D. T., A new 6-hydroxy-4-sphingenine-containing ceramide in human skin. *J. Lipid Res.* **1999**, *40* (8), 1434-9.
21. van Smeden, J.; Hoppel, L.; van der Heijden, R.; Hankemeier, T.; Vreeken, R. J.; Bouwstra, J. A., LC/MS analysis of stratum corneum lipids: ceramide profiling and discovery. *J. Lipid Res.* **2011**, *52* (6), 1211-21.
22. Boiten, W.; Absalah, S.; Vreeken, R.; Bouwstra, J.; van Smeden, J., Quantitative analysis of ceramides using a novel lipidomics approach with three dimensional response modelling. *Biochimica et Biophysica Acta (BBA) - Molecular and Cell Biology of Lipids* **2016**, *1861* (11), 1652-1661.
23. Janssens, M.; van Smeden, J.; Gooris, G. S.; Bras, W.; Portale, G.; Caspers, P. J.; Vreeken, R. J.; Kezic, S.; Lavrijsen, A. P.; Bouwstra, J. A., Lamellar lipid organization and ceramide composition in the stratum corneum of patients with atopic eczema. *J. Invest. Dermatol.* **2011**, *131* (10), 2136-8.
24. van Smeden, J.; Janssens, M.; Boiten, W. A.; van Drongelen, V.; Furio, L.; Vreeken, R. J.; Hovnanian, A.; Bouwstra, J. A., Intercellular skin barrier lipid composition, and organization in Netherton syndrome patients. *J. Invest. Dermatol.* **2014**, *134* (5), 1238-1245.
25. Schreiner, V.; Gooris, G. S.; Pfeiffer, S.; Lanzendorfer, G.; Wenck, H.; Diembeck, W.; Proksch, E.; Bouwstra, J., Barrier characteristics of different human skin types investigated with X-ray diffraction, lipid analysis, and electron microscopy imaging. *J. Invest. Dermatol.* **2000**, *114* (4), 654-60.
26. J.A. Bouwstra, E. H. M., *Cosmetic formulation principles and practice*. CRC Press: Boca Raton, 2019.
27. Crumrine, D.; Khnykin, D.; Krieg, P.; Man, M.-Q.; Celli, A.; Mauro, T. M.; Wakefield, J. S.; Menon, G.; Mauldin, E.; Miner, J. H.; Lin, M.-H.; Brash, A. R.; Sprecher, E.; Radner, F. P. W.; Choate, K.; Roop, D.; Uchida, Y.; Gruber, R.; Schmuth, M.; Elias, P. M., Mutations in Recessive Congenital Ichthyoses Illuminate the Origin and Functions of the Corneocyte Lipid Envelope. *J. Investig. Dermatol.* **2019**, *139* (4), 760-768.
28. Eckl, K.-M.; Tidhar, R.; Thiele, H.; Oji, V.; Hausser, I.; Brodesser, S.; Preil, M.-L.; Önal-Akan, A.; Stock, F.; Müller, D.; Becker, K.; Casper, R.; Nürnberg, G.; Altmüller, J.; Nürnberg, P.; Traupe, H.; Futerman, A. H.; Hennies, H. C., Impaired Epidermal Ceramide Synthesis Causes Autosomal Recessive Congenital Ichthyosis and Reveals the Importance of Ceramide Acyl Chain Length. *J. Investig. Dermatol.* **2013**, *133* (9), 2202-2211.
29. Motta, S.; Monti, M.; Sesana, S.; Caputo, R.; Carelli, S.; Ghidoni, R., Ceramide composition of the psoriatic scale. *Biochim. Biophys. Acta* **1993**, *1182* (2), 147-51.
30. Groen, D.; Gooris, G. S.; Bouwstra, J. A., New insights into the stratum corneum lipid organization by X-ray diffraction analysis. *Biophys. J.* **2009**, *97* (8), 2242-2249.
31. Uche, L. E.; Gooris, G. S.; Beddoes, C. M.; Bouwstra, J. A., New insight into phase behavior and permeability of skin lipid models based on sphingosine and phytosphingosine ceramides. *Biochim. Biophys. Acta* **2019**, *1861* (7), 1317-1328.

CURRICULUM VITAE

Lorretta Uche was born on the 27th of February 1969 in Nigeria. She obtained a bachelor's degree in Pharmacy from the University of Nigeria Nsukka in 1991. Thereafter, she undertook a one-year internship program at the University of Nigeria Teaching Hospital Enugu in drug dispensing and compounding. Afterward, she did the mandatory one-year National Youth Service at the Essential Drugs division of the Ministry of Health and Social Welfare Port-Harcourt. She then worked as a community Pharmacist in New Life Care Pharmacy Port-Harcourt for two years.

In 1997 she obtained a master's degree in Pharmaceutical Technology (with distinction) from Kings College, London. Her dissertation investigated the effect of oil structure on microemulsion formation and was supervised by Prof. Jayne Lawrence. She was awarded the Abbott Laboratories Prize for best student in Pharmaceutical Technology and the College Prize for the best student from all of the Pharmacy Departments three MSc degrees. Thereafter, she joined Juhel Nigeria Limited, a pharmaceutical manufacturing company as a Production Pharmacist. In the year 2000, she was awarded the World Bank Robert S. McNamara Fellowship to investigate the Regulation of the Pharmaceutical industry in Nigeria. She worked in the Pharmaceutical industry for 15 years during which she gained experience in various sections including drug formulation, quality assurance, and regulatory affairs.

In 2017, she was admitted to a PhD position at Leiden Academic Centre for Drug Research, Leiden University under the supervision of Prof. Joke Bouwstra and Dr. Charlotte Beddoes. Her project focused on using lipid model membrane systems as a tool to unravel the underlying factors for skin barrier impairment in inflammatory skin diseases.

In November 2021, she was employed as Pharmaceutical Scientist, Manufacturing Science and Technology at Abbott laboratories, Weesp, Netherlands

LIST OF PUBLICATIONS

Uche, L. E.; Gooris, G. S.; Beddoes, C. M.; Bouwstra, J. A., *New insight into phase behavior and permeability of skin lipid models based on sphingosine and phytosphingosine ceramides*. *Biochim. Biophys. Acta*, **2019**; 1861(7): p. 1317-1328.

Uche, L. E.; Gooris, G. S.; Bouwstra, J. A.; Beddoes, C. M., *Barrier Capability of Skin Lipid Models: Effect of Ceramides and Free Fatty Acid Composition*, *Langmuir*, **2019**; 26;35(47):15376-15388

Uche, L. E.; Gooris, G. S.; Bouwstra, J. A.; Beddoes, C. M., *High concentration of the ester-linked ω -hydroxy ceramide increases the permeability in skin lipid model membranes*, *Biochim. Biophys. Acta*, **2021**; 1863(1): p. 183487-183497.

Uche, L. E.; Gooris, G. S.; Bouwstra, J. A.; Beddoes, C. M., *Increased Levels of Short-Chain Ceramides Modify the Lipid Organization and Reduce the Lipid Barrier of Skin Model Membranes*, *Langmuir* **2021**; 37 (31), 9478-9489.

